NASA CR-145119

CORRELATION OF AH-1G AIRFRAME TEST DATA WITH A NASTRAN MATHEMATICAL MODEL

MAR 1977
RECEIVED
NASA STI FACILITY
INPUT BRANCH

REPORT NUMBER 699-099-016

FEBRUARY, 1976

Prepared under NASA Contract NAS1-13801

(NASA-CR-145119) CORRELATION OF AH-1G AIRFRAME TEST DATA WITH A NASTRAN MATHEMATICAL MODEL (Bell Helicopter Co.) 160 p HC A08/MF A01 CSCL 13M

N77-19488

Unclas

G3/39 21647

BELL HELICOPTER TEXTRON

P. O. Box 482

FORT WORTH, TEXAS 76101

for

NATIONAL AERONAUTICS & SPACE ADMINISTRATION

CONTENTS

	Page
SUMMARY	1
INTRODUCTION	1
SYMBOLS	3
AH-1G AIRFRAME STRUCTURE AND MATH MODEL DESCRIPTION	4
Airframe Structure Description	4
NASTRAN Math Model Description	5
TEST DATA AND NASTRAN ANALYSIS COMPARISON	8
Fuselage and Wings Static Tests and Analysis	8
Tailboom and Vertical Fin Static Tests and Analysis	14
Airframe Vibration Tests and Analysis	18
CONCLUSIONS	27
APPENDIX A FREQUENCY RESPONSE DATA COMPARISONS FOR DIFFERENT AMOUNTS OF DAMPING	63
APPENDIX B FREQUENCY RESPONSE DATA COMPARISONS (MAGNITUDE AND PHASE)	81
APPENDIX C FORCED RESPONSE MODE SHAPE COMPARISONS	141
APPENDIX D DESCRIPTION OF DIGITAL DATA REDUCTION TECHNIQUE	153
REFERENCES	155

ILLUSTRATIONS

Figure		Page
1	NASTRAN Model of the AH-1G Helicopter Airframe	29
2	Fuselage Structure Schematic	30
3	Main Rotor Pylon	31
4	Wings and Carry Through Structure	32
5	Tailboom and Vertical Fin	33
6	NASTRAN Fuselage Structure Model	34
7	NASTRAN Main Rotor Pylon Model	35
8	NASTRAN Wings and Carry Through Structure Model	36
9	NASTRAN Tailboom and Vertical Fin Model	37
10	Fuselage Structure Mounted on Base Plate	38
11	Fuselage Vertical and Torsion Test Setup	39
12	Fuselage Lateral Test Setup	40
13	Wing Test Setup	41
14	Typical Graphical Data Reduction Technique	42
15	Fuselage Vertical Load-Deflection Comparison	43
16	Fuselage Torsion Torque-Rotation Comparison	44
17	Fuselage Lateral Load-Deflection Comparison	45
18	Wing Beamwise Load-Deflection Comparison	46
19	Wing Torsion Torque-Rotation Comparison	47
20	Tailboom Test Setup	48
21	Load Application and Typical Dial Indicator	49
22	Vertical Fin Test Setup (Lateral Test Shown)	50
23	Tailboom Vertical Load-Deflection Comparison	51

ILLUSTRATIONS (Concluded)

Figure		Page
24	Tailboom Lateral Load-Deflection Comparison	52
25	Tailboom Torsion Torque-Rotation Comparison	53
26	Vertical Fin Lateral Load-Deflection Comparison	54
27	Vertical Fin Torsion Torque-Rotation Comparison	55
28	Vertical Fin Chordwise Load-Deflection Comparison	56
29	Wing Store	57
30	Accelerometer Locations for Shake Tests	58
31	Suspension and Shaker Locations for Vertical and Lateral Tail Shake Tests	59
32	Suspension and Shaker Locations for Main Rotor Hub Shake Tests	60
33	Shake Test Data Reduction Flow Chart	61
34	Comparison of Frequency Response Using 0% and 2% Damping	62

TABLES

		Page
I	Comparison of Weight and Inertia Parameters . . .	21
II	Calculated Airframe Natural Frequencies	23
III	Comparison of Natural Frequencies - Vertical Test	25
IV	Comparison of Natural Frequencies - Lateral Test	25

CORRELATION OF AH-1G AIRFRAME TEST DATA WITH A NASTRAN MATHEMATICAL MODEL*

By James D. Cronkhite and Victor L. Berry

Bell Helicopter Textron

SUMMARY

The purpose of the study was to provide test data for evaluating a mathematical vibration model of the Bell AH-1G helicopter airframe. The math model was developed and analyzed using the NASTRAN structural analysis computer program (Reference 1).

Data from static and dynamic tests were used for comparison with the math model. Static tests of the fuselage and tailboom were conducted to verify the stiffness representation of the NASTRAN model. Dynamic test data were obtained from shake tests of the airframe and were used to evaluate the NASTRAN model for representing the low frequency (below 30 Hz) vibration response of the airframe.

In general, the results of the comparisons show good agreement between the NASTRAN analysis and test. Problems encountered during the test data reduction and subsequent correlation are discussed in detail.

INTRODUCTION

This report documents the results of static and dynamic tests and comparison of results from those tests with NASTRAN finite element analyses of the Bell AH-1G attack helicopter airframe. The principal objective is to determine the validity of the NASTRAN mathematical model for predicting the vibration response of the airframe.

The NASTRAN vibration analysis was performed under an earlier contracted effort with the Army, Contract DAAF03-73-C-0122. The math model was developed to represent the low frequency (below 30 Hz) vibration response of the AH-1G helicopter airframe. This frequency range covers airframe vibration response to predominant main rotor excitation frequencies and to recoil loads when firing large caliber, turret-mounted guns from the

*The contract research effort which has lead to the results in this report was financially supported by USAAMRDL (Langley Directorate).

ORIGINAL PAGE IS OF POOR QUALITY

nose of the helicopter. Predominant main rotor excitation frequencies of the Bell two bladed rotor are two- and four-per-rev (10.8 and 21.6 Hz), and large caliber automatic weapon firing rates are generally in the range of 5 to 15 Hz.

The mathematical model is a linear elastic representation of the airframe structure with items such as the gun turret, fuel, main and tail rotors and crew modeled as lumped masses. The AH-1G NASTRAN model is shown in Figure 1. The model was delivered to the Army in January 1974. The version of NASTRAN used was public version, level 15.1. Very detailed documentation of the NASTRAN model was provided to the Army in the contract final report, Reference 2.

The purpose of this effort is to compare the NASTRAN model with test results to validate the model in light of the assumptions made, i.e., that an elastic structural model could represent airframe vibration modes below 30 Hz. Since dynamic response must be cauculated, both stiffness and mass modeling techniques are required. Stiffness modeling can be correlated directly from static load-deflection test data, but mass modeling can be correlated only indirectly with shake test data which contains both stiffness and mass effects. Good correlation between analytical and test results for both static and dynamic tests implies that both stiffness and mass modeling are correct. If only static test correlation is good, then the error should be in the mass modeling.

Three sets of tests were conducted:

- static fuselage load-deflection tests performed at the Rock Island Arsenal,

- static tailboom load-deflection tests conducted at Bell Helicopter, and

- airframe vibration tests also conducted at Bell but under another contract, Army Contract DAAJ02-73-C-0105.

For each of the above tests, the test procedure, description of the test article, instrumentation, and data reduction techniques are discussed. The results of the NASTRAN analyses are also presented and compared to the test results. For the vibration test, a discussion of significant dynamic characteristics such as damping effects, frequency response, and airframe mode shapes is also presented. More extensive details pertaining to test fixtures, procedures, and results are given in References 3 through 5.

SYMBOLS

BL	butt line
BS	boom station
CG	center of gravity
FNS	fin station
FS	fuselage station
g	gravitational unit (1 g = 386 in./sec^2)
Hz	Hertz, cycles per second
in.	inch
lb	pound
LVDT	linear variable differential transformer
sec	second
WL	water line
WS	wing station

AH-1G AIRFRAME STRUCTURE AND MATH MODEL DESCRIPTION

In the interest of completeness, descriptions of the airframe structure and NASTRAN math model are included herein. More detailed descriptions can be found in Reference 2.

Airframe Structure Description

Fuselage. - The fuselage structure is built around the main beams running the length of the fuselage (FS 61 to 300). The beams are made up of vertical webs and upper and lower caps. The left-hand main beam is shown by the shaded area in Figure 2. The main beams give the primary vertical bending stiffness in the fuselage structure and differential bending of the main beams provides torsional stiffness in the open sections of the forward fuselage (FS 61 to 138).

The main beams are tied together by the lower horizontal floors (FS 46 to 138), WL 46; FS 93 to 138, WL 55; FS 138 to 300, WL 35.97), the forward fuel cell cover (FS 152 to 186, WL 77), and the engine deck (FS 213 to 300, WL 65) to give the fuselage lateral stiffness. The torsion sections are closed in the forward fuel cell area (FS 148.5 to 186) and the aft fuselage (FS 213 to 300) but open on top of the main beams in the main rotor pylon and wing area (FS 186 to 213).

The ammo shelf (FS 93 to 138, WL 27) does not significantly affect the vertical or lateral bending stiffness of the fuselage structure but does influence the torsional stiffness because of the shear tie at the FS 93 bulkhead.

An XM-28 gun turret is mounted under the gunner's floor (FS 61.25 to 93). Four fittings distribute the recoil loads into the main beams.

Main rotor pylon. - The main rotor pylon located at FS 200 above WL 65 provides the structural tie between the main rotor and the fuselage. It is attached to the fuselage through five elastomeric mounts and a lift link. The mounting arrangement is shown in Figure 3. This lift link is the primary vertical load path and is pinned to the center wing carry through beam or "lift beam." The elastomeric mounts are designed to produce low pylon rocking frequencies to isolate the main rotor in-plane vibratory loads from the fuselage and to react the main rotor torque.

Wings and carry through structure. - The wings on the AH-1G are designed primarily as stores supports, not as aerodynamic lifting surfaces. The wings and carry through structure are shown in Figure 4. The stores attachment points are at BL 42.5 and 60.

The wing is a two-cell box structure having aluminum skins, three spars and three ribs. The carry through consists

ORIGINAL PAGE IS
OF POOR QUALITY

of three beams that are attached to the three wing spars by pinned connections at the fuselage contour. The forward carry through beam is attached to the FS 186.25 bulkhead. The center carry through beam or "lift beam" is attached at the fuselage contour and is pin connected in the center to the lift link. The aft spar carry through is attached to the FS 213.94 bulkhead.

Tailboom and vertical fin. - The tailboom and vertical fin structure are shown in Figure 5. The tailboom is bolted to the fuselage at four attachment fittings located at the four main longerons of the tailboom and the four main beam caps of the fuselage.

The tailboom is of semimonocoque construction having aluminum skins, stringers and longerons. The longerons and stringers are supported by bulkhead frames spaced down the length of the boom. A typical cross section of the tailboom is shown in Figure 5. The tail rotor driveshaft and cover on top of the boom are assumed nonstructural.

The vertical fin has a two cell cambered airfoil section with two spars and a trailing edge strip. The tail rotor driveshaft and cover on the front of the fin is assumed nonstructural as well as the top portion of the fin which extends above the 90° gearbox. A typical fin cross section is shown in Figure 5. The 90° gearbox and the tail rotor mast shown in Figure 5 provide the connection between the tail rotor and the top of the vertical fin structure. The tail rotor mast is supported on bearings inside the gearbox and the gearbox is bolted to the top of the fin.

NASTRAN Math Model Description

The idealization of the airframe into a finite element model is briefly described in this section. The emphasis in the idealization is on developing a model adequately representing the low frequency vibration modes of the airframe with the fewest degrees of freedom possible. Representation of the fuselage structure in the area of the XM-28 gun turret and of the wing structure in the area of the wing stores is given special attention. The gun turret and stores themselves are represented as rigid masses, as are the main and tail rotors, the engine, and useful weight items such as the crew, fuel and ammunition.

The complete model, shown in Figure 1, consists of structural elements from the NASTRAN library (see Reference 1) such as scalar springs, rods, bars, shear panels, triangular and quadrilateral membranes. There was no use of general elements, substructuring, or DMAPing in the model. The entire structure had

ORIGINAL PAGE IS
OF POOR QUALITY

to be represented due to the effects of unsymmetrical sections in the fuselage and of the tail rotor offset to the right side.

Fuselage Idealization. - The fuselage is a built-up idealization using primarily rods and shear panels in the bending sections. Instead of using an elastic line or 'beam' representation, built-up modeling is used because of the complex structure in the forward and center fuselage areas. The forward fuselage has open sections making it difficult to calculate the elastic axis location and torsional stiffness properties important in determining the structural response to lateral gunfiring. In the center fuselage, where the wing carry through, pylon support and fuselage structures intersect, built-up modeling is required to represent the complex redundant structure.

The primary fuselage bending structure is modeled with rods and shear panels. The belly structure is also modeled with rods and shear panels except where triangular membranes are required due to geometry. The nose structure skins are modeled with membranes, and bulkheads are modeled with membranes surrounded by rods. Multipoint constraint equations representing rigid elements are used to tie the landing gear, tailboom and gun turret mass to the fuselage. Bar elements are used only for the pylon support structure. The NASTRAN fuselage idealization is shown in Figure 6.

Main rotor pylon idealization. - The main rotor pylon is modeled as an elastic line using bar elements. The mast is pinned to the transmission case at mast bearing locations. The elastomeric pylon mounts are modeled with scalar spring elements, and multipoint constraint equations are used to tie the transmission elastic line to the mount locations. The lift link is represented with a bar, pinned and rigidly offset from grid points on the transmission and lift beam. The NASTRAN model is shown in Figure 7.

Significant deficiencies are apparent in the main rotor pylon idealization. There are no provisions in the pylon model for "pendulum" stiffening or differential stiffening effects resulting from the helicopter being suspended in a gravity field. Also, the elastomeric mounts which have material nonlinearities are idealized as linear springs. These effects along with transmission dynamic effects that are not represented in the math model could result in significant discrepancies in dynamic response between the NASTRAN idealization and the actual pylon.

Wings and carry through structure idealization. - The wings and carry through are built-up idealizations because of the complex interface between these structures involving pinned connections at the fuselage contour. The wing spar caps, carry through beam caps and attachment lugs are modeled with bars and the spar and beam webs with shear panels and rods. The wing skins are represented by quadrilateral membranes which preserve the beamwise (vertical) bending and torsional stiffness but are somewhat too

stiff in chordwise (fore-and-aft) bending. The pinned connections at the attachment lugs are modeled with multipoint constraint equations. The NASTRAN model is shown in Figure 8.

Tailboom and vertical fin idealizations. - The tailboom and vertical fin are modeled as elastic lines using bar elements with calculated bending and torsional stiffness properties. The elastic axis is assumed to be on the geometric center of the tailboom and along the center spar of the vertical fin (refer to Figure 5 for typical sections and Figure 9 for the NASTRAN model).

In calculating the tailboom stiffness properties, the attached skins were considered fully effective. This is not totally accurate since the tailboom is of semimonocoque sheet-stringer design. This type of design compensates for skin buckling and the corresponding reduced element areas at stress levels near the ultimate design stress. Since this analysis is based on stress levels resulting from 1 g level flight conditions rather than stress levels resulting from 4.5 g ultimate conditions,consideration of the skins as being fully effective is believed accurate.

TEST DATA AND NASTRAN ANALYSIS COMPARISONS

Fuselage and Wings Static Tests and Analysis

Test Procedure. - Static load-deflection tests of the AH-1G fuselage and wings were conducted at Rock Island Arsenal. The purpose of the tests was to determine the stiffnesses of the fuselage and wing structures. The test setup, instrumentation and load-deflection data are documented in the Rock Island test report (Reference 3).

The test article was AH-1G ship number 15048. The fuselage had fire damage in the area under the main rotor pylon (FS 186 - FS213). The damaged structure was repaired with stiffened sheet resulting in good structural integrity. Although the stiffness was not identical, it was fairly representative of the original fuselage. The repair changes were well documented so that the NASTRAN math model could be changed accordingly so that there was a direct correspondence between the test article and the math model. The side contour panels (FS 61 - FS 186) that are not used in the NASTRAN model were removed and the side doors of the ammo compartment (FS 93 - FS 138) were propped open during the tests for compatibility between test and analysis.

The five static load-deflection tests of the fuselage and wing are summarized as follows:

Load condition	Maximum load
Fuselage vertical	1000 lb
Fuselage torsion	20,000 in.-lb
Fuselage lateral	1000 lb
Wing beamwise	1000 lb
Wing torsion	28,000 in.-lb (left) 19,200 in.-lb (right)

In the fuselage load-deflection tests, the stiffness of the entire fuselage was determined for each direction of loading, i.e., vertical, lateral and torsion. The mounting location chosen for the fuselage was the four bolt attachment points at the tailboom junction. The location for the applied load was chosen at the nose of the fuselage where a loading fixture could be mounted at the gun turret attachment points. Figure 10 shows the fuselage positioned on the base mounting plate with load cells at each of the four mounting locations. Linear variable differential transformers (LVDT's) were used for deflection measurements. These were located at several stations

along the fuselage and at the four base attachment points where measurements were taken with respect to ground.

There were three separate fuselage load-deflection tests conducted: vertical, torsion and lateral. A maximum alplied load of 1000 lb was used for the vertical and lateral tests and a maximum torque of 20,000 (in.-lb) was used for the torsion test. The test setup that was used for the fuselage vertical and torsion tests is shown in Figure 11. The fuselage was rotated 90 degrees about its roll axis and the wings were removed for the lateral load-deflection test as shown in Figure 12.

Because of some instrumentation location problems, the lateral fuselage test was rerun using dial indicators for measuring deflections. For this test the ammo doors were closed to see if there was any stiffening from the doors.

For the wing load-deflection tests, the wings were left attached to the fuselage. The fuselage mounting for the fuselage vertical and torsion tests (Figure 11) was used for the wing tests. An instrumentation fixture was developed to allow measurement of wing deflections relative to the fuselage at the wing root. Wing elastic deflections could then be measured directly. This would eliminate having to calculate wing deflections from measurements taken with respect to ground which would also include fuselage and base deflections.

Two wing load-deflection tests were conducted: beamwise (vertical) and torsion. The setup for the wing test is shown in Figure 13. Wing loads were applied through a fixture at each wing tip. A maximum beamwise downward load of 1000 lb was used at each wing tip. The wing torsion load was intended to be a 20,000 in.-lb torque applied equally and in opposite directions at each wing tip. However, the left wing upward load (refer to Figure 13) was made twice the other three applied loads by mistake. The maximum load was then 800 lb at all locations but the left upward load which was 1600 lb. This resulted in a maximum torque of 19,200 (in.-lb) (800 lb loads with a 24 in. couple arm) applied to the right wing tip and a 28,800 (in.-lb) countertorque and 800 lb chordwise shear applied to the left wing tip.

Data Reduction. - The signals from the LVDT measuring devices and load transducers were recorded on tape as the tests were being run. Load versus deflection plots were obtained by playing the recorded data through an automated data reduction system at the Ware Simulation Center at the Rock Island Arsenal.

Data was taken for three or more cycles of loading for each test. The absolute deflections at maximum load for all load conditions were then averaged. Following this, corrections were made for

deflections due to rotation of the base of the fuselage with respect to ground.

Typical graphical data reduction methods used in determining deflections at maximum load are shown in Figure 14. A straight line through the data was used to approximate the load-deflection curve and define the deflection at maximum load. The deflection at zero load (Δ_o) was considered an error and was subtracted off the deflection at maximum load.

Base rotation deflections often showed a preload effect with little or no deflection up to a certain load level. Above that load level the deflection would increase. A typical example of how these curves were reduced is shown in Figure 14(b).

Base rotations were accounted for in the following manner. Deflections were measured on the fuselage structure at the four corners of the base. Deformations of the support structure, load cells and fuselage attachment fittings were accounted for in the measurements. Rotations were calculated using the pairs of deflections on the left hand and right hand sides for the vertical test and the pairs of deflections on the upper and lower sides for the lateral test. For a maximum load of 1000 lb, the resulting base rotations and corresponding deflections at the nose of the fuselage (FS 61) are as follows:

	Vertical test		Lateral test	
Base rotation (rad)	Left hand	.0005477	Upper	.0004402
	Right hand	.0005984	Lower	.0008724
	Average	.0005734	Average	.0006589
Deflection at FS 61 due to rotation (in.)	Left hand	.1305	Upper	.1049
	Right hand	.1426	Lower	.2079
	Average	.1366	Average	.1570

On the lateral test, the base rotations varied by nearly a factor of two with the lower side being consistently larger than the upper side. A possible explanation for this is that the base plate on which the fuselage was mounted had a built-up 3° angle (see Figure 10) making the upper attachment points about 1½ in. higher than the lower. This would result in the base being symmetrical for the vertical loading and unsymmetrical for the lateral loading.

NASTRAN Analysis. - The NASTRAN model was modified to reflect the structure repair changes. Documentation of these changes can be found in the test report (Reference 3). The fuselage

was then cantilever boundaried at the four tailboom attachment locations for the fuselage and wing loading conditions. Structure deflections were determined using the static solution in NASTRAN, rigid format 1.

For the fuselage loading conditions, the load was applied through a rigid (stiff) fixture that was attached at the gun turret mounting locations corresponding to the load fixture used in test. Maximum vertical, lateral and torsion loads were applied separately to the load fixture and the corresponding structure deflections computed for direct comparison with the reduced test data.

For the wing loading conditions, the instrumentation fixture (see Figure 13) was represented in the NASTRAN model. This was done by using stiff bars attached to the fuselage at the same location as test. Grid points were located identically at the measured grid point on the wing and tied to the fixture (stiff bars). Then the fixture grid point was tied to the wind structure grid point by a 1.0 (lb/in.) spring oriented in the direction being measured. This value of spring rate should not stiffen the structure being measured and allows direct calculation of the relative wing deflection from the spring force, i.e., 1.0 lb force in the spring equals 1.0 inch deflection.

The wing loads were applied at the center spar at the outboard rib of each wing. The maximum beamwise and torsion loads were applied separately and the relative wing deflections were computed from the spring forces between the fixture and the wing.

Comparison of results. -

1. Vertical load-deflection comparison (Figure 15).

   - NASTRAN results are stiffer than the test results (about 15% stiffer up to FS 93). NASTRAN results at FS 61 are about 25% stiffer than test.

   - The deflection shape is in good agreement between NASTRAN and test except in the nose area between FS 61 and FS 93 where the test appears softer.

   - There may be a steady translation of the base since the deflections from test do not project to a zero deflection at FS 300. However, this could be due to the difficulty in measuring the much smaller deflections near the base.

   - Possible explanations for the NASTRAN results being stiffer than test are:

(1) the actual structure is not as stiff as the idealized NASTRAN model indicates,

(2) the stiffness of the load fixture, modeled as rigid in NASTRAN, is affecting the deflections between FS 61 and FS 93,

(3) the side panels and ammo doors that were removed during the test helped stabilize the structure in the forward end of the fuselage or may be partially effective when installed, thereby providing stiffness lost due to cutouts in the cockpit area, joints, etc.,

(4) errors in instrumentation and loading calibration or in the data reduction, or

(5) that the fuselage structure of ship number 15048 being from a 1968 model helicopter may be "looser" than a new structure.

2. Torsion torque-rotation comparison (Figure 16)

- It was found after initial comparisons of the data that the NASTRAN model was much stiffer in the forward fuselage than test. In an attempt at improving the correlation, the ammo bay structure (FS 93 - FS 138) was removed in the NASTRAN model. This modification was warranted since the shelf is free on both sides except for hinged doors which were propped open during the test. The correlation was found to improve with the shelf removed.

- With the ammo bay removed, the NASTRAN results are about 10 to 15 percent stiffer than test.

- The deflection shapes are in good agreement.

- Possible explanations for the NASTRAN results being stiffer are the same as those discussed for the vertical test above.

3. Lateral load-deflection comparison (Figure 17)

- At FS 93, the NASTRAN results are between 5 and 25 percent stiffer than test. The large spread in the test data is due to the variation in base rotations used in the calculations (refer to data reduction discussion). Using the average test value, the correlation is similar to that of the previous vertical and torsion tests.

- As mentioned in the discussion of the test procedure, the lateral test was rerun with dial indicators instead of LVDT's. The deflections measured with the dial indicators are about 15 percent lower than the other test and agree very well with the NASTRAN results.

4. Wing beamwise comparison (Figure 18)

The correlation of the wing tests with NASTRAN was not expected to be good for two reasons. The first is the complicated joint between the wing and the fuselage (see Figure 4) which tended to be sloppy could be affected by such things as the fit and torque of the bolts tying the wing and fuselage together. The second reason was the order of the maximum deflections to be measured was considerably lower than for the fuselage test. Such factors as possible joint sloppiness or deflections of the fuselage where the instrumentation fixture was attached could strongly affect the measurements.

- The agreement between NASTRAN and test is better than expected with the NASTRAN deflection at the tip of the wing being about 15 percent stiffer than test.

- There appears to be very little bending in the wing with most of the deflection due to rotation of the wing attachment joint (WS 18 - WS 20)

5. Wing torsion comparison (Figure 19)

- The NASTRAN results are about 15 percent softer than test.

- There appears to be a steady shift in the test data which could be due to warping of the fuselage structure where the instrumentation fixture is attached. This could cause warping and bending deflections in the fixture that could affect the measurements.

- If the rotation at the wing root (WS 21) is corrected to agree with the NASTRAN curve at the wing root, the wing tip would show NASTRAN about 15 percent stiffer than test which is similar to that of the previous tests.

The results of the fuselage comparisons can be summarized as follows:

- NASTRAN results are about 15 percent stiffer than test.

- The lateral test was rerun using dial indicators instead of LVDT's which measured deflections that were about 15 percent stiffer than previous tests and agreed well with NASTRAN.

- Removing the ammo shelf in the NASTRAN model improved correlation in the forward fuselage for the torsion test.

- Base rotations varied greatly on the lateral fuselage test and had a significant effect on the deflections.

The wing comparisons can be summarized as follows:

- The agreement was better than expected with the NASTRAN results at the wing tip about 15 percent stiffer than test for the beamwise loading and about 15 percent softer than test for the torsion loading.

- The test data indicated most of the wing deflection for the beamwise loading was due to rotation at the attachment joint.

- The test data also indicates a steady shift in the wing torsion test data due to deflection of the instrumentation fixture. If this was taken into account, it would make the NASTRAN data 15 percent stiffer than test.

Tailboom and Vertical Fin Static Tests and Analysis

Test Procedure. - The static load-deflection tests of the tailboom and vertical fin were conducted by the Mechanical Test Lab at Bell Helicopter Textron. The purpose of the tests was to validate the stiffness representation of the tailboom and vertical fin structure used in the NASTRAN math model. The setup, instrumentation and test data are documented in Reference 4.

The test article was the tailboom from the helicopter at Rock Island Arsenal that was used for the fuselage static testing, AH-1G ship number 15048. The basic structure of the tailboom was in good condition with only minor preparation, such as replacing fasteners for access doors, having to be done before testing.

The tailboom was mounted to a base fixture at the four fuselage attachment points at BS 41.32 for the tailboom and vertical fin loading conditions. Structure deflections up to 1.0 in. were measured with dial indicators. Deflections expected to be greater than 1.0 in. were measured with tube scales which were attached to the structure through a string and pulley arrangement. The small base rotation and translation deflections were measured electrically with strain-leaf indicators which were small cantilevers with strain-gaged flexures.

The six static load-deflection tests of the tailboom and vertical fin and maximum applied load for each are summarized as follows:

Load condition	Maximum load
Tailboom vertical	1000 lb
Tailboom lateral	1000 lb
Tailboom torsion	40,000 in.-lb
Vertical fin lateral	500 lb
Vertical fin torsion	13,000 in.-lb
Vertical fin chordwise	500 lb

Three loading conditions were used in the tailboom testing: vertical, lateral and torsion. The test setup for the vertical loading condition is shown in Figure 20. The instrumentation for measuring base deflection and structure deflections was attached to a framework built around the tailboom and base and attached to ground.

The load fixture for the tailboom tests is shown in Figure 21. The fixture was located at BS 227. The maximum load for the vertical and lateral tests was 1000 lb. The maximum torque for the tailboom torsion test was 40,000 in.-lb.

Three loading conditions were used in the vertical fin testing: lateral, torsion and chordwise. An instrumentation fixture was used for the vertical fin tests so that elastic deflection of the fin could be measured with respect to the base of the fin. Testing of the fin was not as extensive as the tailboom and only two sets of measurements were taken along the fin for each load condition. A typical vertical fin test setup is shown in Figure 22.

Vertical fin loads were applied through the tail rotor gearbox and mast in the lateral, torsion and chordwise directions. Maximum lateral and chordwise loads were 500 lb. The maximum fin torsion load was 13,000 in.-lb.

Data reduction. - Deflections were tabulated for each test as the loading was applied. The deflections were plotted as load versus deflection curves and are included in Reference 4. The deflections corresponding to the maximum load were used in the comparison with the NASTRAN analysis. The calculated deflections represented the rigidly cantilevered structure deflection with respect to ground and therefore any base rotation that occurred in test had to be removed before comparison with NASTRAN could be made.

Deflections were measured at the four corners of the base. As in the fuselage tests, the base rotations were calculated using the left hand and right hand pairs of deflections for the vertical loading and the upper and lower pairs of deflections for the lateral loading. The average base rotations were used for comparison with NASTRAN. For a maximum load of 1000 lb,

base rotations and resulting deflections at the aft end of the tailboom (BS 206) are as follows:

	Vertical test		Lateral test	
Base rotation (rad)	Right hand	.000318	Lower	.00086
	Left hand	.000720	Upper	.00102
	Average	.000519	Average	.00094
Deflection at BS 206 due to base rotation (in.)	Right hand	.0524	Lower	.1418
	Left hand	.1190	Upper	.1681
	Average	.0857	Average	.1550

A possible explanation for the large variation in base rotation for the vertical loading is believed to be caused by local deflection of the lower left hand tailboom attachment fitting under compression load. This deflection was considerably higher than the other deflections and resulted in a large rotation on the left hand side. The measurement was not taken directly on the fitting but rather on an adjacent bulkhead web. For the lateral loading, the lower left hand fitting was in tension and unusual deflections were not indicated.

NASTRAN Analysis. - The forward end (BS 41.32) of the NASTRAN tailboom model was cantilevered in all six degrees of freedom for the tailboom and vertical fin loading conditions. Loads were applied to the model at the same locations as test. Structure deflections were determined using the static analysis solution in NASTRAN, rigid format 1.

The relative fin deflections for the fin loading condition were determined by a separate analysis with the fin cantilever boundaried at the fin base (FNS 59.06). The calculated fin deflections would then correspond to the relative deflections measured in test.

Comparison of Results. -

1. Tailboom vertical load-deflection comparison (Figure 23)

   - There is fairly good agreement between the NASTRAN and test results with NASTRAN being slightly softer - about 4 percent when compared to the average deflections at the aft end (BS 206). There were significant differences in the base rotations measured on the left hand and right hand sides which resulted in about a 14 percent variation in the deflections.

   - The curve shapes agree well, NASTRAN being slightly softer at the aft end of the tailboom.

2. Tailboom lateral load-deflection comparison (Figure 24)

   - As with the vertical loading, there is good agreement between NASTRAN and test results with NASTRAN slightly softer at the aft end of the tailboom (about 7 percent).

   - Again the curve shapes agree well, NASTRAN being slightly softer in the aft end.

3. Tailboom torsion load-deflection comparison (Figure 25).

   - There is good agreement except at the aft end of the tailboom (BS 206). There was a large variation in the test data at that location as indicated by the band of measured rotations in the figure. Test varies from 19 percent to 45 percent stiffer than NASTRAN with the average being about 28 percent stiffer at BS 206.

   - The curve shapes agree well except for the BS 206 location.

4. Vertical fin lateral load-deflection comparison (Figure 26)

   - Deflections measured relative to the base of the fin are about 25 percent lower than NASTRAN.

   - There is good agreement when comparing the total deflections of the fin with respect to the tailboom base (NASTRAN results are about 3 percent softer than test).

   - The relative fin bending deflections are only about 10 percent of the total deflections at the top of the fin.

5. Vertical fin torsion torque-rotation comparison (Figure 27)

   - The test is considerably stiffer than NASTRAN (about 35 percent) for the torsional rotations of the fin.

6. Vertical fin chordwise load-deflection comparison (Figure 28)

   - The test gets stiffer towards the top of the fin when compared to NASTRAN. Test is about 20 percent stiffer at FNS 10.

   - The total vertical deflections with respect to the tailboom base show better agreement with test. Test was about 10 percent stiffer than NASTRAN.

Results of the tailboom and vertical fin comparisons are summarized as follows:

- There is excellent agreement for the tailboom loading conditions both in curve shape and deflection magnitude. The only exception is a torsion data point at BS 206 which is considerably stiffer (about 35 percent average) than NASTRAN,

but there is a lot of scatter in the data at that particular point.

- The vertical fin tests which were not as extensive or as conclusive as the tailboom tests, indicate relative deflections considerably stiffer than NASTRAN (about 20 percent to 35 percent stiffer).

- The relative fin deflections represent a small part of the total deflections with respect to the tailboom base at the top of the fin (about 10 percent for the fin lateral loading).

- The total deflection at the top of the fin for the fin lateral and chordwise loadings were in good agreement. NASTRAN was about 3 percent softer for the lateral loading and about 10 percent softer for the chordwise loading.

Airframe Vibration Tests and Analysis

General. - Correlation with shake tests was done to evaluate the NASTRAN model in light of the assumptions made, i.e., an elastic structural model aimed at representing the low frequency (below 30 Hz) vibration response of the airframe. Test results were obtained from shake tests conducted as a part of Army contract DAAJ02-73-C-0105.

The shake testing was conducted on an AH-1G helicopter, ship number 28391. The helicopter was configured with clean wings (no stores) and with 325 lb rocket pods at the inboard store stations on the stub wings. These particular stores were chosen to be consistent with a flight test program done under contract DAAJ02-73-C-0105. The configuration with stores was tested in order to evaluate the effect of wing stores on airframe vibration.

Vertical and lateral excitations applied to the tail of the airframe were the principal shake tests used for evaluation of the NASTRAN model. However, comparisons with shake tests where the force is applied to the main rotor hub were also made. The structural dynamics characteristics of the soft-mounted pylon (see Figure 3) that depend on its loading or mounting nonlinearities were expected to cause significant discrepancies between the test results and NASTRAN math model results since the math model does not include effects of large motions (differential stiffening or "pendulum" stiffening) or material nonlinearities in the elastomeric mounts. Shaking at the main rotor hub through the pylon would then result in an excitation to the airframe structure that is not as well defined as it would be when shaking at the tail. However, shaking at the hub is of interest in determining in-flight airframe vibration response. The

exciting force from the main rotor is at the hub and one would like to know the transfer function between the excitation at the hub and response at locations on the airframe.

Accelerometers were used for measuring vibration response of the airframe. Accelerometer locations were selected to correspond as closely as possible to grid point locations in the NASTRAN model to facilitate correlation.

Different values of modal damping were used in the NASTRAN analysis to determine an appropriate value for the comparison with test data. The criteria used for evaluating the amount of damping to be used was that the response near resonances should be higher than test results while trying to maintain a shape of the curve that was representative of the test curve. This is considered to be a conservative but representative method of determining the airframe vibration response analytically. In the response valleys, however, this approach would be unconservative since more damping generally increases the response in these areas. In a design analysis the effects of both low (up to 2 percent) and high (up to 5 percent) values of damping of the airframe structure modes should be considered; the low values of damping for evaluating near resonance responses and higher values of damping for evaluating response in the valleys.

The method of comparison between the shake tests and the NASTRAN analysis was to overlay frequency response data or forced response mode shape data for the same boundary conditions, applied force and response locations for test and analysis and comment on their agreement. The comparison figures are presented in Appendices A, B and C. The correlation is discussed in later sections of the report.

Test procedure. - The AH-1G helicopter was suspended from the main rotor hub by a long cable and soft bungee (the bungee was removed for the lateral and fore-and-aft hub shakes). The suspension system was intended to support the helicopter in a way that would allow free vibration of the airframe in the manner that it would vibrate in flight. The vertical mode of the helicopter on the suspension system with bungee was below 1.3 Hz and should not affect the airframe vibration response at higher frequencies (4 Hz and above). The main and tail rotors were replaced with dummy hubs that were ballasted to represent the rotor weights. Two helicopter weight configurations were tested: clean wing and inboard wing stores. The left wing store is shown in Figure 29. The shake testing is described in more detail in Reference 5.

The shake tests were run with a single sinusoidal applied force and sweeping frequency from 2 to 40 Hz. NASTRAN frequency

response results were used as a guide in the testing. The test conditions used for correlation are the following:

Applied force direction/location	Configuration
Vertical/tail (FS 485)	Clean wing
Vertical/tail	Stores
Lateral/tail	Clean wing
Lateral/tail	Stores
Vertical/hub	Clean wing
Lateral/hub	Clean wing
Fore-and-aft/hub	Clean wing

After a frequency sweep was completed, forced response mode shape data was obtained by dwelling at frequency response peaks. Response was measured by accelerometers distributed along the airframe. The excitation force was measured by transducers located between the airframe and the shaker. The accelerometer locations used in the tests are shown in Figure 30.

Shaker locations and the suspension of the helicopter for the vertical and lateral tail shake tests are shown in Figure 31 and for the main rotor hub shake tests in Figure 32. Note that the bungee is used for the vertical hub shake but the stiff cable alone is used for the lateral and longitudinal hub shake tests. This minimizes the effect of the suspension system on hub vibration when shaking horizontally at the hub. It was assumed that vertical response when shaking horizontally at the hub is not significant; otherwise the stiff cable suspension could affect the response.

Data reduction. - Accelerometer and force transducer data were reduced on-site to monitor the testing and off-site to obtain complete results for correlation with the NASTRAN analysis. A flow diagram of the on-site and off-site data reduction procedures is shown in Figure 33.

The on-site data reduction was used to monitor the testing and check the digital data reduction technique. Frequency response plots were made for a few accelerometers. These plots along with a mode shape meter were used to locate frequencies upon which to dwell for taking mode shape data.

The mode shape meter visually displays the relative response of several accelerometers along the airframe and allows quick identification of modes without having to guess or feel the structure by hand. No data were recorded from the mode shape meter.

ORIGINAL PAGE IS
OF POOR QUALITY

The off-site data reduction procedure was used to generate the test data used for correlation. This procedure involved digitizing the on-board analog FM tapes on which the accelerometer and force transducer signals were recorded and then digitally analyzing the data to generate frequency response (magnitude and phase) plots and forced mode shape plots. These plots were then used directly for comparison with the NASTRAN analysis. The digital data reduction technique is explained in Appendix D.

Frequency response plots from the on-site system were compared to the off-site digital data reduction system to verify the digital technique. Plots for response locations at the nose, tail and hub (hub shakes only) were compared and showed that the shape of the frequency response magnitudes were always in good agreement, but there was sometimes a steady shift between the two curves. Since the magnitudes were plotted on logarithmic scale this indicated the difference was a constant multiplying factor which could have occurred in calibration of the digital data. The comparison curves in Appendices A and B are noted whenever this error was known to occur. No shifts occurred in the tail shake test data, but a few shifts did occur in the hub shake test data.

NASTRAN analysis. - The only changes made to the NASTRAN model documented in Reference 2 involved stores and measurement locations on the tailboom. All weights associated with the outboard stores (about 520 lb) for the clean wing configuration were removed. Store mass properties (Figure 29) were added at each inboard store location to represent the stores configuration.

Some additional grid points had to be added with rigid (stiff) bars connecting them to the structural model in order to directly compute the NASTRAN response at the same location as the test and to apply the tail shaker loads. This was done at the tailboom/fuselage junction, the elevator and the location of the lateral and vertical shaker forces.

A comparison of the weight, CG and inertias of the NASTRAN model with available test data is as follows:

TABLE I. COMPARISON OF WEIGHT AND INERTIA PARAMETERS

	Clean wing		Stores	
	Test	NASTRAN	Test	NASTRAN
Weight (lb)	8214	8394	8888	9044
CG: FS	196.1	192.9	196.8	193.2
WL	--	70.6	--	68.65
Inertia (lb-in.^{2})				
Roll	--	11.4×10^6	--	13.0×10^6
Pitch	--	61.9×10^6	--	62.5×10^6
Yaw	--	52.0×10^6	--	53.3×10^6

The natural frequencies for the clean wing and stores configurations are given in Table II.

The NASTRAN frequency response analysis, Rigid Format 11 (see Reference 1), was used to determine the magnitude and phase versus frequency results needed for correlation with the test data. Free vibration modes of the airframe were excited by a sinusoidal 1 lb force at the same forcing location as the shake test. Response was determined from 0 to 32.5 Hz in increments of .10 Hz. Magnitude and phase plots were generated on a Calcomp 763 digital plotter. These plots were then overlayed on the test frequency response plots for direct comparison.

The effect of damping on frequency response characteristics of the NASTRAN model was determined by varying the modal damping. Values of constant 0 percent, 2 percent and 5 percent modal damping were used as well as a linear variation in damping (0 percent at 0 Hz, 2 percent at 10 Hz, 4 percent at 20 Hz, etc.).

Effect of damping on frequency response comparisons. - It was found early in the study that using zero damping in the NASTRAN response analysis gave results that were difficult to interpret. Every mode of the structure would show up on the frequency response curves because of slight coupling that occurs due to structure and mass asymmetries. It became a problem to determine whether the response of a particular mode was significant to the shape of the frequency response curve. A comparison of NASTRAN response with 0 percent and 2 percent modal damping is shown in Figure 34. The conclusion drawn from this is that some amount of damping, say 1 to 2 percent, is needed to obtain reasonable frequency response results from analysis.

Comparisons between test and NASTRAN using different values of modal damping are shown in Appendix A. Responses at the gunner seat, the tail (FS 485)and 90° gearbox, and the hub (hub shakes only) are compared using 2 percent, 5 percent and linear damping.

As would be expected, the effects of increased damping shown by these comparisons are:

- the frequency response curve is smoothed out,

- the response near a resonance is lower, and

- low response areas are raised.

TABLE II - CALCULATED AIRFRAME NATURAL FREQUENCIES

Mode	Natural Frequency - Hertz	
	Clean Wing	W/Stores
Main rotor pylon fore-and-aft rocking (pylon pitch)	3.034	3.022
Main rotor pylon lateral rocking (pylon roll)	3.899	3.459
First fuselage lateral bending	7.149	7.050
First fuselage vertical bending	7.952	7.900
Skid	14.570	14.570
First fuselage torsion	15.672	15.305
Second fuselage vertical bending	17.491	17.261
Second fuselage lateral bending	17.504	16.563
Fuselage roll/engine lateral	18.760	18.167
Skid	19.841	19.837
Fuselage torsion/wing yaw	21.498	20.249
Wing asymmetric torsion	--	21.561
Skid	23.428	23.426
Third fuselage vertical bending	24.978	23.953
Main rotor mast lateral bending	25.285	25.557
Third fuselage lateral bending	25.759	24.580
Main rotor mast fore-and-aft bending	26.986	26.404
Wing symmetric torsion	--	28.294
Skid	29.037	28.705
Fourth fuselage vertical bending	31.949	31.553
Fuselage torsion	34.040	32.266

The tail lateral response comparisons shown in Figures A-6 and A-8 are good examples of these effects.

After comparing the NASTRAN results using different amounts of damping with test, it was concluded that using a constant 2 percent modal damping would result in a representative shape of the frequency response curve. Also, this was a slightly lower value of damping than test and would therefore be conservative (higher) in high response or resonance areas of the frequency range. Attempts at determining modal damping from the test frequency response curves using a "half power point" technique indicated about 3 percent constant modal damping with greater values at some of the higher frequencies.

Frequency-response comparisons. - When comparing frequency response results in Appendix B, the frequency placement of peaks, overall amplitudes of response, and curve shape representation of the test curve by the NASTRAN analysis were primarily considered. The phase relationship was sometimes useful in locating resonances but was more difficult to compare than magnitudes and was often jumping back and forth between ±180°.

Forced response mode shapes were helpful in finding correspondence between peaks of the test and NASTRAN curves. Comparisons of forced response mode shapes for the lateral and vertical tail shake of the clean wing configuration are given in Appendix C. The NASTRAN mode shape was determined by multiplying the magnitude at a response location by the cosine of the phase angle at that location minus the phase angle of the reference location.

General comments on the comparison of the frequency response curves of Appendix B are listed below.

1. Vertical tail shake - clean wing (Figures B-1 to B-8)

   - Response amplitudes, shape and peaks agree well through main rotor four-per-rev (21.6 Hz). At higher frequencies, the measured forward responses (farthest from excitation) are reduced while the aft response points (nearest the excitation) remain high. Attenuation of the force by the intervening structure between the excitation point and the forward response locations is suspected.

   - The NASTRAN pylon fore-and-aft rocking mode at 3 Hz is lower than test (about 4 Hz) as indicated in Figure B-1, B-4, B-5 and B-6. This is probably due to "pendulum" stiffening (differential stiffness) of the pylon caused by suspending the helicopter at the hub in a gravity field. This effect is not represented in the NASTRAN model.

- From the frequency response curves and the forced response mode shapes in Appendix C (Figures C-1 to C-4) the following comparison of airframe modes show good agreement between test and NASTRAN.

TABLE III. COMPARISON OF NATURAL FREQUENCIES - VERTICAL TEST

Mode	Test	NASTRAN
Fore-and-aft pylon	3.9	3.0
1st vertical bending	8.0	8.0
Fuselage torsion	15.5	15.7
2nd vertical bending	18.0	17.5

NOTE: See Figures B-2, B-4 and B-6 for examples.

2. Vertical tail shake - with stores (Figures B-9 to B-16)

- As in the clean wing configuration, test and analysis responses agree well. The pilot seat (Figure B-10) and 90° gearbox (Figure B-14) magnitudes and phases are good examples.

- The wing stores do not have a big effect on the response. The lowest NASTRAN wing frequency is calculated to be at 21.5 Hz and does not show up strongly in the NASTRAN or test curves. There is a store mode (probably a store sway mode) with weak response in a valley at about 11 Hz on the test curve. This mode shows up much stronger in the lateral shake test. The NASTRAN model had the stores rigidly attached to the wing and would not represent this mode.

3. Lateral tail shake - clean wing (Figures B-17 to B-24)

- Response amplitudes and shape agree well except in the area of the fuselage torsion/wing yaw mode which amplifies the NASTRAN response in the 20 - 25 Hz range. This mode is suspected to be a weak mode at 22.5 Hz that appears to be highly damped on the test curve.

- A comparison of modes derived from the frequency response curves and forced response mode shapes in Appendix C (Figure C-5 to C-8) is given below:

TABLE IV. COMPARISON OF NATURAL FREQUENCIES - LATERAL TEST

Mode	Test	NASTRAN
1st lateral bending	7.1	7.15
Fuselage torsion	15.5	15.7
2nd lateral bending	18.9	17.5
3rd lateral bending	24.4	25.8

4. Lateral tail shake - with stores (Figures B-25 to B-32)

   - The store mode mentioned in the vertical tail shake comparison shows up strong at 11 Hz and would not be represented in the NASTRAN model.

   - Except for the store mode at 11 Hz, curves agree well. Figures B-28, B-29 and B-30 are good examples.

5. Hub vertical shake (Figures B-33 to B-40)

   - Except for the 1st vertical bending mode, the test data is relatively flat and does not show as much response as NASTRAN.

   - The test curves look rather rough and "noisy".

   - The suspension system or dummy hub might be affecting the response. An instrumentation or data reduction problem or some transient dynamics in the pylon system is suspected.

6. Hub Lateral Shake (Figures B-41 to B-48)

   - The pylon roll mode is at 5 Hz for the test compared to 4 Hz calculated by NASTRAN. The difference is probably due to "pendulum" stiffening effects on the soft-mounted pylon not represented in the NASTRAN model.

   - The lateral hub response test curves show a very strong mode at 19 Hz that is not in the NASTRAN model. This is probably a suspension mode or a mode of the dummy hub, neither of which is modeled in NASTRAN.

   - The airframe response amplitudes apparently agree well but it is probably just a coincidence. The effect of the pylon dynamics were expected to cause force attenuation and result in a highly damped looking response of the airframe at higher frequencies. That the high airframe response amplitudes agree fairly well with NASTRAN in the 15 to 25 Hz range could be due to the effect of the high hub response at 19 Hz cancelling the effect of force attenuation through the pylon.

7. Hub fore-and-aft shake (Figures B-49 to B-56)

   - The hub response from test appears to have a steady shift making it too low. This agrees with the fore-and-aft hub response being lower by a constant factor when compared to the on-site data reduction frequency response plot. The hub response had to be multiplied by 1.35 to agree with the on-site plot.

- As with the lateral hub shake there is a strong mode at 19 Hz. The same discussion for the lateral hub shake applies here.

In summary, the NASTRAN frequency response characteristics agree well with the test results for the vertical and lateral tail shake conditions. There is good agreement in overall amplitudes, forced response mode shapes, peak responses and general curve shape through main rotor four-per-rev (21.6 Hz). Agreement is not as good for the hub shake conditions. The problems are believed to be associated with pylon dynamics, the suspension system and the dummy main rotor hub.

CONCLUSIONS

Tests were conducted to evaluate the NASTRAN vibration analysis of the AH-1G helicopter airframe. Static load-deflection tests of the fuselage and tailboom were performed for comparative evaluation of the stiffness modeling. Sinusoidal vibration testing was done in order to evaluate the dynamic modeling. In general, the agreement between test and analysis was good. The analysis was considered representative of the low frequency vibration characteristics through the range of main rotor and automatic weapon firing excitation frequencies. For the Bell two-bladed rotor, predominant main rotor excitation frequencies are two-per-rev (10.8 Hz) and four-per-rev (21.6 Hz) and large caliber automatic weapon firing rates are in the 5 - 15 Hz frequency range.

The following comments summarize the results of the study:

1. The vibration shake tests with excitation at the tail of the airframe were the principal tests used in the evaluation of the vibration analysis. The NASTRAN frequency response characteristics agreed well with these tests in overall amplitudes, forced response mode shapes, peak responses and general curve shape through four-per-rev.

2. Significant dynamic response differences showed up between NASTRAN and test for the hub shake tests and were believed to be associated with pylon dynamics not represented in the math model and the suspension system and dummy main rotor hub that were used for the test.

3. The effects of damping on the comparison of frequency response characteristics were considered in the analysis. Although a constant 2 percent modal damping was used in most of the comparisons, it is felt that damping should be

varied in a design analysis to see its effect in both the high response (resonance) and low response (antiresonance) frequency ranges.

4. For most of the fuselage static test comparisons, the NASTRAN results were about 15 percent stiffer than test. However, one of the tests (lateral) was rerun using two different methods of measuring deflections, LVDT's and dial indicators. The dial indicators showed much better agreement with the NASTRAN analysis. The conclusion then is that the analysis is between 0 and 15 percent stiff.

5. The NASTRAN analysis, using fully effective skin for the representation of the semimonocoque sheet-stringer tailboom, showed good agreement with test. The analysis was generally about 0 to 5 percent softer than the average test values.

More needs to be learned about the analysis of the main rotor pylon dynamics and representing skin effectivity of sheet-stringer structures such as the AH-1G tailboom. Pylon dynamics are important in the analysis of main rotor induced airframe vibrations. Proper accounting of skin effectivity under compression loads encountered in flight is important in accurate determination of the stiffness of semimonocoque structures.

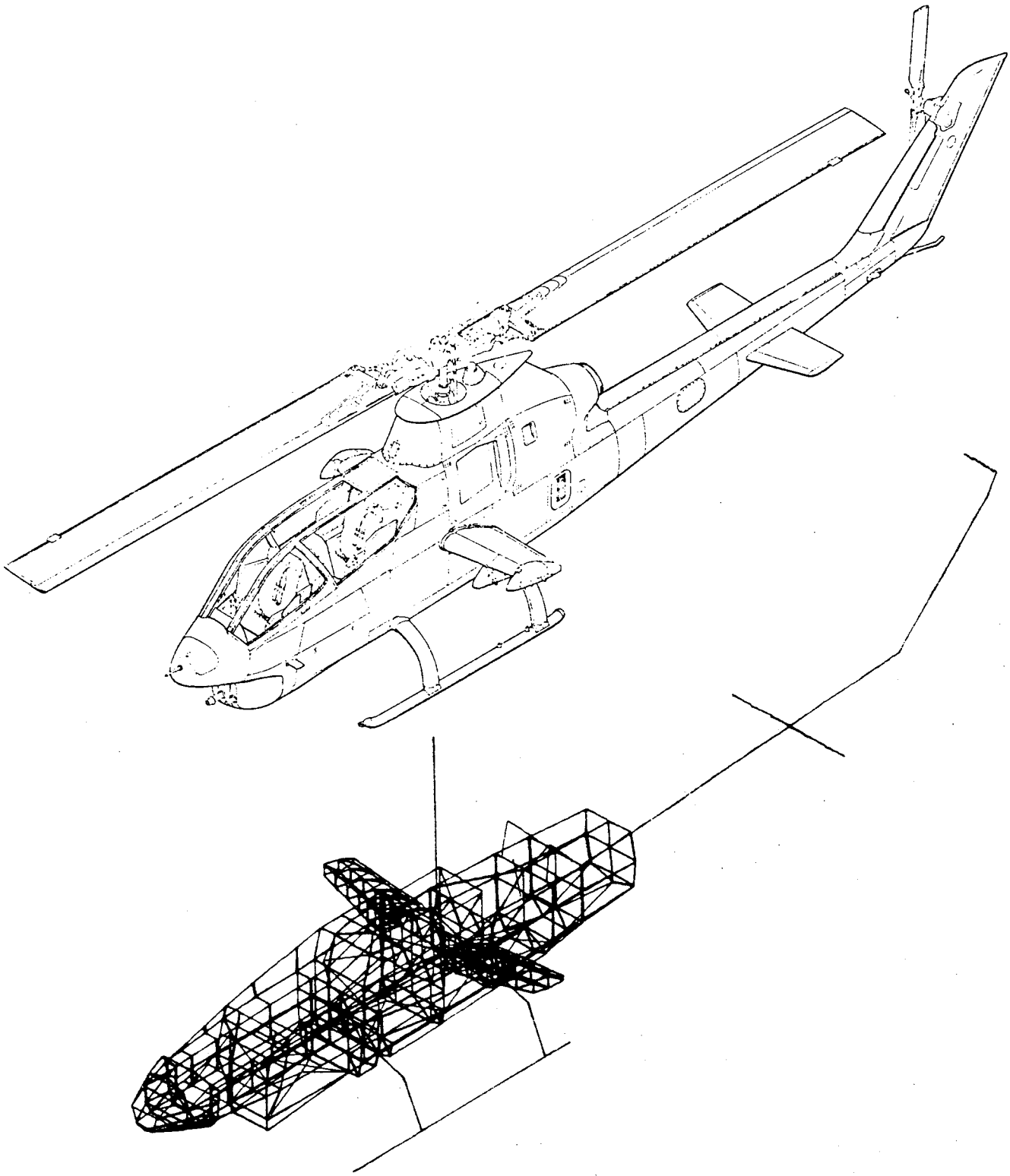

Figure 1. NASTRAN Model of the AH-1G Helicopter Airframe.

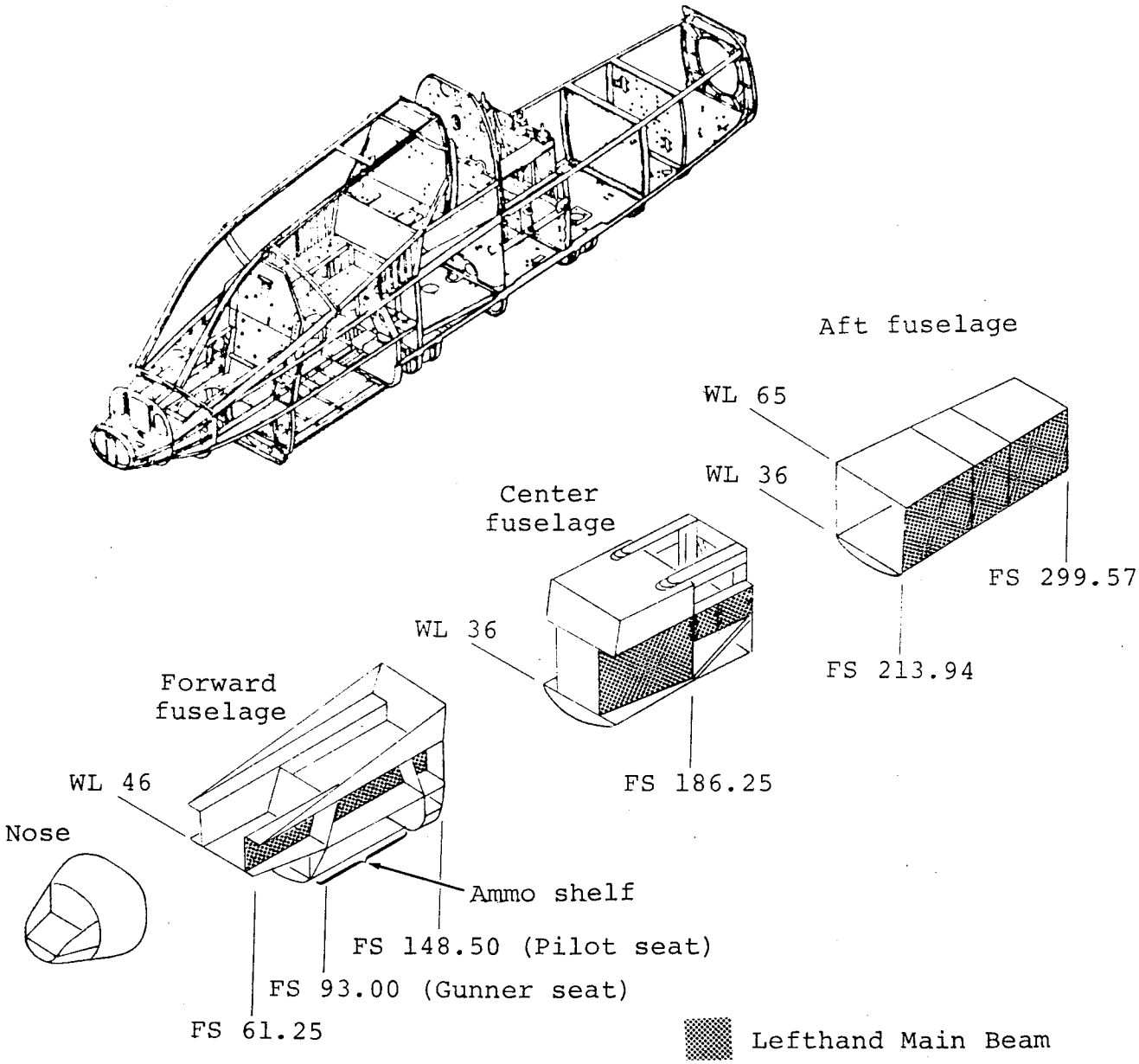

Figure 2. Fuselage Structure Schematic.

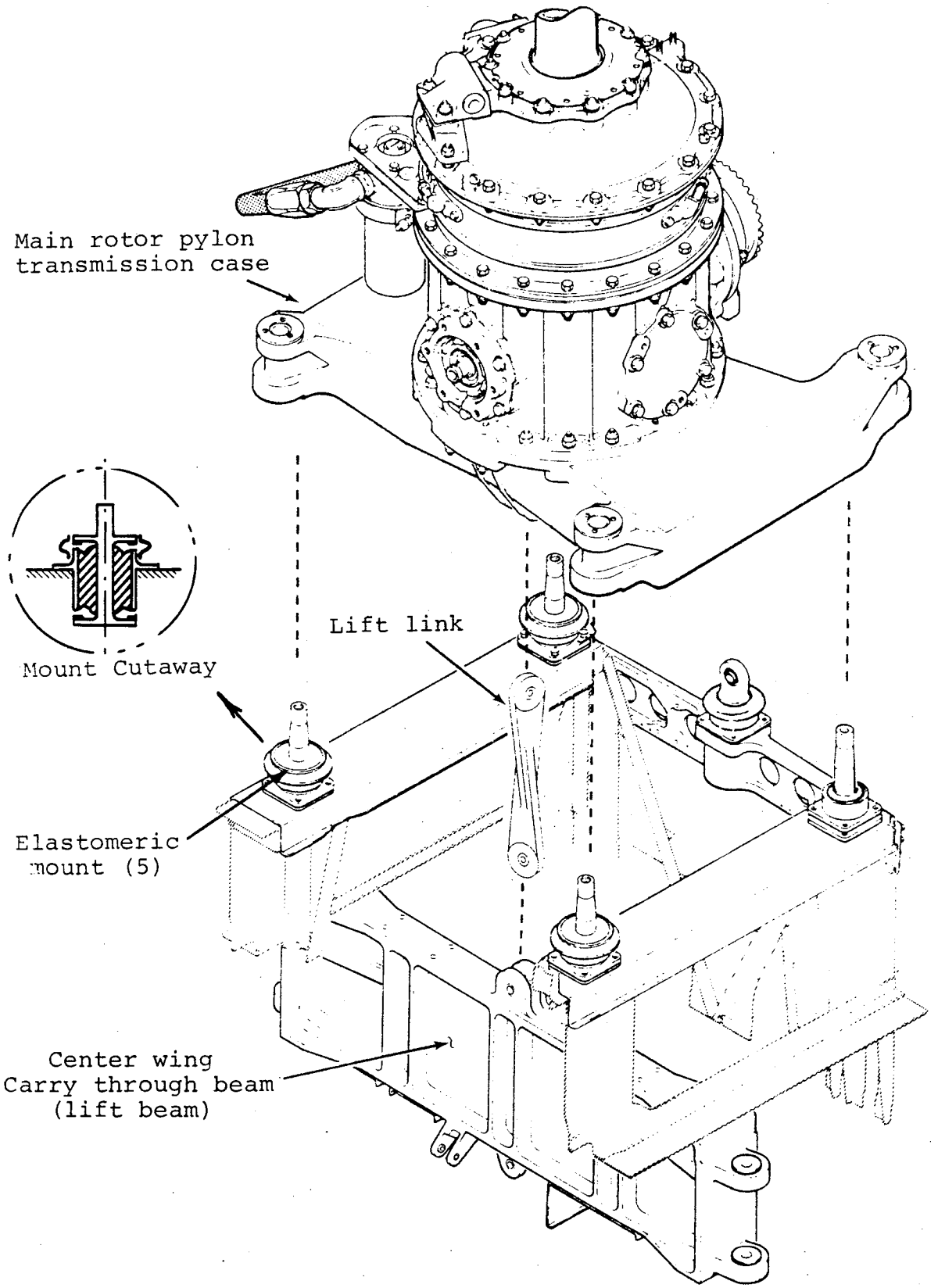

Figure 3. Main Rotor Pylon.

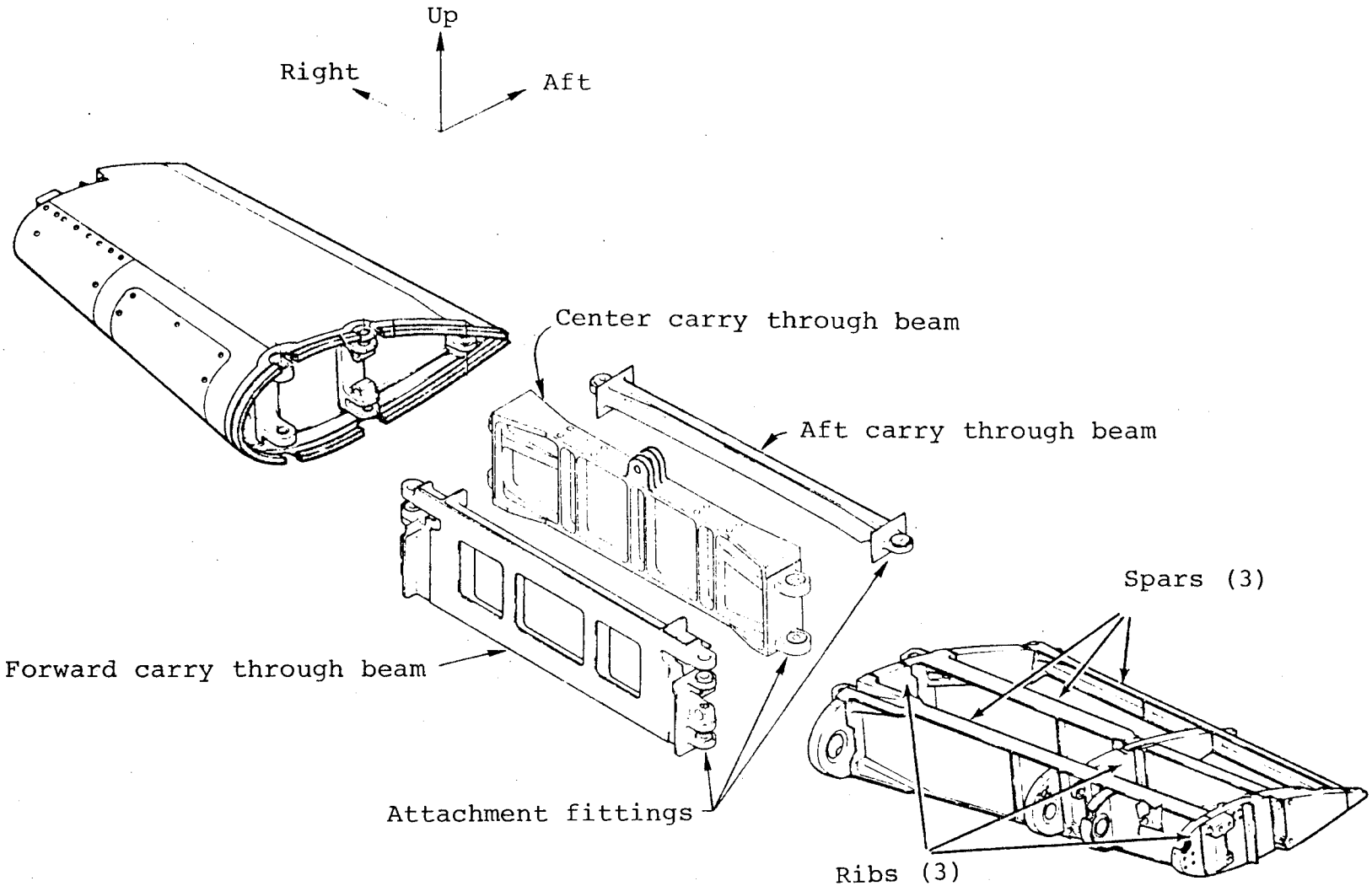

Figure 4. Wings and Carry Through Structure.

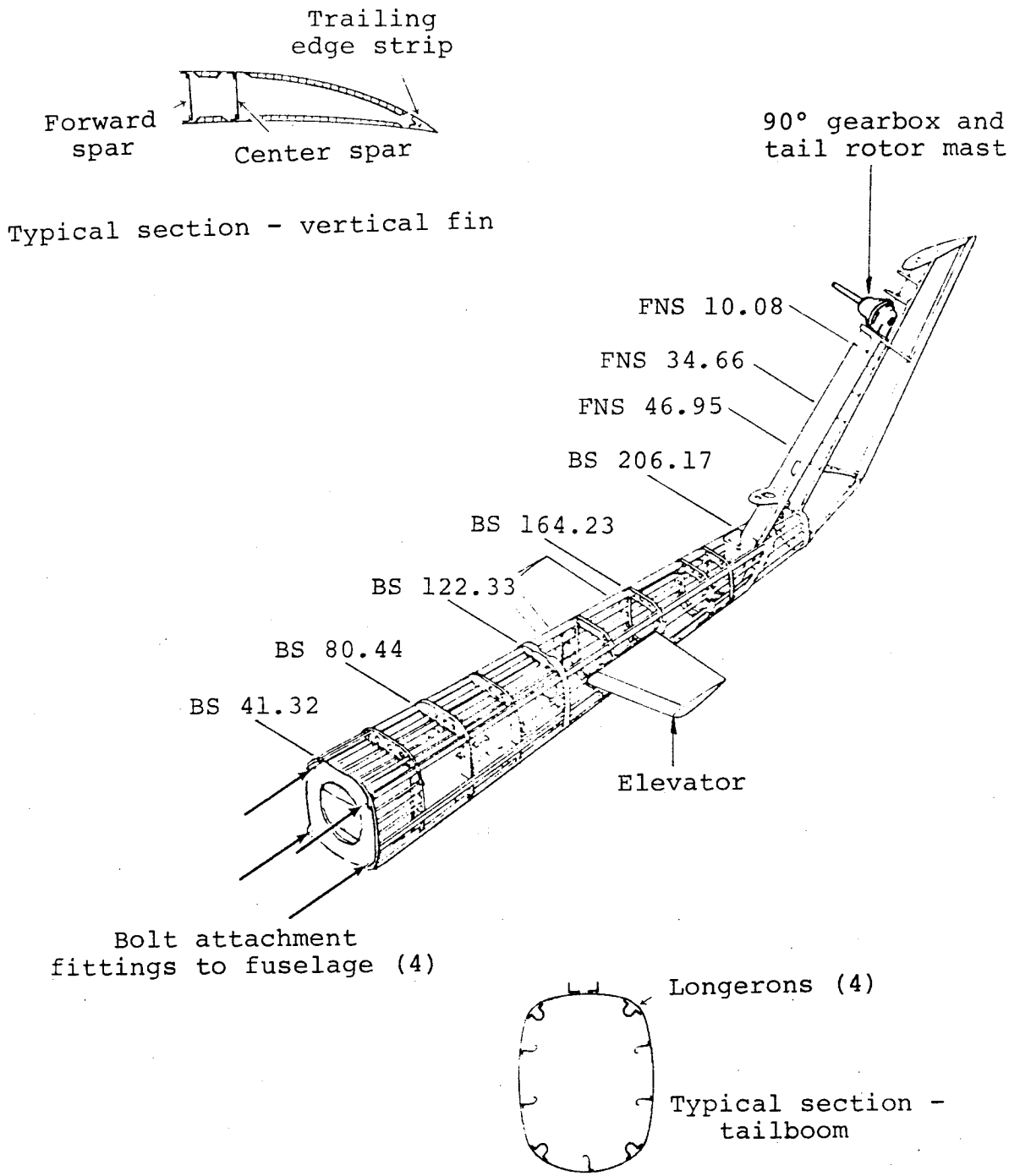

Figure 5. Tailboom and Vertical Fin.

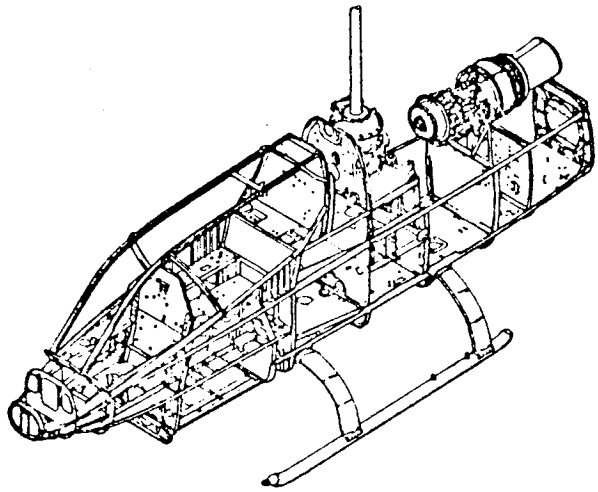

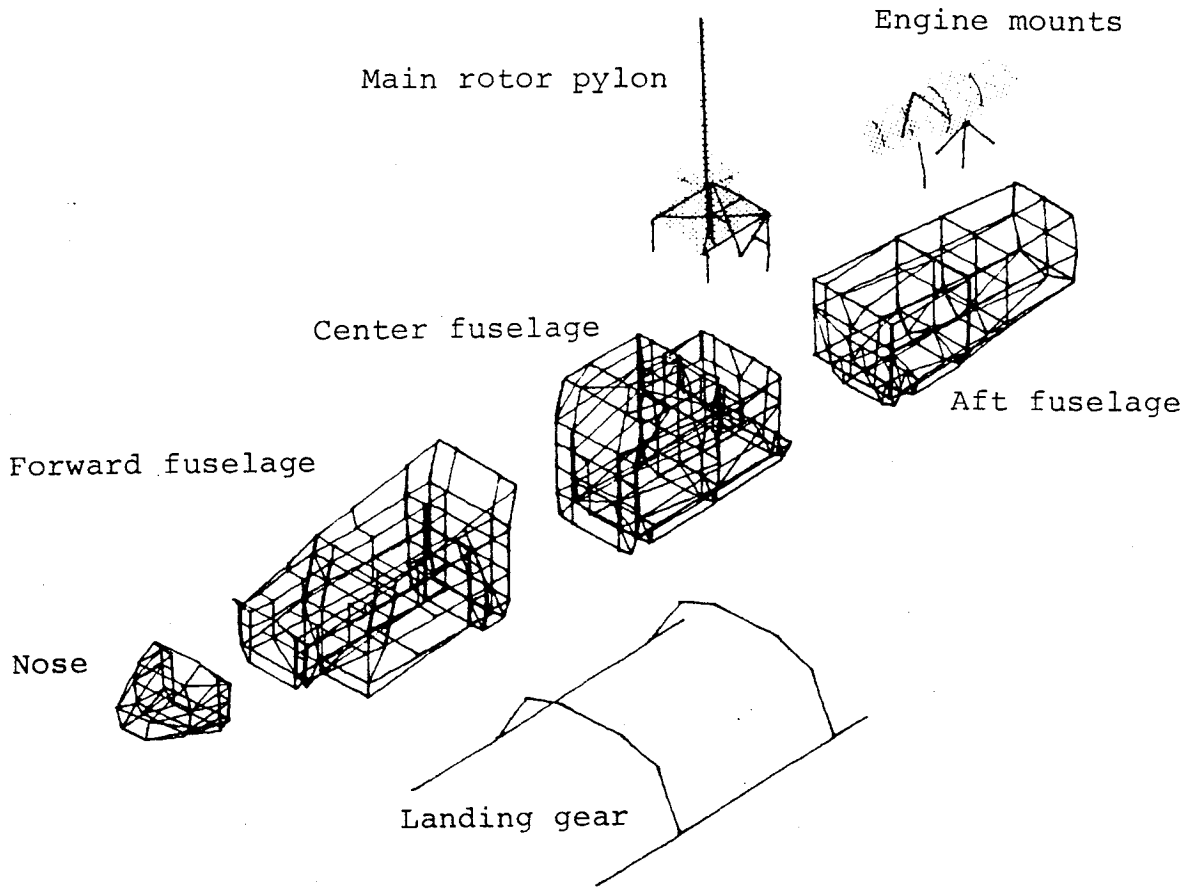

Figure 6. NASTRAN Fuselage Structure Model.

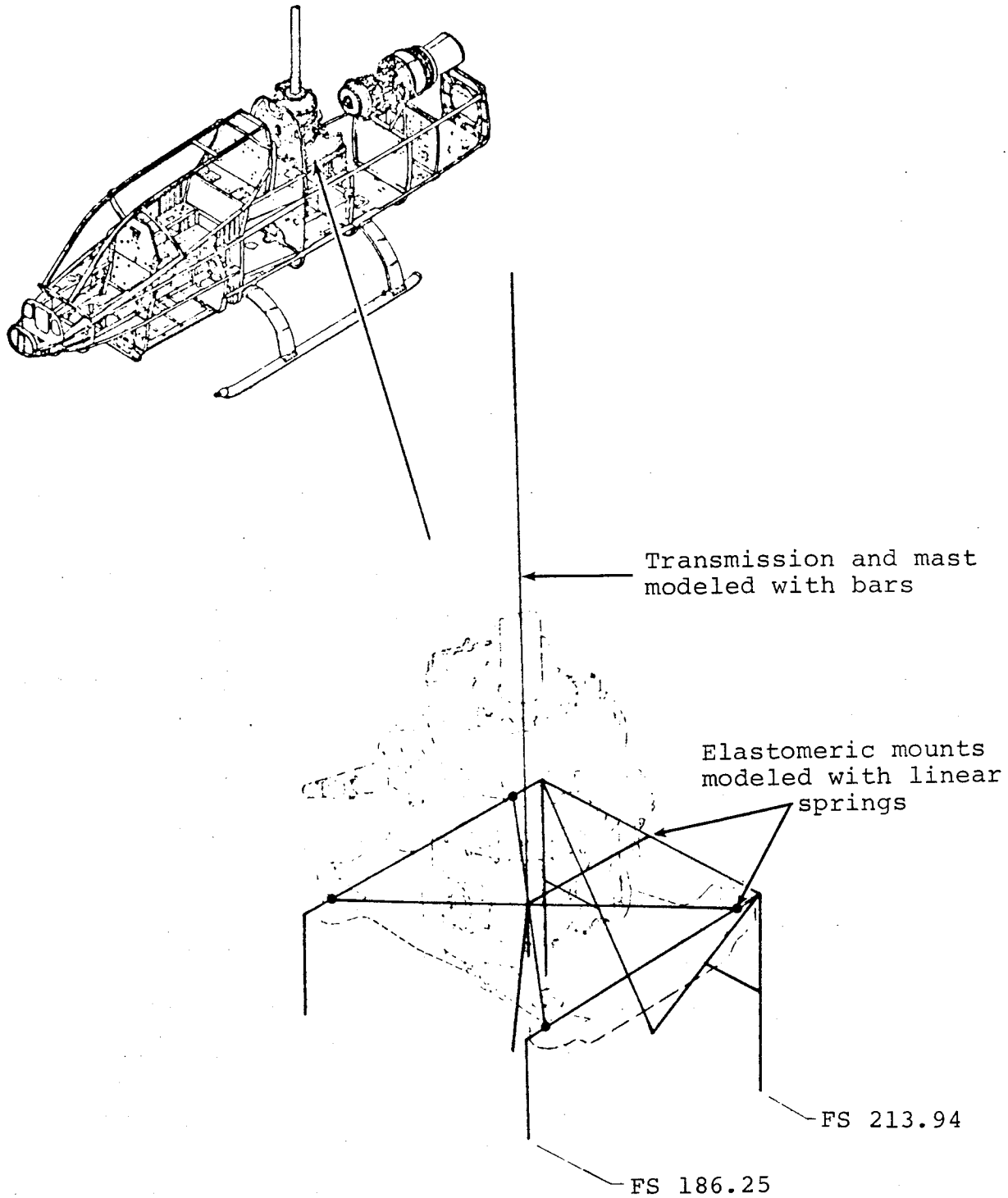

Figure 7. NASTRAN Main Rotor Pylon Model.

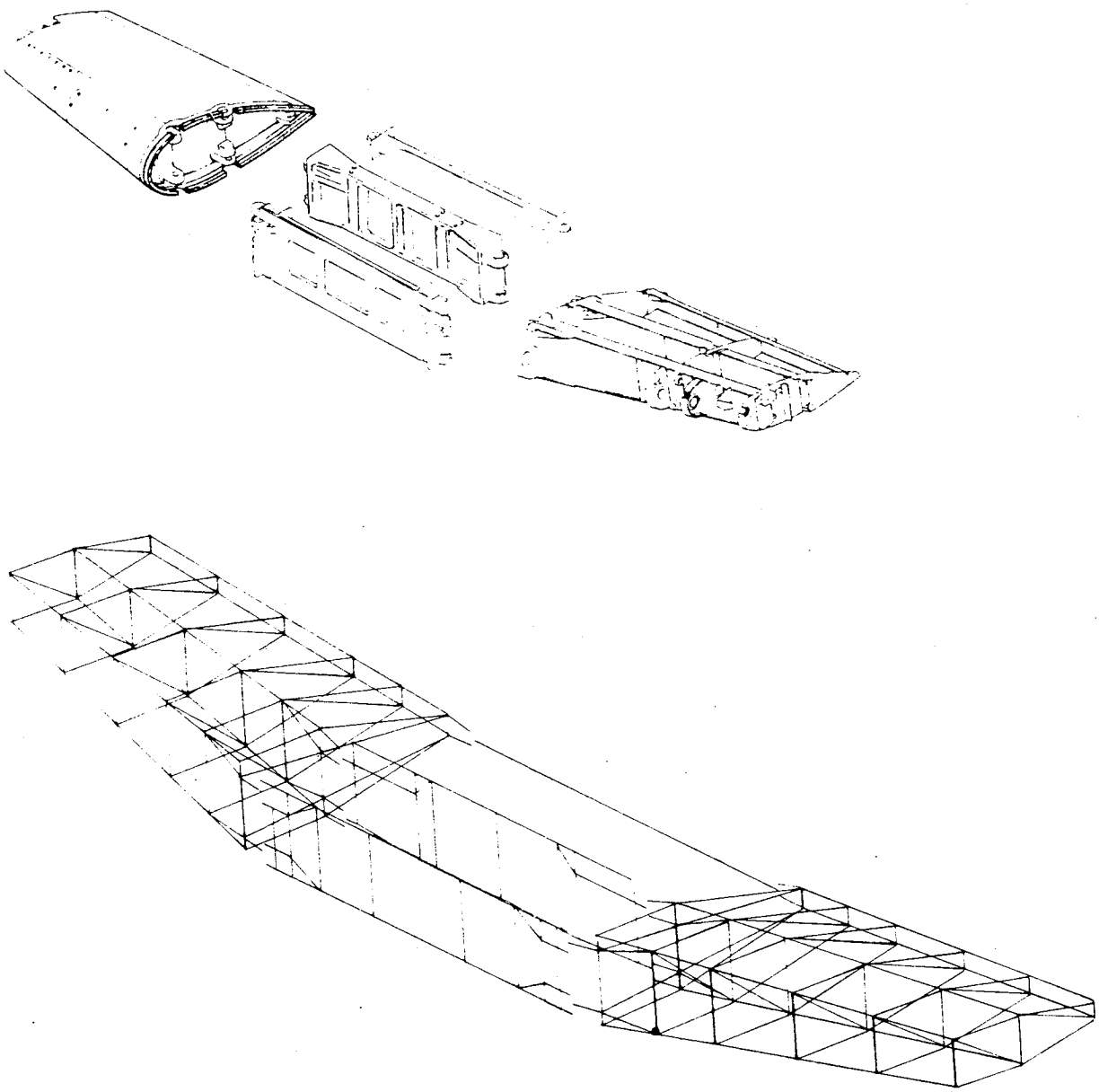

Figure 8. NASTRAN Wings and Carry Through Structure Model.

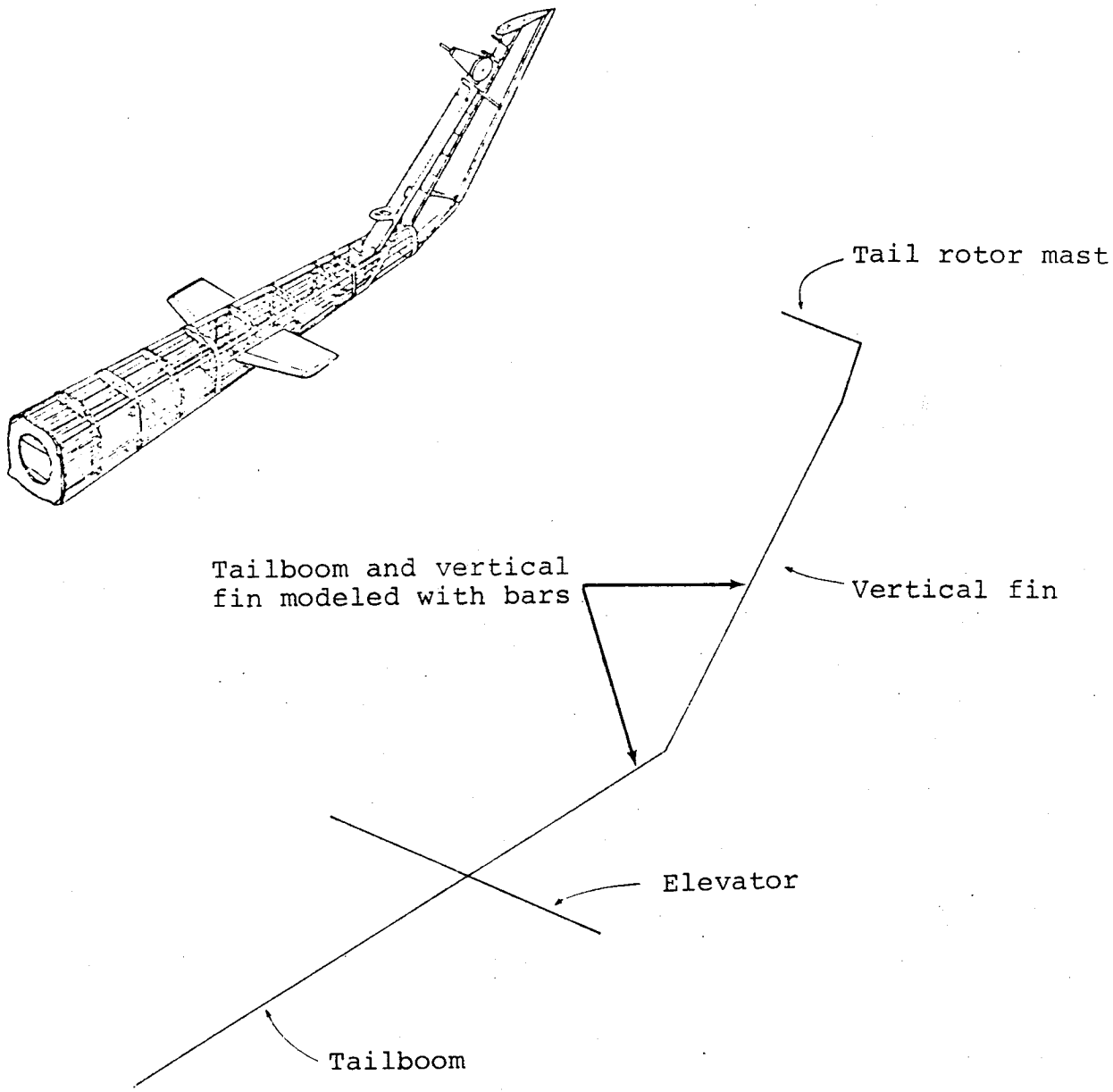

Figure 9. NASTRAN Tailboom and Vertical Fin Model.

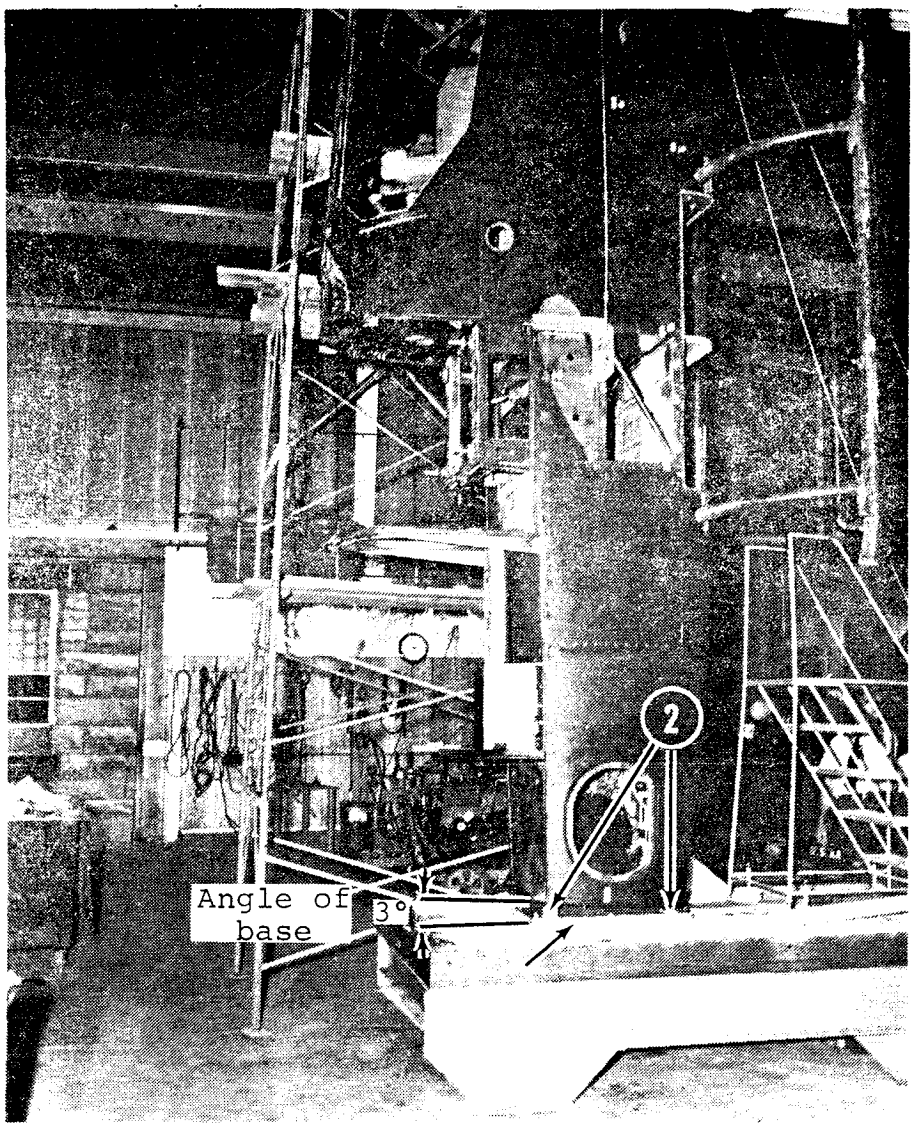

1 Base plate
2 Load cell mounting points (4)

Figure 10. Fuselage Structure Mounted on Base Plate.

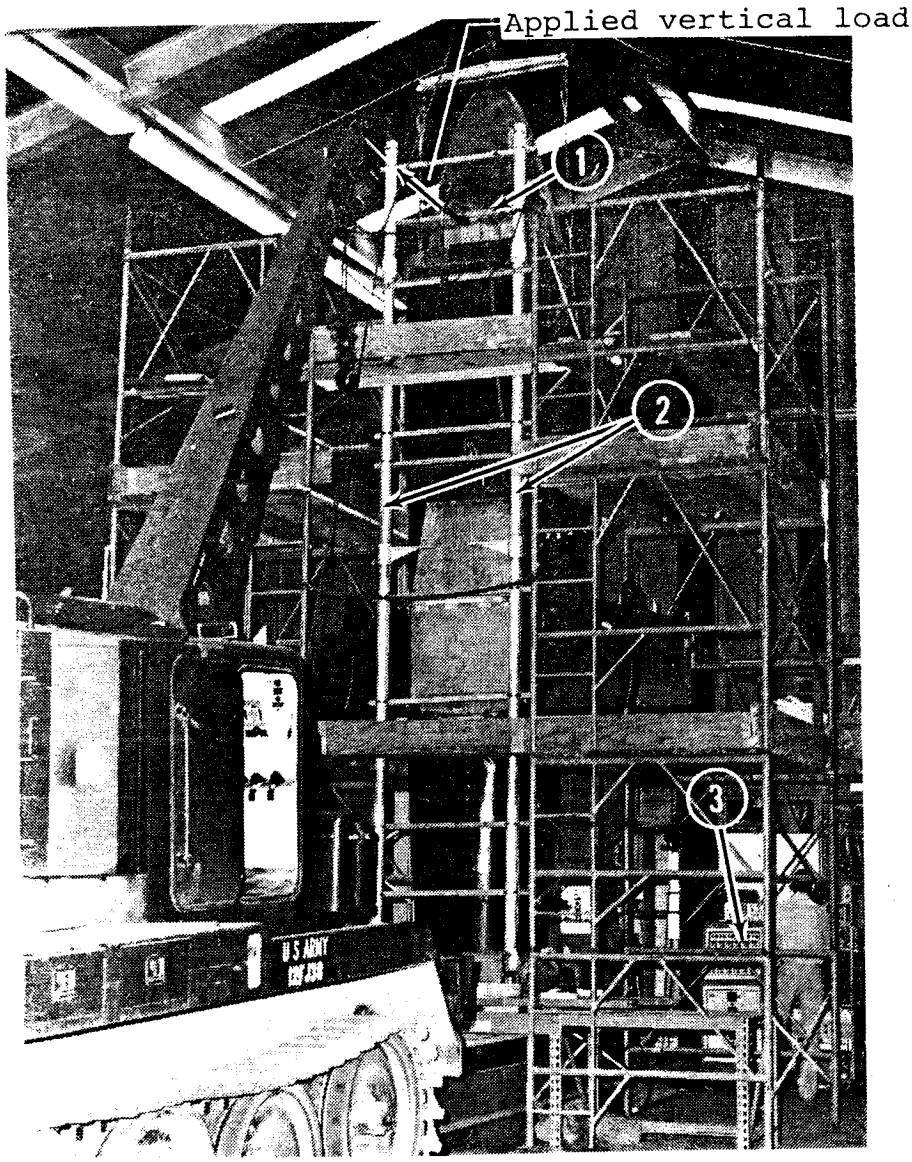

1 Load fixture
2 Instrumentation support fixtures
3 Data recording system

Figure 11. Fuselage Vertical and Torsion Test Setup.

ORIGINAL PAGE IS
OF POOR QUALITY

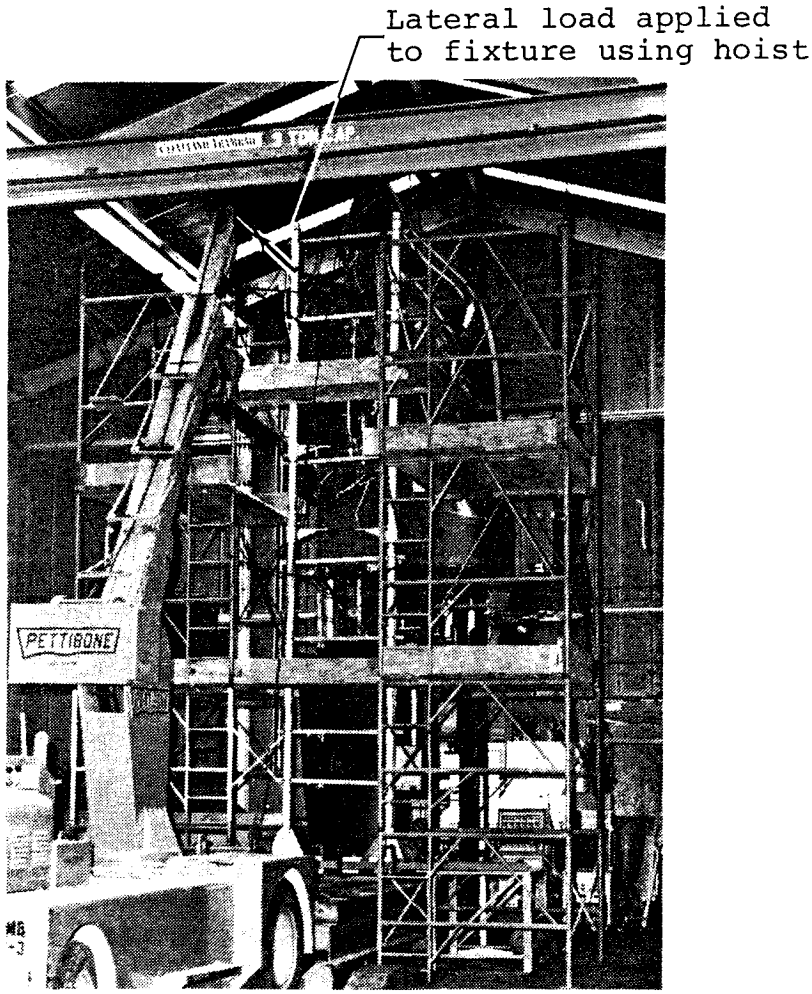

Figure 12. Fuselage Lateral Test Setup.

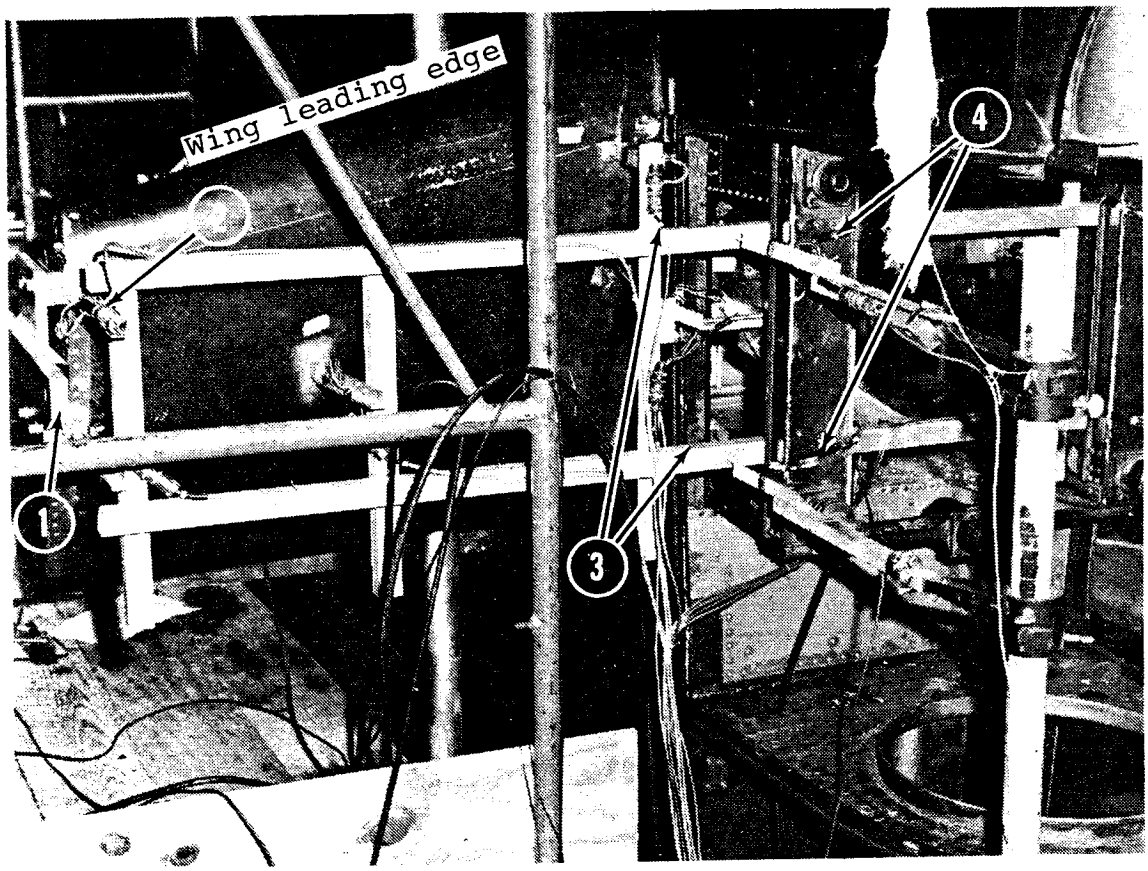

1 Load fixture
2 Typical LVDT
3 Instrumentation fixture
4 Instrumentation fixture clamped to fuselage structure

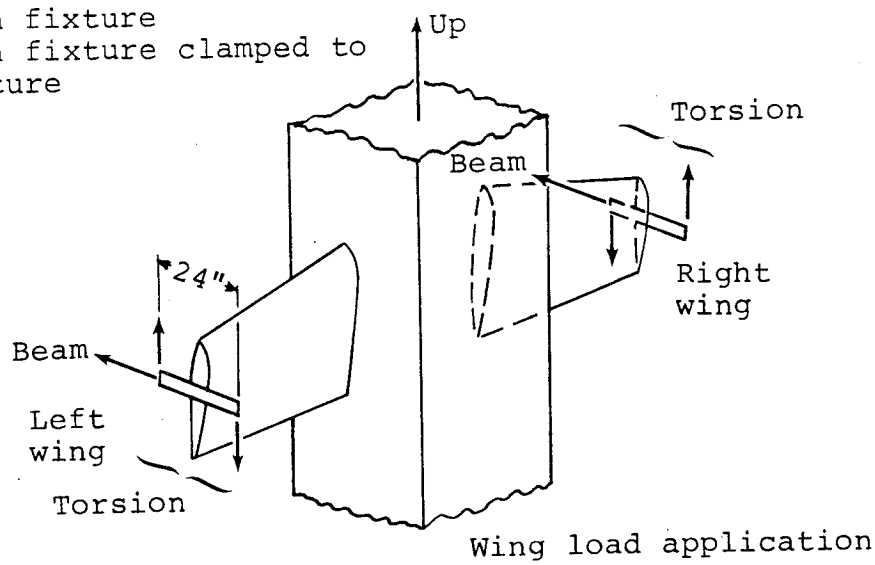

Figure 13. Wing Test Setup.

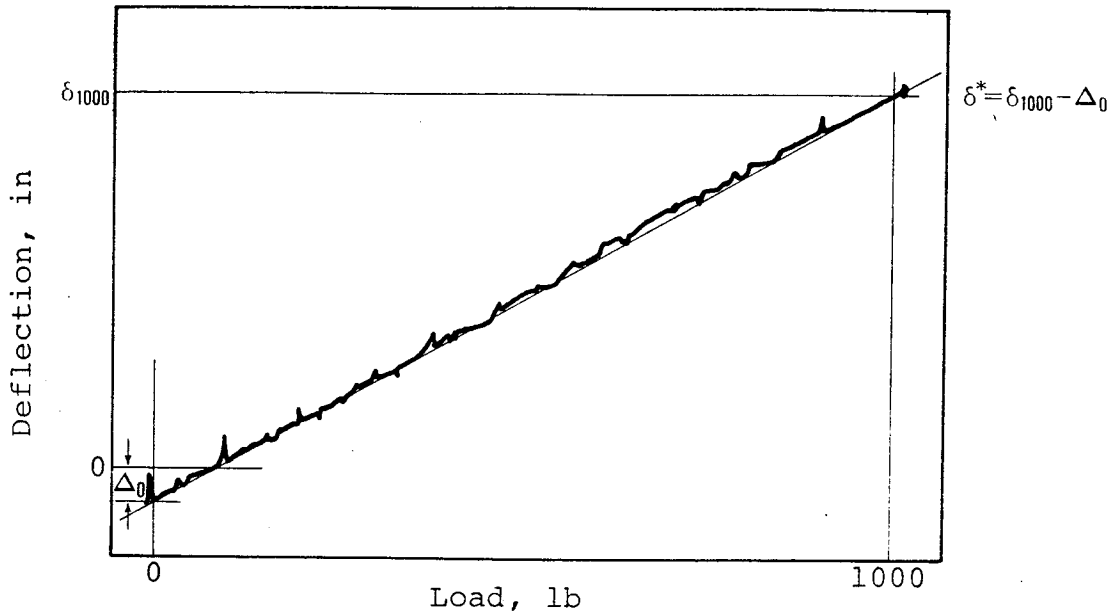

(a) Typical load-deflection curve

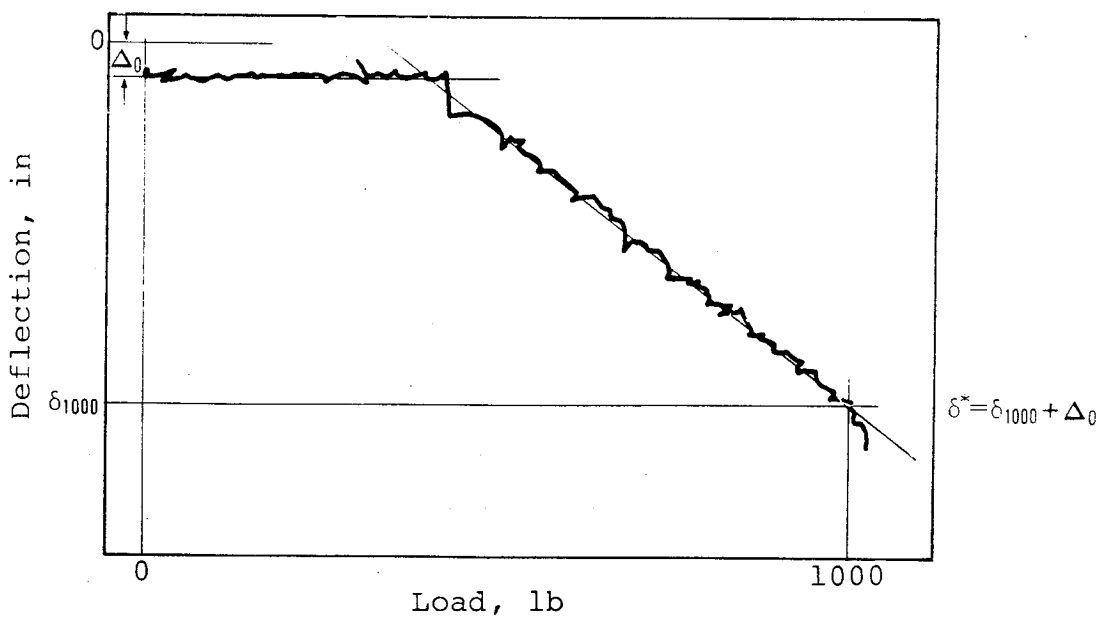

(b) Example of base deflection curve indicating a preload effect

δ^*~Final deflection at maximum load (1000 lb) used for comparison with NASTRAN math model

Figure 14. Typical Graphical Data Reduction Technique.

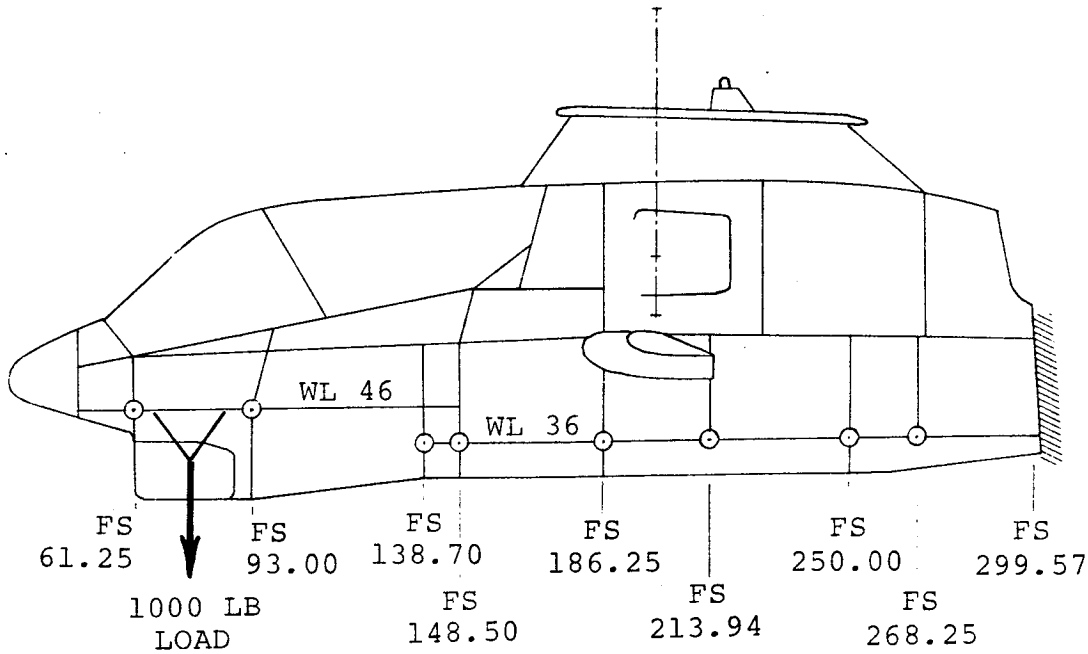

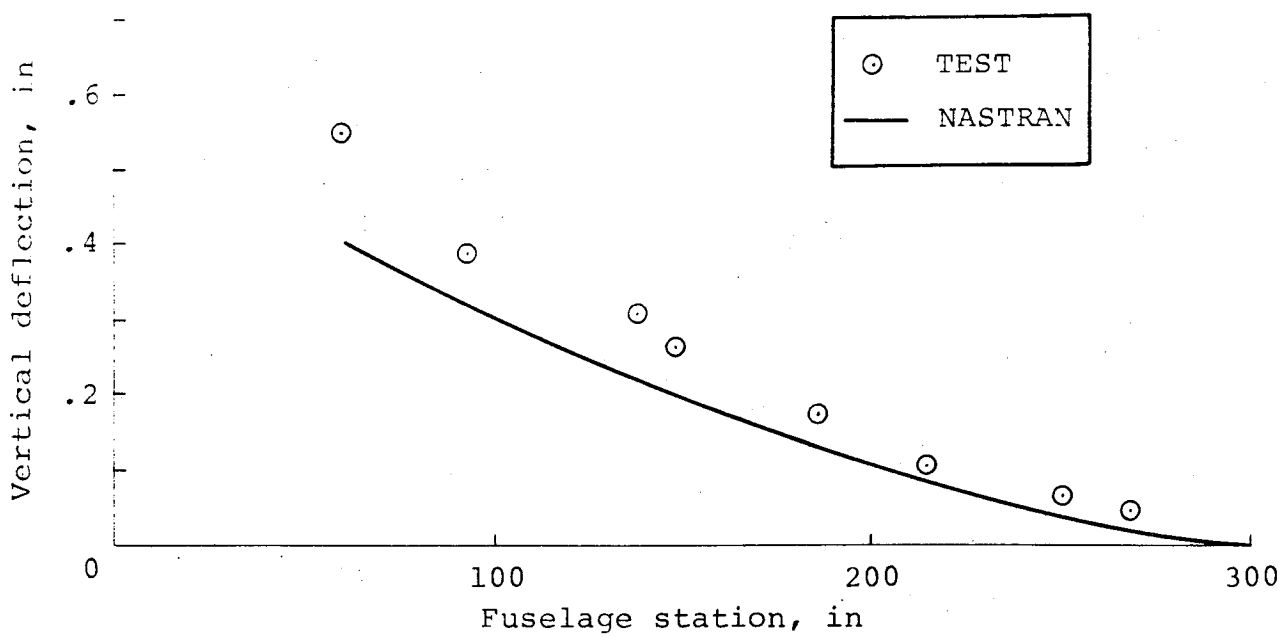

Figure 15. Fuselage Vertical Load-Deflection Comparison.

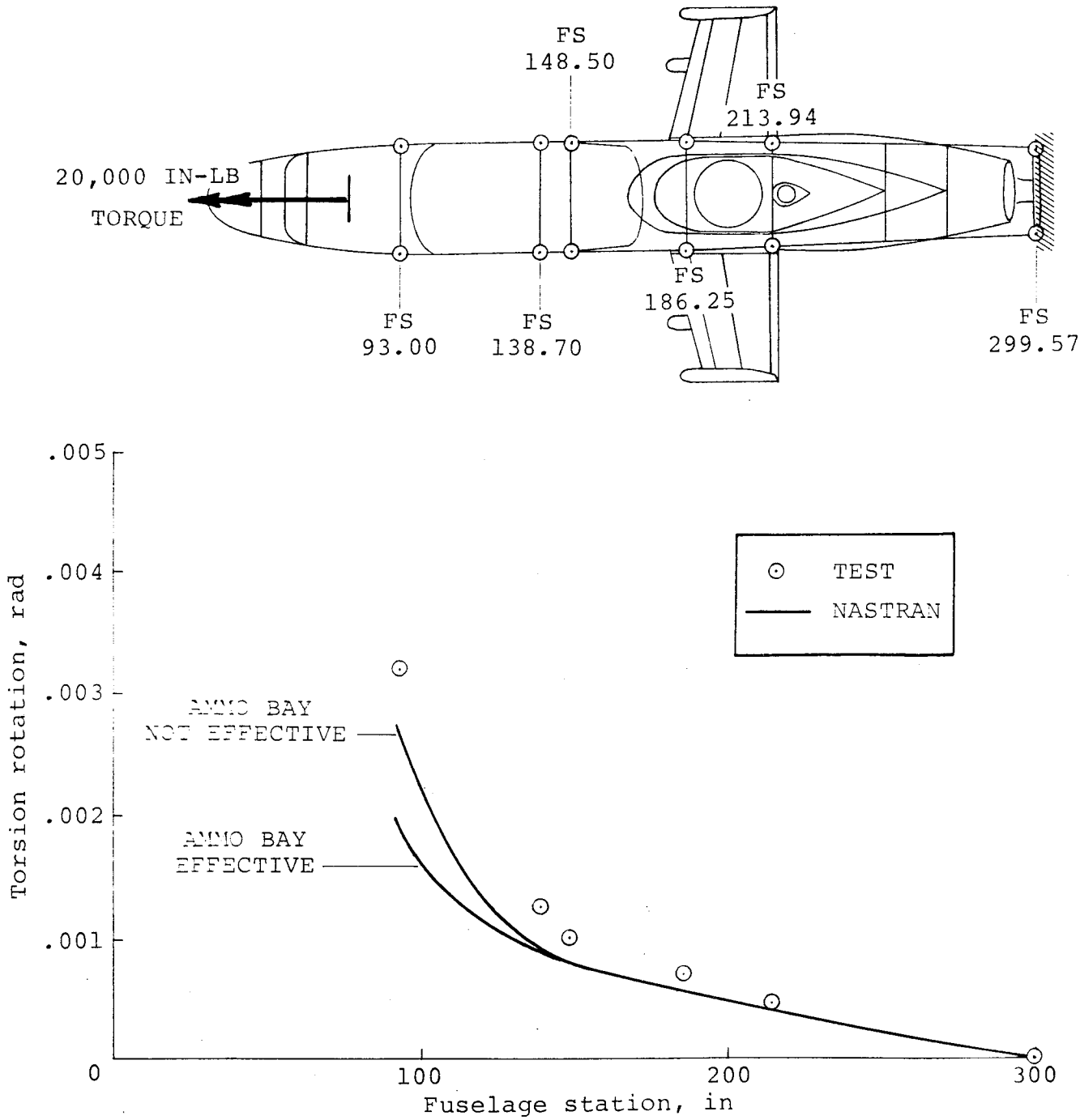

Figure 16. Fuselage Torsion Torque-Rotation Comparison.

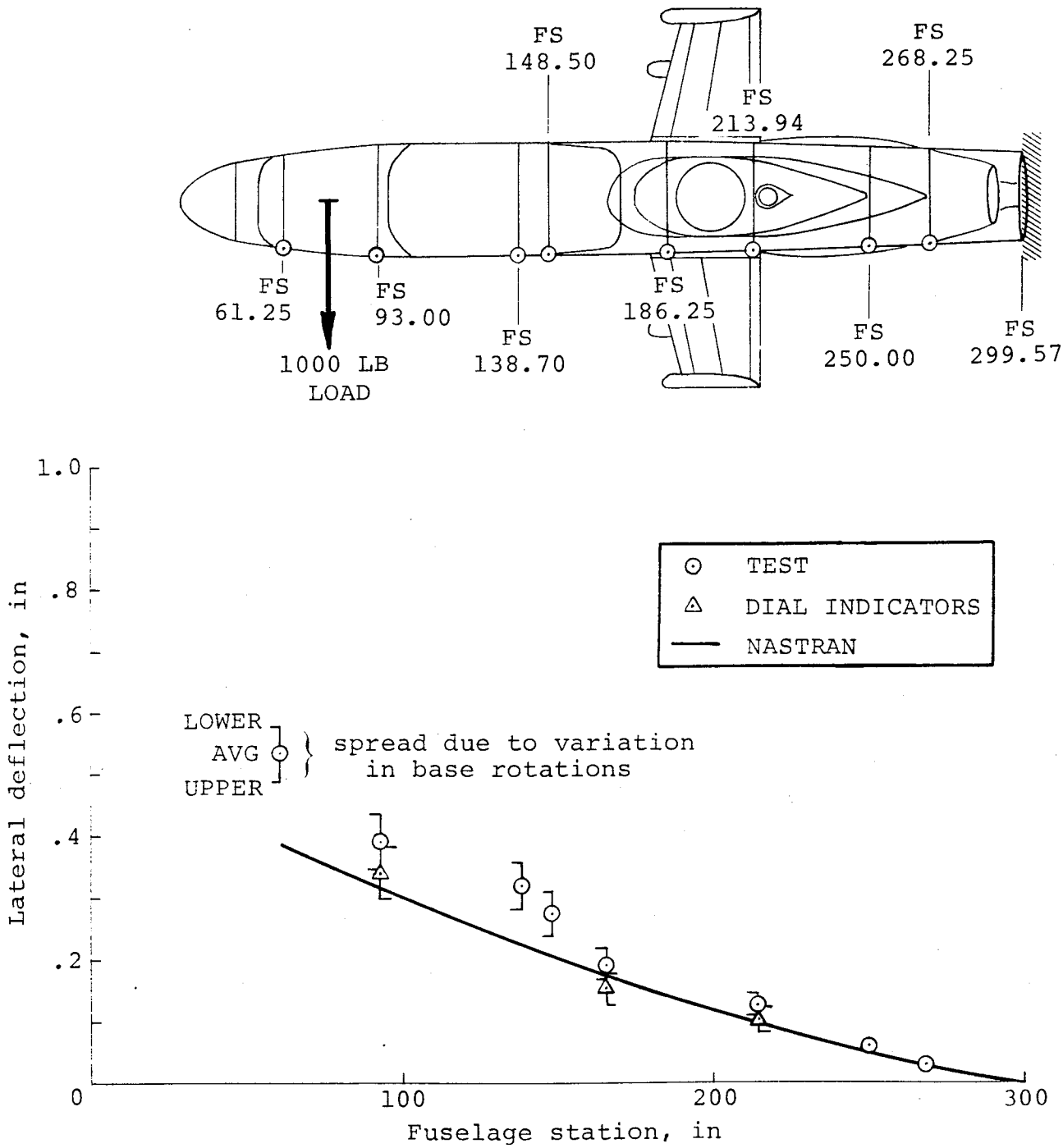

Figure 17. Fuselage Lateral Load-Deflection Comparison.

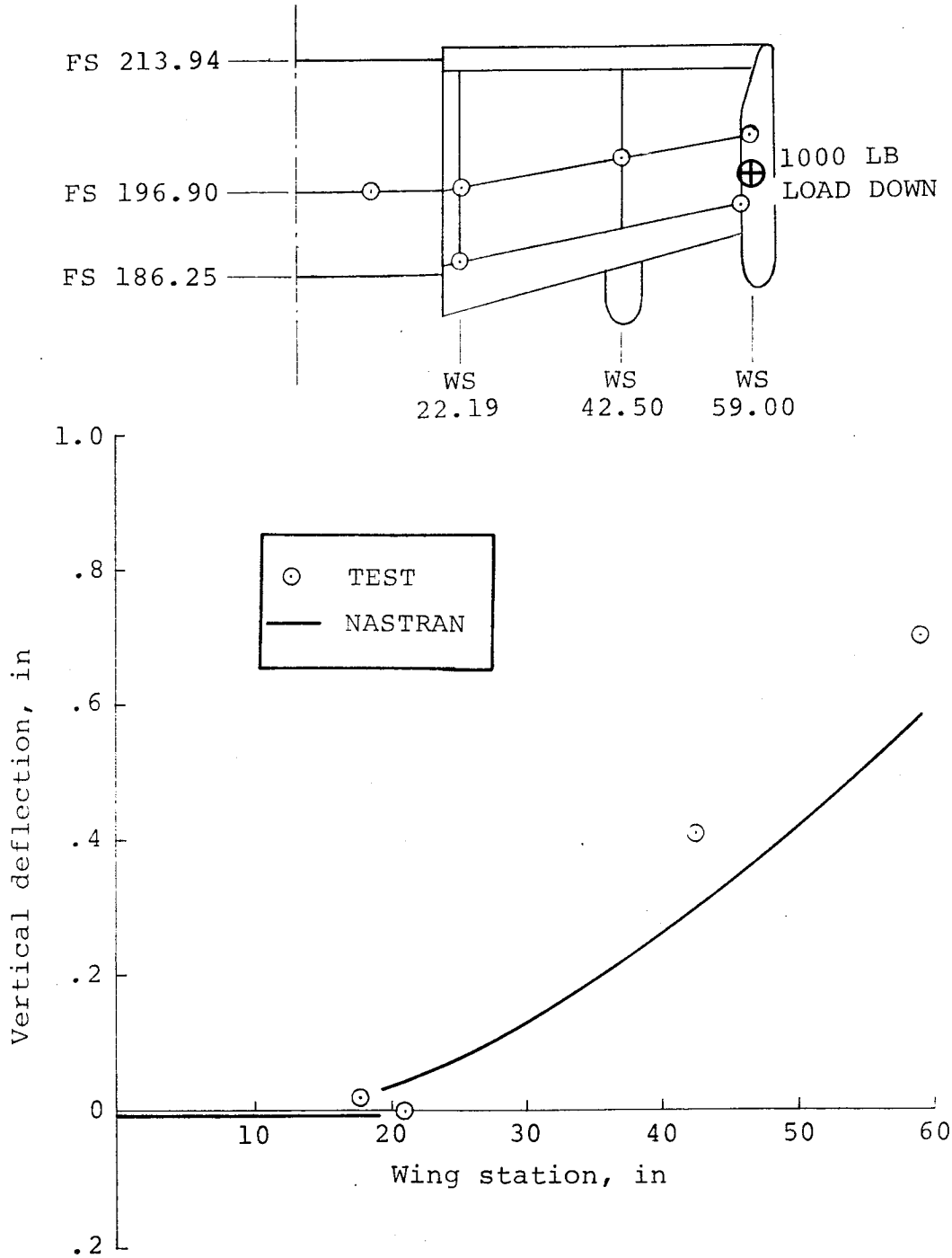

Figure 18. Wing Beamwise Load-Deflection Comparison.

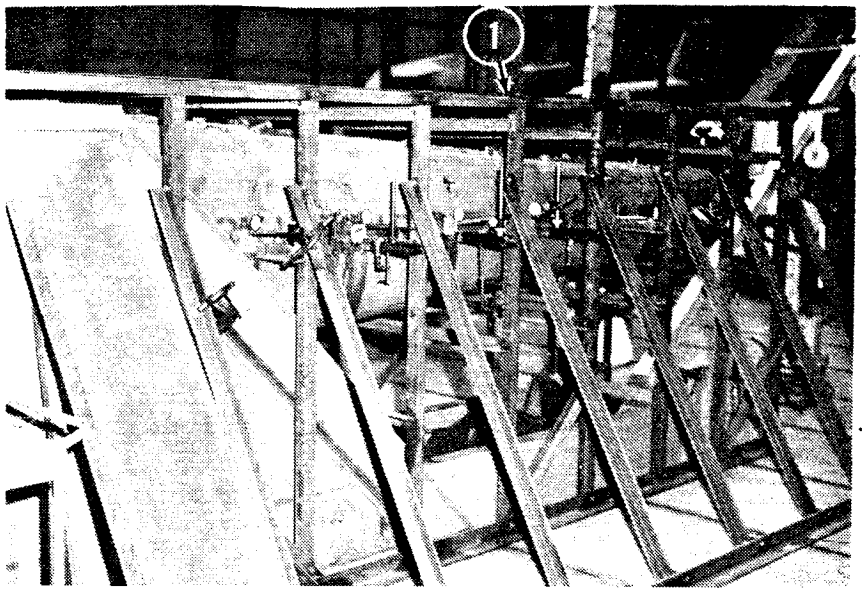

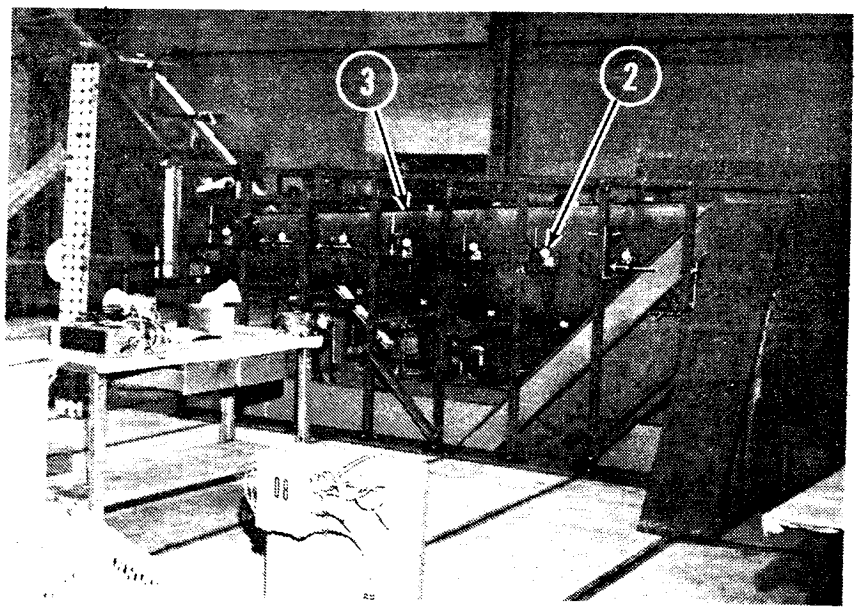

1 Indicator support fixture
2 Typical dial indicator (set for vertical deflection measurement
3 Tailboom installation

Figure 20. Tailboom Test Setup.

ORIGINAL PAGE IS
OF POOR QUALITY

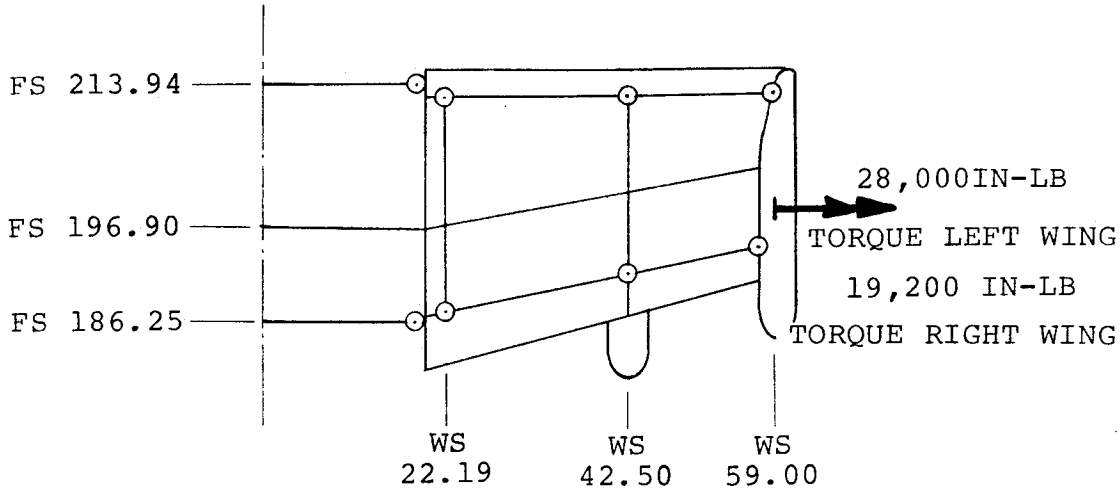

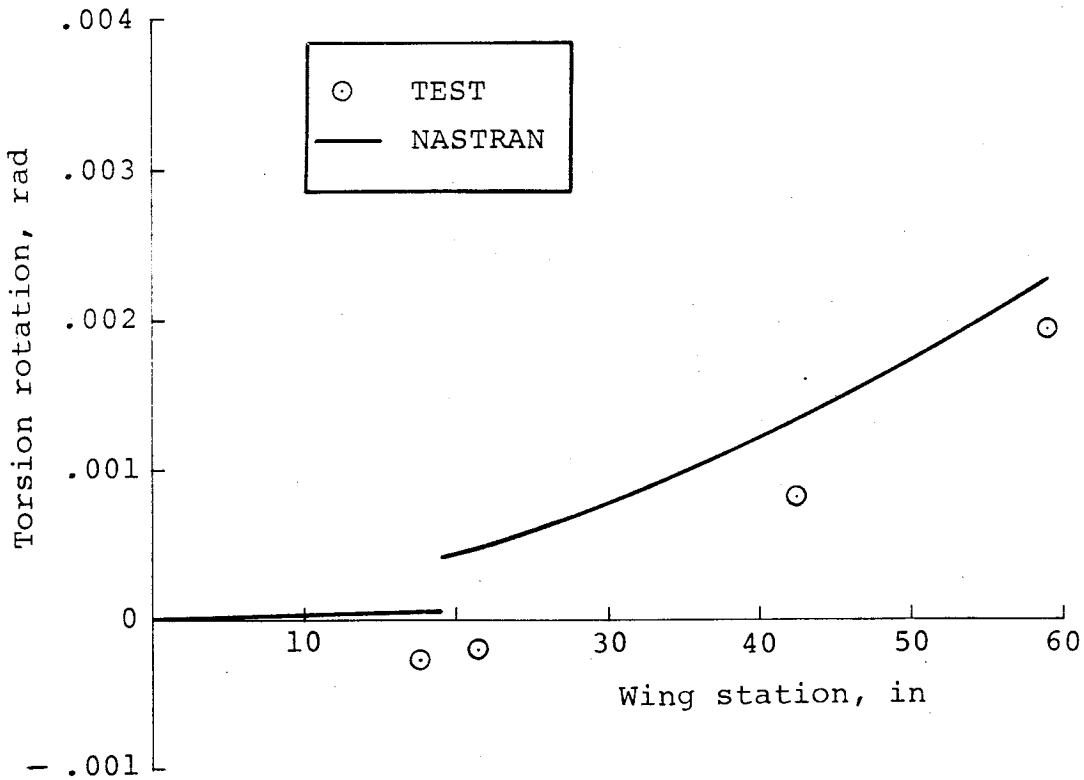

Figure 19. Wing Torsion Torque-Rotation Comparison

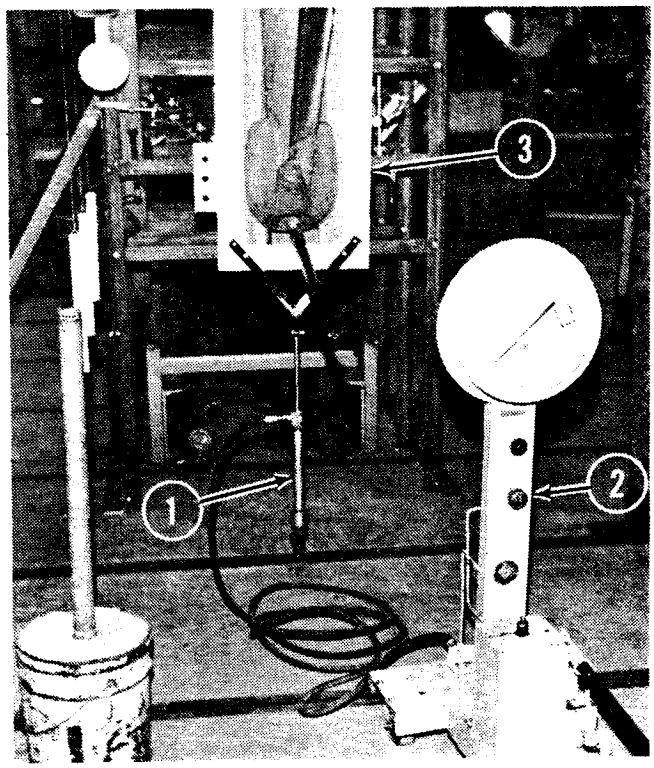

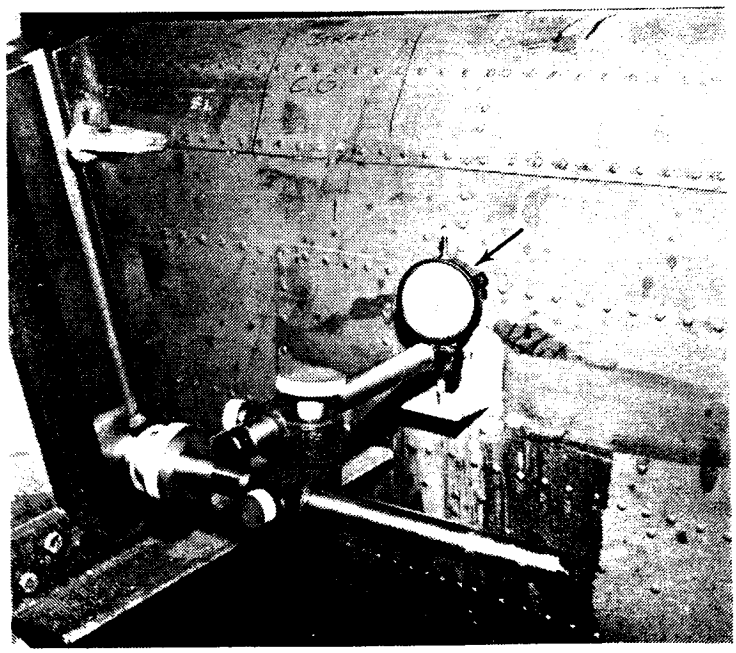

1 Hydraulic cylinder for applying vertical load
2 Hand pump with calibrated gage
3 Fixture for applying load to tailboom
4 Typical dial indicator installation

Figure 21. Load Application and Typical Dial Indicator.

ORIGINAL PAGE IS
OF POOR QUALITY

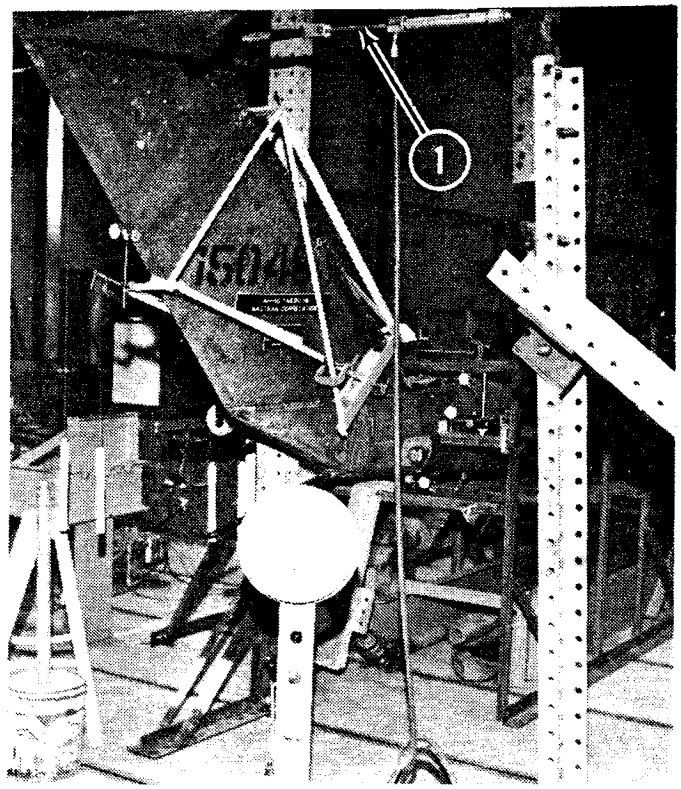

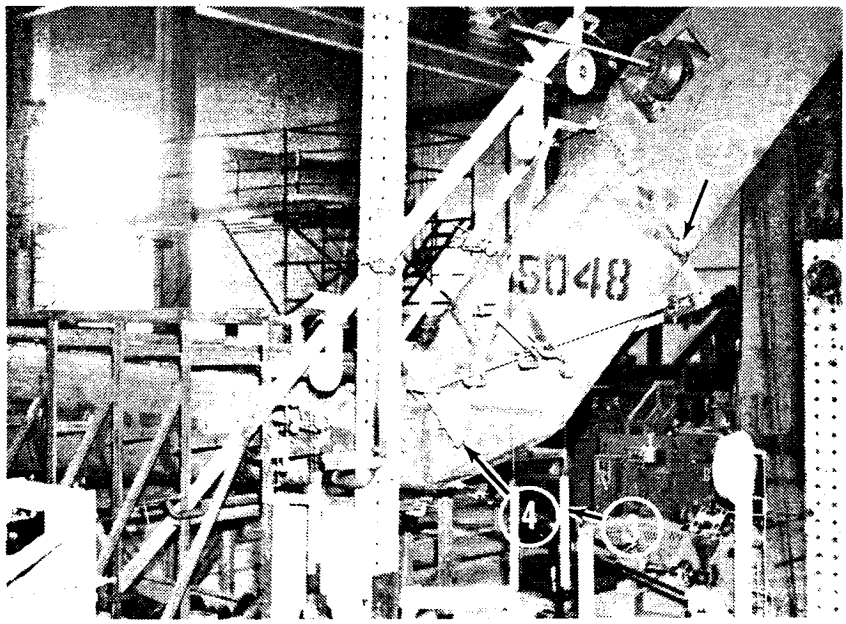

1 Hydraulic cylinder for applying load
2 Typical dial indicator - measures relative deflection
3 Tube scale - measures total deflection
4 Base for dial indicator fixture

Figure 22. Vertical Fin Test Setup (Lateral Test Shown).

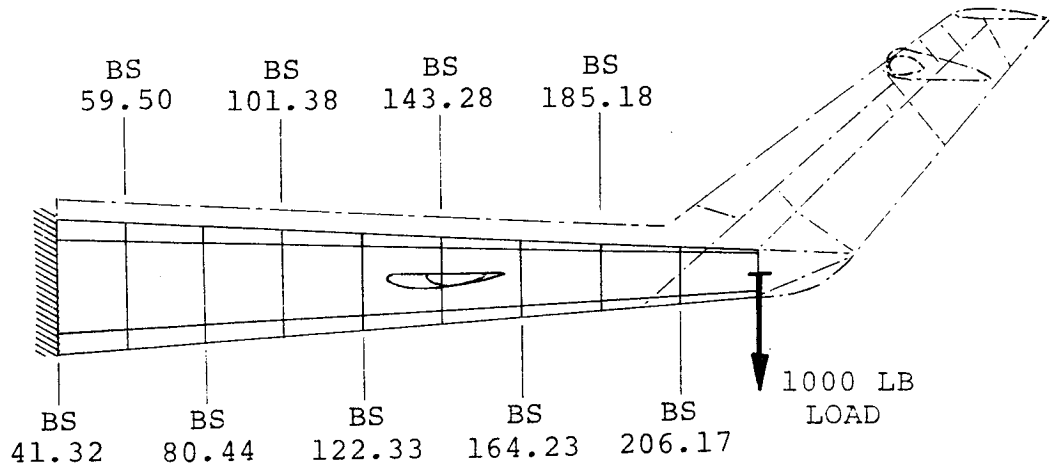

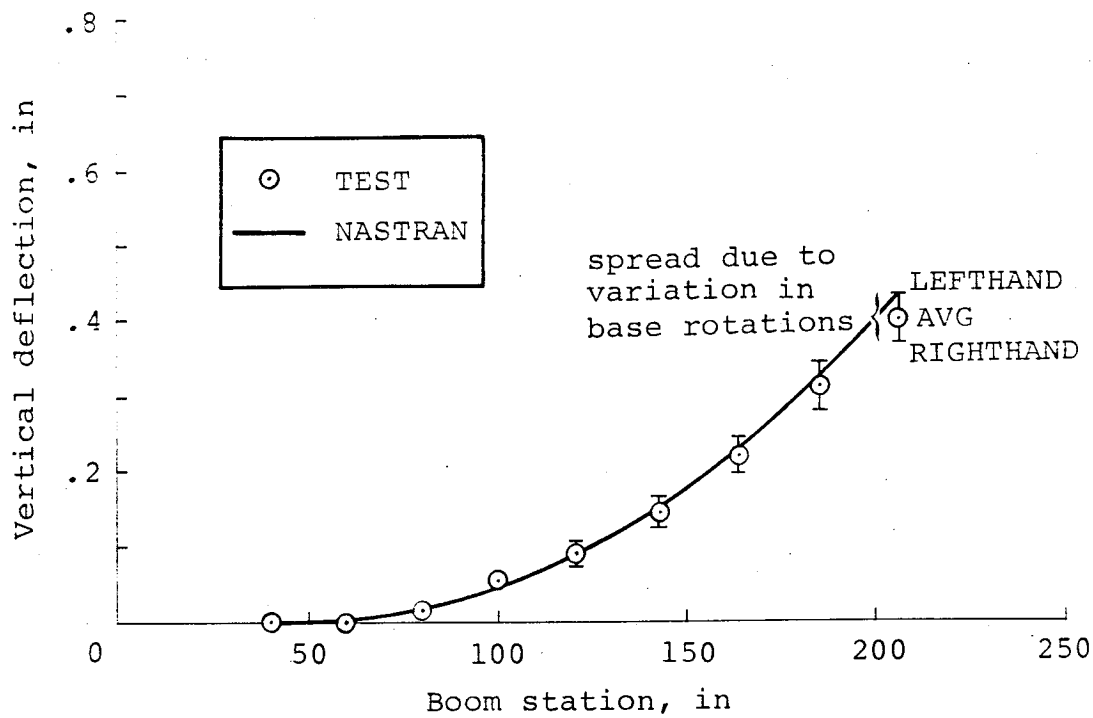

Figure 23. Tailboom Vertical Load-Deflection Comparison.

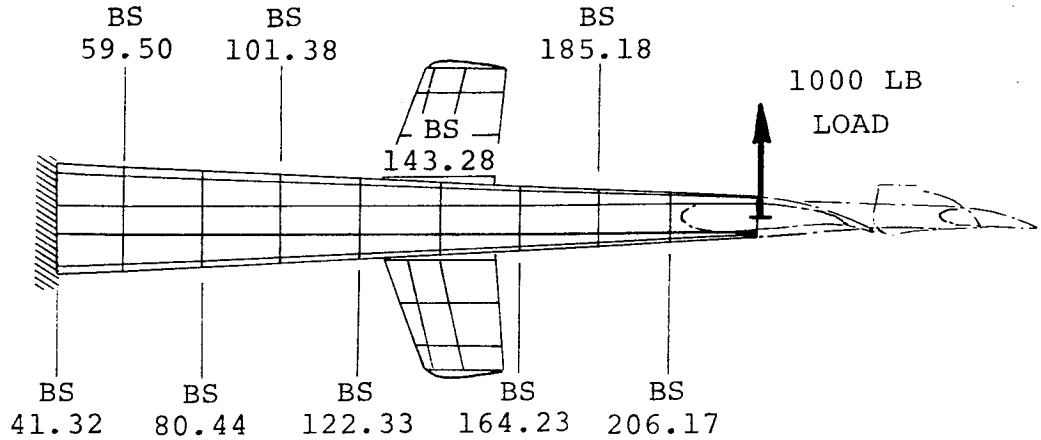

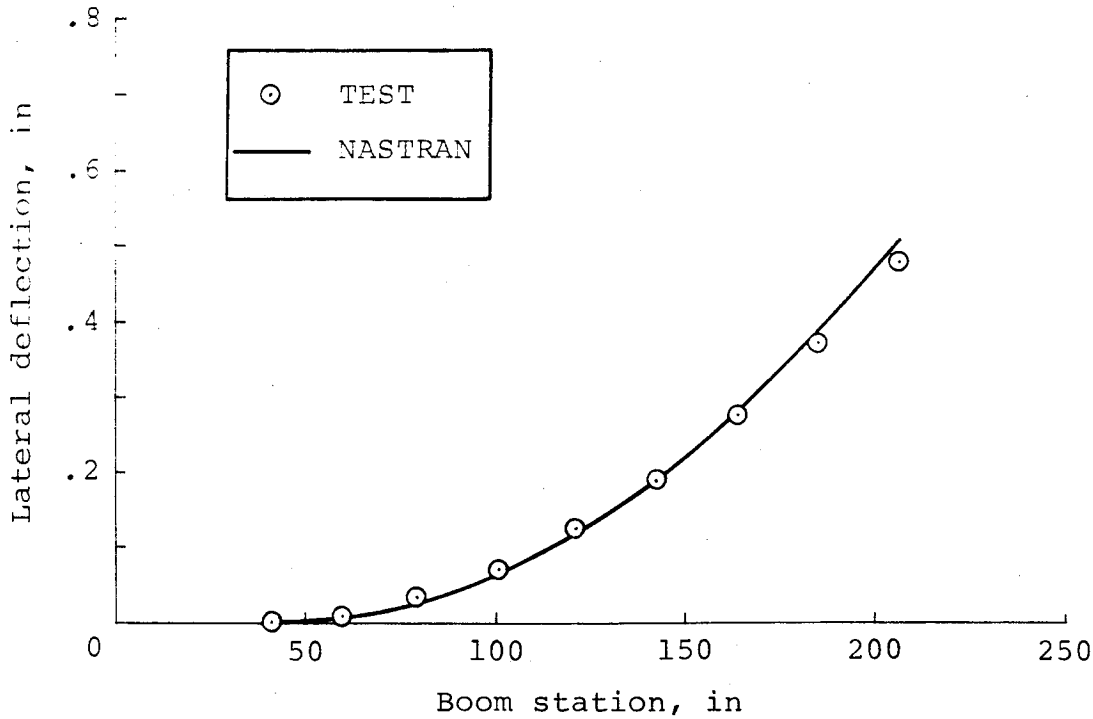

Figure 24. Tailboom Lateral Load-Deflection Comparison.

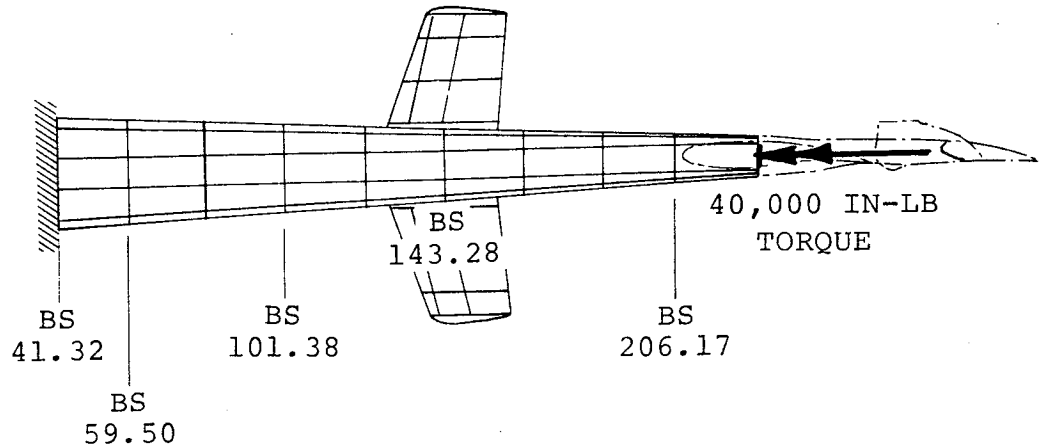

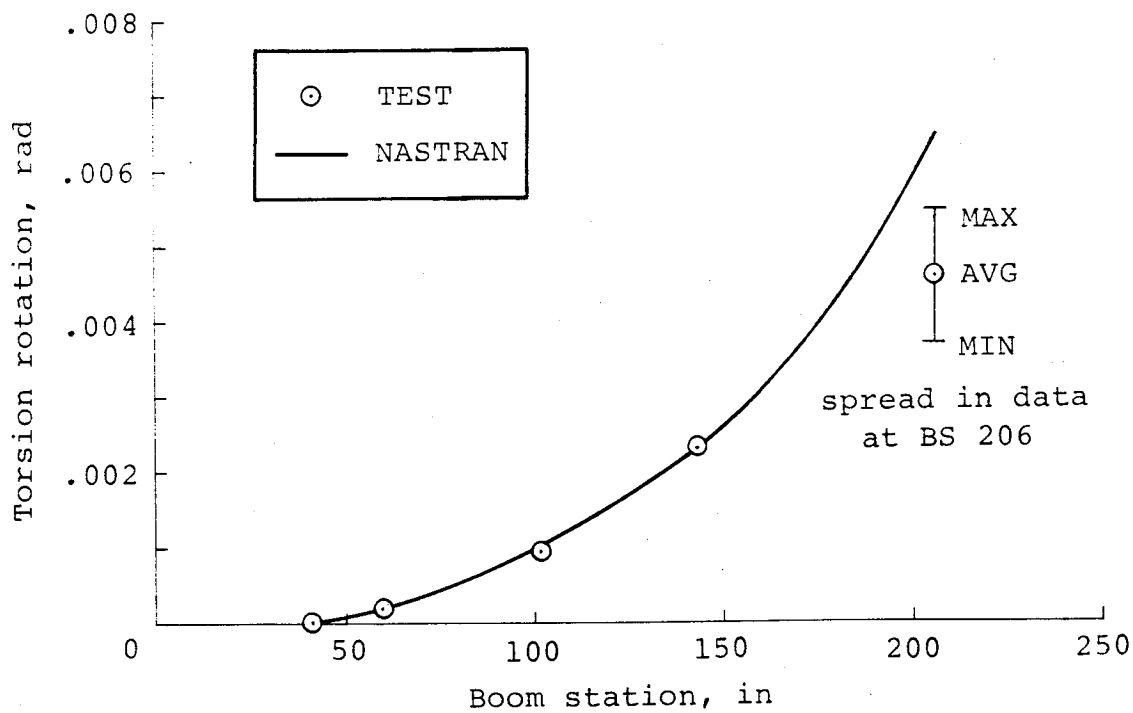

Figure 25. Tailboom Torsion Torque-Rotation Comparison.

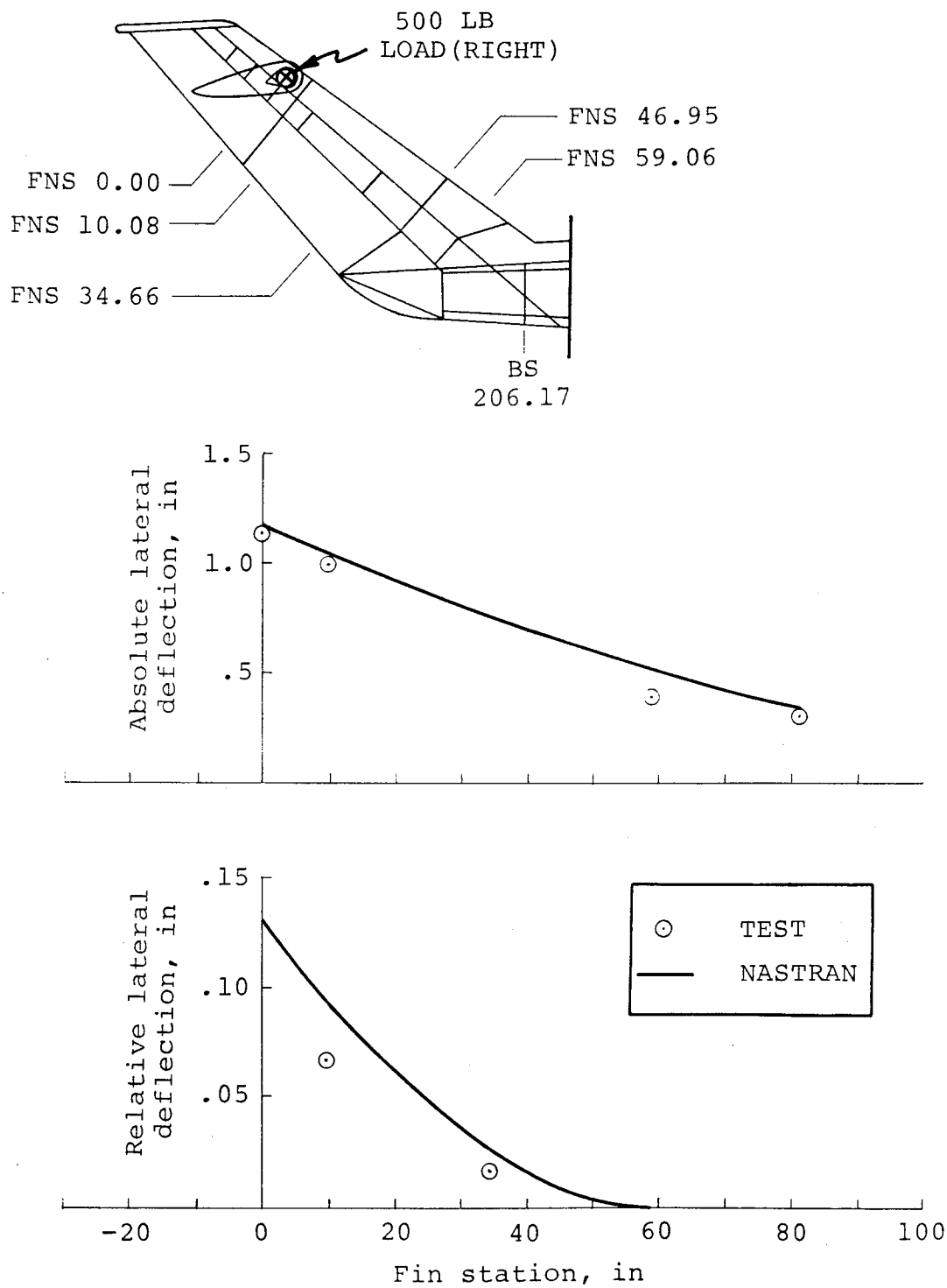

Figure 26. Vertical Fin Lateral Load-Deflection Comparison.

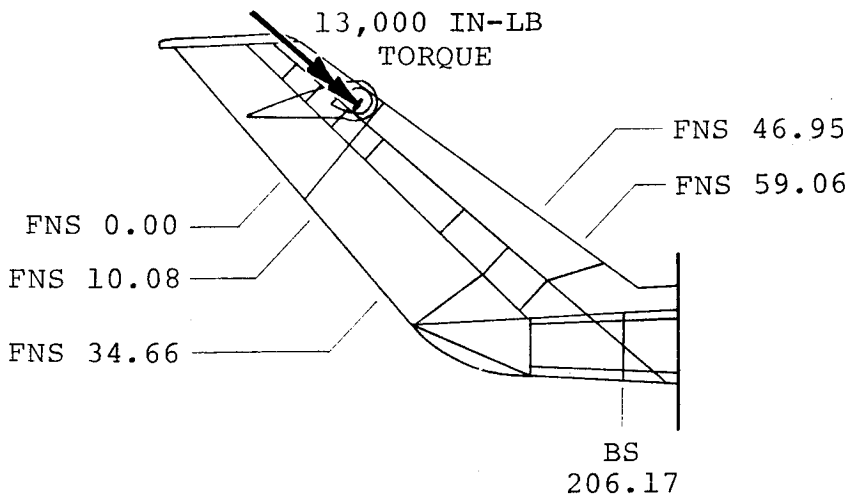

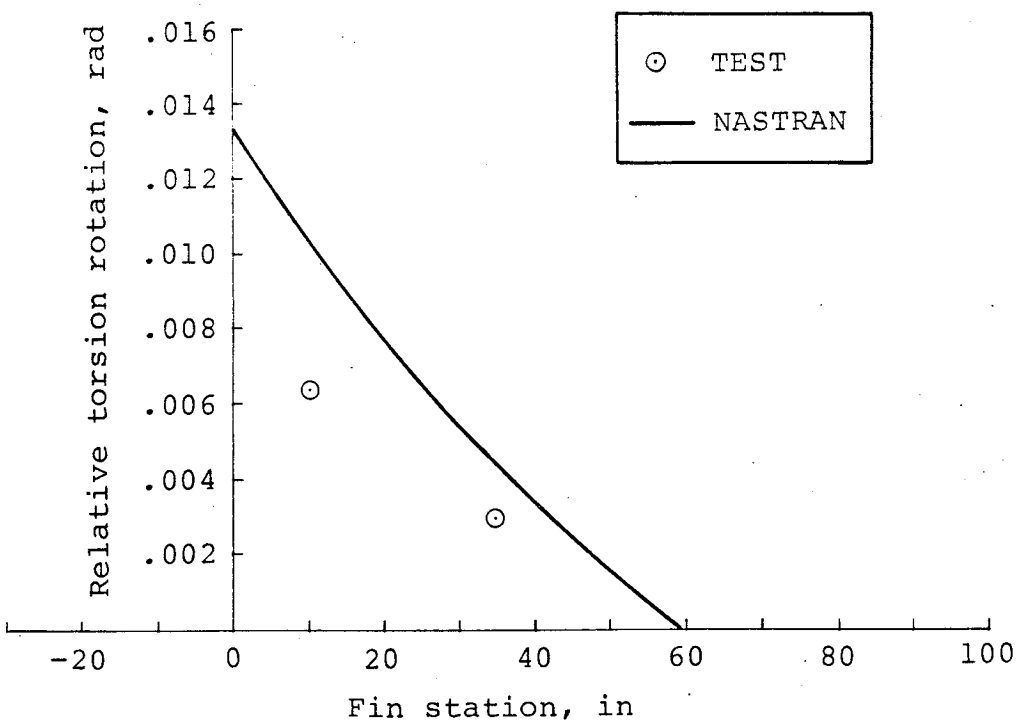

Figure 27. Vertical Fin Torsion Torque-Rotation Comparison.

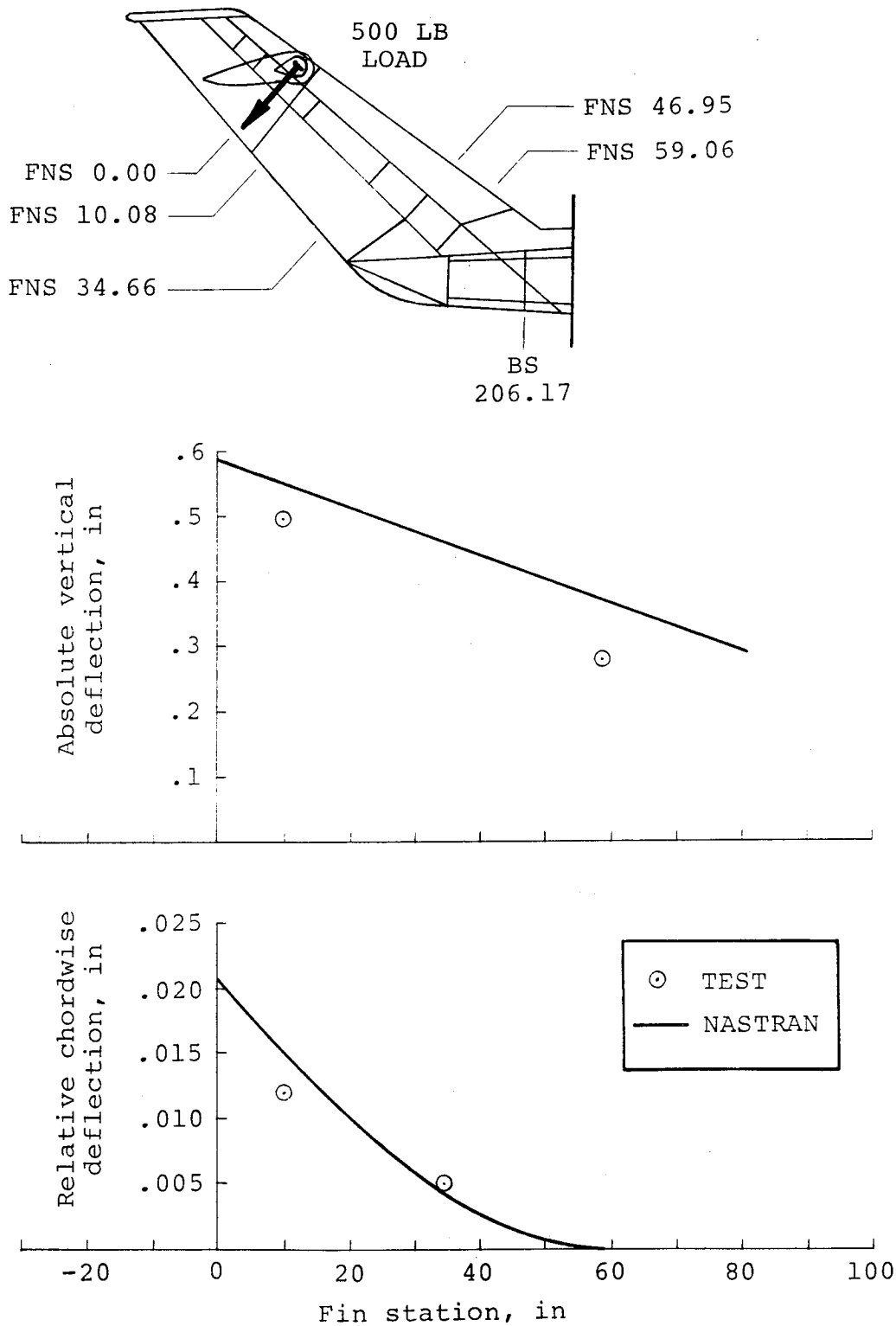

Figure 28. Vertical Fin Chordwise Load-Deflection Comparison.

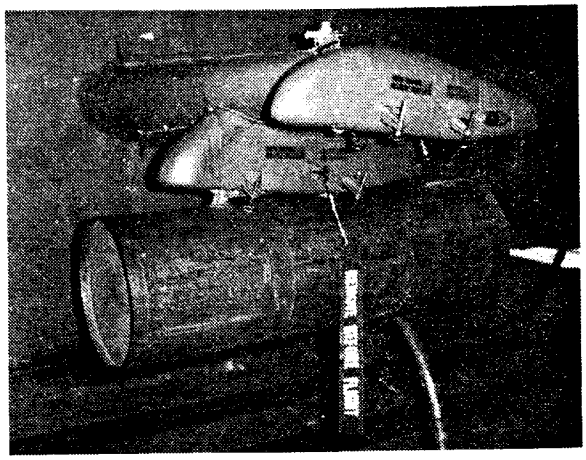

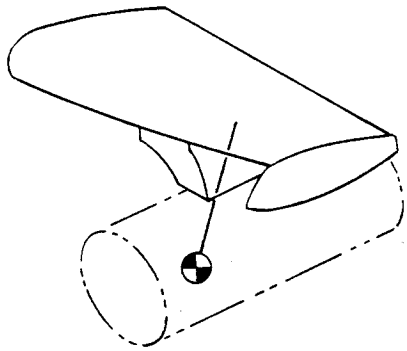

WEIGHT = 325 lb/side

CG: STA 196.25
BL ±42.50
WL 43.41

INERTIAS = ROLL = 19995 lb-in^2
PITCH = 61132 lb-in^2
YAW = 61132 lb-in^2

Figure 29. Wing Store.

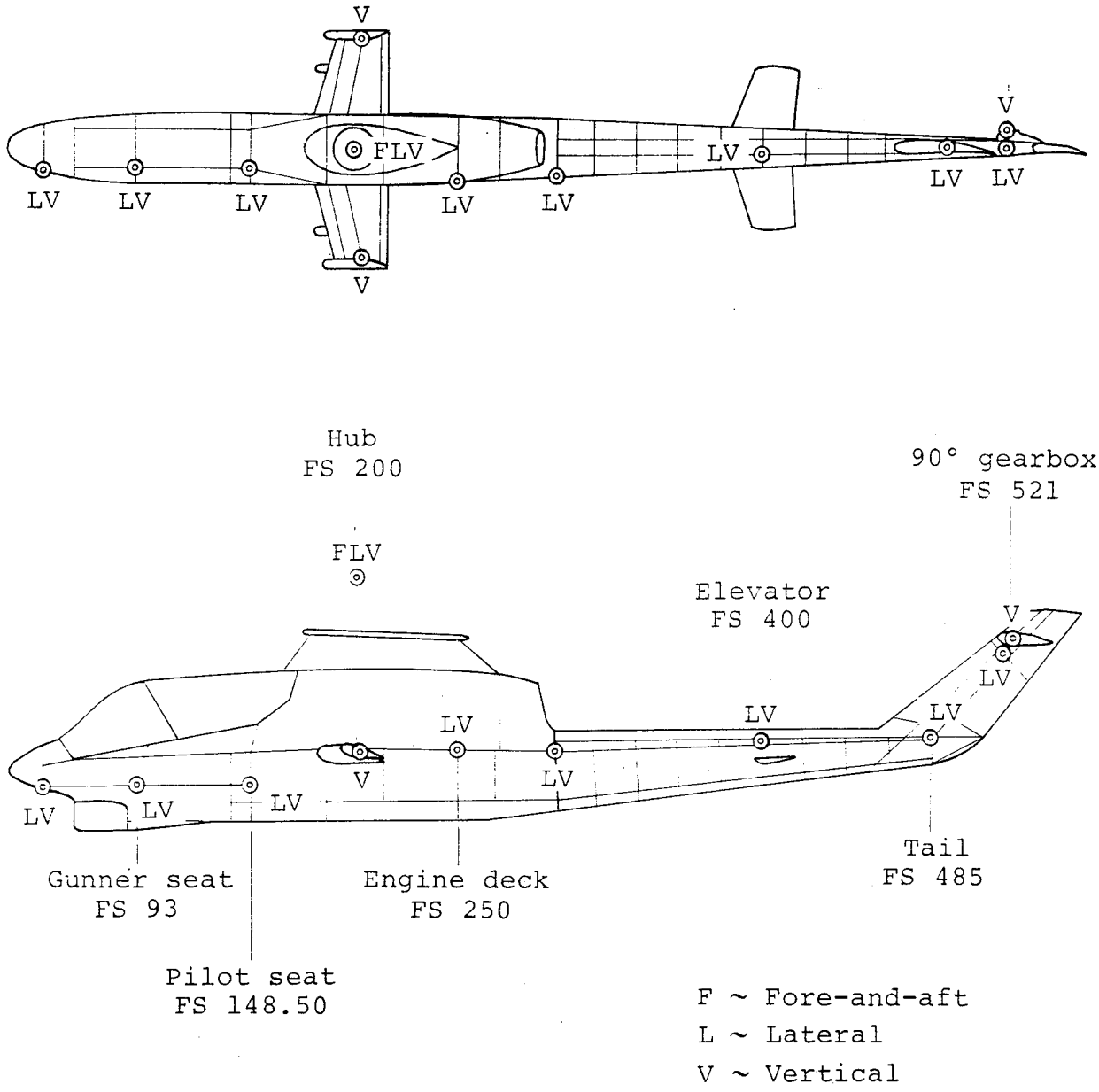

Figure 30. Accelerometer Locations for Shake Tests.

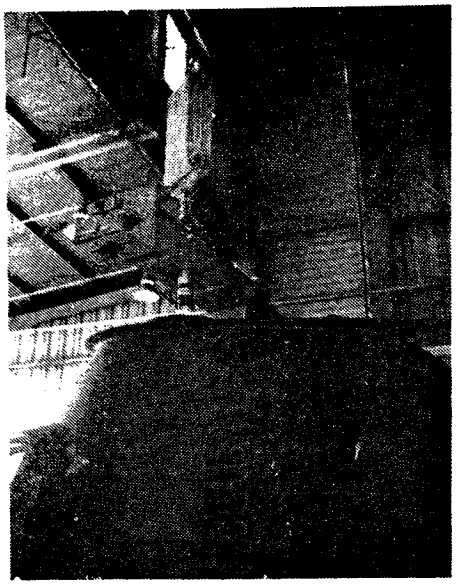

Bungee suspension

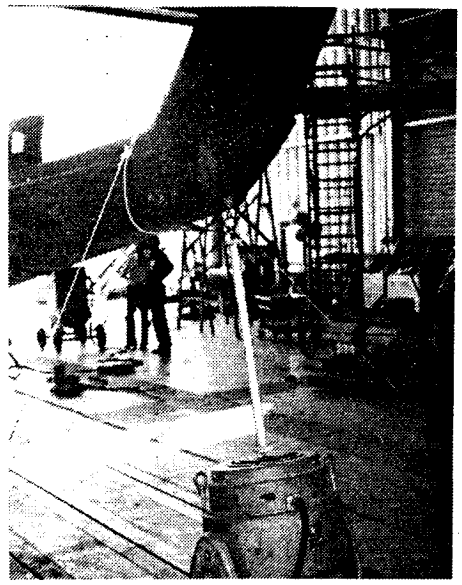

Vertical tail shake

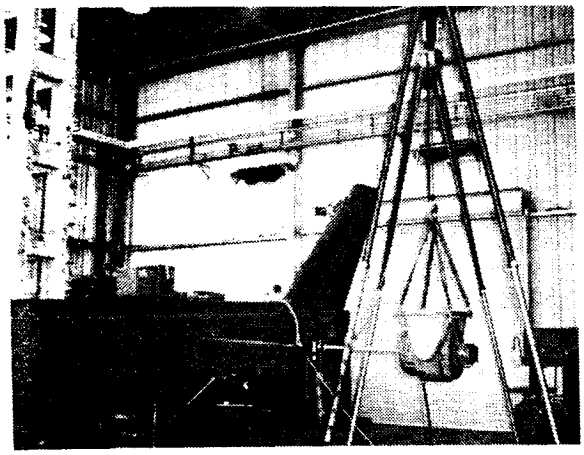

Lateral tail shake
shaker suspension

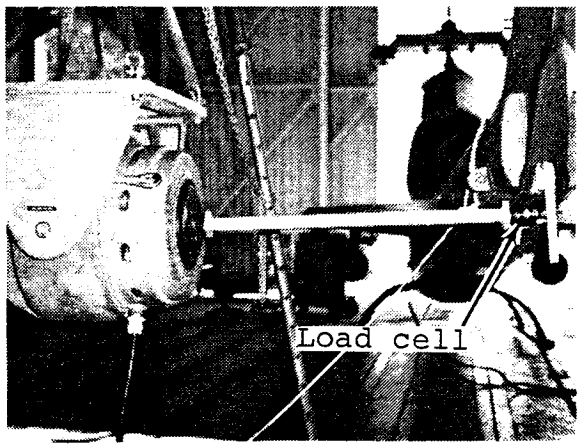

Lateral tail shake

Figure 31. Suspension and Shaker Locations for Vertical and Lateral Tail Shake Tests.

ORIGINAL PAGE IS
OF POOR QUALITY

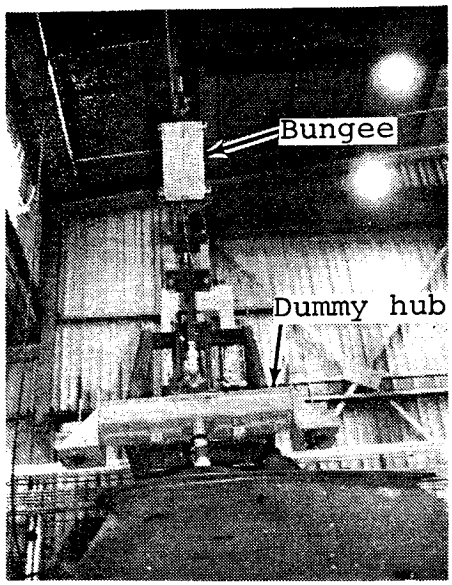

Vertical hub shake
bungee suspension

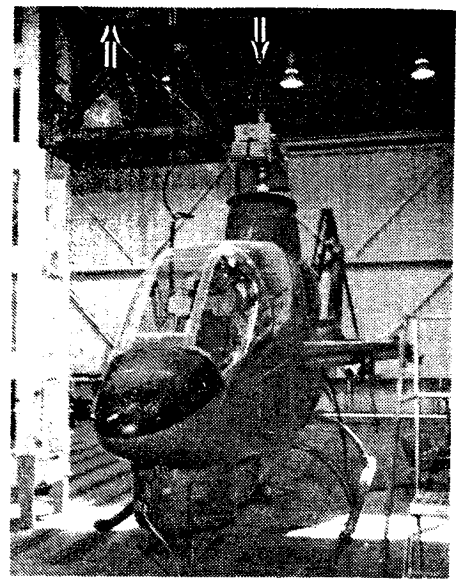

Vertical hub shake

Cable suspension
without bungee

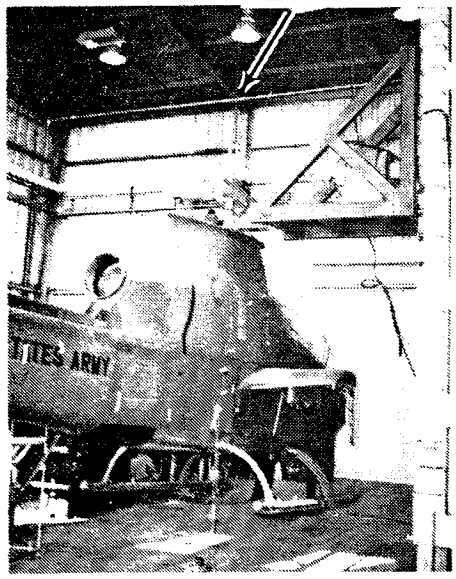

Lateral hub shake

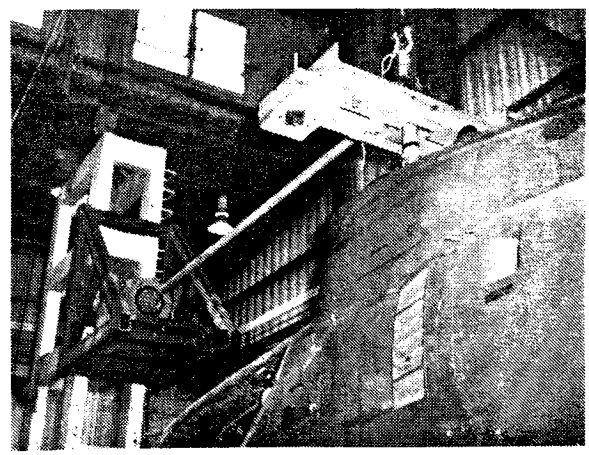

Fore-and-aft hub shake

Figure 32. Suspension and Shaker Locations for Main Rotor Hub Shake Tests.

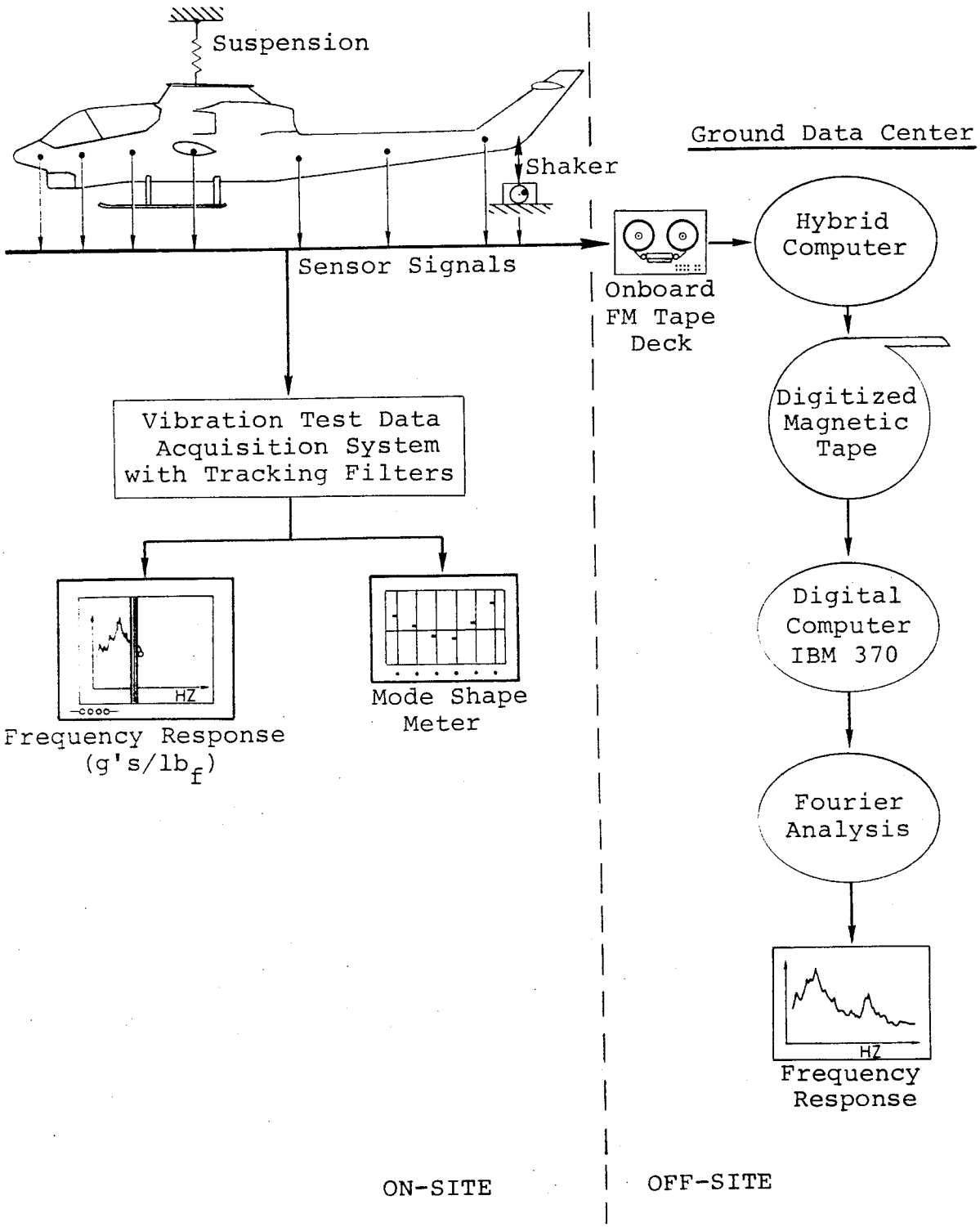

Figure 33. Shake Test Data Reduction Flow Chart.

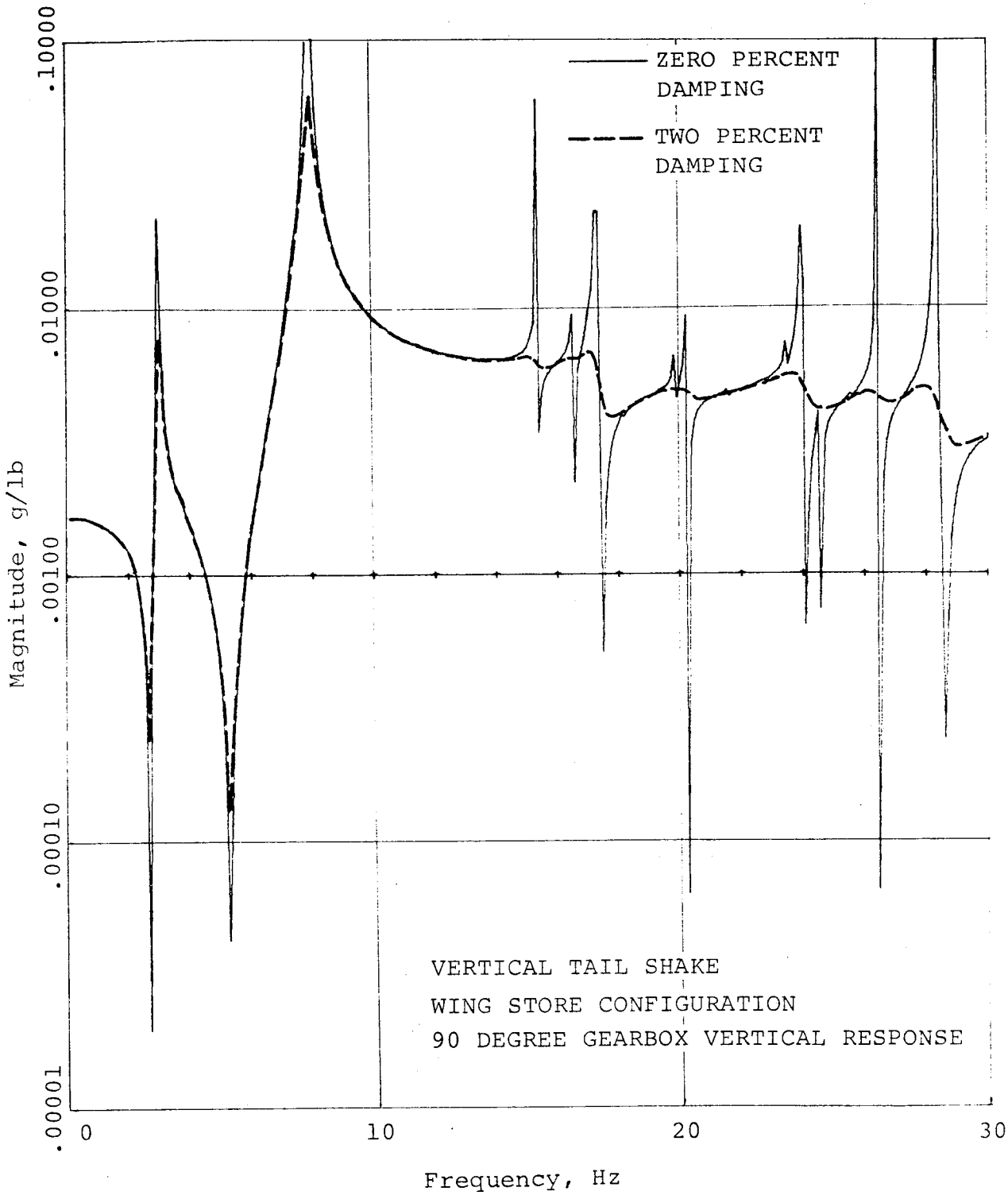

Figure 34. Comparison of Frequency Response Using 0% and 2% Damping.

APPENDIX A

FREQUENCY RESPONSE DATA COMPARISONS FOR DIFFERENT AMOUNTS OF DAMPING

This appendix contains figures showing frequency response comparisons between NASTRAN and test results for different values of model damping in NASTRAN. The values of damping that were used for each comparison were constant 2 percent and 5 percent damping and linear damping (0 percent at 0 Hz, 2 percent at 10 Hz, 4 percent at 20 Hz, etc.). The figure number, forcing condition, helicopter configuration and response location for each comparison are given in Table A1. Main rotor two-per-rev (10.8 Hz) and four-per-rev (21.6 Hz) excitation frequencies are indicated on the figures.

TABLE A1. - FREQUENCY RESPONSE DATA COMPARISONS

Figure number	Applied force location/direction	Configuration	Response location/direction
A-1	Tail/vertical	Clean wing	Gunner seat/vertical
A-2	Tail/vertical	Clean wing	Tail/vertical
A-3	Tail/vertical	With stores	Gunner seat/vertical
A-4	Tail/vertical	With stores	Tail/vertical
A-5	Tail/lateral	Clean wing	Gunner seat/lateral
A-6	Tail/lateral	Clean wing	Tail/lateral
A-7	Tail/lateral	With stores	Gunner seat/lateral
A-8	Tail/lateral	With stores	Tail/lateral
A-9	Hub/vertical	Clean wing	Hub/vertical
A-10	Hub/vertical	Clean wing	Gunner seat/vertical
A-11	Hub/vertical	Clean wing	90° gearbox/vertical
A-12	Hub/lateral	Clean wing	Hub/lateral
A-13	Hub/lateral	Clean wing	Gunner seat/lateral
A-14	Hub/lateral	Clean wing	90° gearbox/vertical
A-15	Hub/fore-and-aft	Clean wing	Hub/fore-and-aft
A-16	Hub/fore-and-aft	Clean wing	Gunner seat/vertical
A-17	Hub/fore-and-aft	Clean wing	90° gearbox/vertical

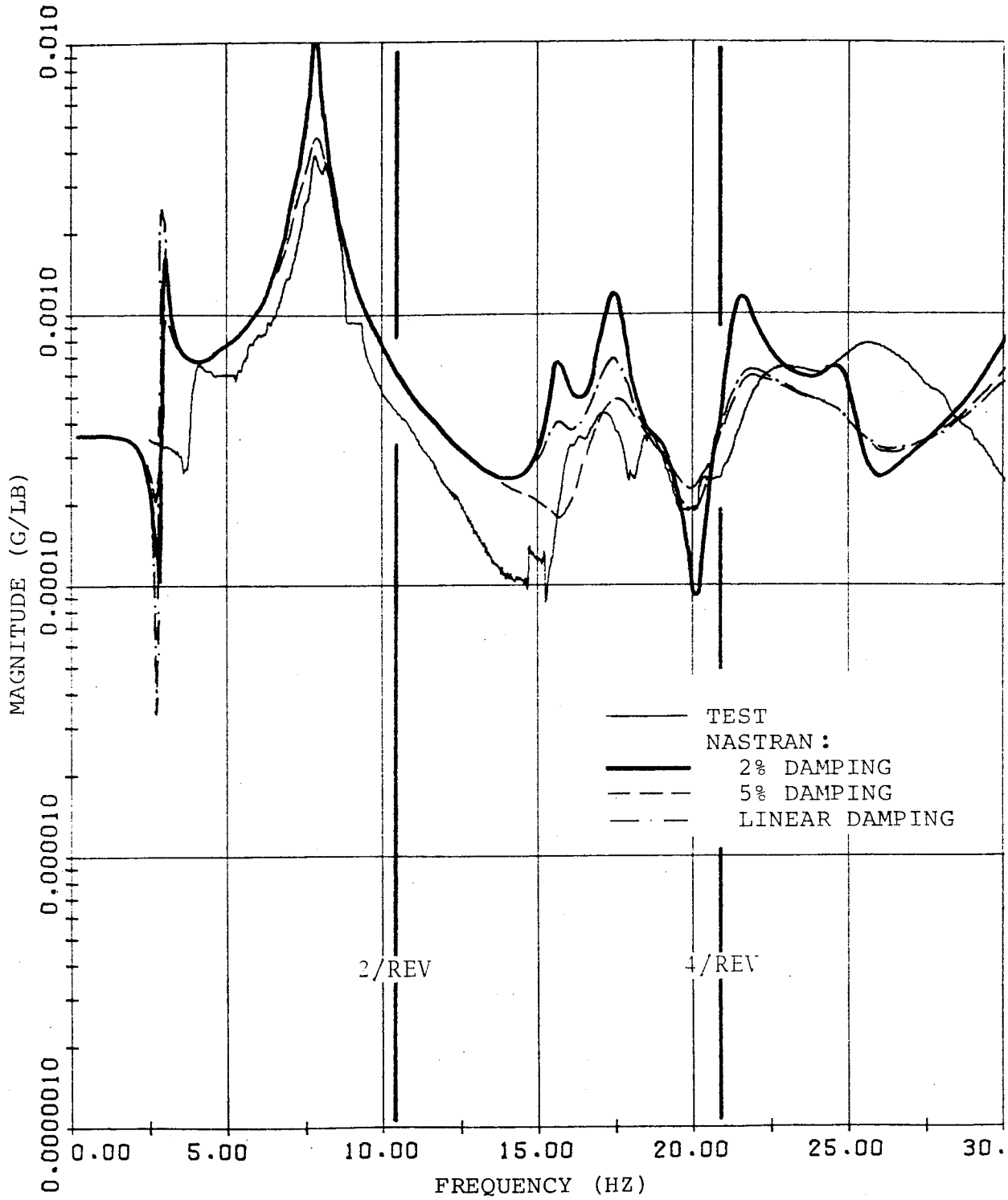

Figure A-1. Frequency Response, Vertical Tail Shake (Clean Wing) 2%, 5% and Linear Damping - Gunner Seat Vertical.

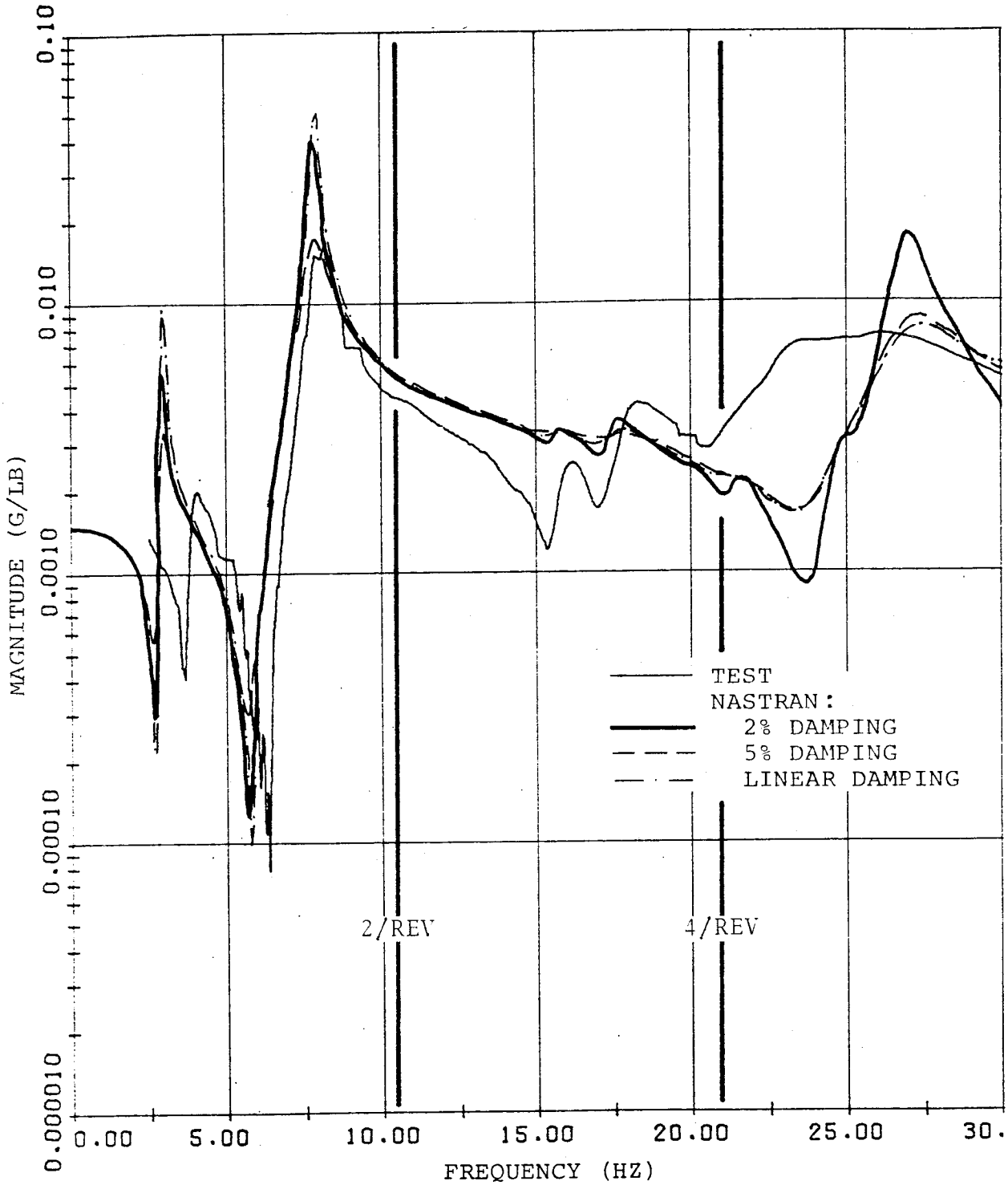

Figure A-2. Frequency Response, Vertical Tail Shake (Clean Wing) 2%, 5% and Linear Damping - Tail Vertical.

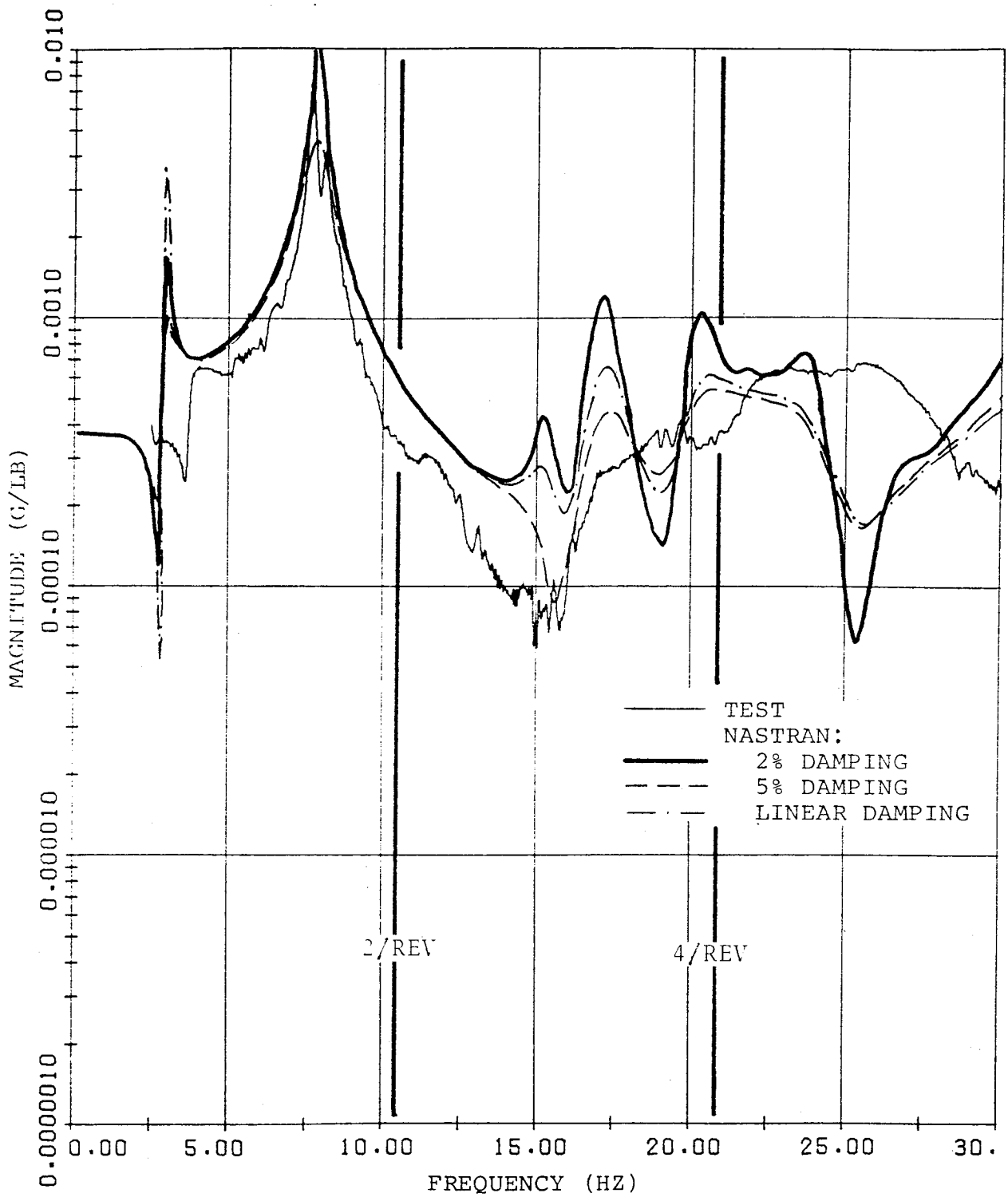

Figure A-3. Frequency Response, Vertical Tail Shake (With Stores) 2%, 5% and Linear Damping - Gunner Seat Vertical.

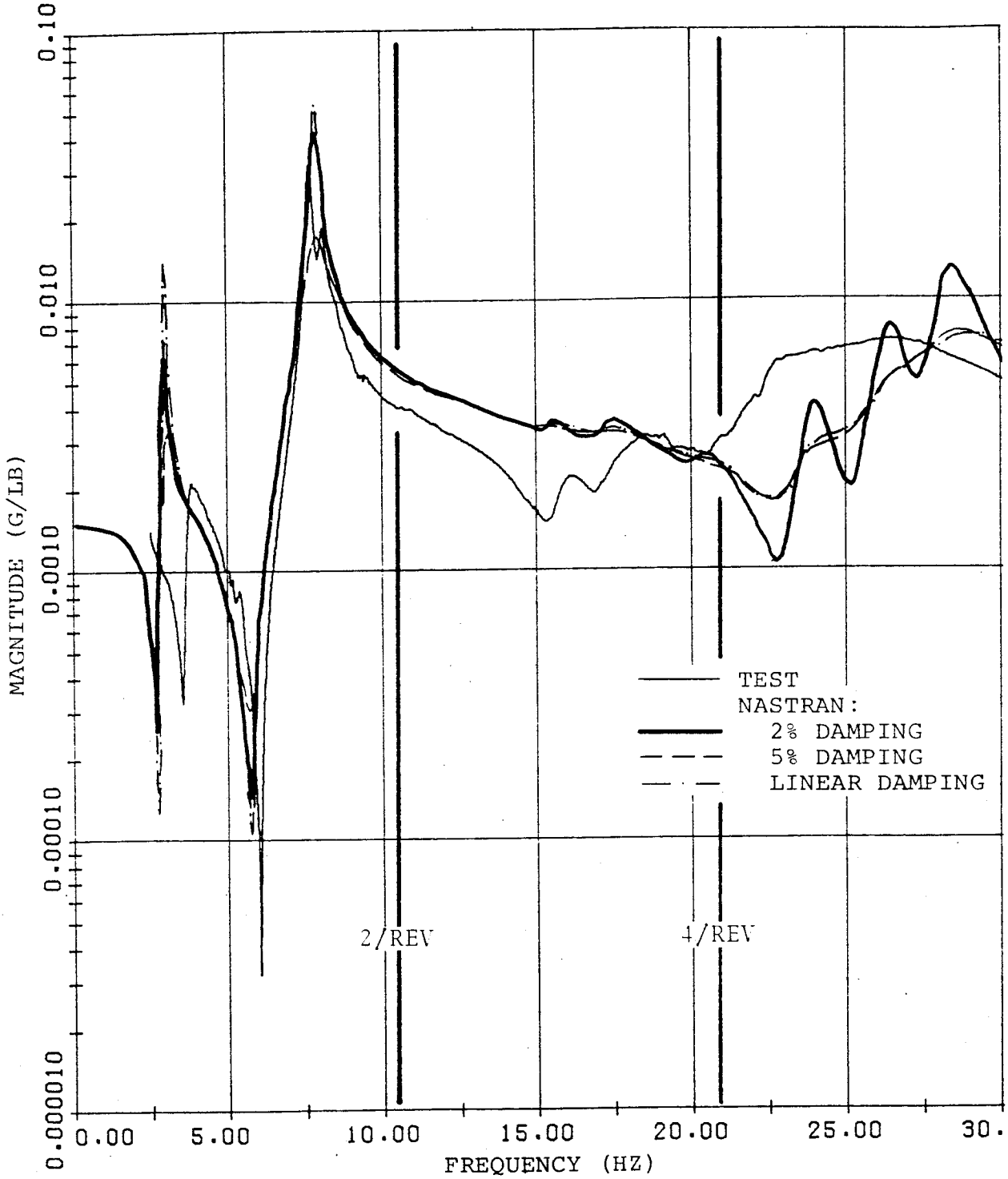

Figure A-4. Frequency Response, Vertical Tail Shake (With Stores) 2%, 5% and Linear Damping - Tail Vertical.

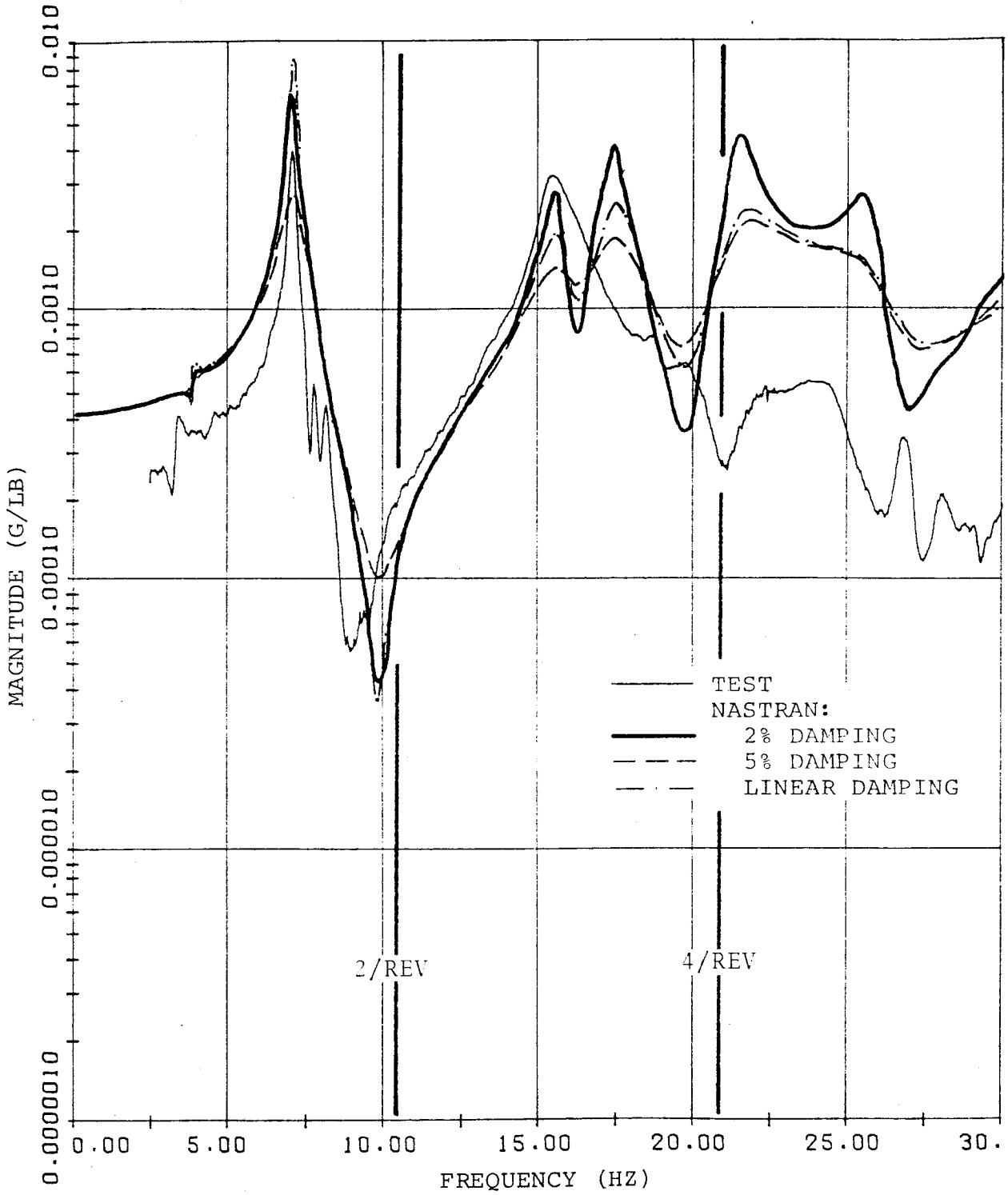

Figure A-5. Frequency Response, Lateral Tail Shake (Clean Wing) 2%, 5% and Linear Damping - Gunner Seat Lateral.

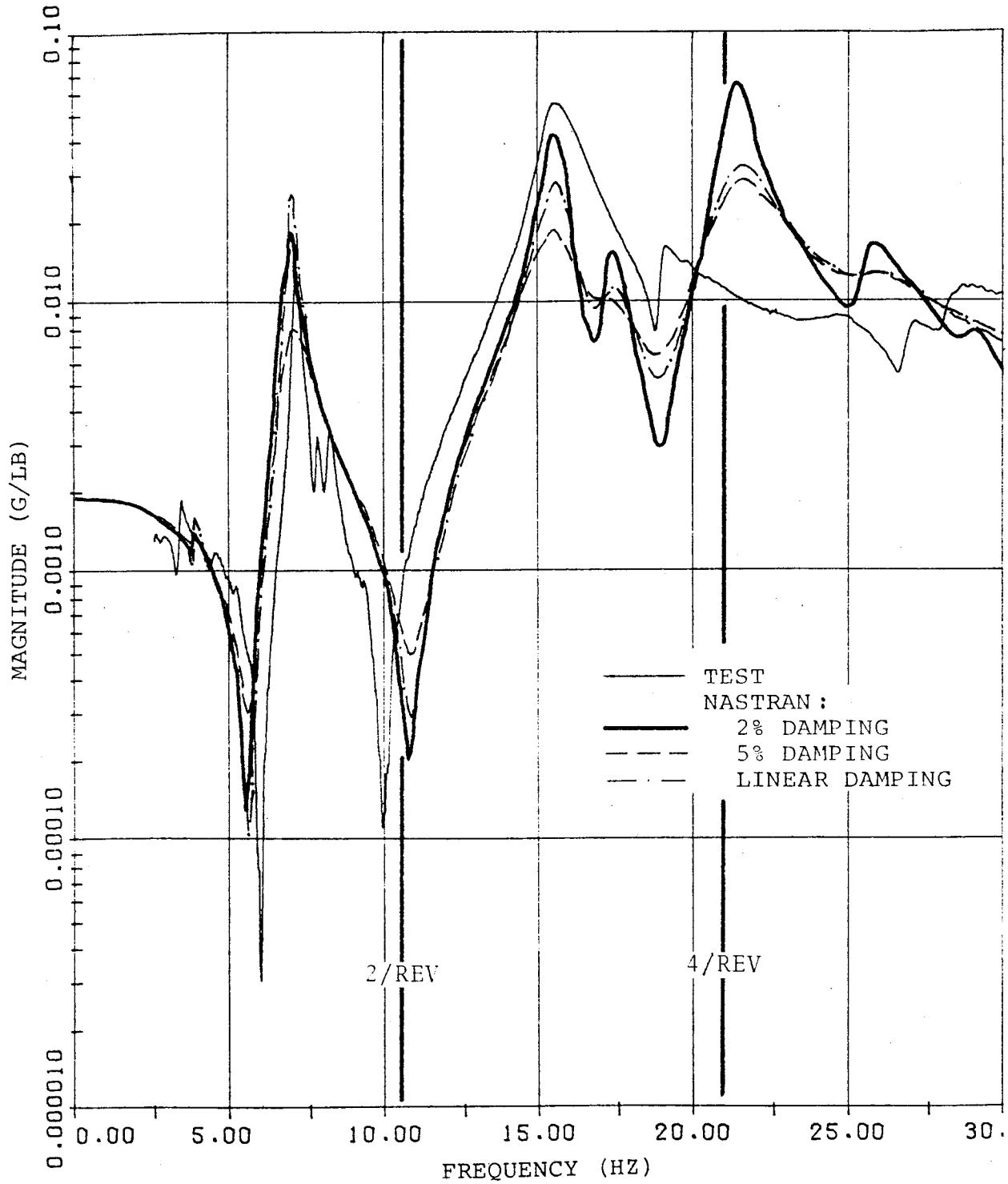

Figure A-6. Frequency Response, Lateral Tail Shake (Clean Wing) 2%, 5% and Linear Damping - Tail Lateral.

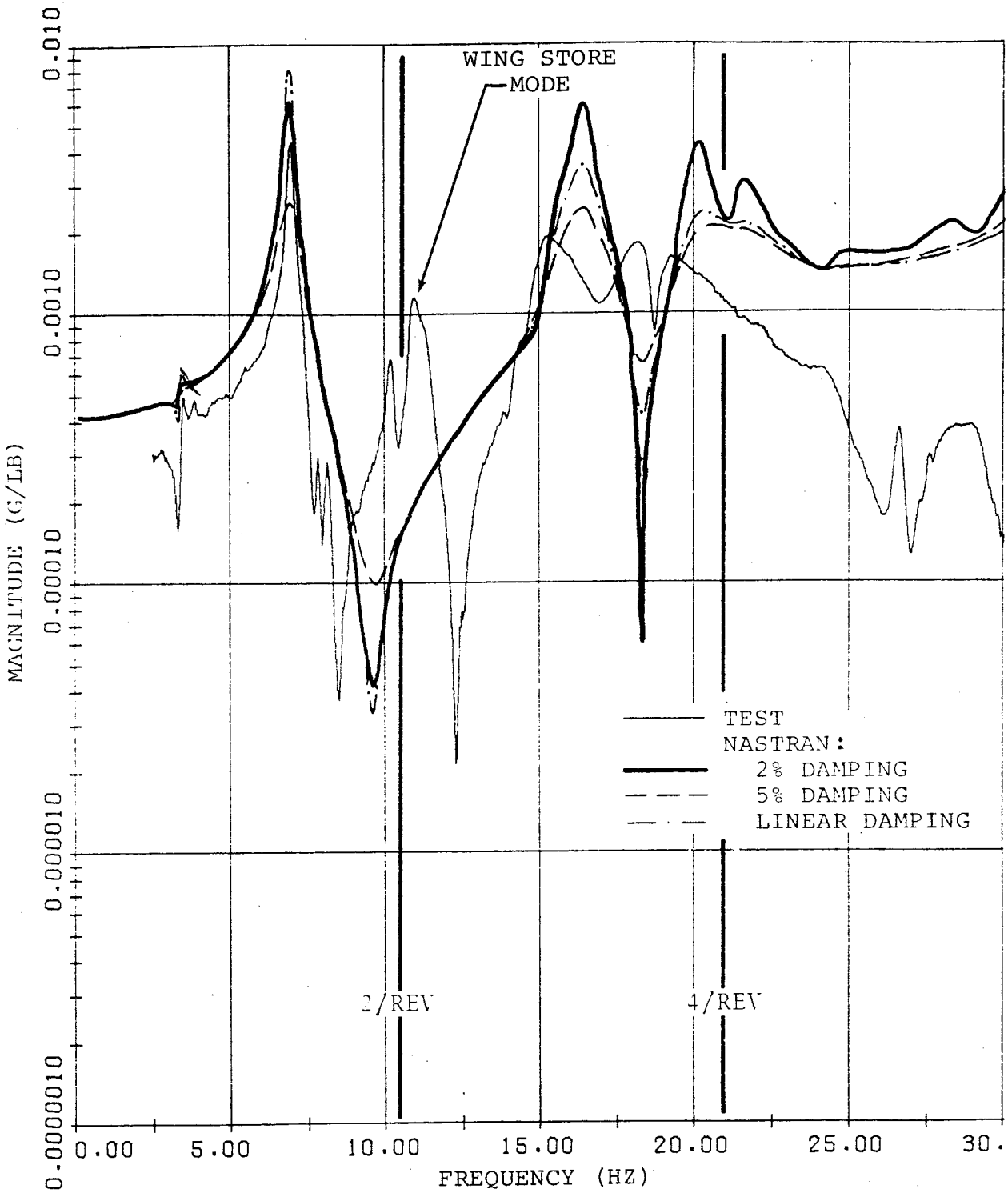

Figure A-7. Frequency Response, Lateral Tail Shake (With Stores) 2%, 5% and Linear Damping - Gunner Seat Lateral.

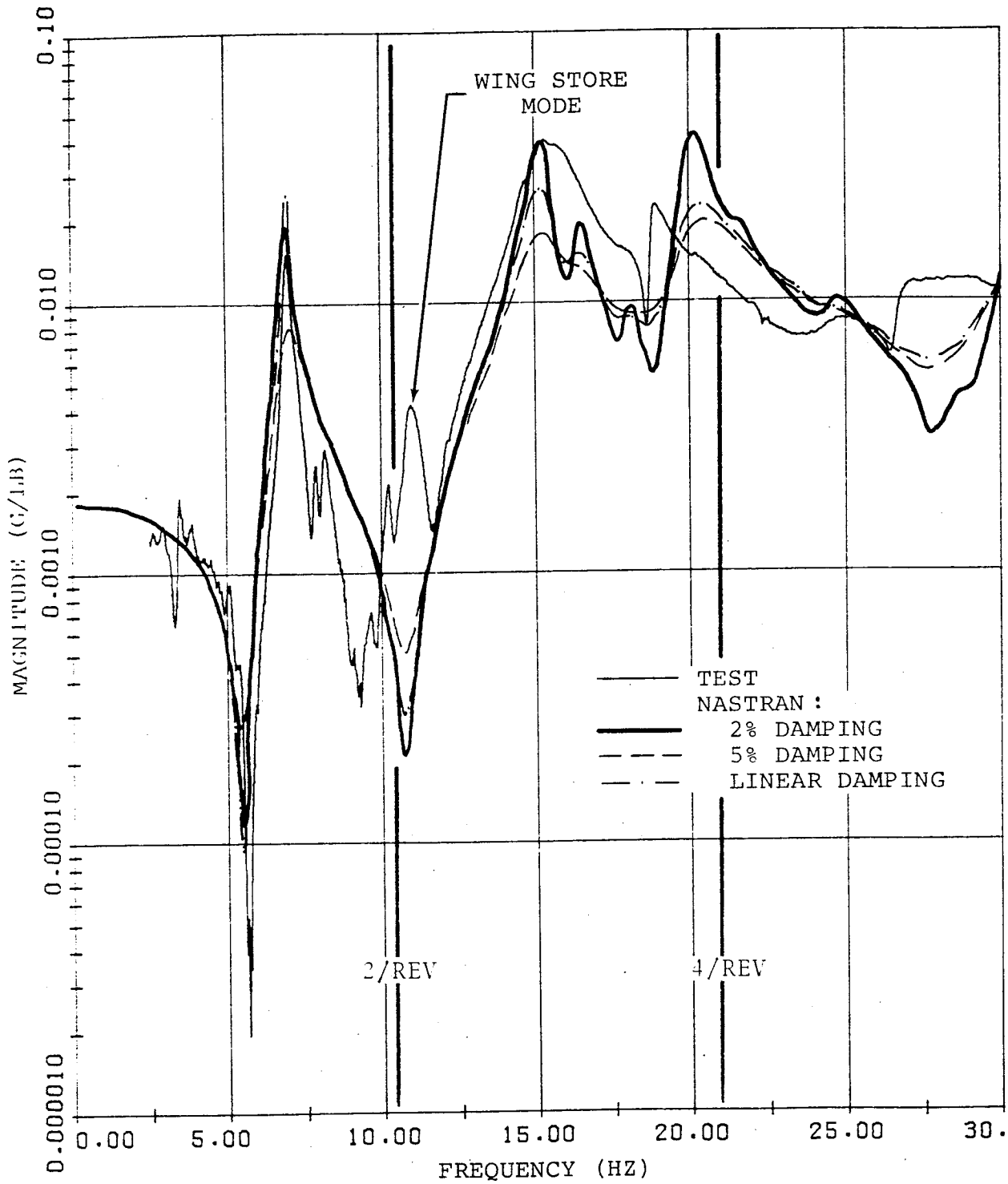

Figure A-8. Frequency Response, Lateral Tail Shake (With Stores) 2%, 5% and Linear Damping - Tail Lateral.

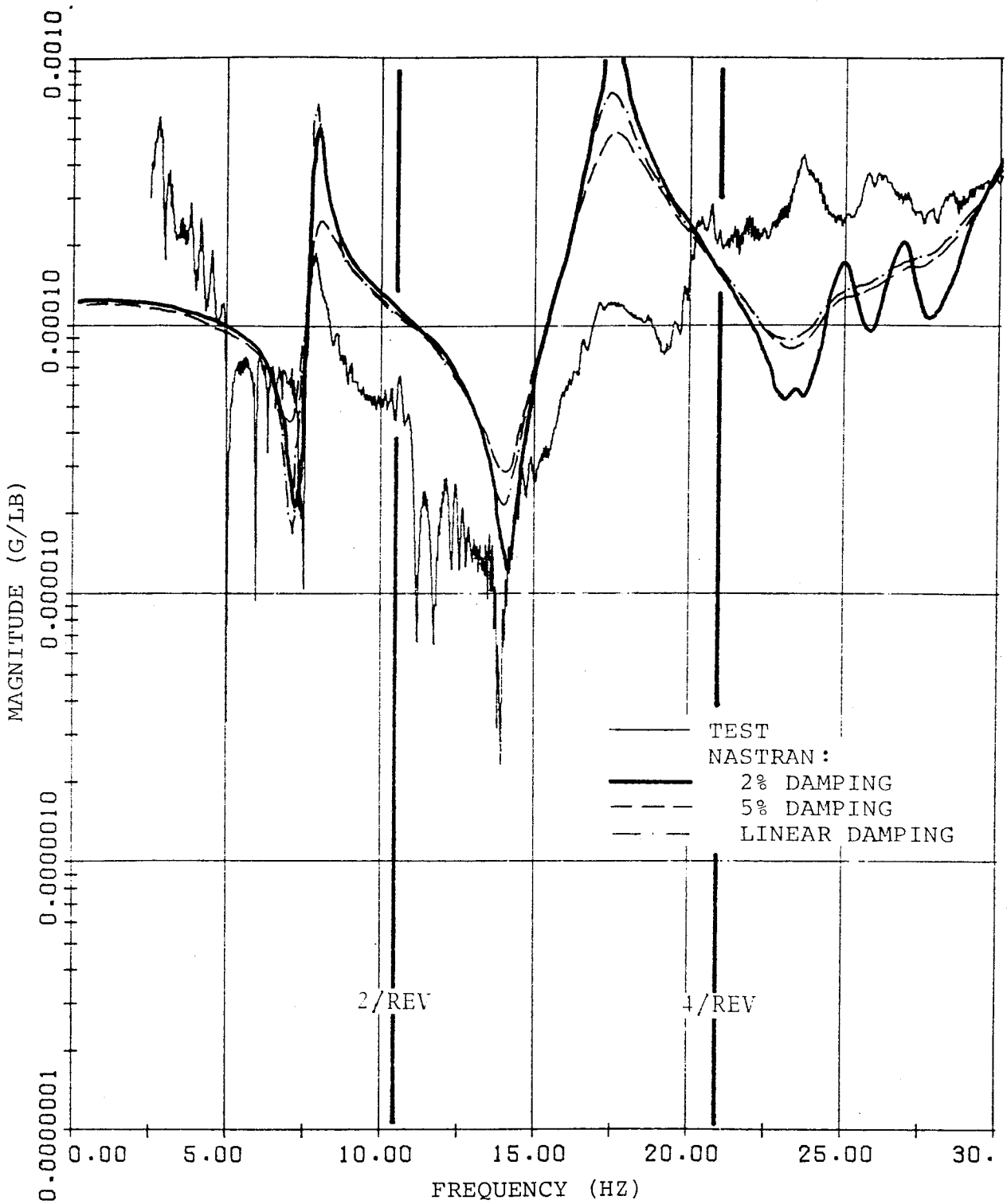

Figure A-9. Frequency Response, Vertical Hub Shake (Clean Wing) 2%, 5% and Linear Damping - Hub Vertical.

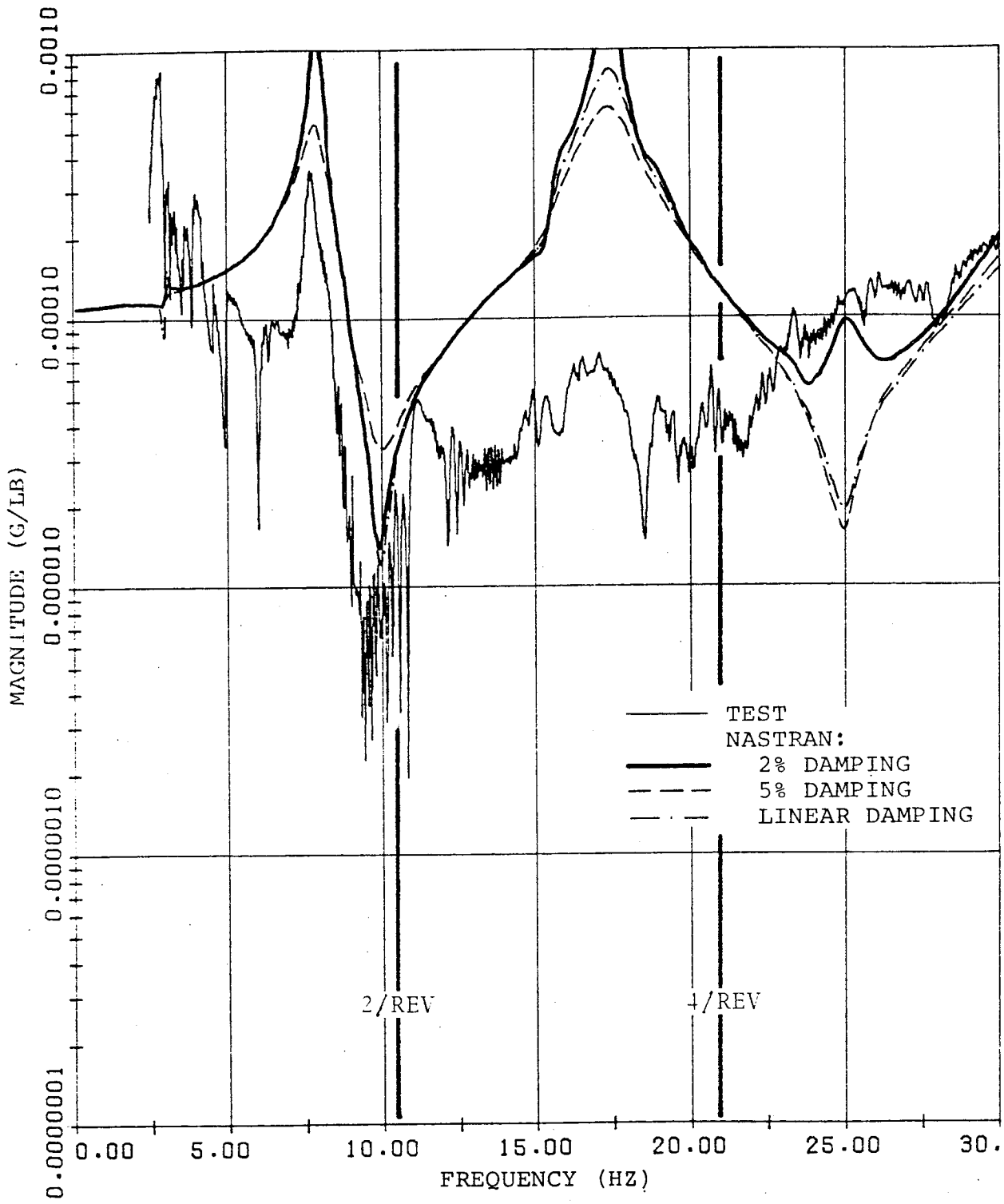

Figure A-10. Frequency Response, Vertical Hub Shake (Clean Wing) 2%, 5% and Linear Damping - Gunner Seat Vertical.

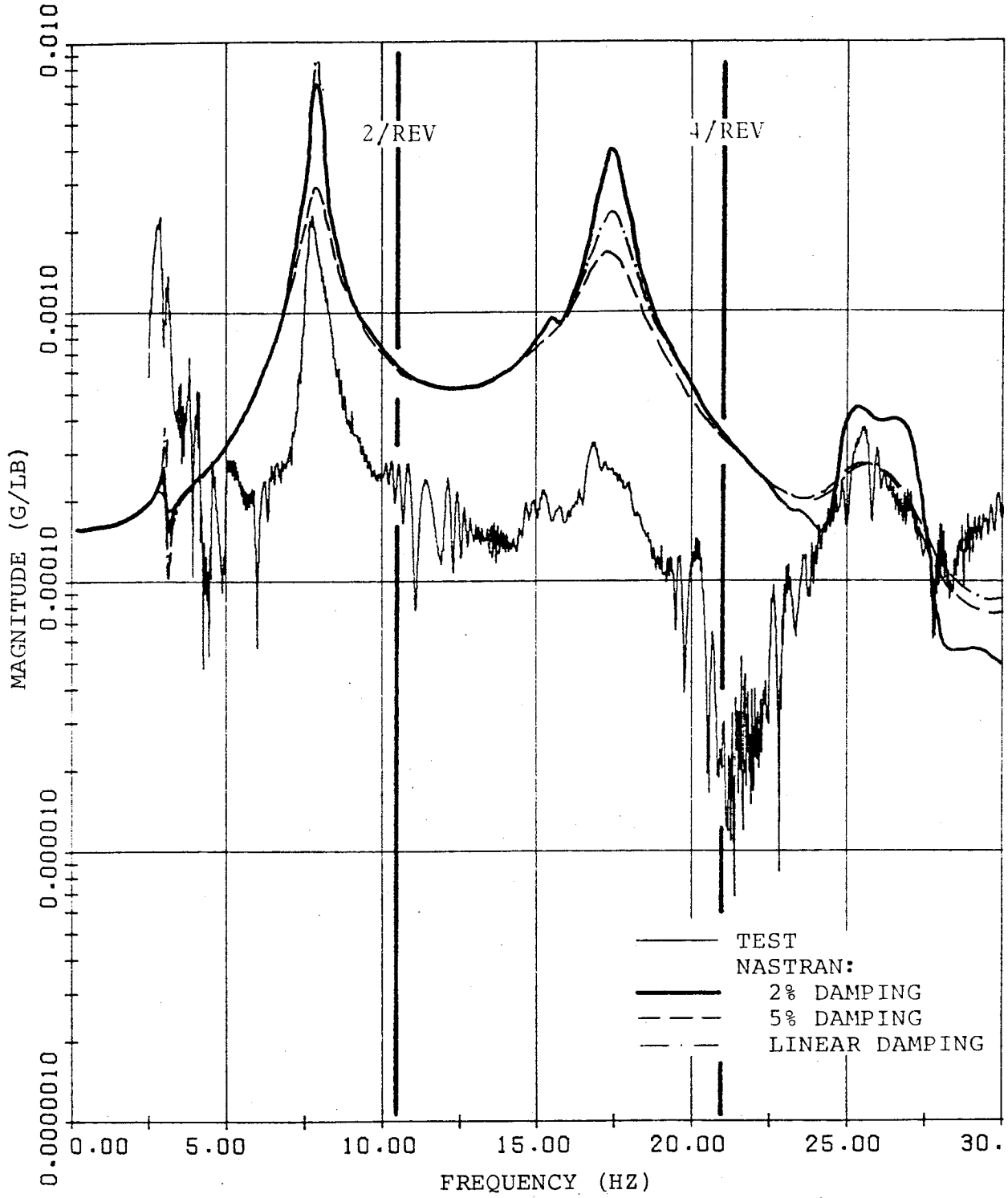

Figure A-11. Frequency Response, Vertical Hub Shake (Clean Wing) 2%, 5% and Linear Damping - 90° Gearbox Vertical.

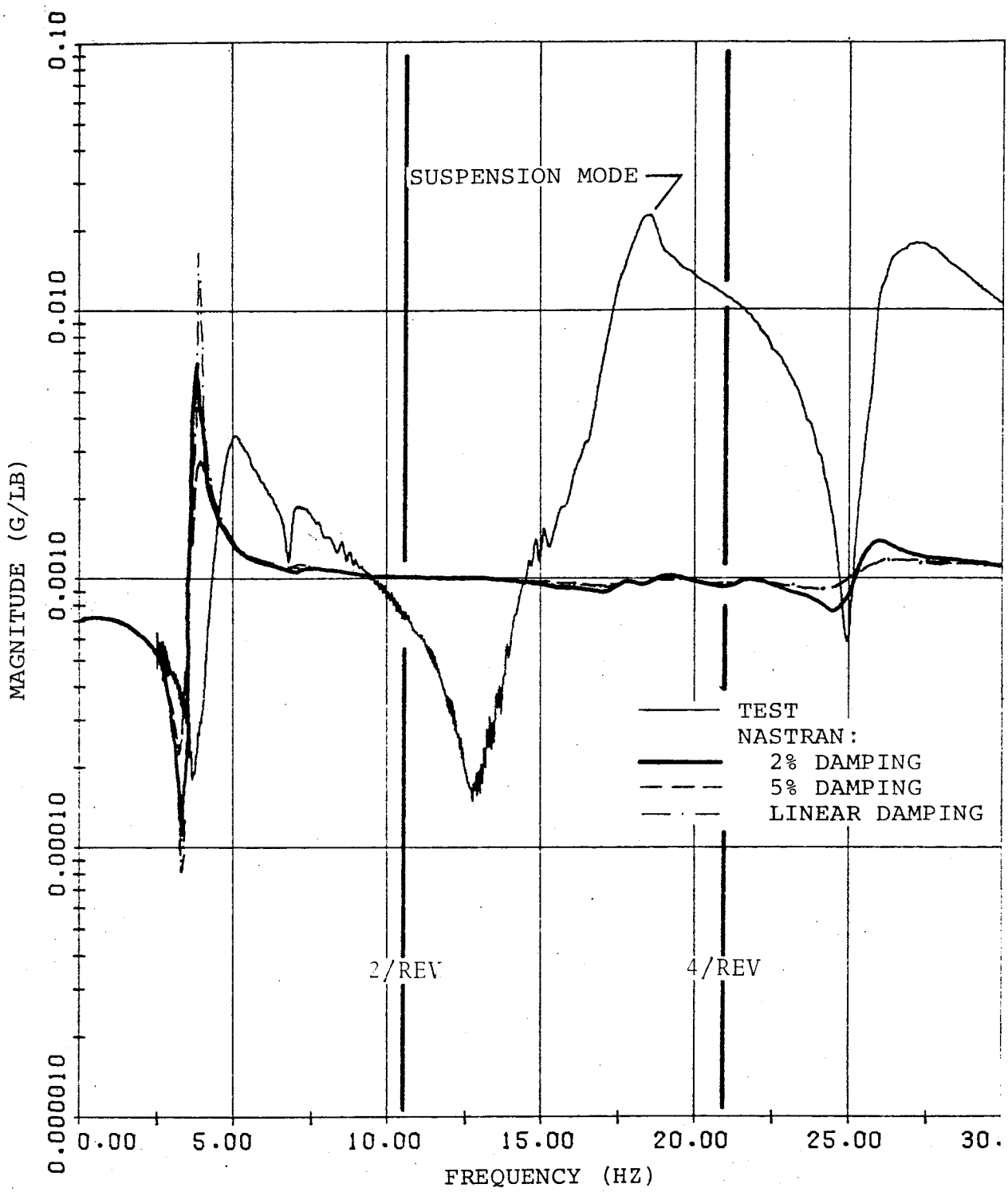

Figure A-12. Frequency Response, Lateral Hub Shake (Clean Wing) 2%, 5% and Linear Damping - Hub Lateral.

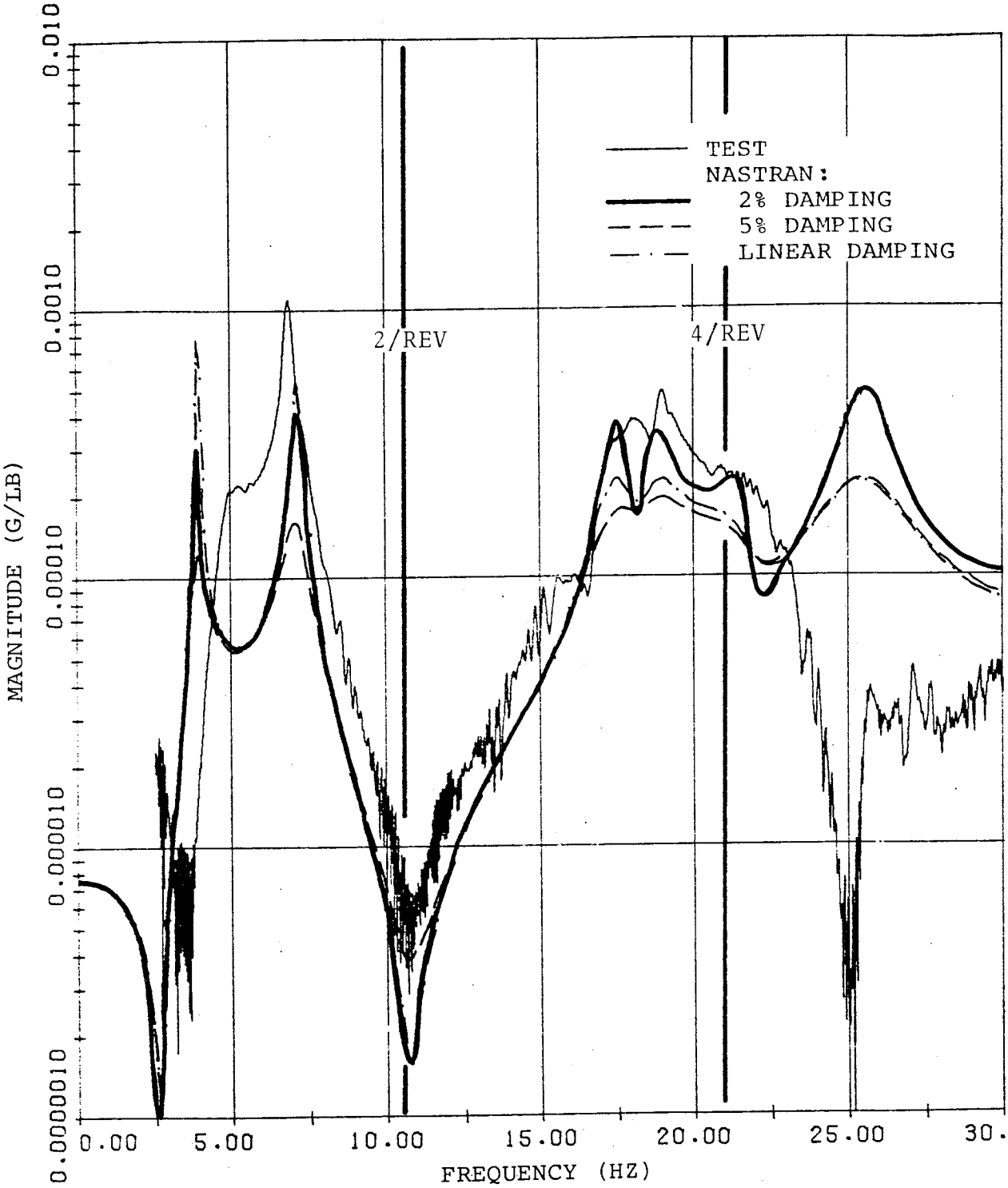

Figure A-13. Frequency Response, Lateral Hub Shake (Clean Wing) 2%, 5% and Linear Damping - Gunner Seat Lateral.

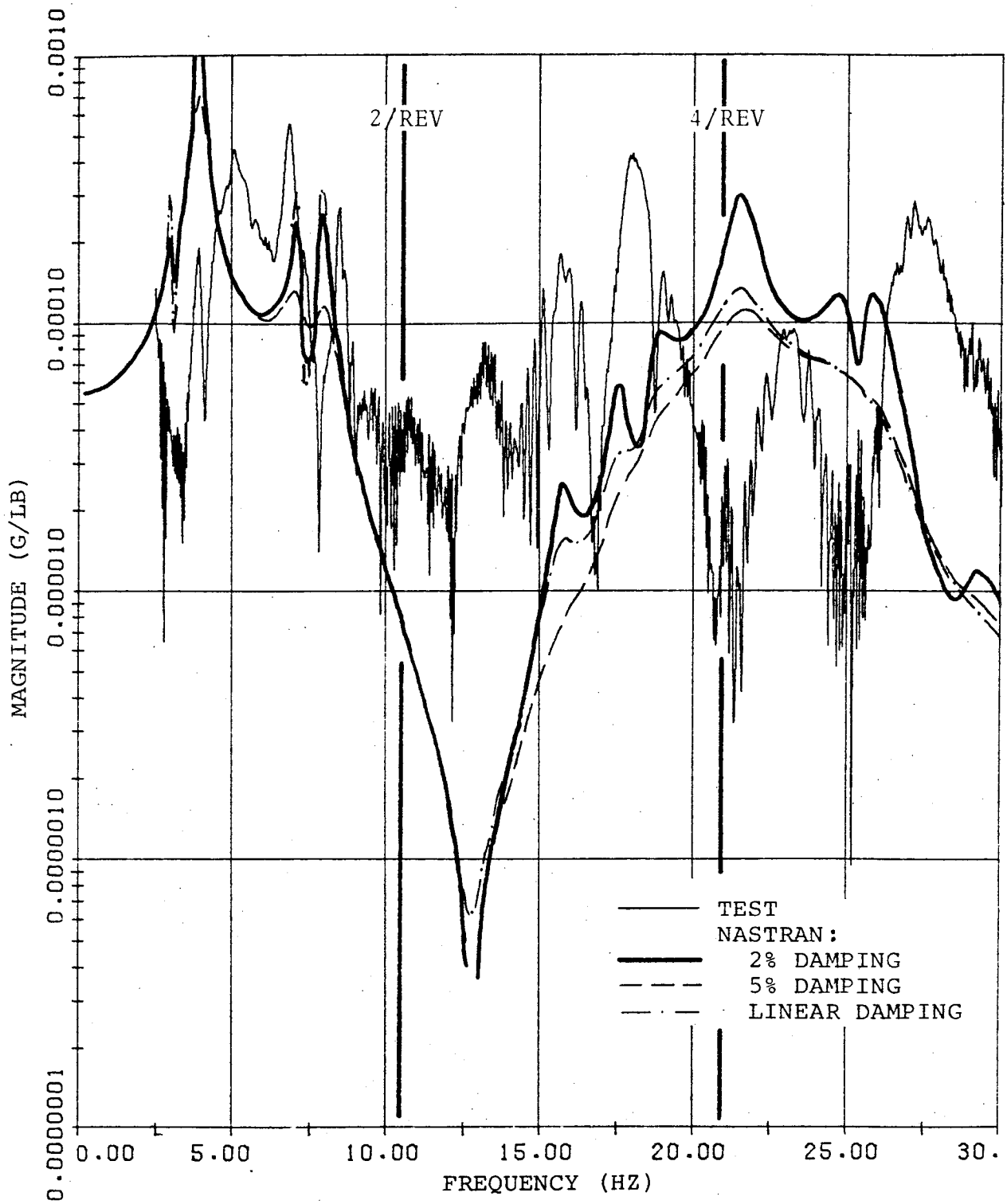

Figure A-14. Frequency Response, Lateral Hub Shake (Clean Wing) 2%, 5% and Linear Damping - 90° Gearbox Lateral.

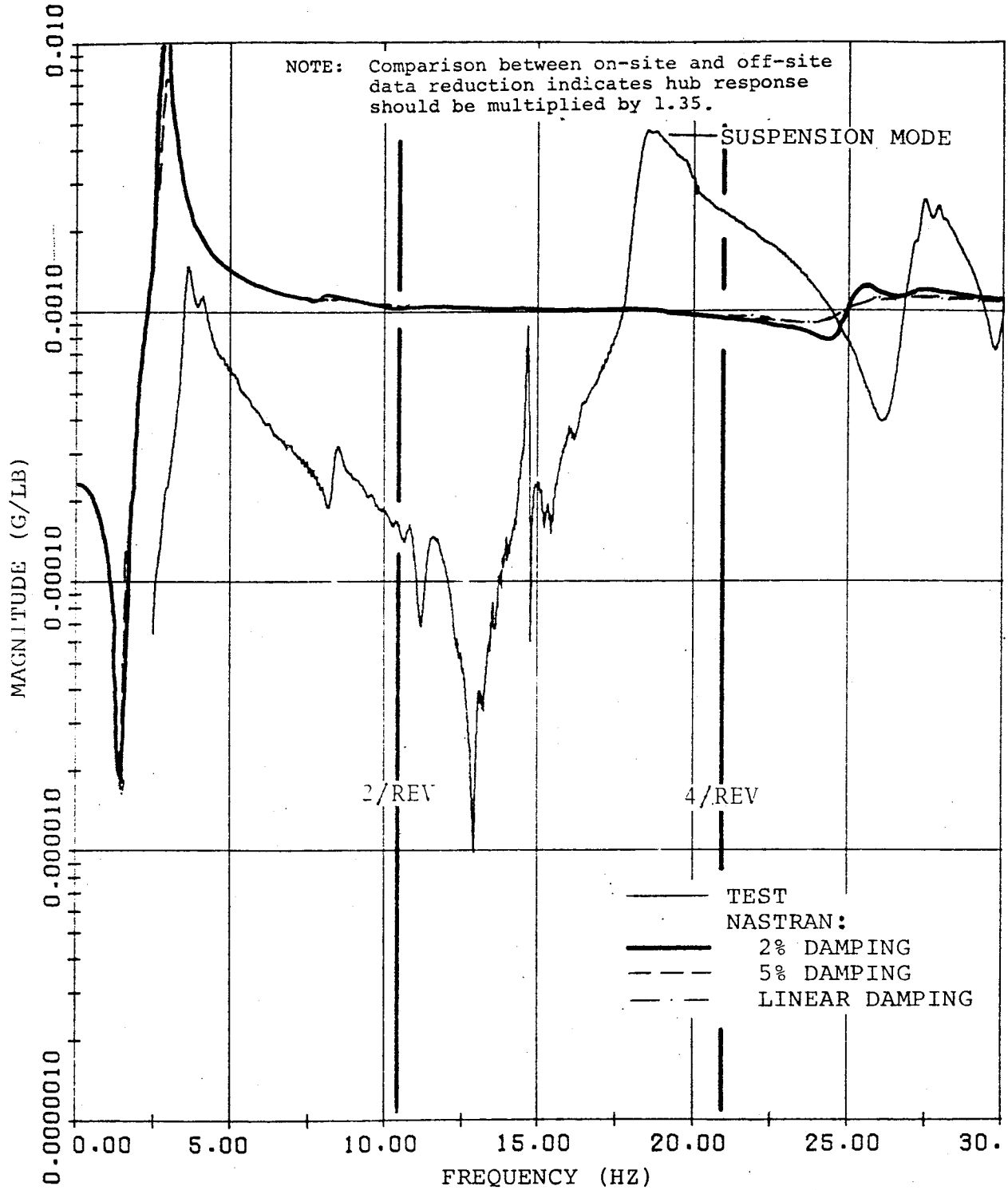

Figure A-15. Frequency Response, Fore-and-Aft Hub Shake (Clean Wing) 2%, 5% and Linear Damping - Hub Fore-and-Aft.

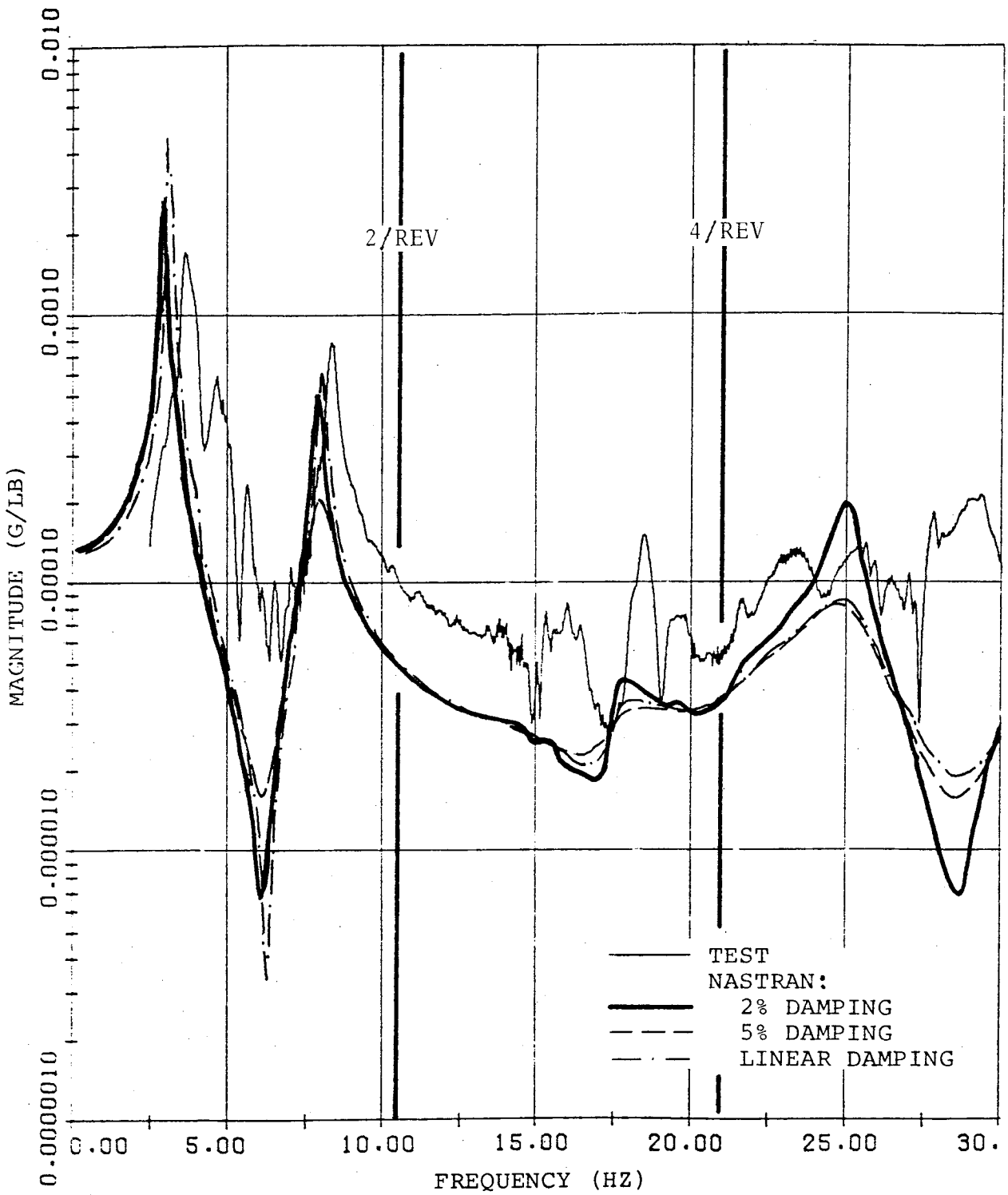

Figure A-16. Frequency Response, Fore-and-Aft Hub Shake (Clean Wing) 2%, 5% and Linear Damping - Gunner Seat Vertical.

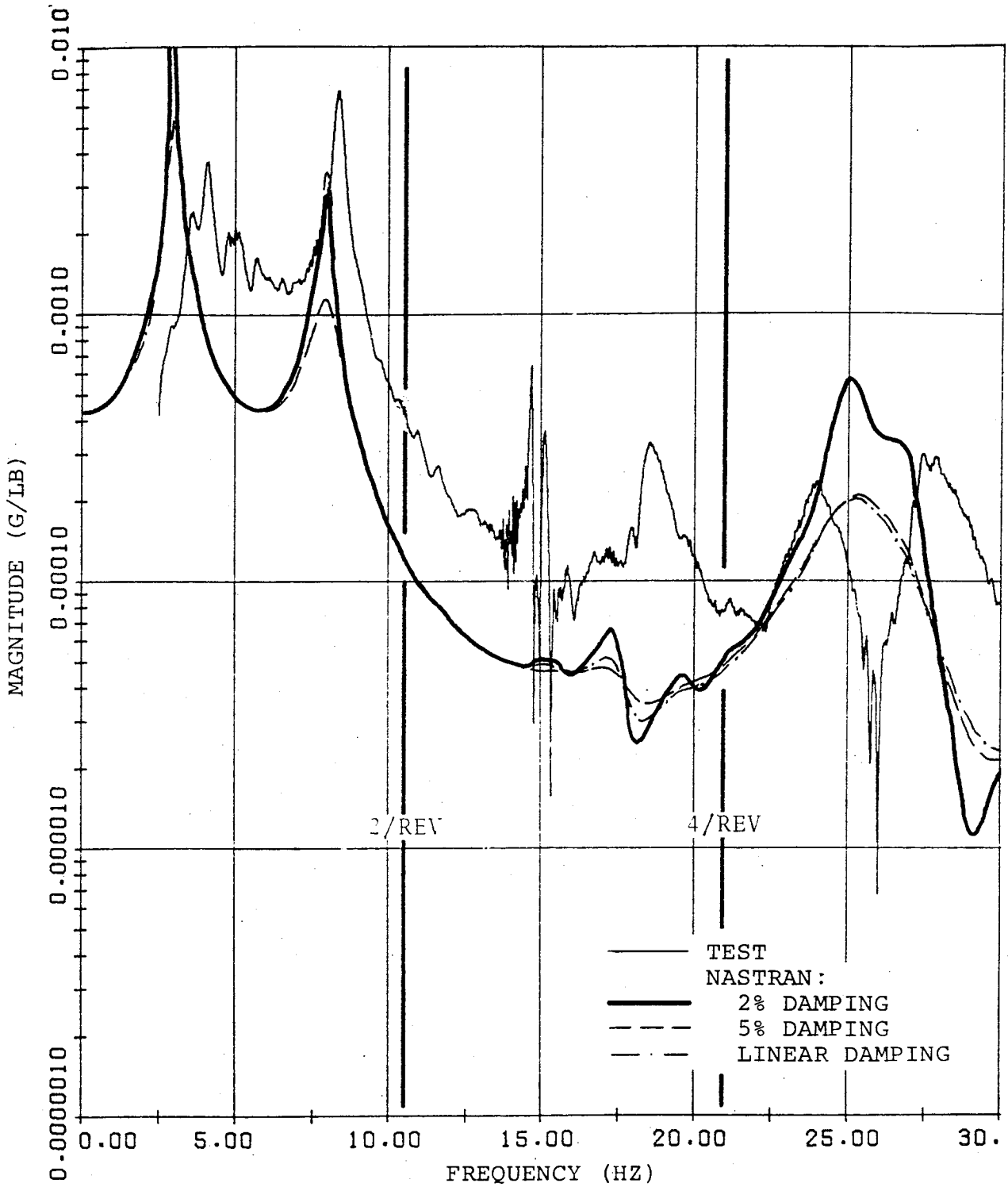

Figure A-17. Frequency Response, Fore-and-Aft Hub Shake (Clean Wing) 2%, 5% and Linear Damping - 90° Gearbox Vertical.

APPENDIX B

FREQUENCY RESPONSE DATA COMPARISONS (MAGNITUDE AND PHASE)

This appendix contains figures showing frequency response comparisons (magnitude and phase) between NASTRAN and test results. The NASTRAN results shown were determined using 2 percent modal damping. The figure number, forcing condition, helicopter configuration and response location for each comparison are given in Table B1. Main rotor two-per-rev (10.8 Hz) and four-per-rev (21.6 Hz) excitation frequencies are indicated on the figure.

TABLE B1. - FREQUENCY RESPONSE DATA COMPARISONS - MAGNITUDE AND PHASE

Figure number	Applied force location/direction	Configuration	Response location/direction
B-1	Tail/vertical	Clean wing	Gunner seat/vertical
B-2	Tail/vertical	Clean wing	Pilot seat/vertical
B-3	Tail/vertical	Clean wing	Engine deck (FS 250)/ vertical
B-4	Tail/vertical	Clean wing	Elevator/vertical
B-5	Tail/vertical	Clean wing	Tail (FS 485)/vertical
B-6	Tail/vertical	Clean wing	90° gearbox/vertical
B-7	Tail/vertical	Clean wing	Left wing tip/vertical
B-8	Tail/vertical	Clean wing	Right wing tip/vertical
B-9	Tail/vertical	With stores	Gunner seat/vertical
B-10	Tail/vertical	With stores	Pilot seat/vertical
B-11	Tail/vertical	With stores	Engine deck (FS 250)/ vertical
B-12	Tail/vertical	With stores	Elevator/vertical
B-13	Tail/vertical	With stores	Tail (FS 485)/vertical
B-14	Tail/vertical	With stores	90° gearbox/vertical
B-15	Tail/vertical	With stores	Left wing tip/vertical
B-16	Tail/vertical	With stores	Right wing tip/vertical
B-17	Tail/lateral	Clean wing	Gunner seat/lateral
B-18	Tail/lateral	Clean wing	Pilot seat/lateral
B-19	Tail/lateral	Clean wing	Engine deck (FS 250)/ lateral
B-20	Tail/lateral	Clean wing	Elevator/lateral
B-21	Tail/lateral	Clean wing	Tail (FS 485)/lateral

TABLE B1. - Continued

Figure number	Applied force location/direction	Configuration	Response location/direction
B-22	Tail/lateral	Clean wing	Top of fin/lateral
B-23	Tail/lateral	Clean wing	Left wing tip/vertical
B-24	Tail/lateral	Clean wing	Right wing tip/vertical
B-25	Tail/lateral	With stores	Gunner seat/lateral
B-26	Tail/lateral	With stores	Pilot seat/lateral
B-27	Tail/lateral	With stores	Engine deck (FS 250)/ Lateral
B-28	Tail/lateral	With stores	Elevator/lateral
B-29	Tail/lateral	With stores	Tail (FS 485)/lateral
B-30	Tail/lateral	With stores	Top of fin/lateral
B-31	Tail/lateral	With stores	Left wing tip/vertical
B-32	Tail/lateral	With stores	Right wing tip/vertical
B-33	Hub/vertical	Clean wing	Hub/vertical
B-34	Hub/vertical	Clean wing	Gunner seat/vertical
B-35	Hub/vertical	Clean wing	Pilot seat/vertical
B-36	Hub/vertical	Clean wing	Engine deck (FS 250)/ vertical
B-37	Hub/vertical	Clean wing	Elevator/vertical
B-38	Hub/vertical	Clean wing	90° gearbox/vertical
B-39	Hub/vertical	Clean wing	Left wing tip/vertical
B-40	Hub/vertical	Clean wing	Right wing tip/vertical
B-41	Hub/lateral	Clean wing	Hub/lateral
B-42	Hub/lateral	Clean wing	Gunner seat/lateral
B-43	Hub/lateral	Clean wing	Pilot seat/lateral

TABLE B1. - Concluded

Figure Number	Applied force location/direction	Configuration	Response location/direction
B-44	Hub/lateral	Clean wing	Engine deck (FS 250)/ Lateral
B-45	Hub/lateral	Clean wing	Elevator/lateral
B-46	Hub/lateral	Clean wing	90° gearbox/vertical
B-47	Hub/lateral	Clean wing	Left wing tip/vertical
B-48	Hub/lateral	Clean wing	Right wing tip/vertical
B-49	Hub/fore-and-aft	Clean wing	Hub/fore-and-aft
B-50	Hub/fore-and-aft	Clean wing	Gunner seat/vertical
B-51	Hub/fore-and-aft	Clean wing	Pilot seat/vertical
B-52	Hub/fore-and-aft	Clean wing	Engine deck (FS 250)/ vertical
B-53	Hub/fore-and-aft	Clean wing	Elevator/vertical
B-54	Hub/fore-and-aft	Clean wing	90° gearbox/vertical
B-55	Hub/fore-and-aft	Clean wing	Left wing tip/vertical
B-56	Hub/fore-and-aft	Clean wing	Right wing tip/vertical

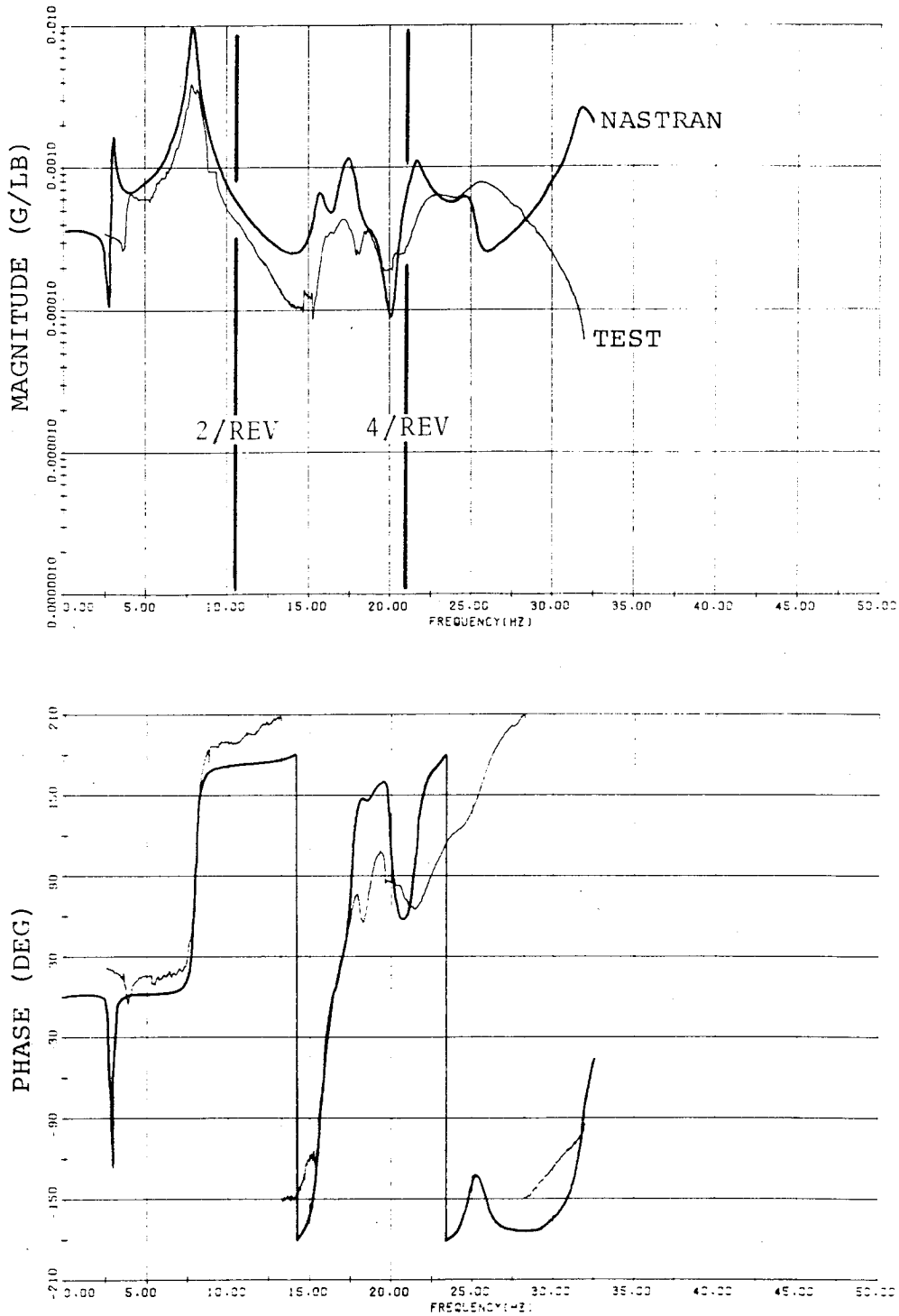

Figure B-1. Tailboom Vertical Shake (Clean Wing) Gunner Seat Vertical Response.

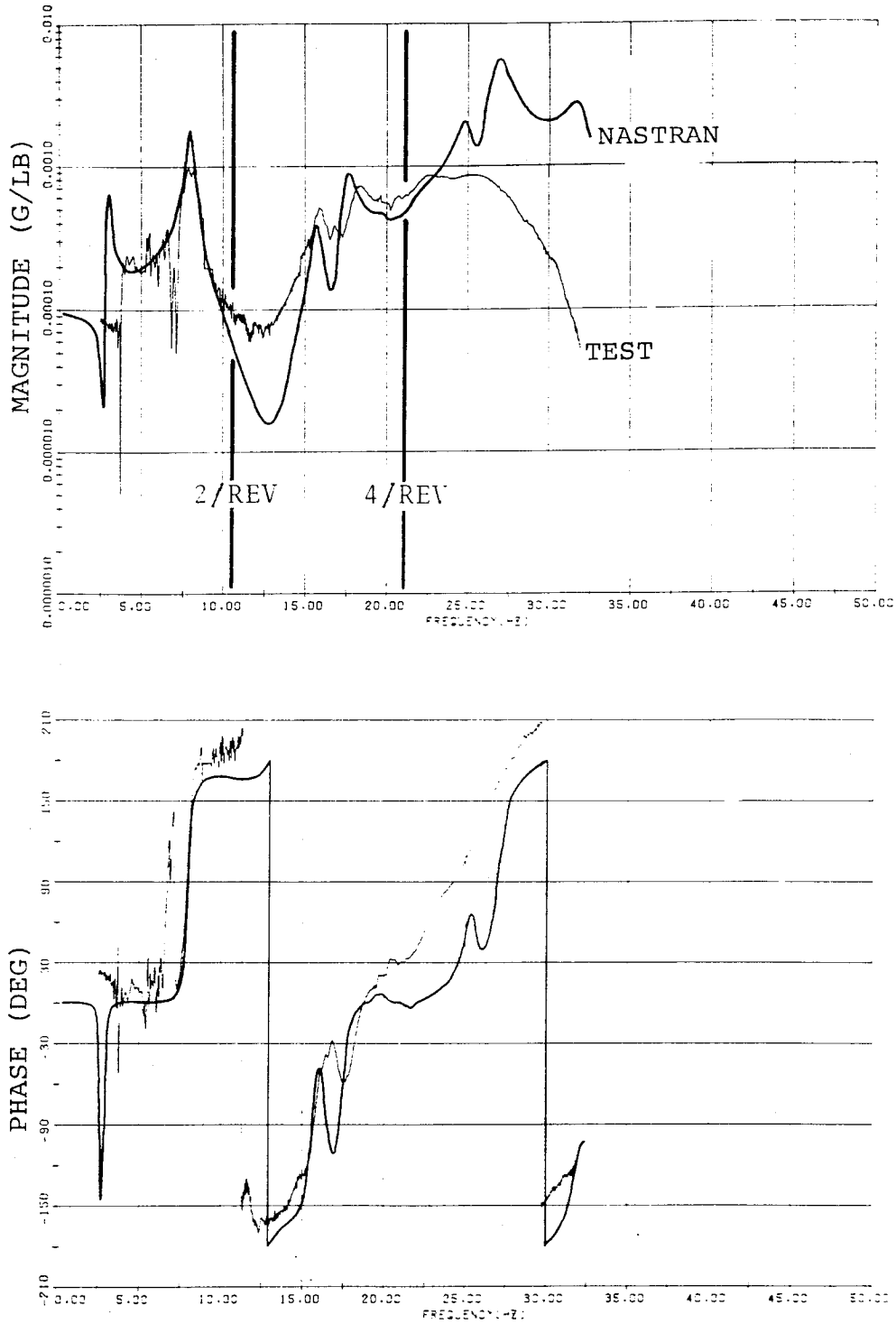

Figure B-2. Tailboom Vertical Shake (Clean Wing) Pilot Seat Vertical Response.

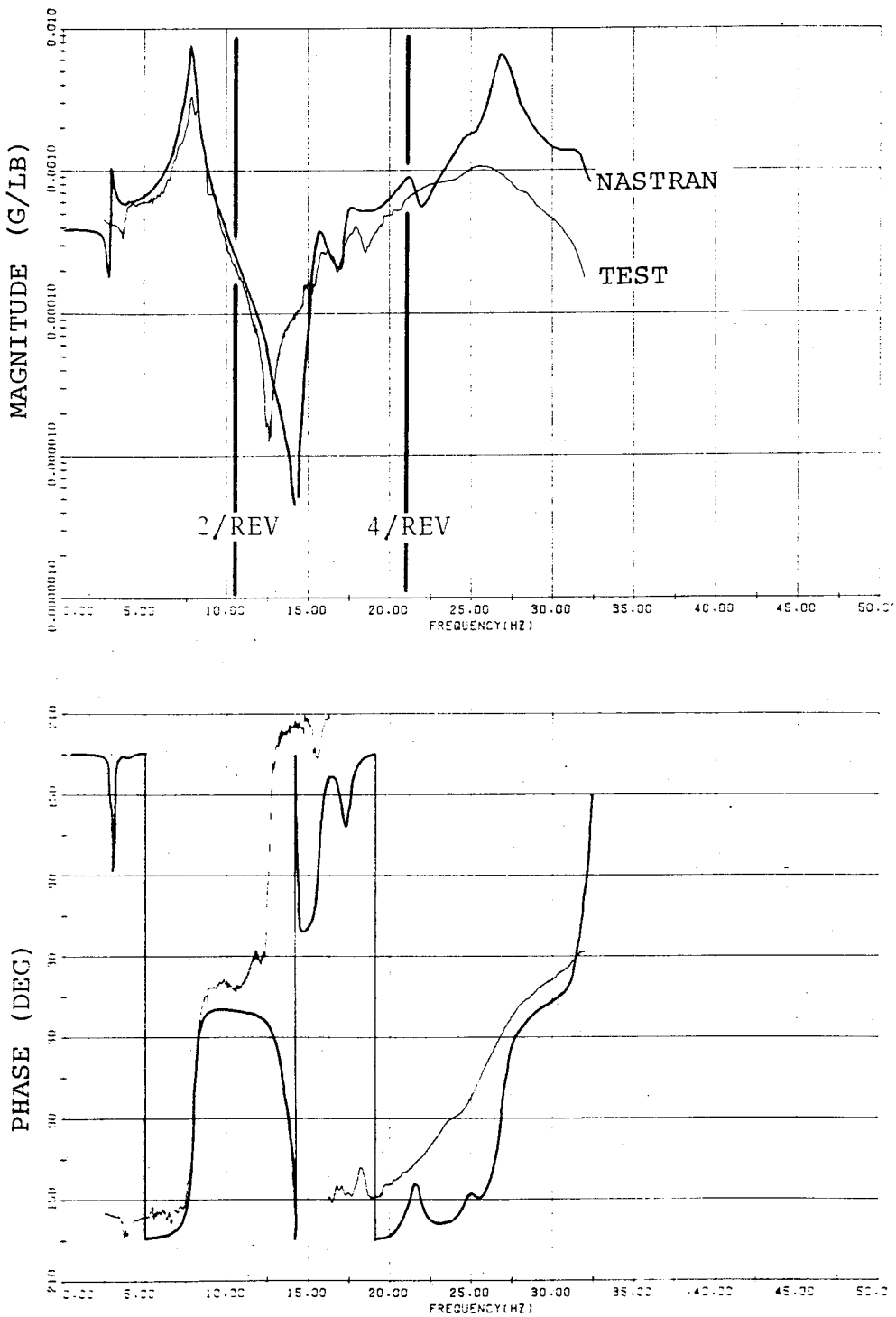

Figure B-3. Tailboom Vertical Shake (Clean Wing) Engine Deck (FS 250) Vertical Response.

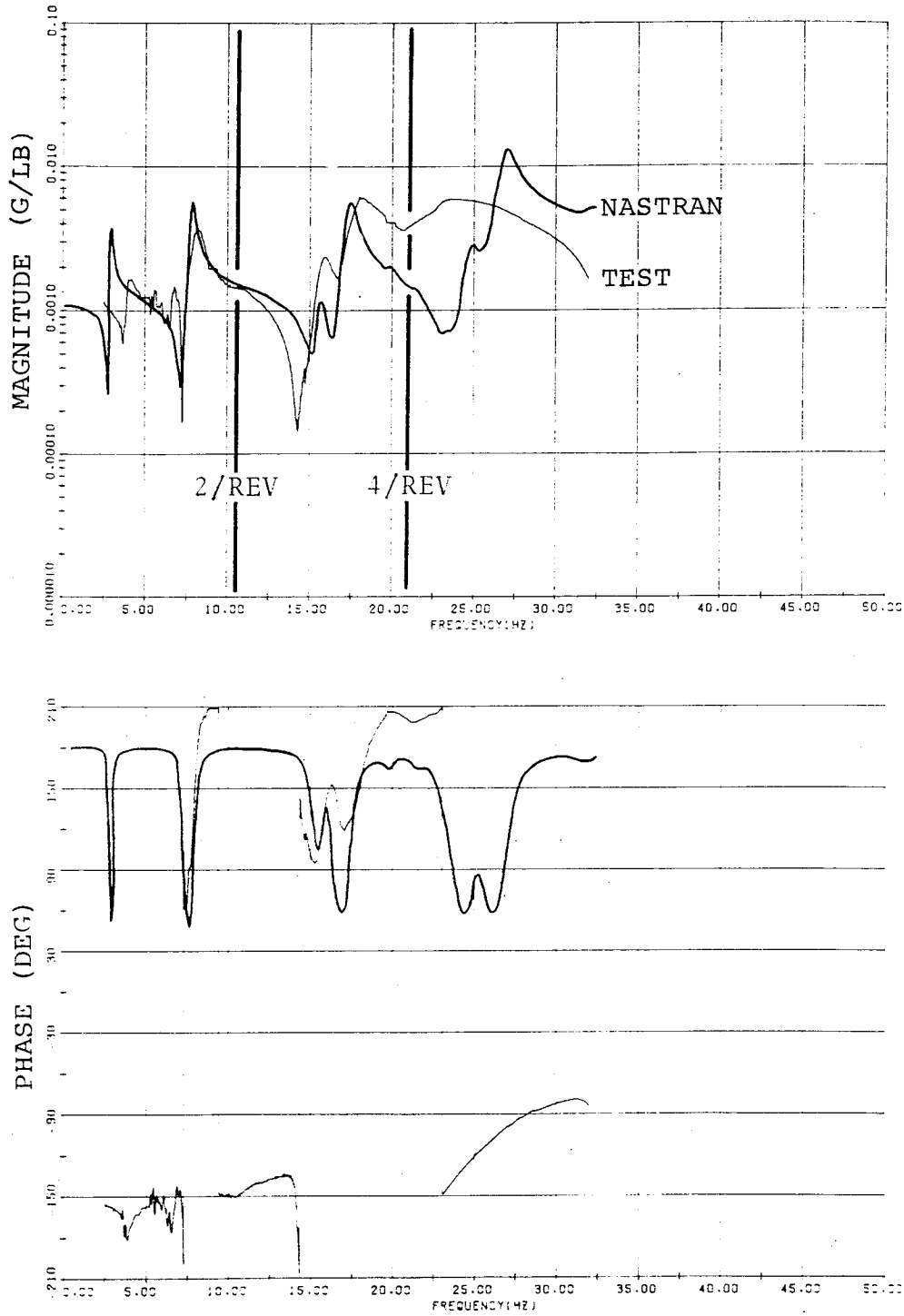

Figure B-4. Tailboom Vertical Shake (Clean Wing) Elevator Vertical Response.

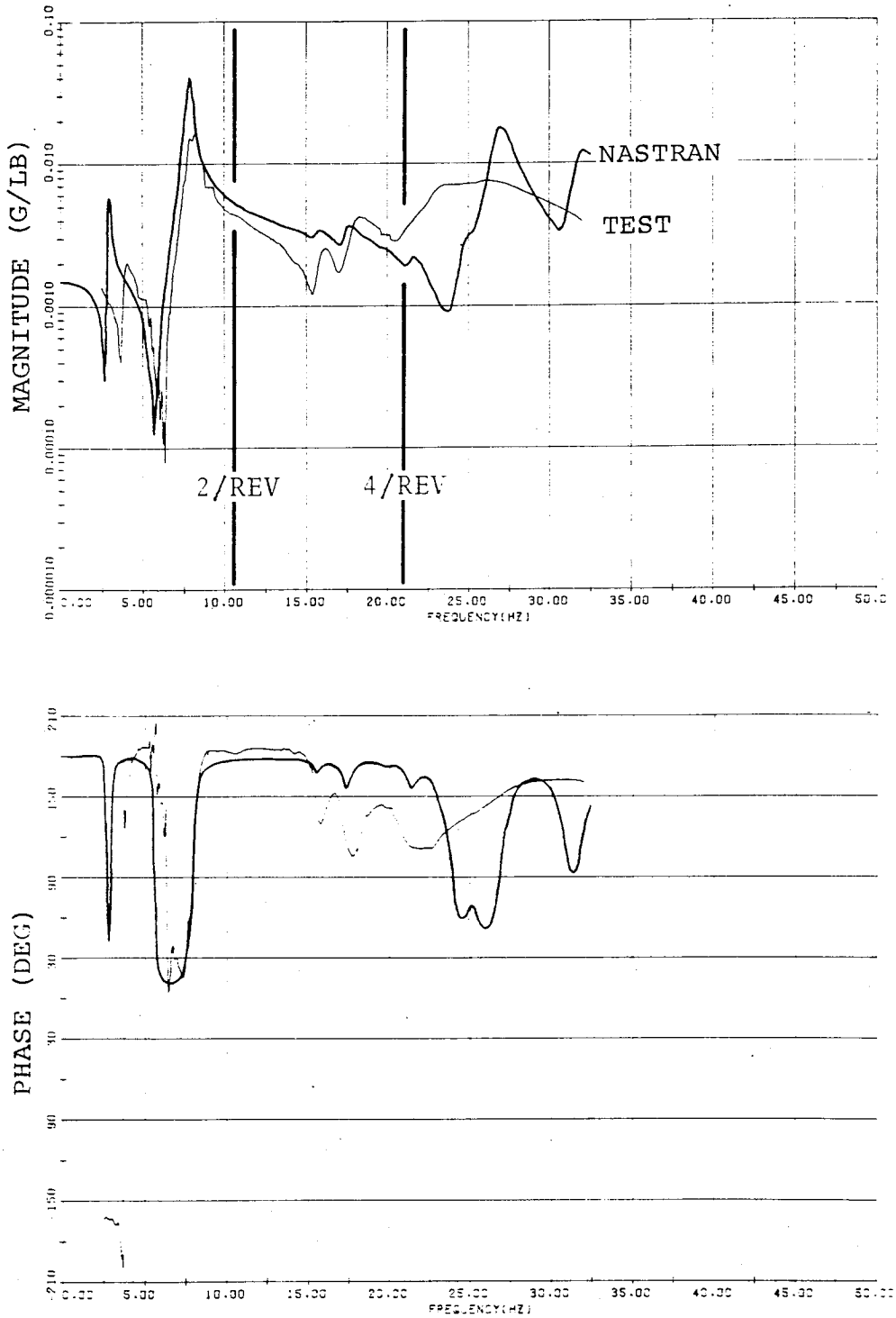

Figure B-5. Tailboom Vertical Shake (Clean Wing) Tail (FS 485) Vertical Response.

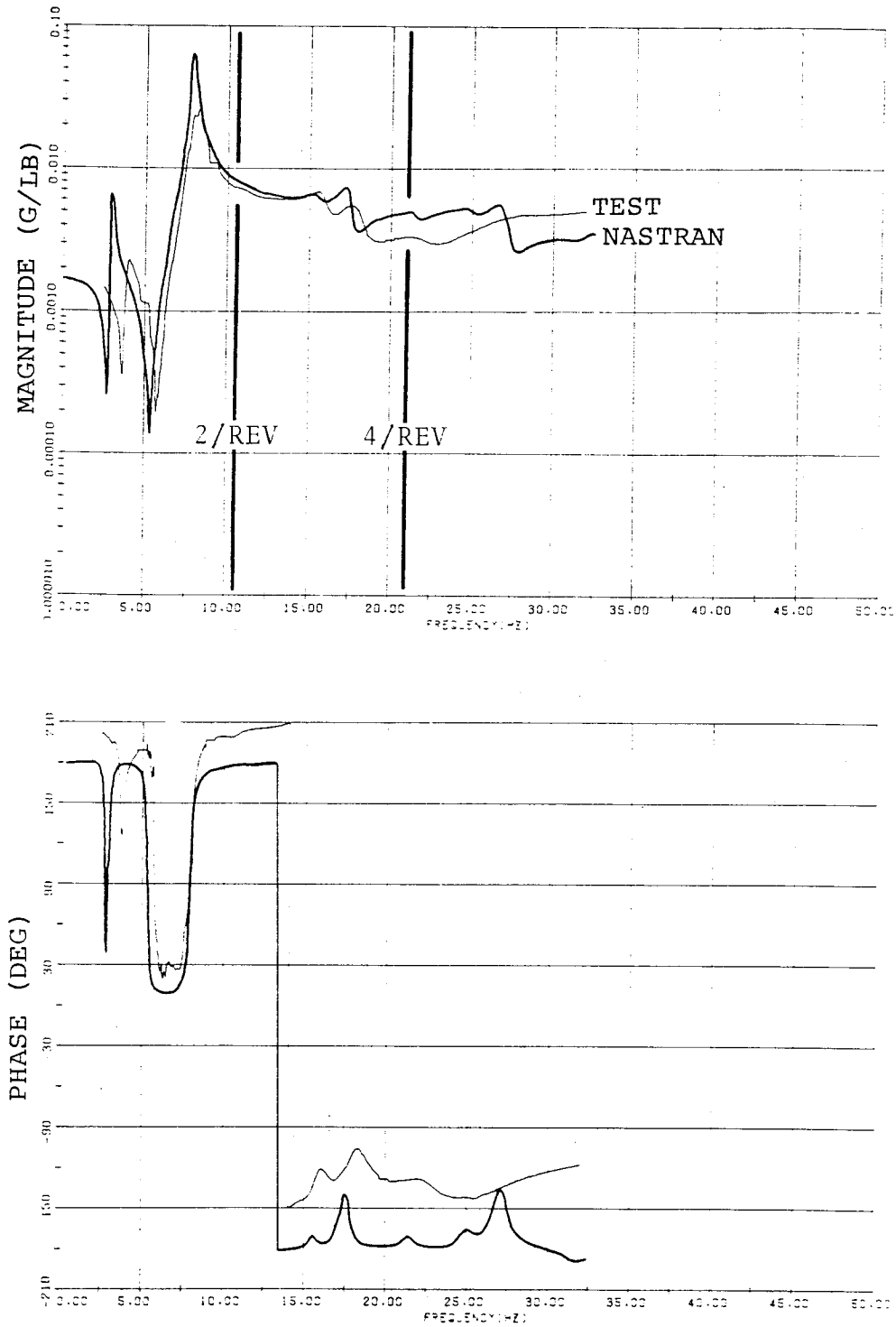

Figure B-6. Tailboom Vertical Shake (Clean Wing) 90° Gearbox Vertical Response.

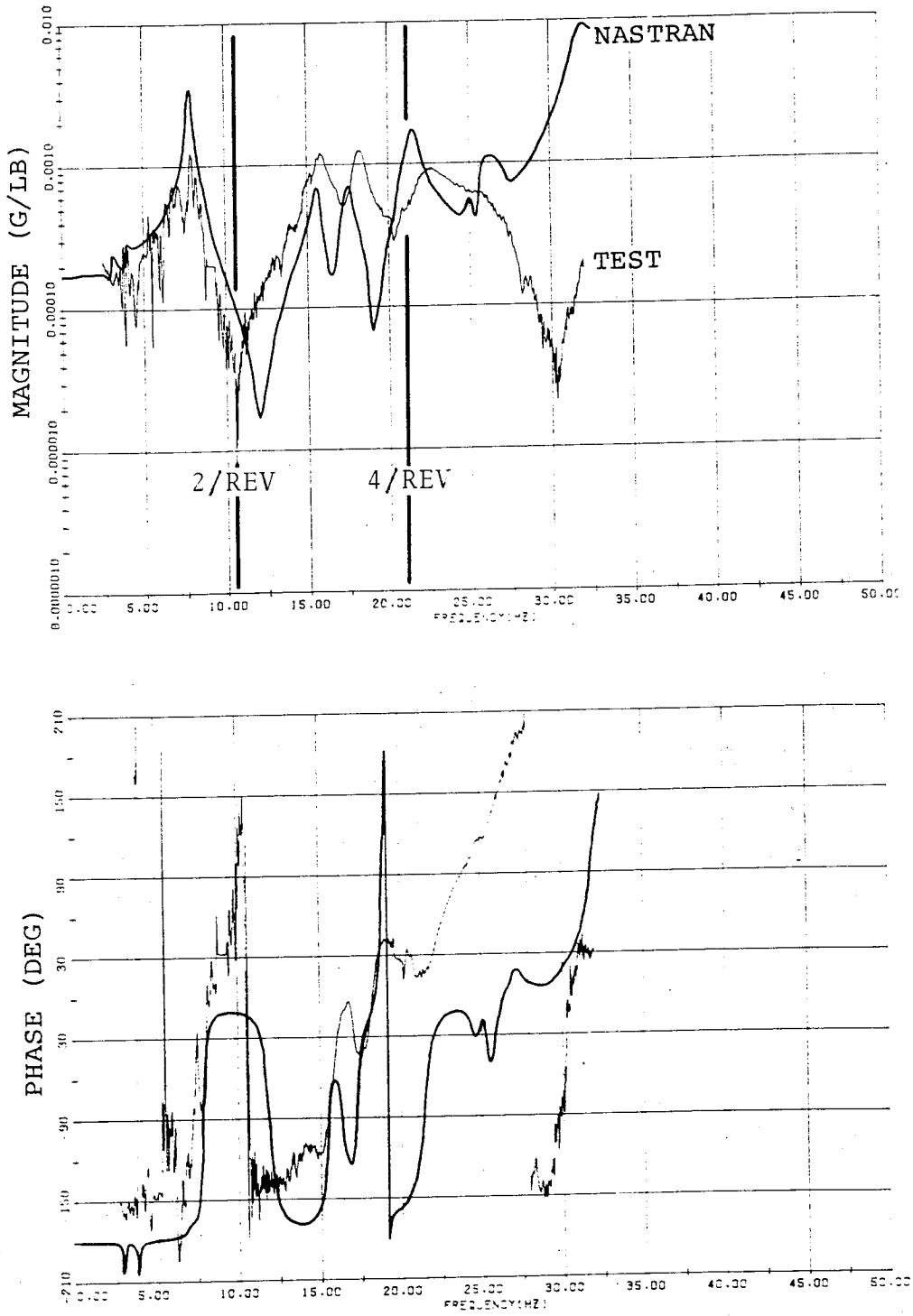

Figure B-7. Tailboom Vertical Shake (Clean Wing) Left Wing Tip Vertical Response.

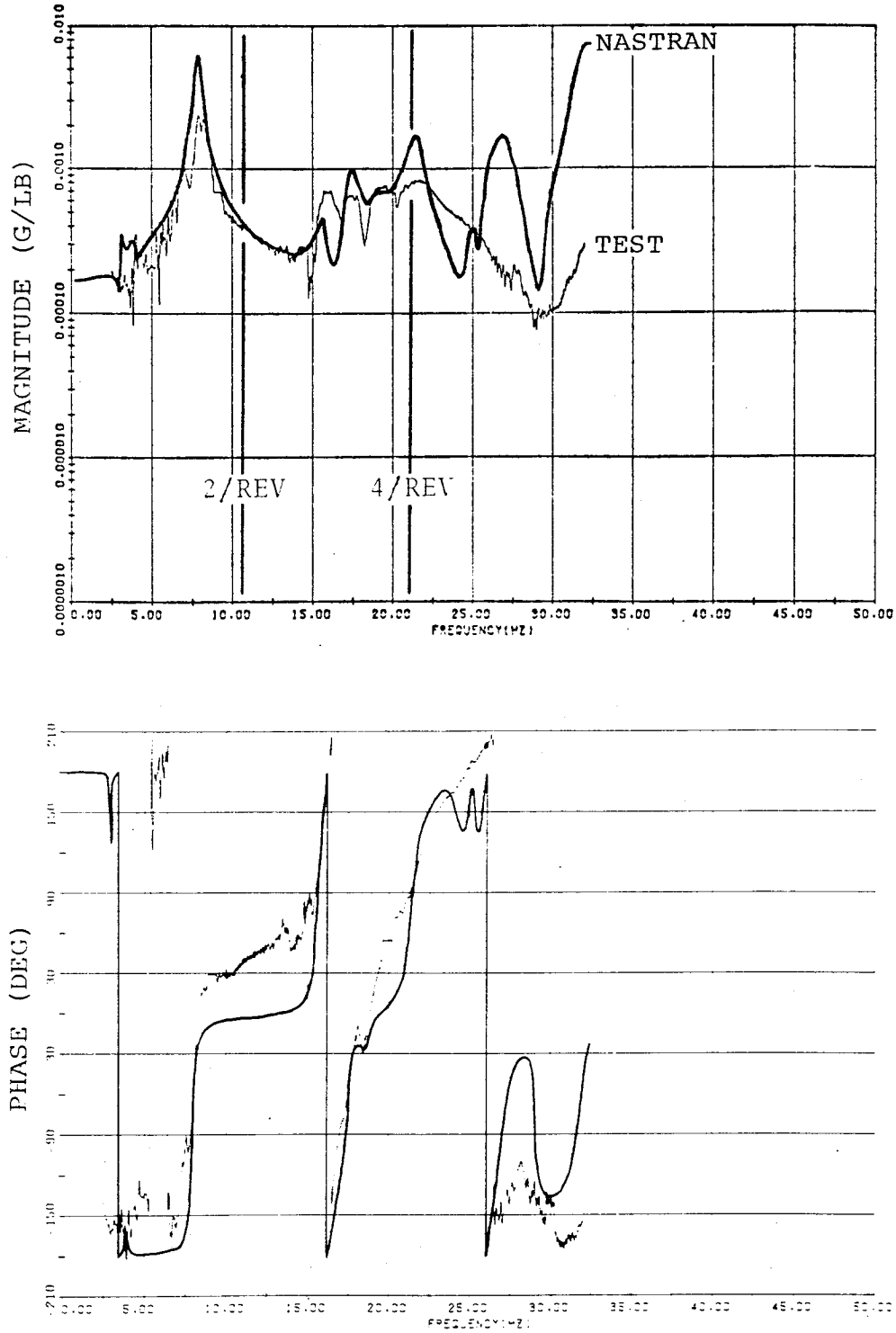

Figure B-8. Tailboom Vertical Shake (Clean Wing) Right Wing Tip Vertical Response.

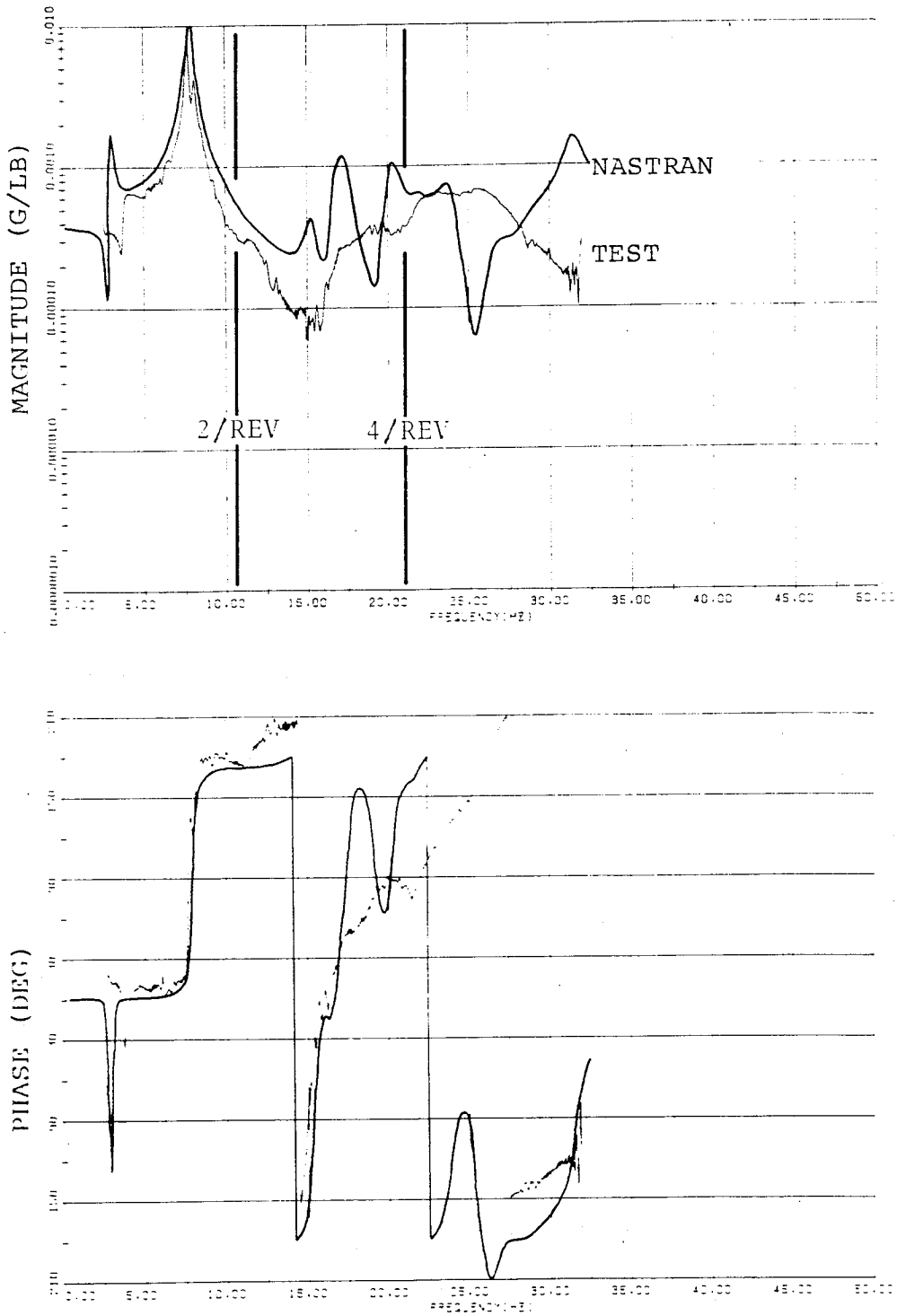

Figure B-9. Tailboom Vertical Shake (With Stores) Gunner Seat Vertical Response.

C-2

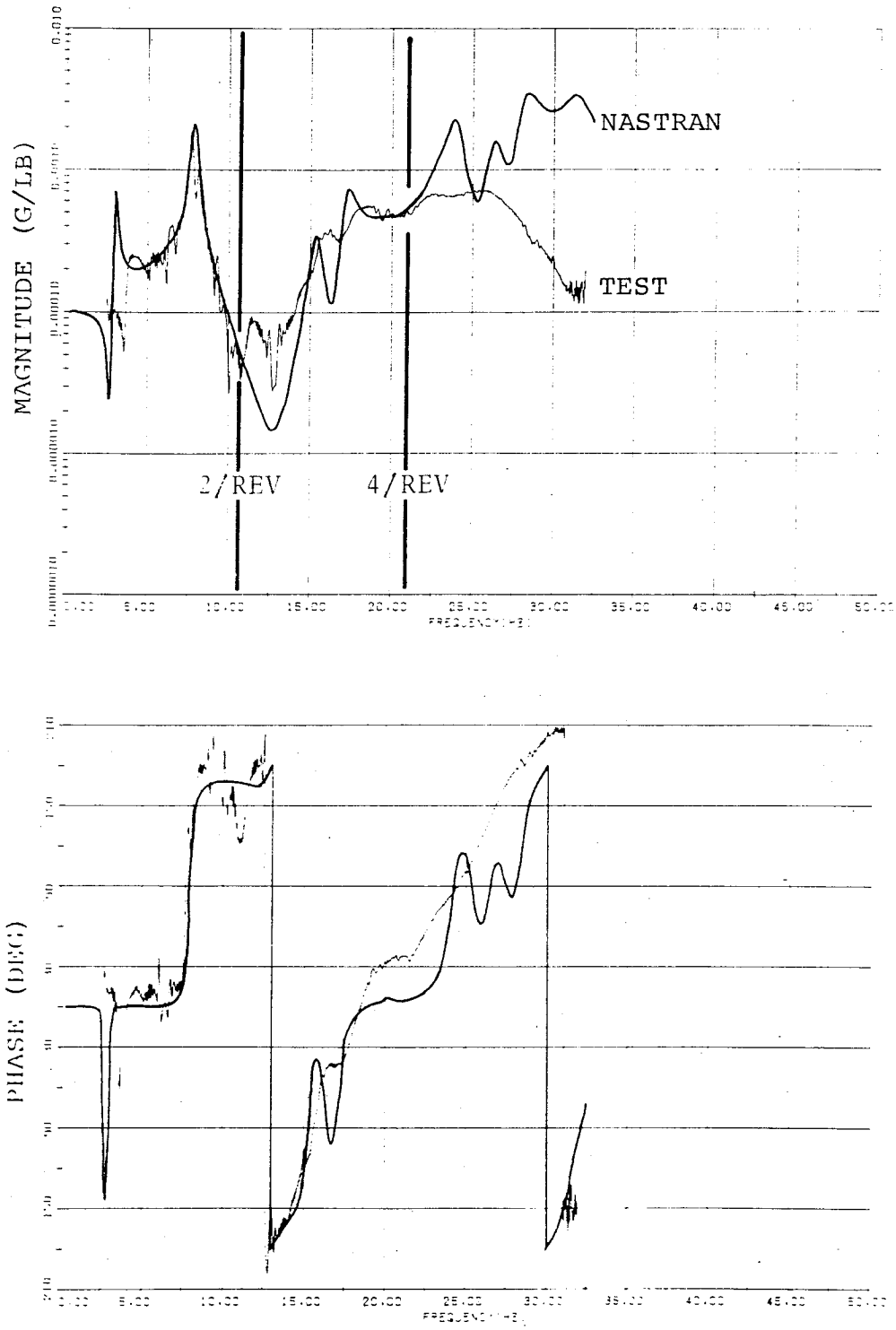

Figure B-10. Tailboom Vertical Shake (With Stores) Pilot Seat Vertical Response.

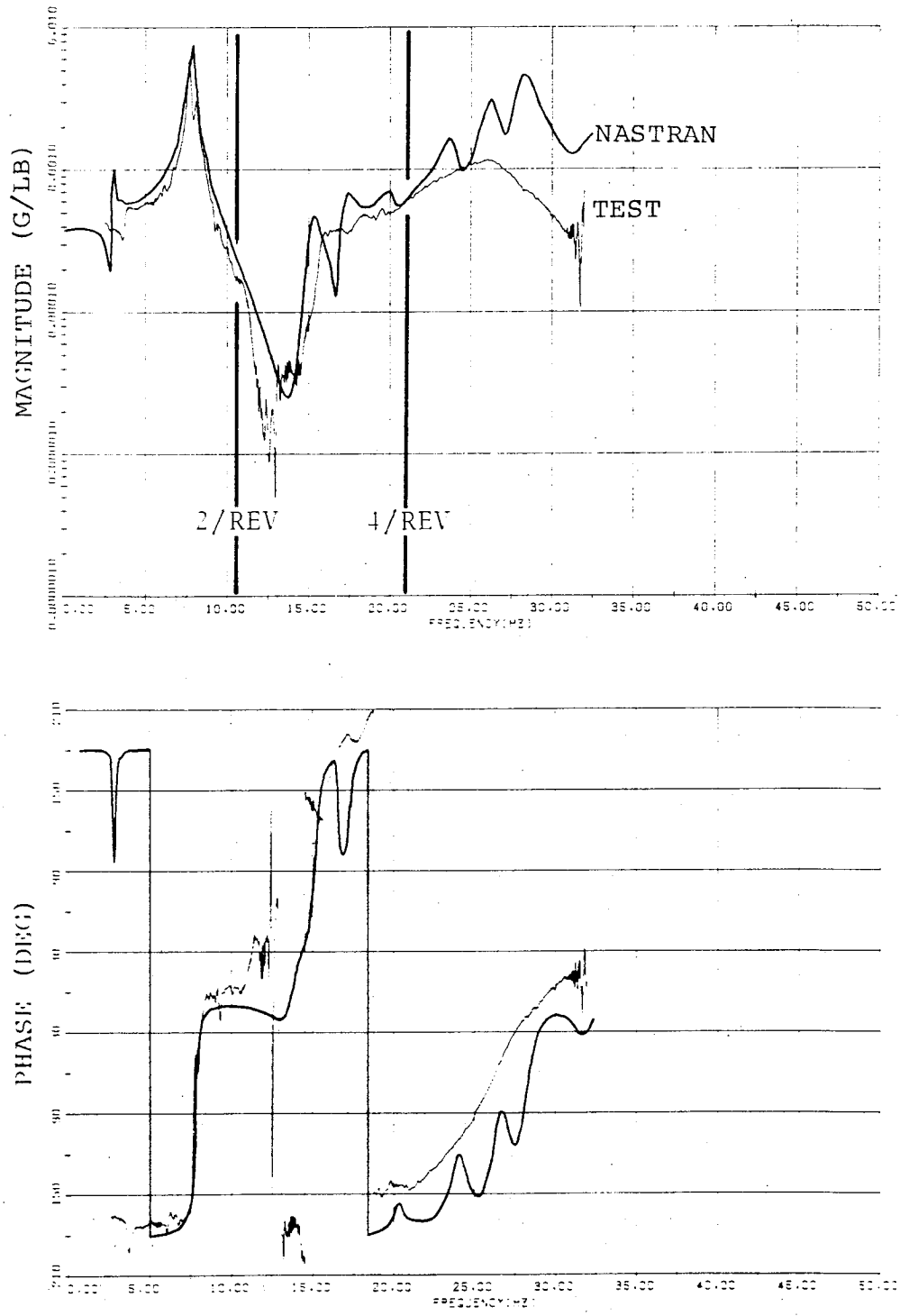

Figure B-11. Tailboom Vertical Shake (With Stores) Engine Deck (FS 250) Vertical Response.

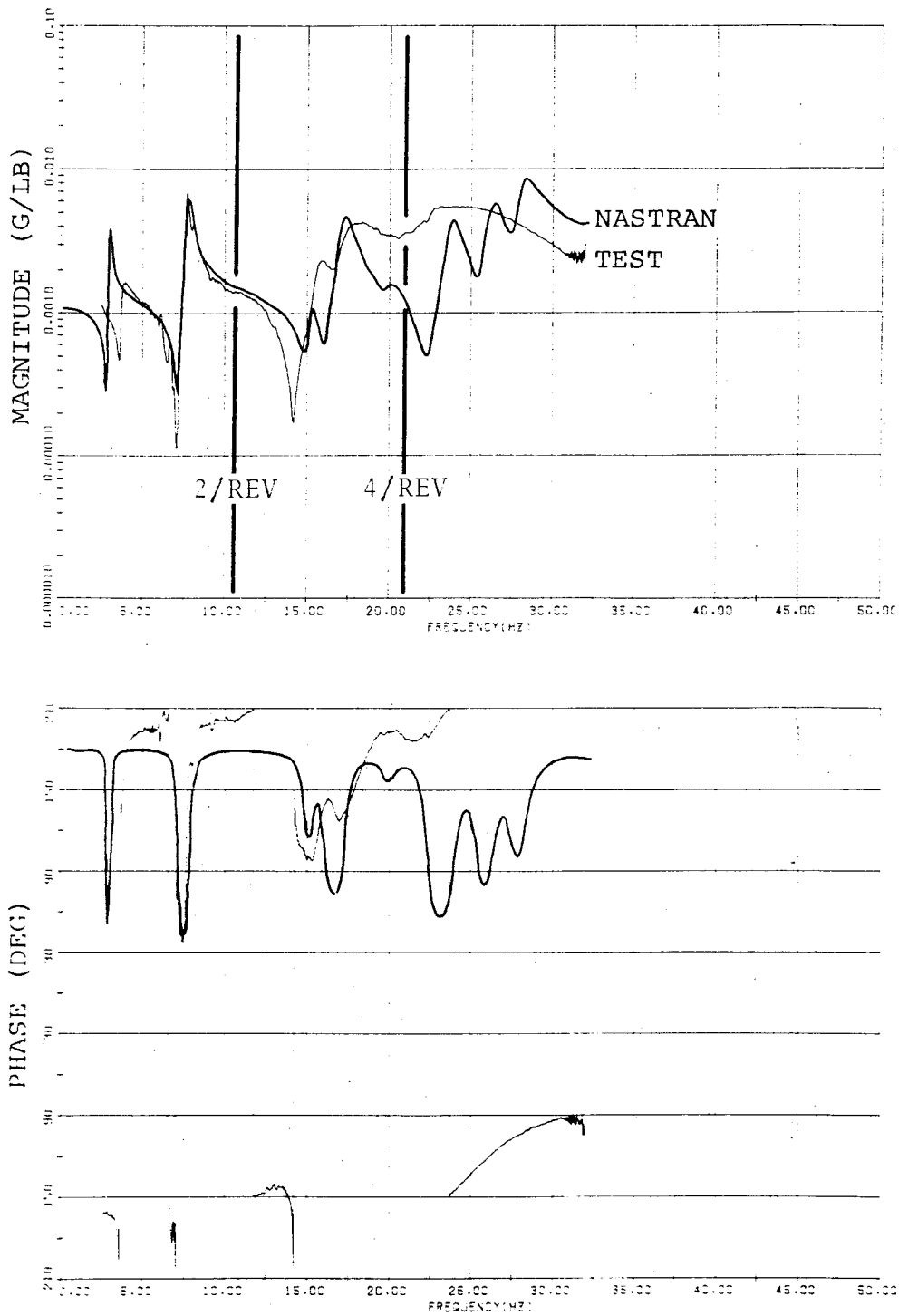

Figure B-12. Tailboom Vertical Shake (With Stores) Elevator Vertical Response.

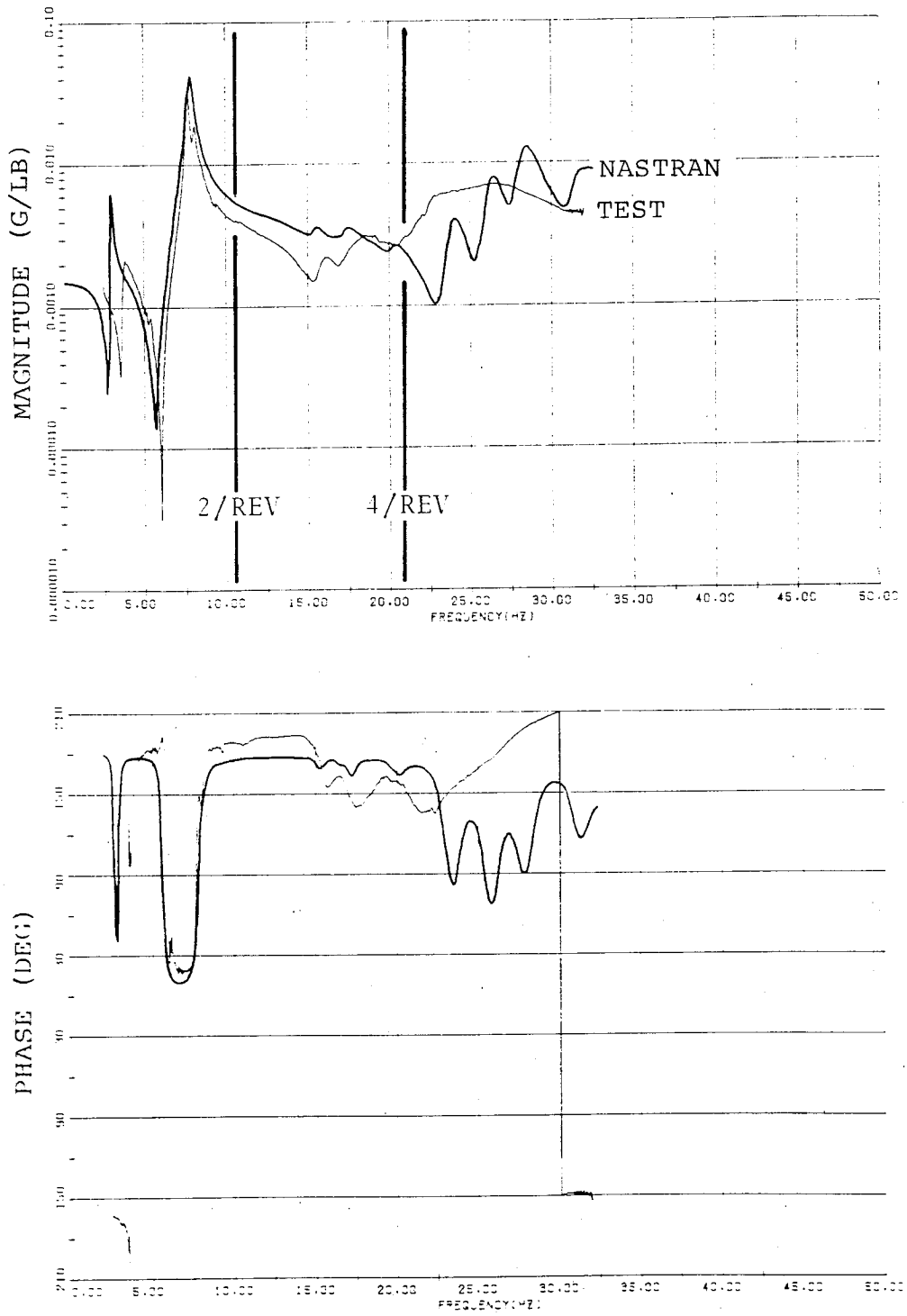

Figure B-13. Tailboom Vertical Shake (With Stores) Tail (FS 485) Vertical Response.

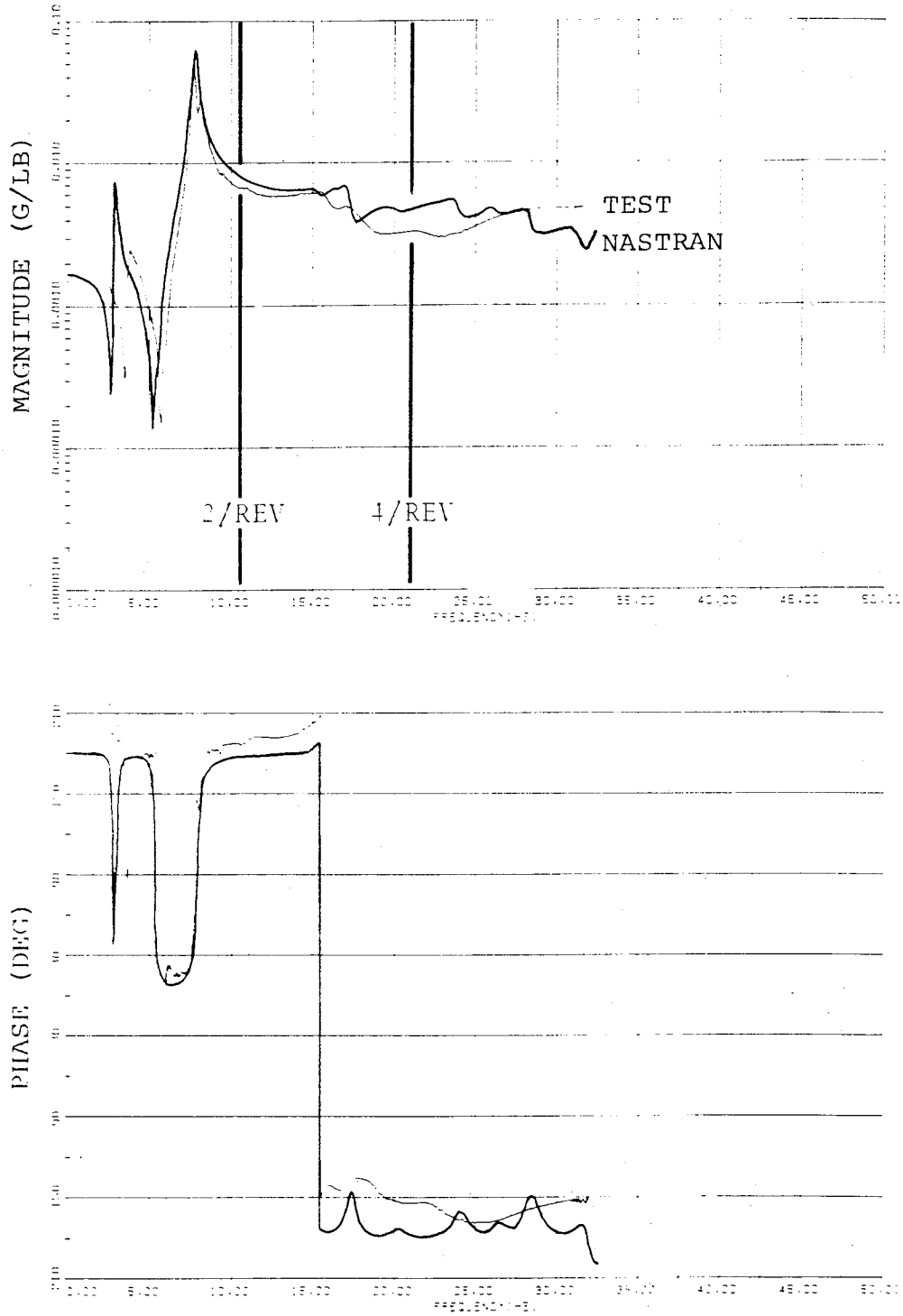

Figure B-14. Tailboom Vertical Shake (With Stores) 90° Gearbox Vertical Response.

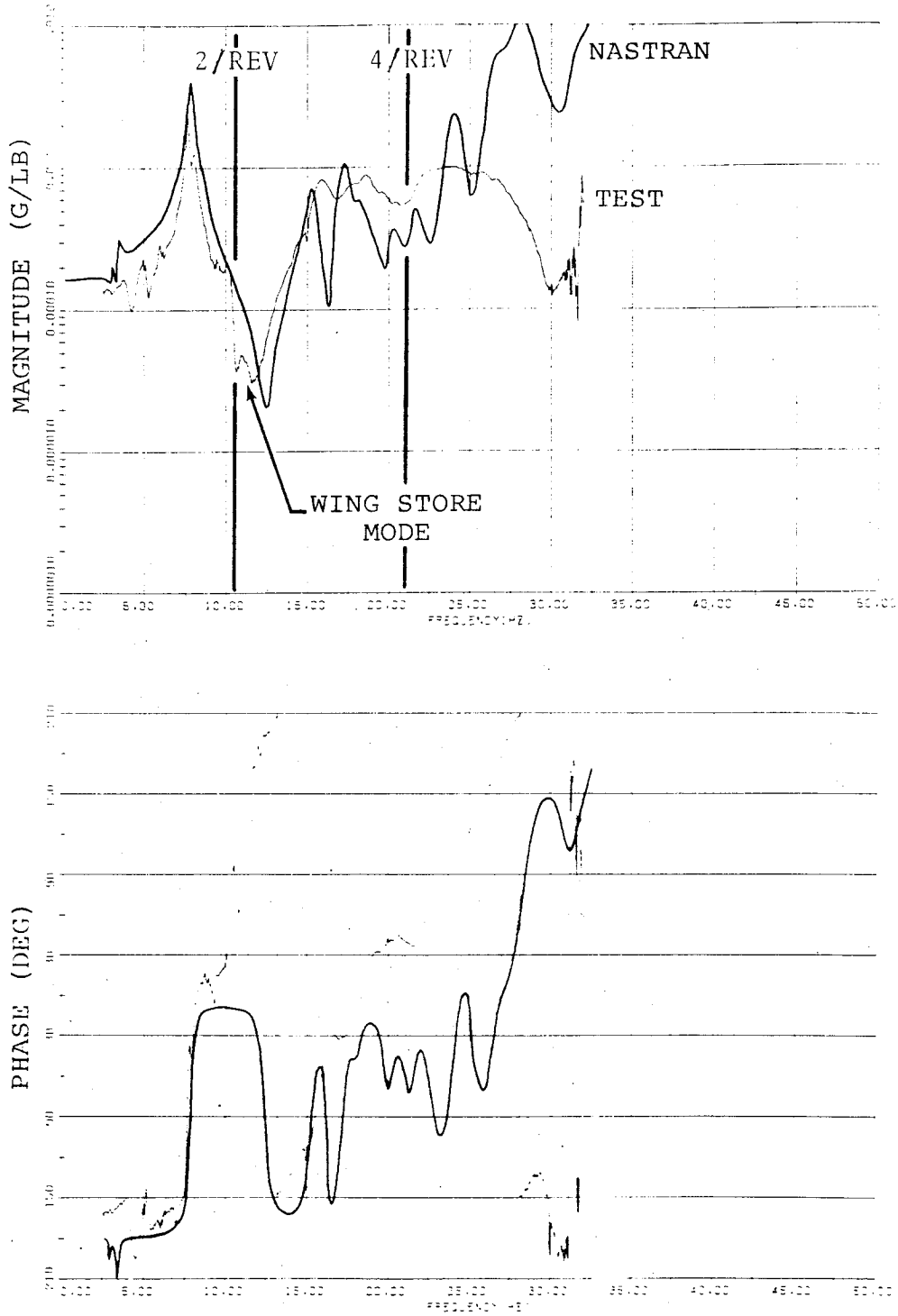

Figure B-15. Tailboom Vertical Shake (With Stores)
Left Wing Tip Vertical Response.

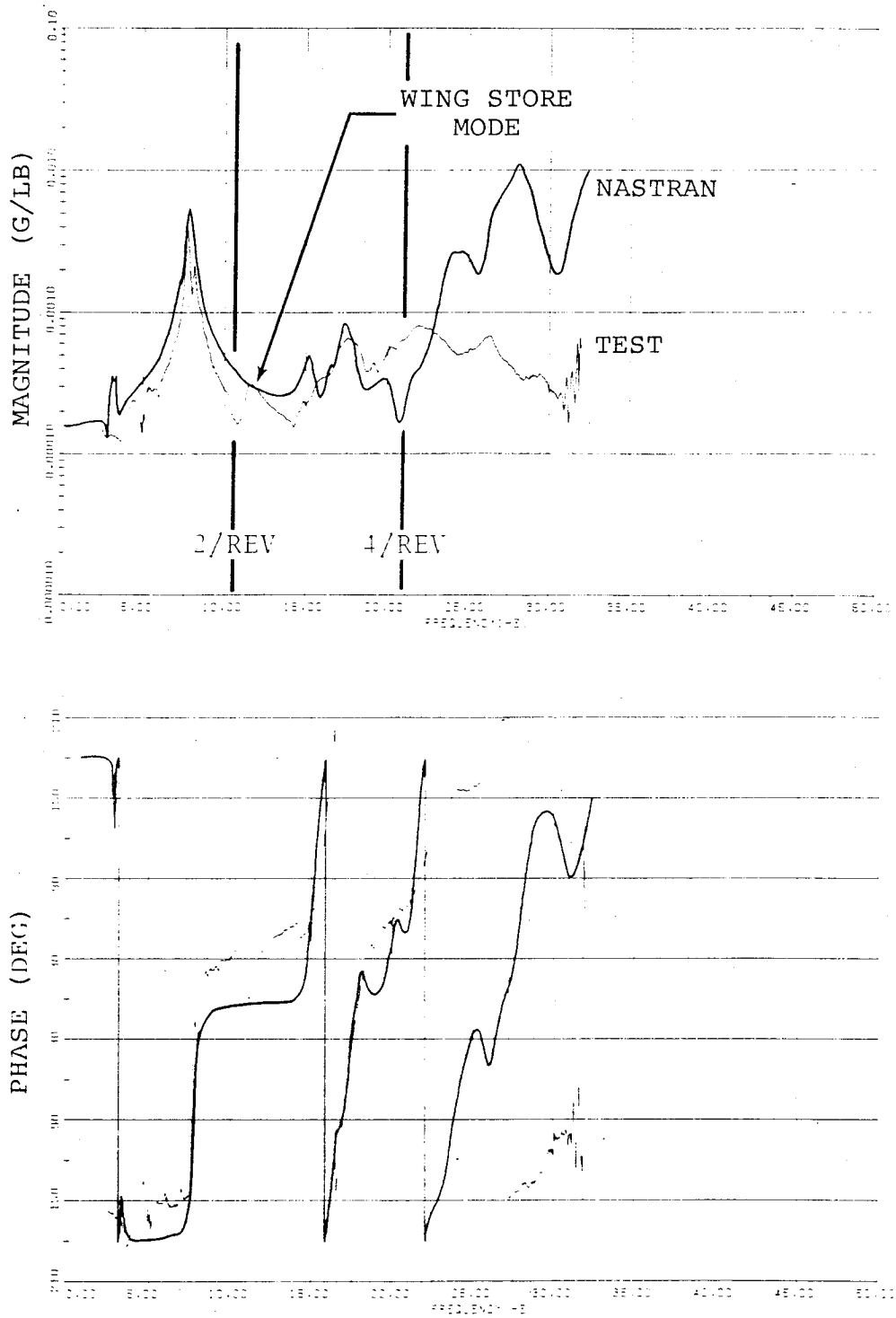

Figure B-16. Tailboom Vertical Shake (With Stores) Right Wing Tip Vertical Response.

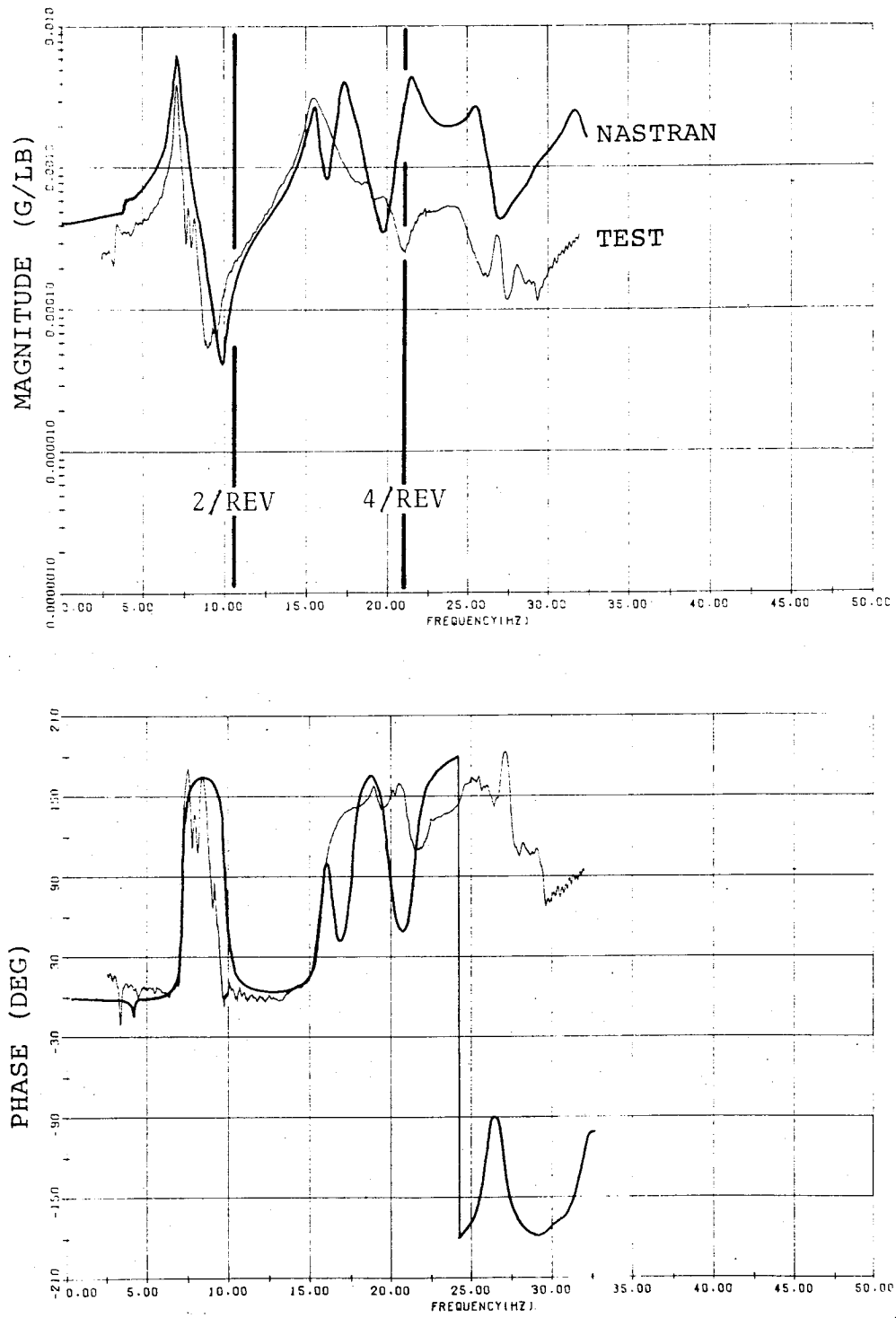

Figure B-17. Tailboom Lateral Shake (Clean Wing) Gunner Seat Lateral Response.

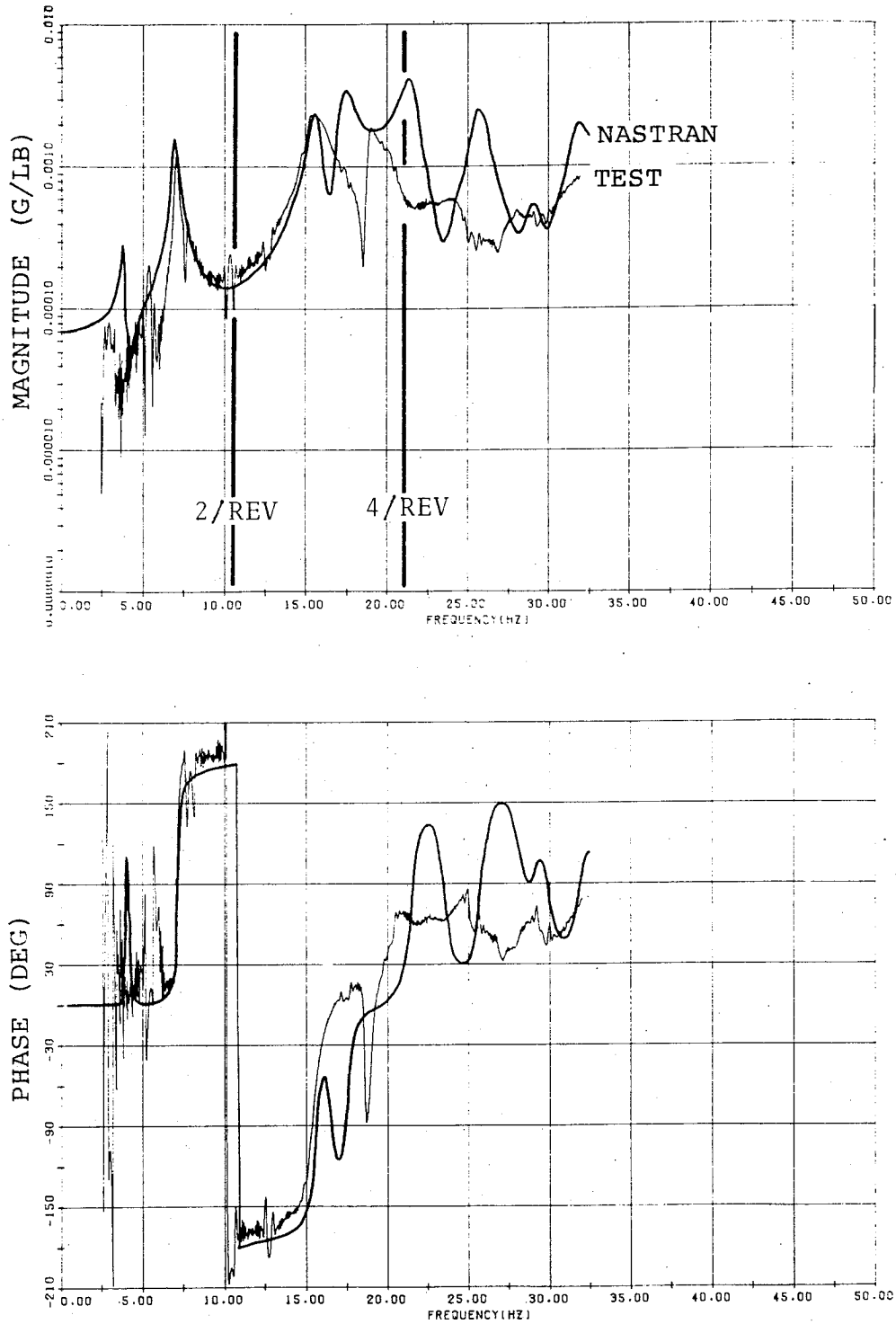

Figure B-18. Tailboom Lateral Shake (Clean Wing) Pilot Seat Lateral Response.

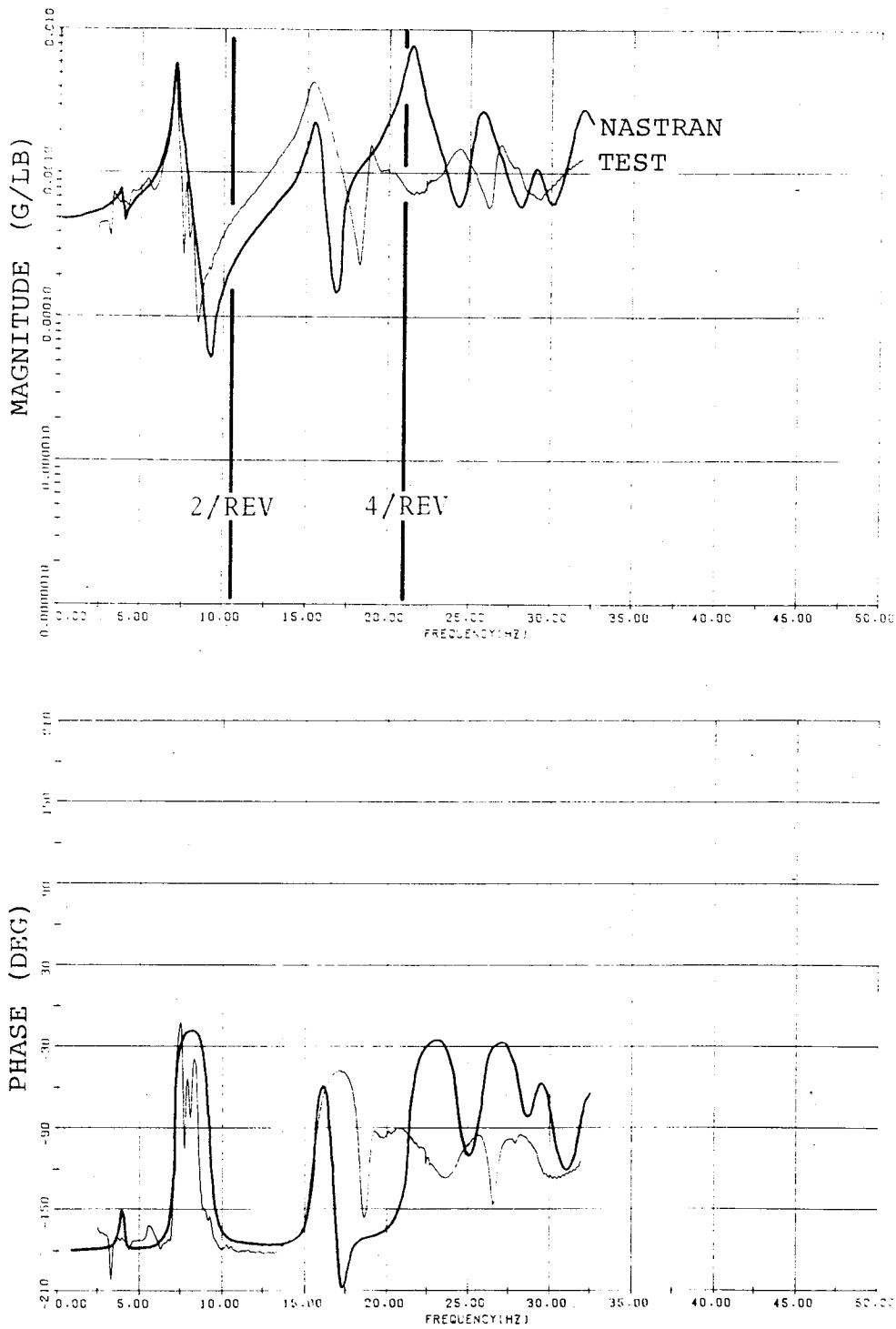

Figure B-19. Tailboom Lateral Shake (Clean Wing) Engine Deck (FS 250) Lateral Response.

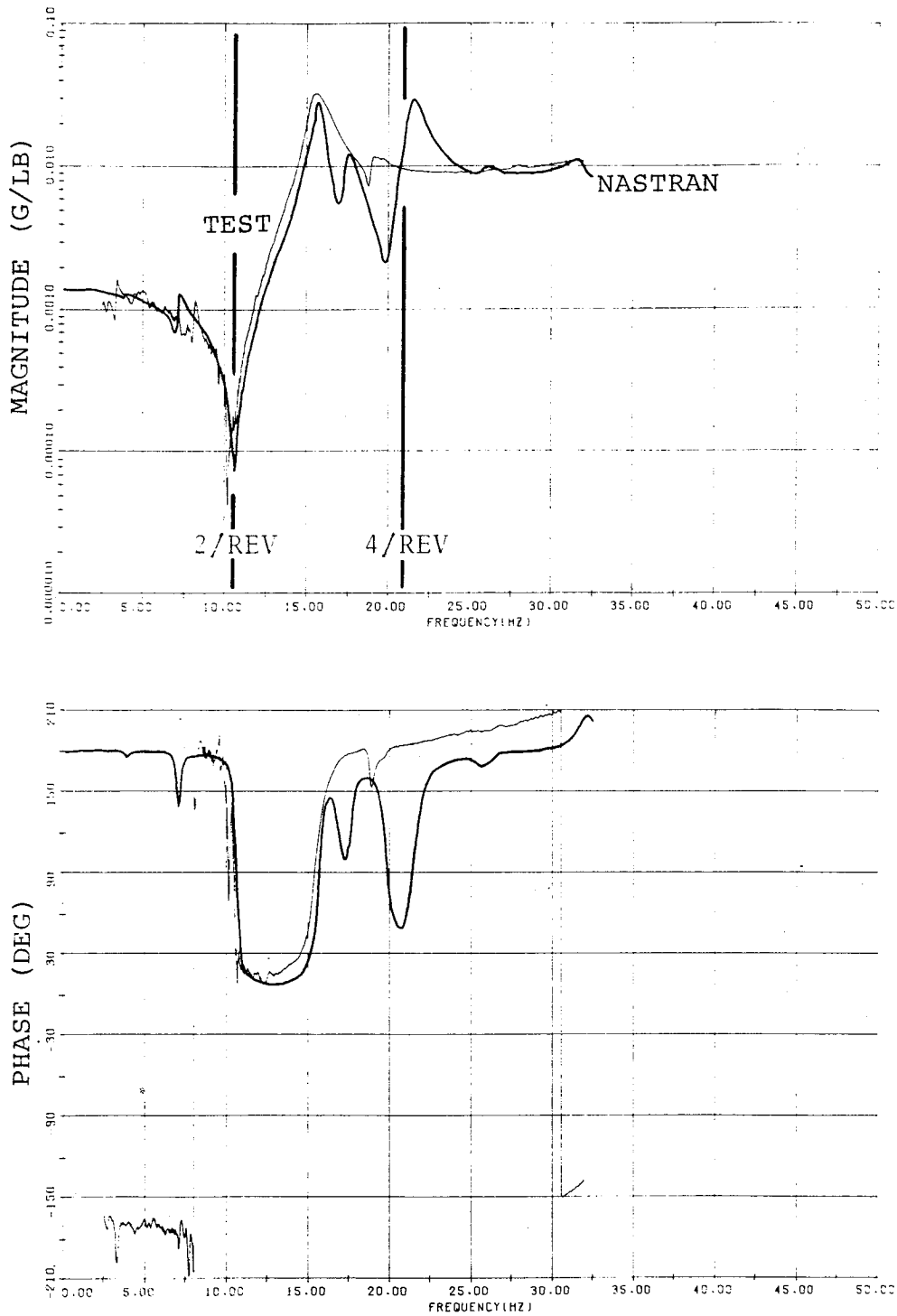

Figure B-20. Tailboom Lateral Shake (Clean Wing) Elevator Lateral Response.

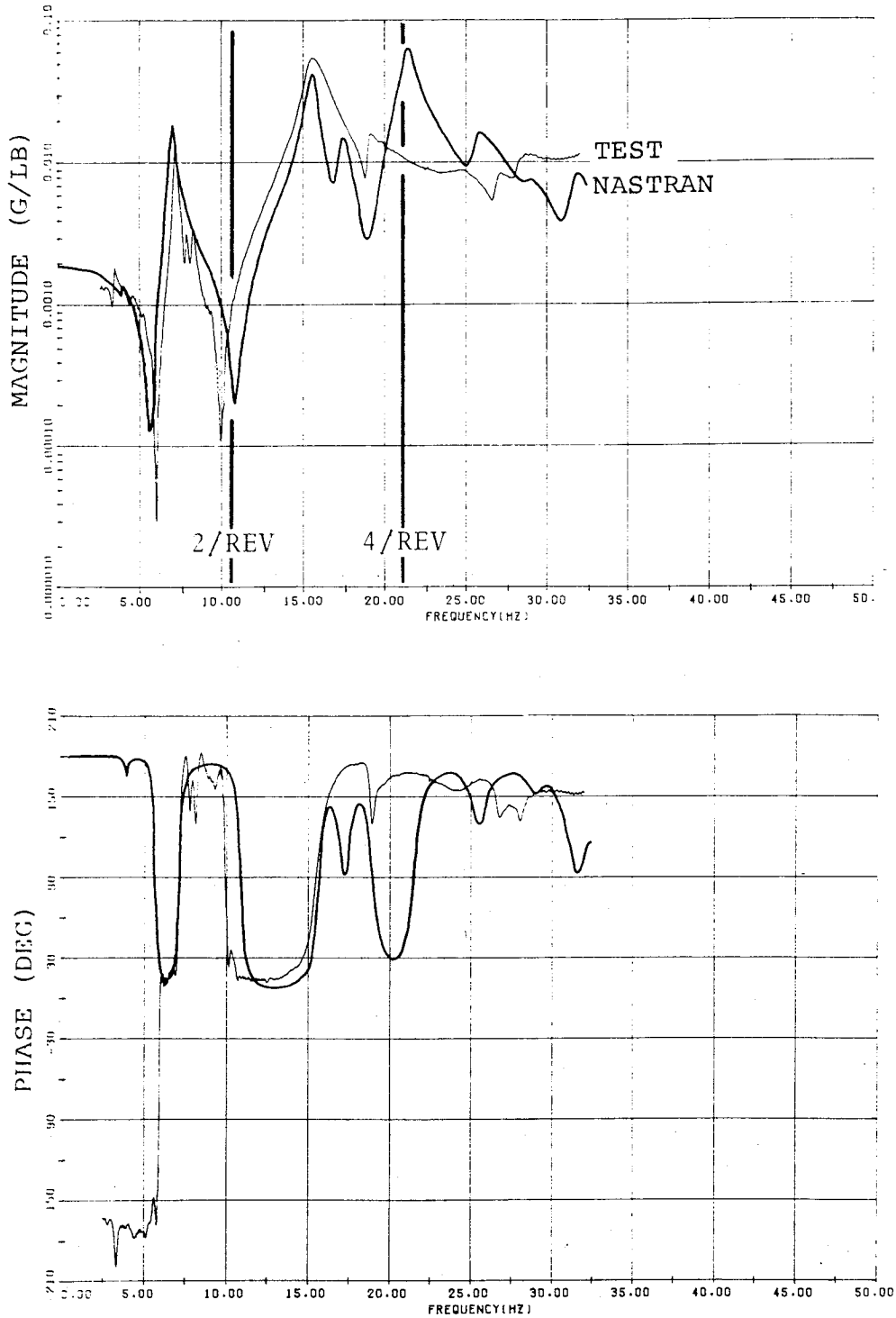

Figure B-21. Tailboom Lateral Shake (Clean Wing) Tail (FS 485) Lateral Response.

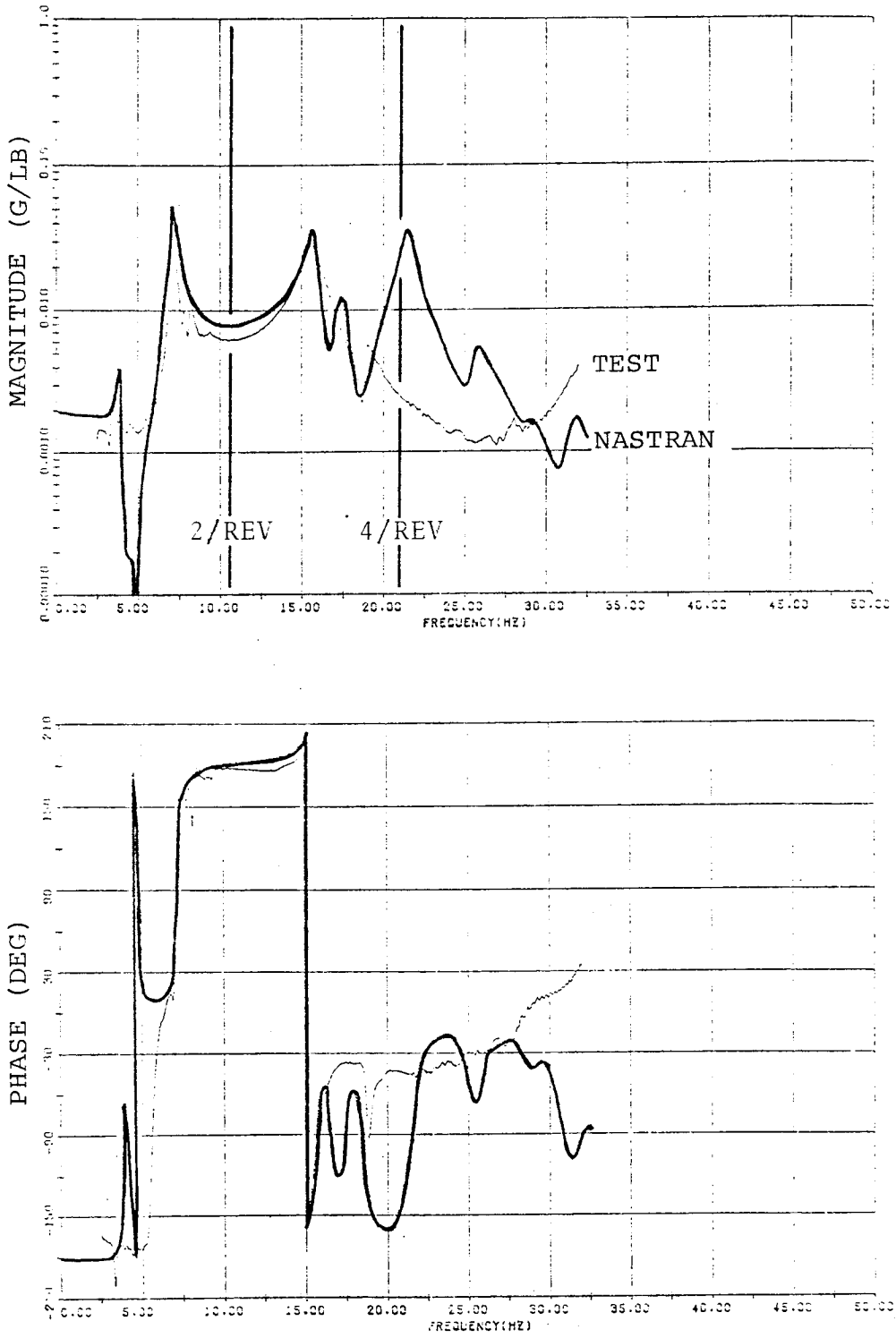

Figure B-22. Tailboom Lateral Shake (Clean Wing) Top of Fin Lateral Response.

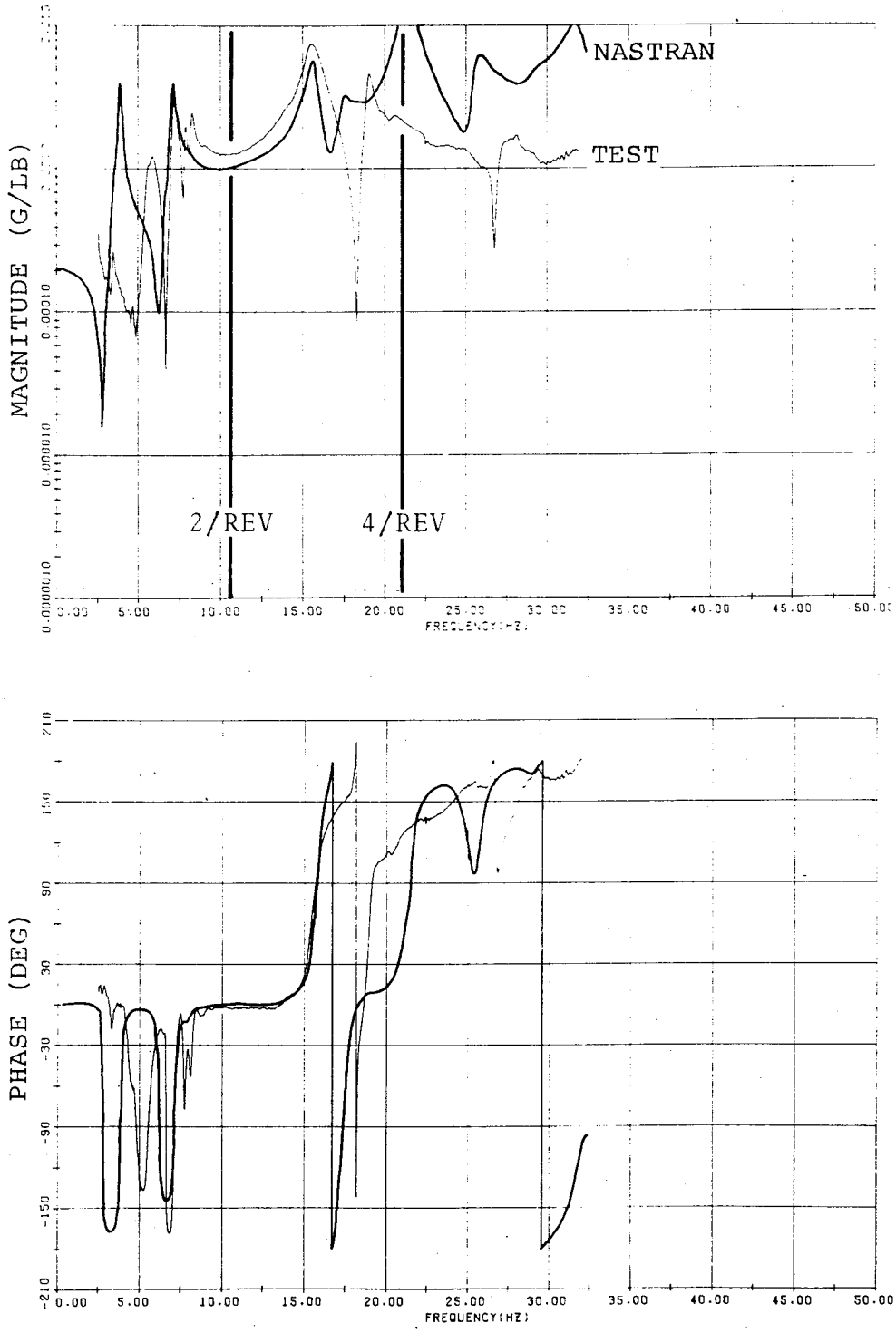

Figure B-23. Tailboom Lateral Shake (Clean Wing) Left Wing Tip Vertical Response.

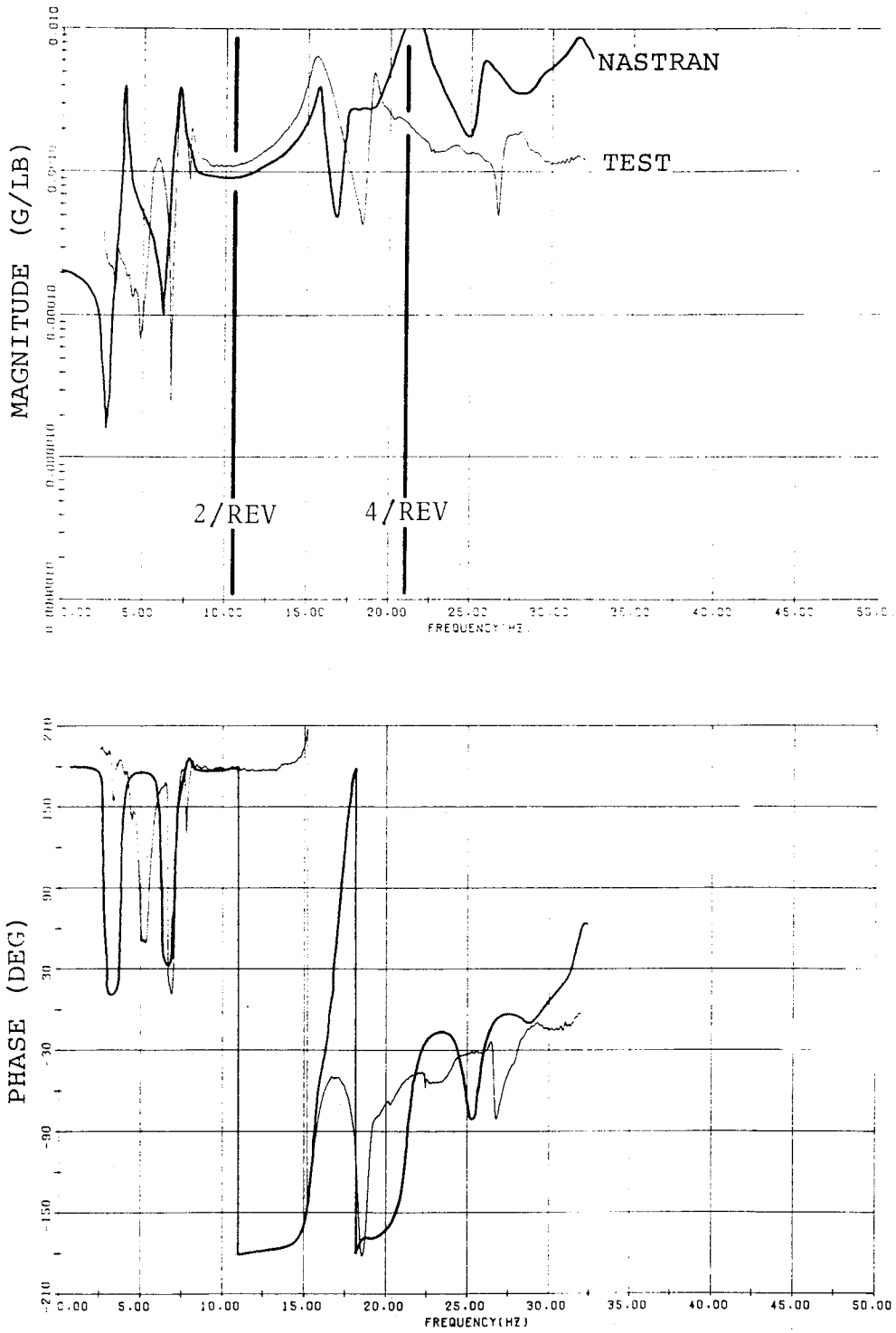

Figure B-24. Tailboom Lateral Shake (Clean Wing) Right Wing Tip Vertical Response.

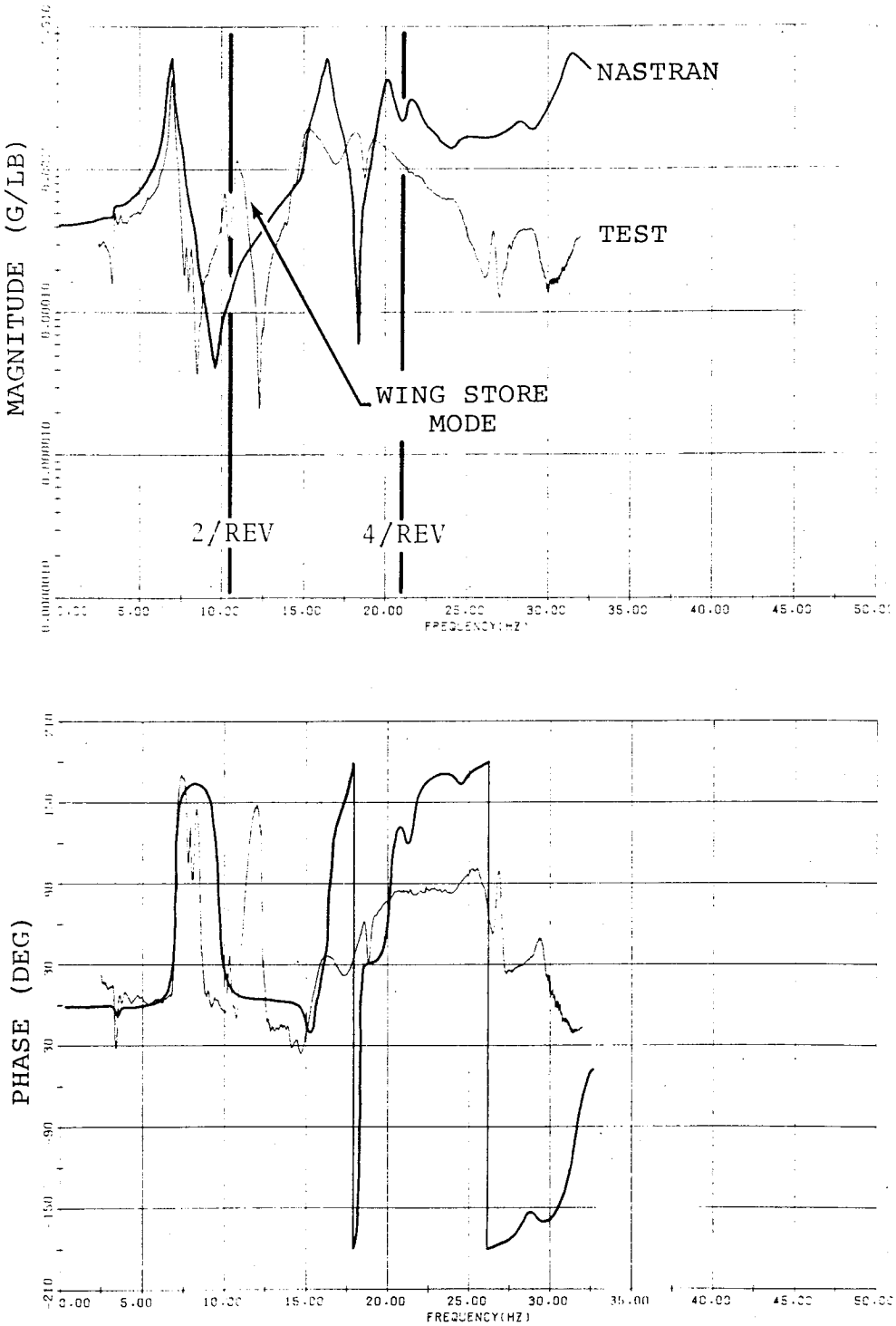

Figure B-25. Tailboom Lateral Shake (With Stores) Gunner Seat Lateral Response.

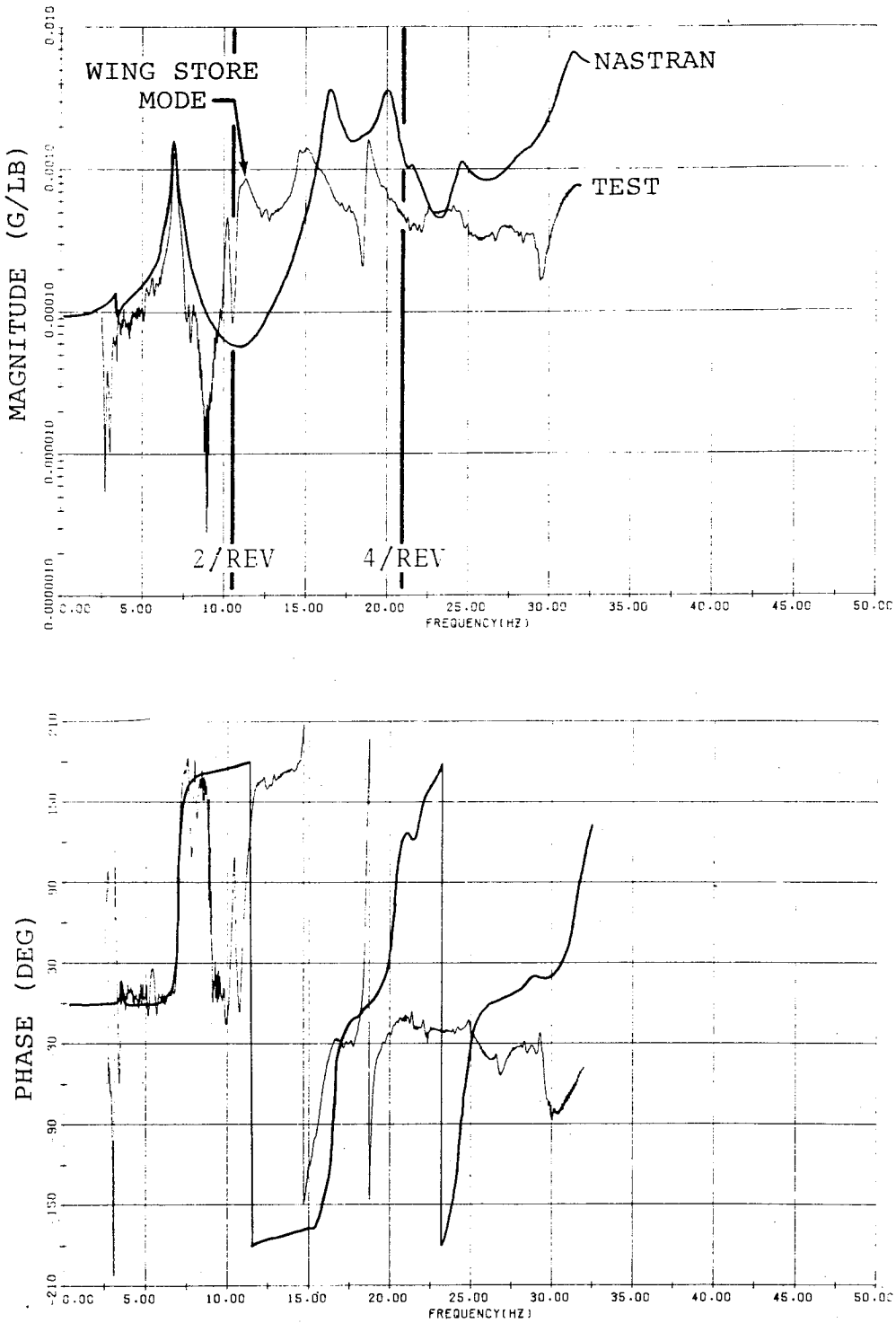

Figure B-26. Tailboom Lateral Shake (With Stores) Pilot Seat Lateral Response.

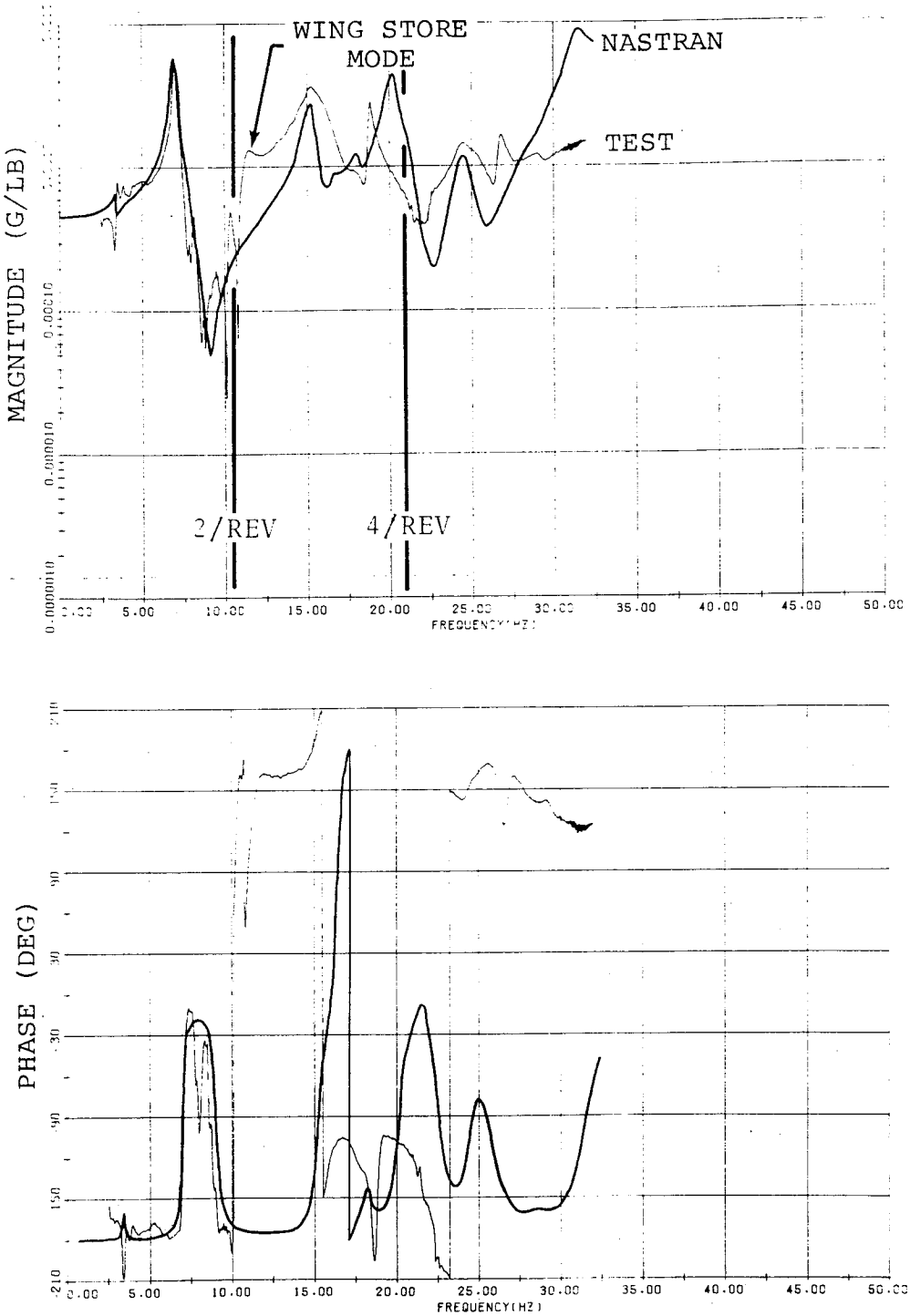

Figure B-27. Tailboom Lateral Shake (With Stores) Engine Deck (FS 250) Lateral Response.

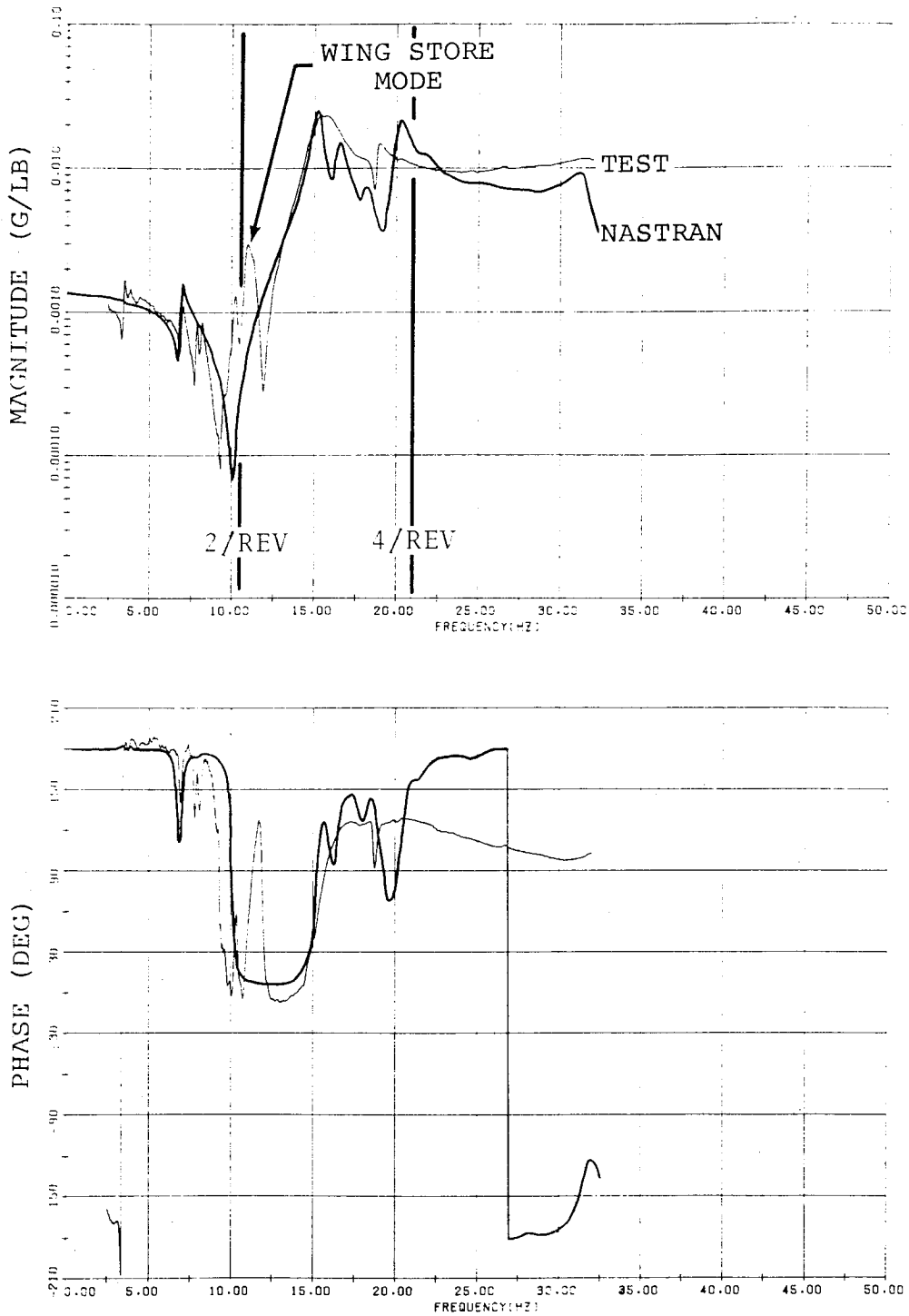

Figure B-28. Tailboom Lateral Shake (With Stores) Elevator Lateral Response.

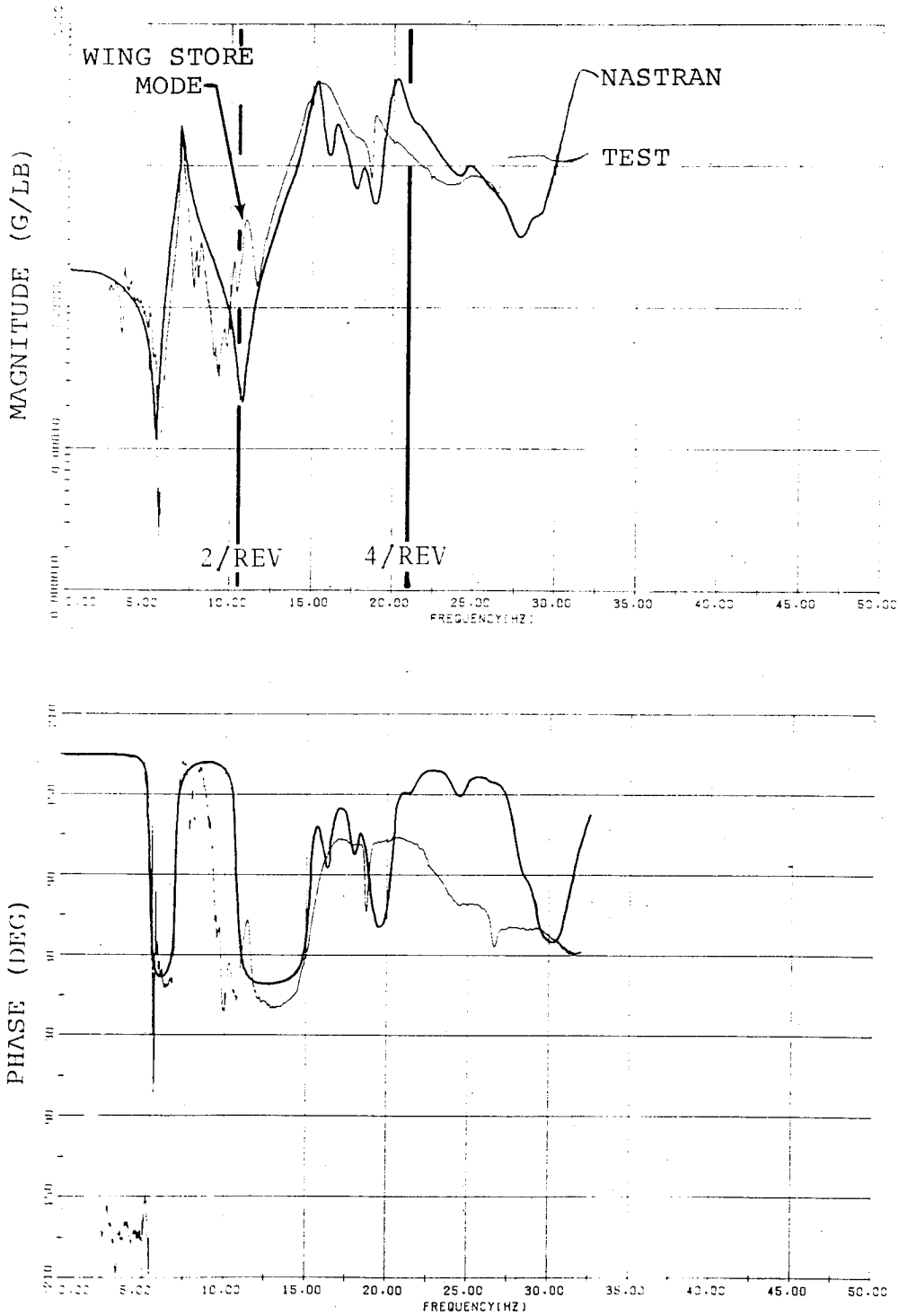

Figure B-29. Tailboom Lateral Shake (With Stores) Tail (FS 485) Lateral Response.

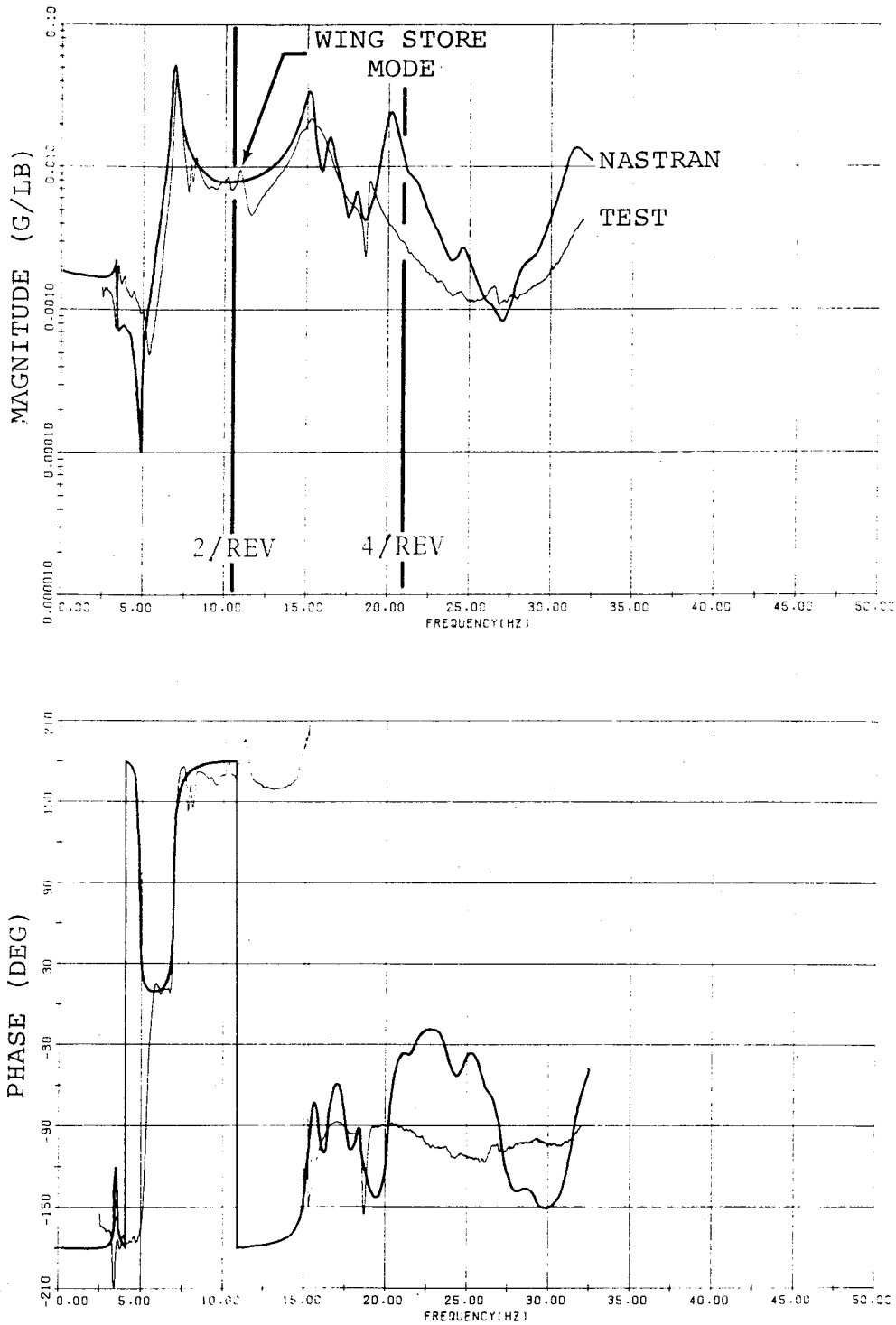

Figure B-30. Tailboom Lateral Shake (With Stores) Top of Fin Lateral Response.

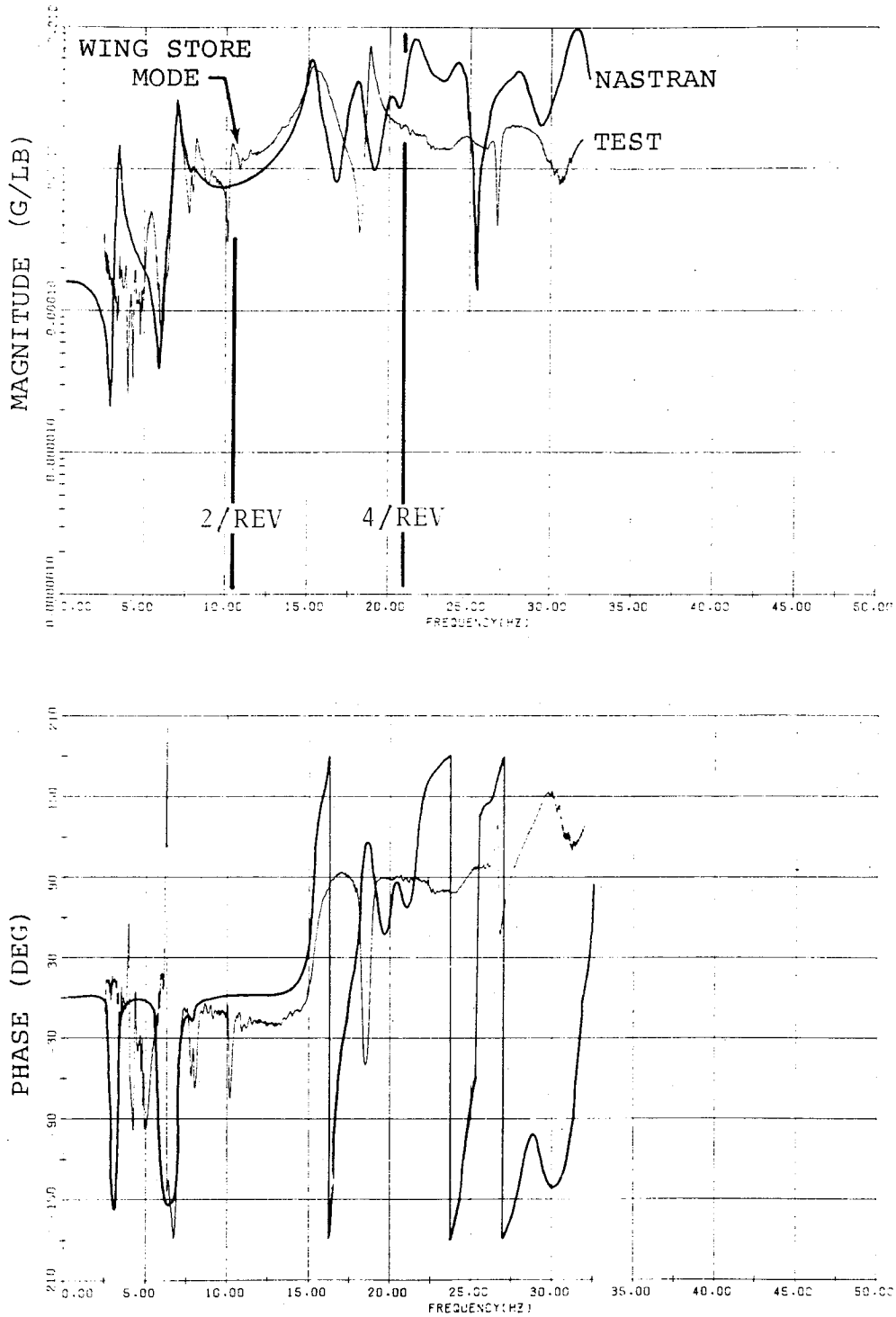

Figure B-31. Tailboom Lateral Shake (With Stores) Left Wing Tip Vertical Response.

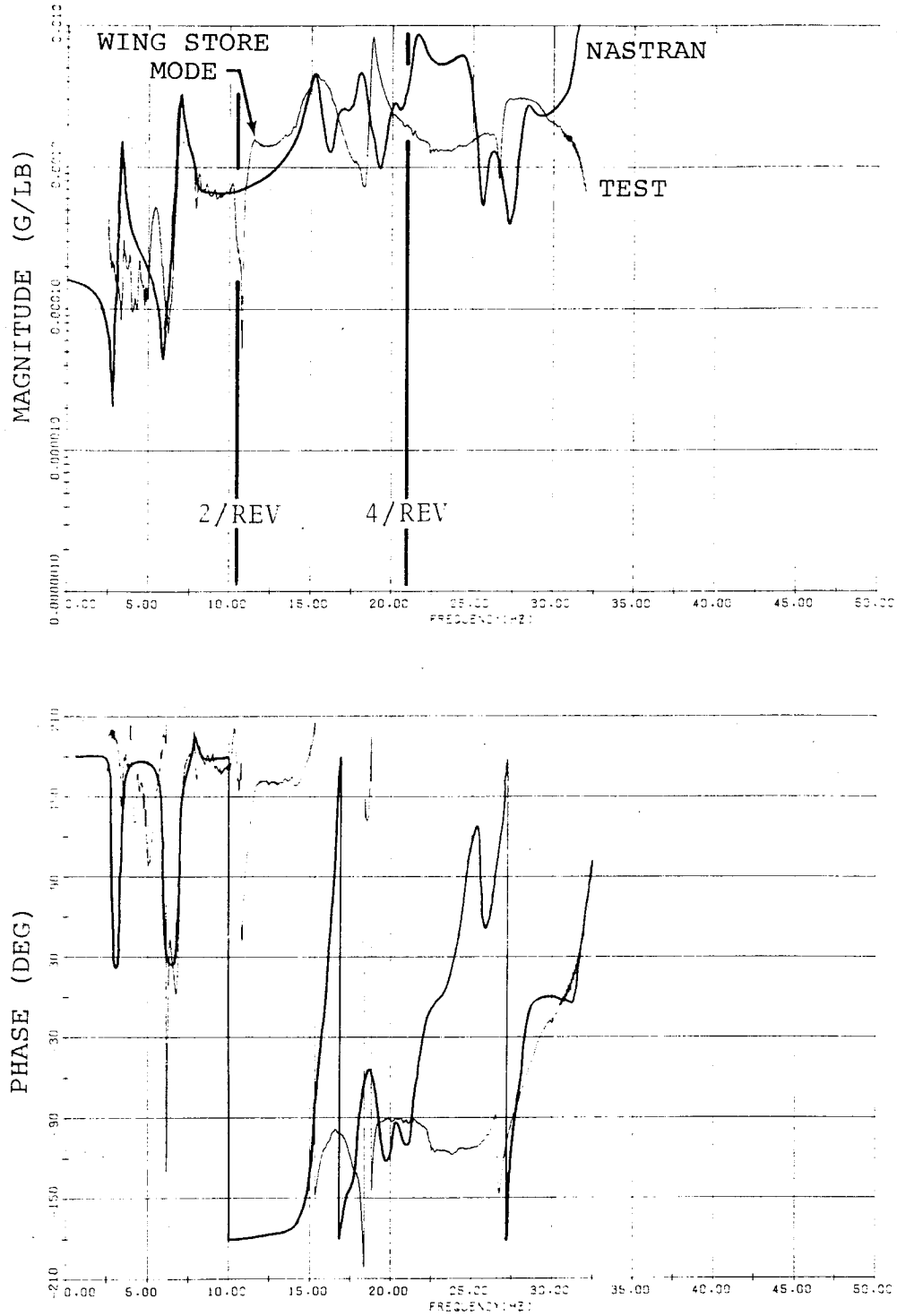

Figure B-32. Tailboom Lateral Shake (With Stores) Right Wing Tip Vertical Response.

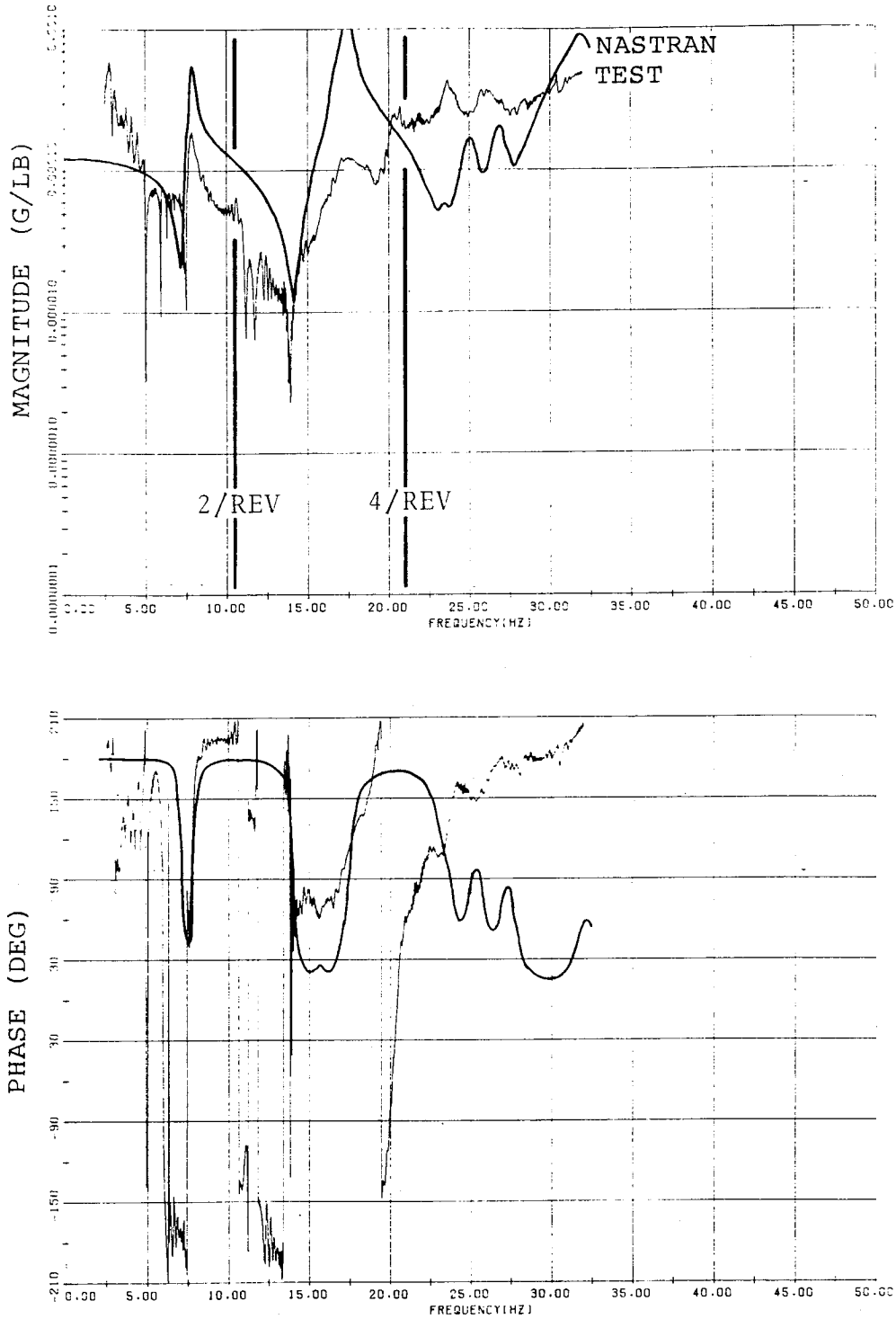

Figure B-33. Main Rotor Hub Vertical Shake (Clean Wing) Hub Vertical Response.

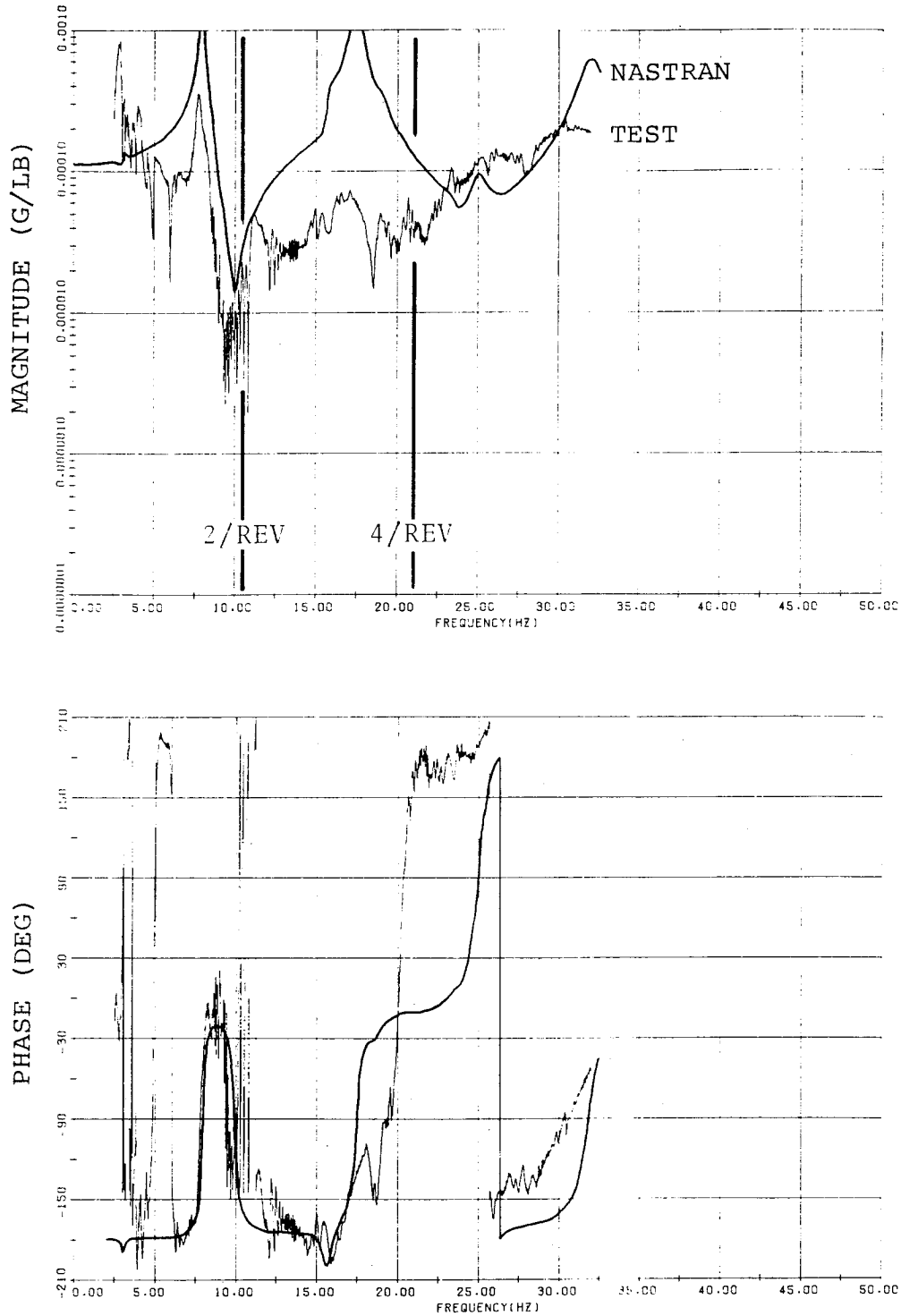

Figure B-34. Main Rotor Hub Vertical Shake (Clean Wing) Gunner Seat Vertical Response.

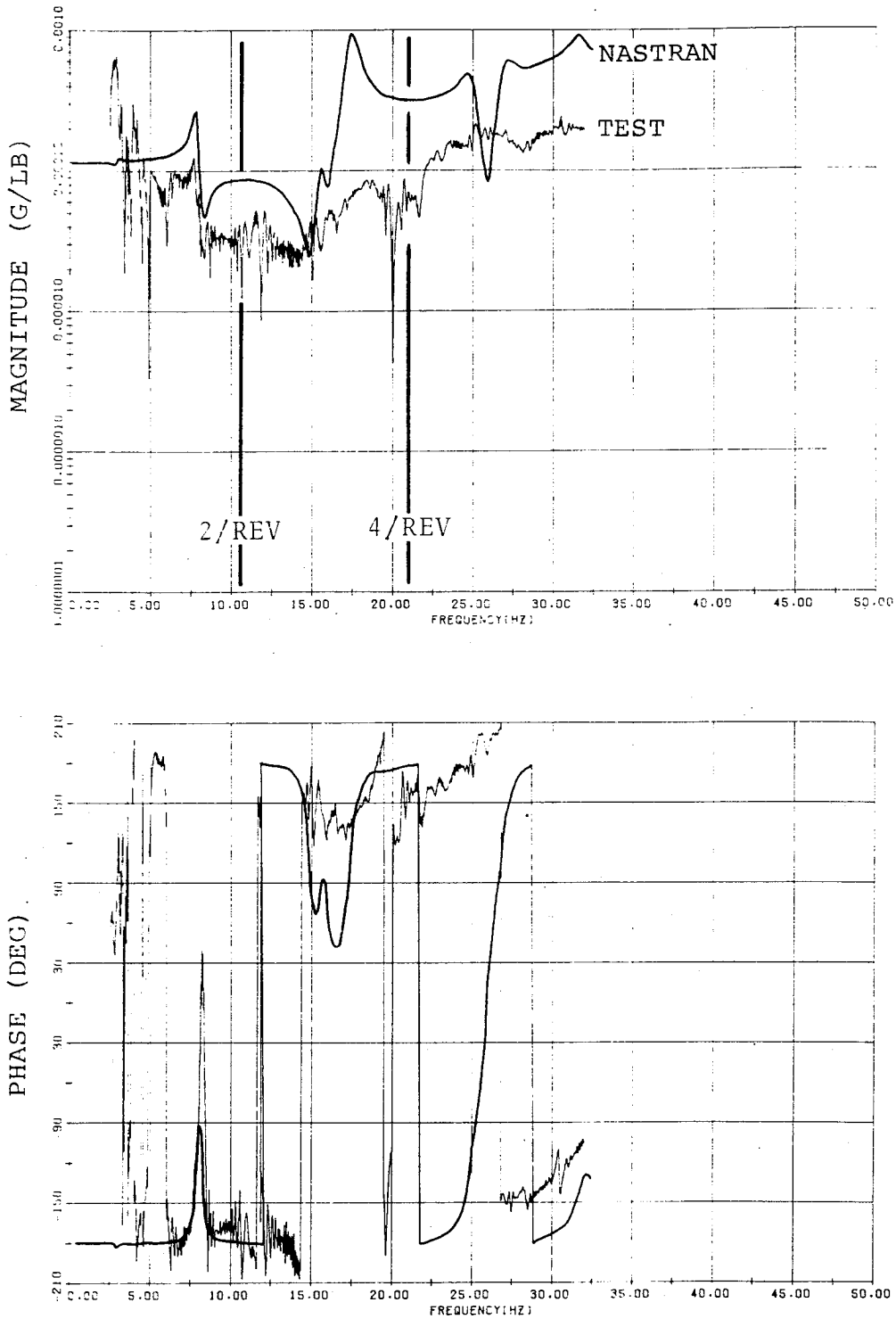

Figure B-35. Main Rotor Hub Vertical Shake (Clean Wing) Pilot Seat Vertical Response.

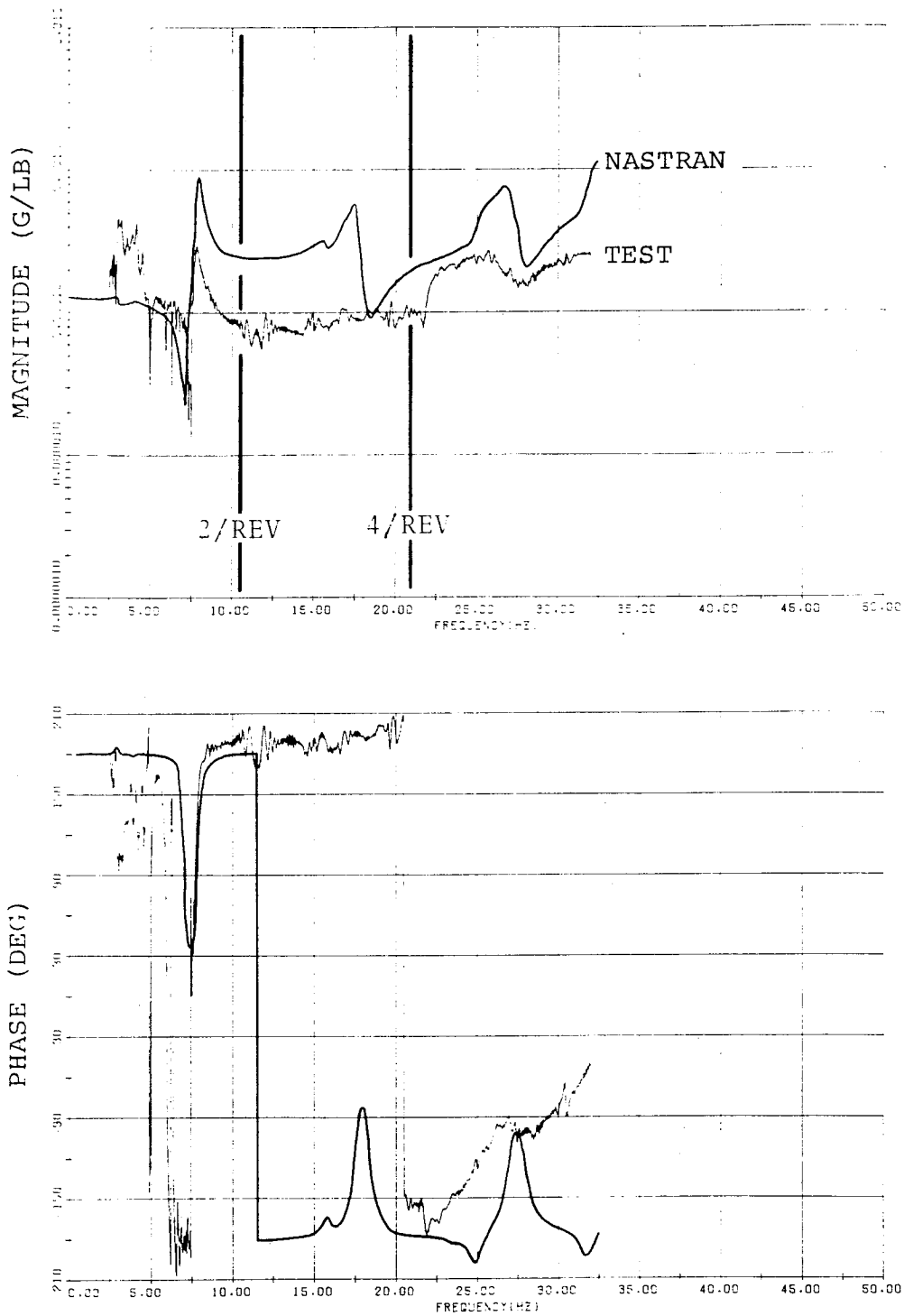

Figure B-36. Main Rotor Hub Vertical Shake (Clean Wing) Engine Deck (FS 250) Vertical Response.

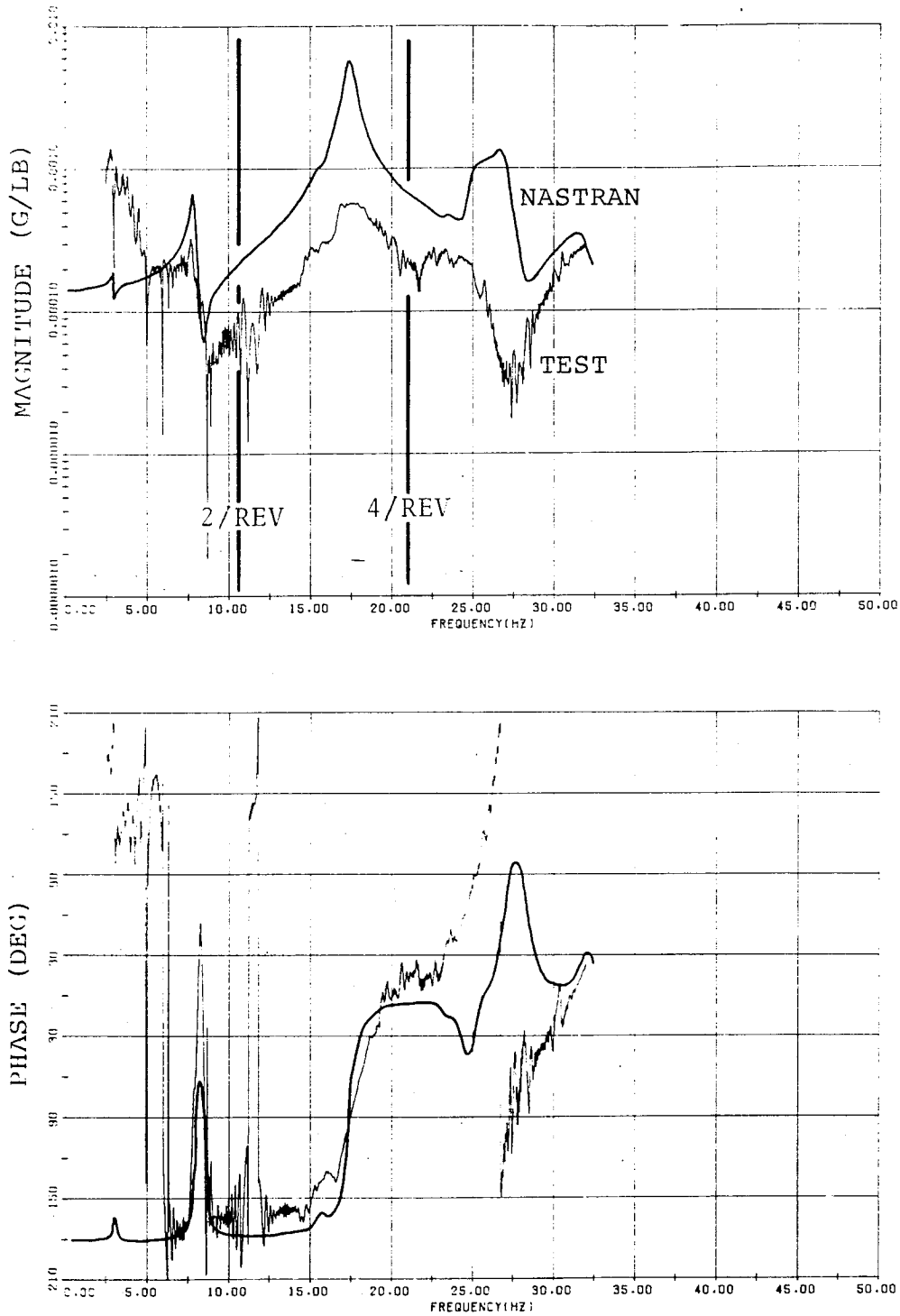

Figure B-37. Main Rotor Hub Vertical Shake (Clean Wing) Elevator Vertical Response.

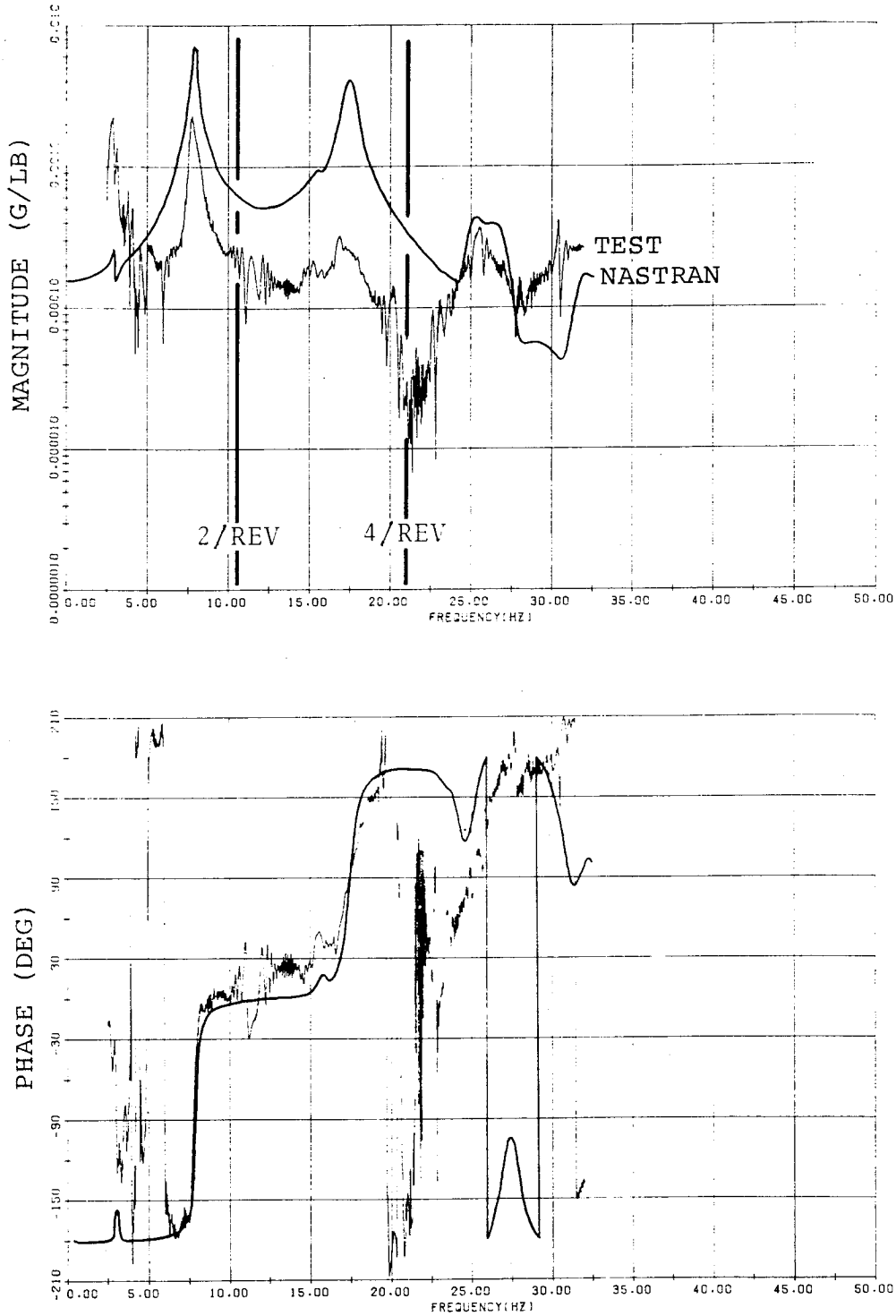

Figure B-38. Main Rotor Hub Vertical Shake (Clean Wing) 90° Gearbox Vertical Response.

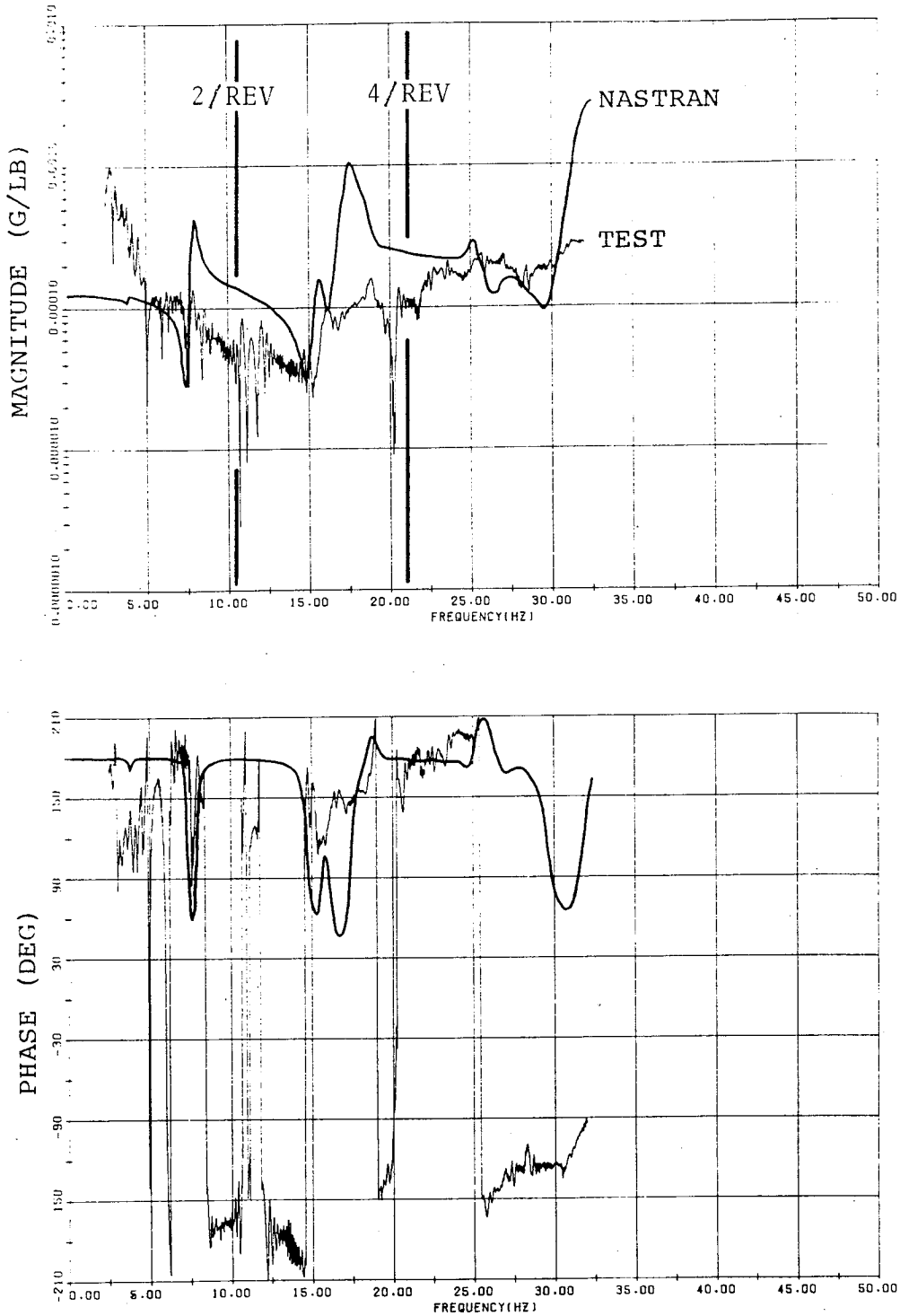

Figure B-39. Main Rotor Hub Vertical Shake (Clean Wing) Left Wing Tip Vertical Response.

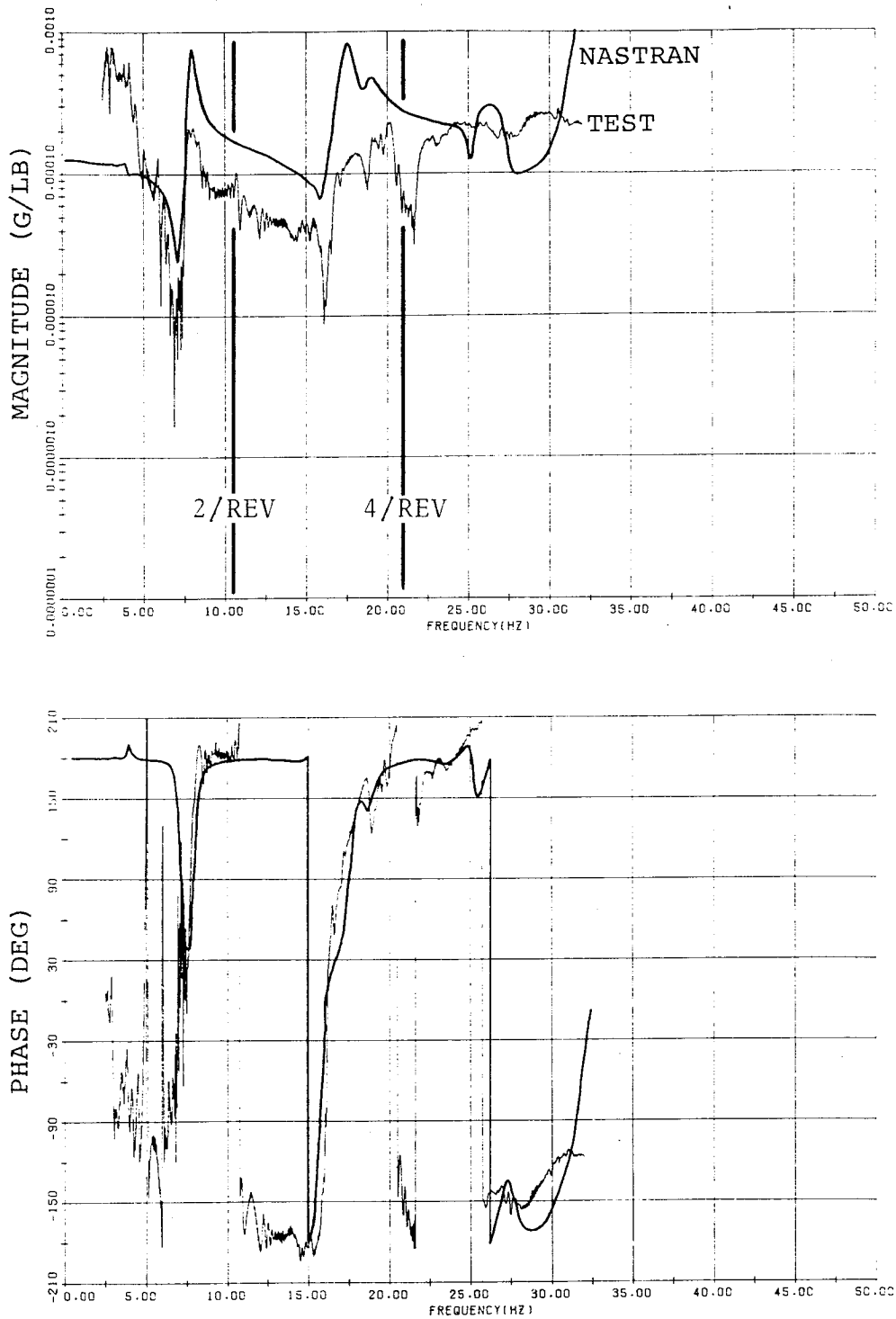

Figure B-40. Main Rotor Hub Vertical Shake (Clean Wing) Right Wing Tip Vertical Response.

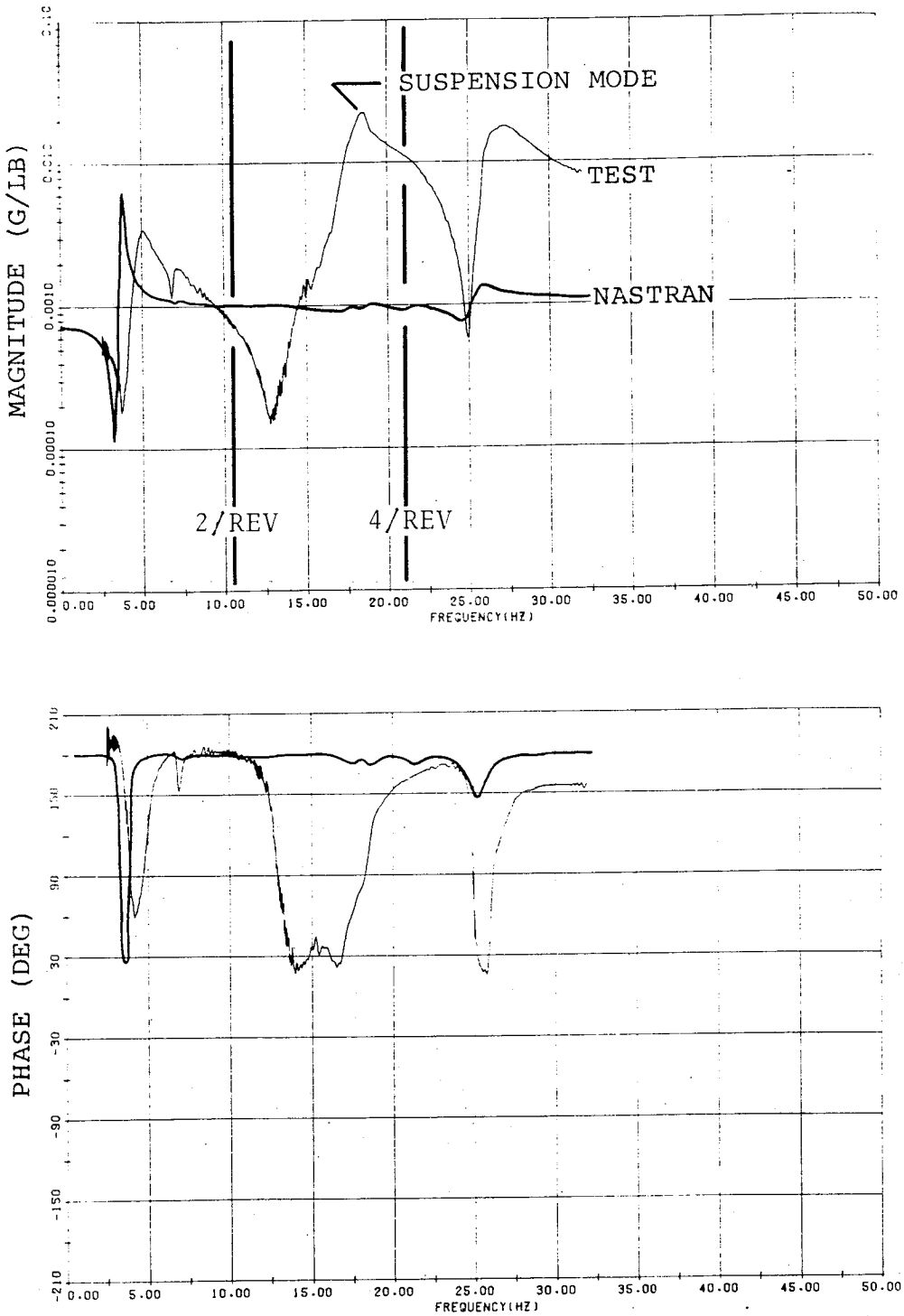

Figure B-41. Main Rotor Hub Lateral Shake (Clean Wing) Hub Lateral Response.

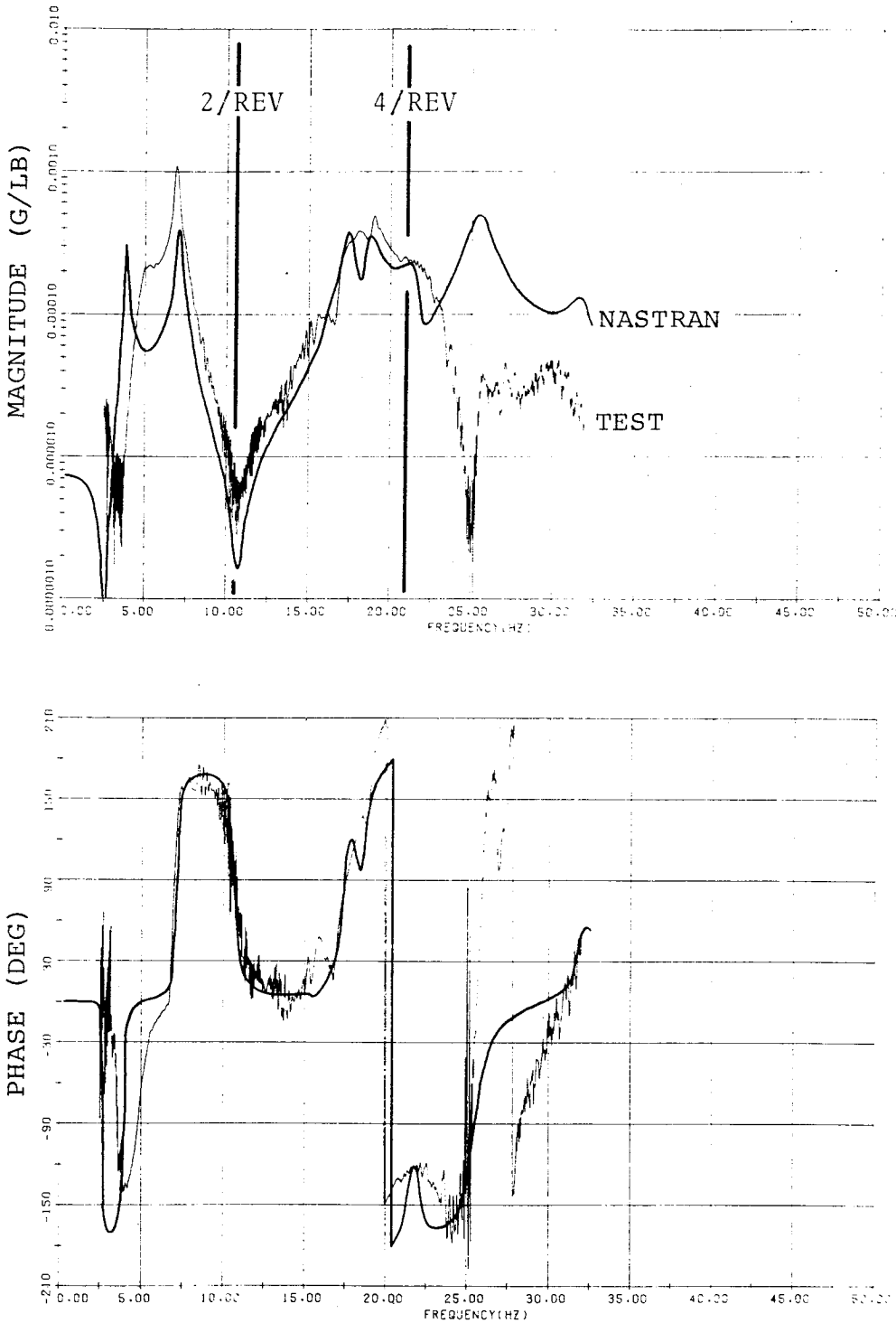

Figure B-42. Main Rotor Hub Lateral Shake (Clean Wing) Gunner Seat Lateral Response.

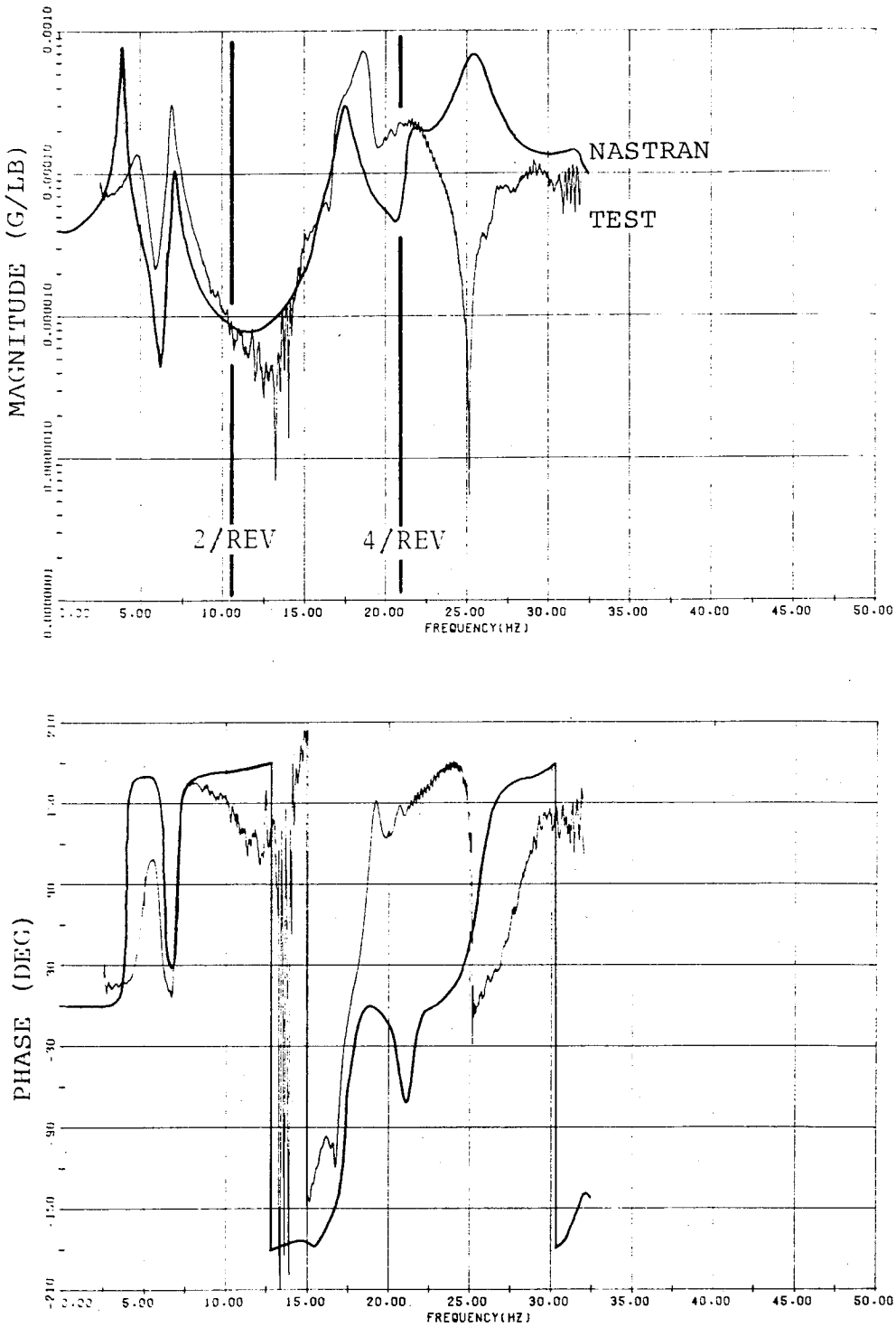

Figure B-43. Main Rotor Hub Lateral Shake (Clean Wing) Pilot Seat Lateral Response.

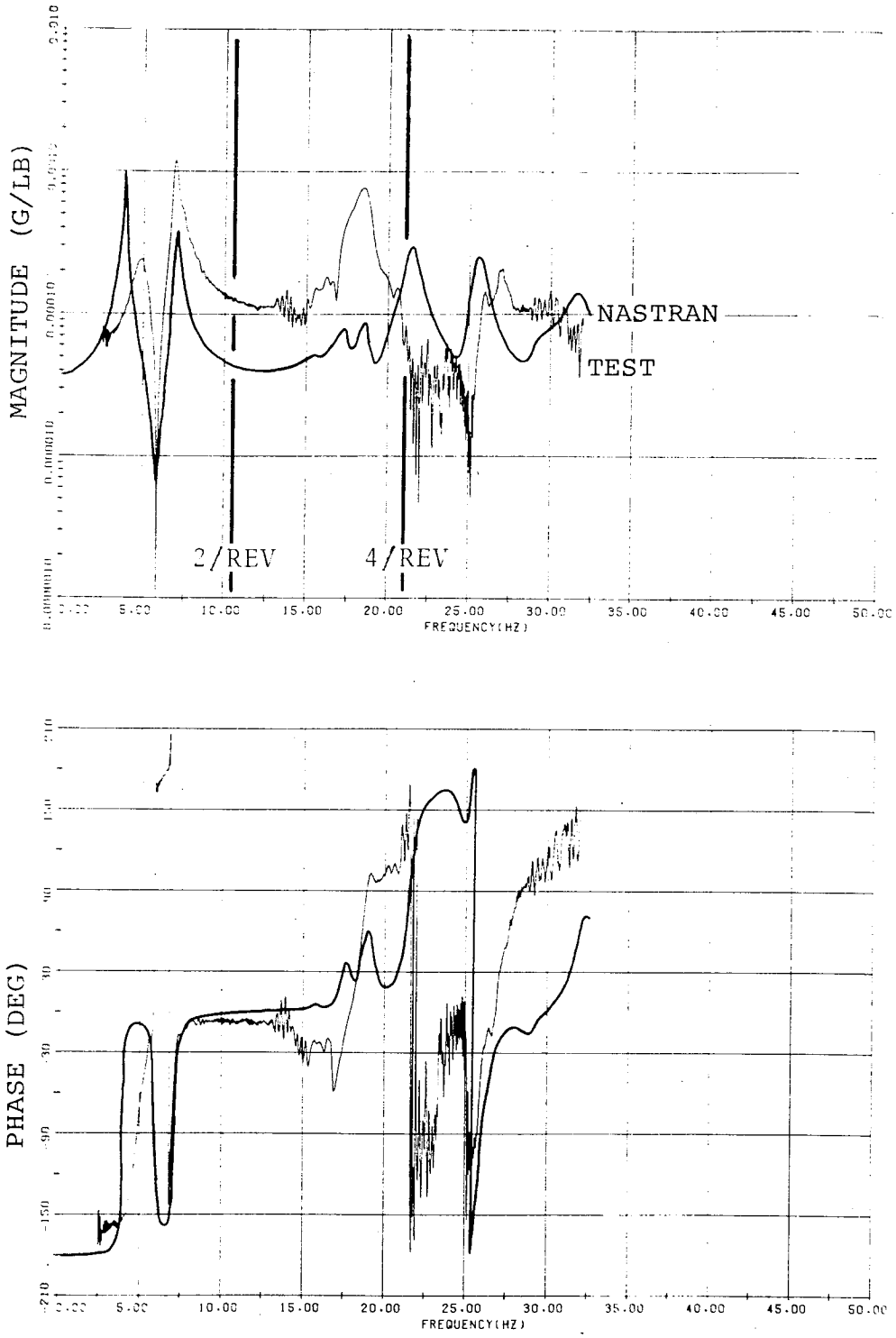

Figure B-44. Main Rotor Hub Lateral Shake (Clean Wing) Engine Deck (FS 250) Lateral Response.

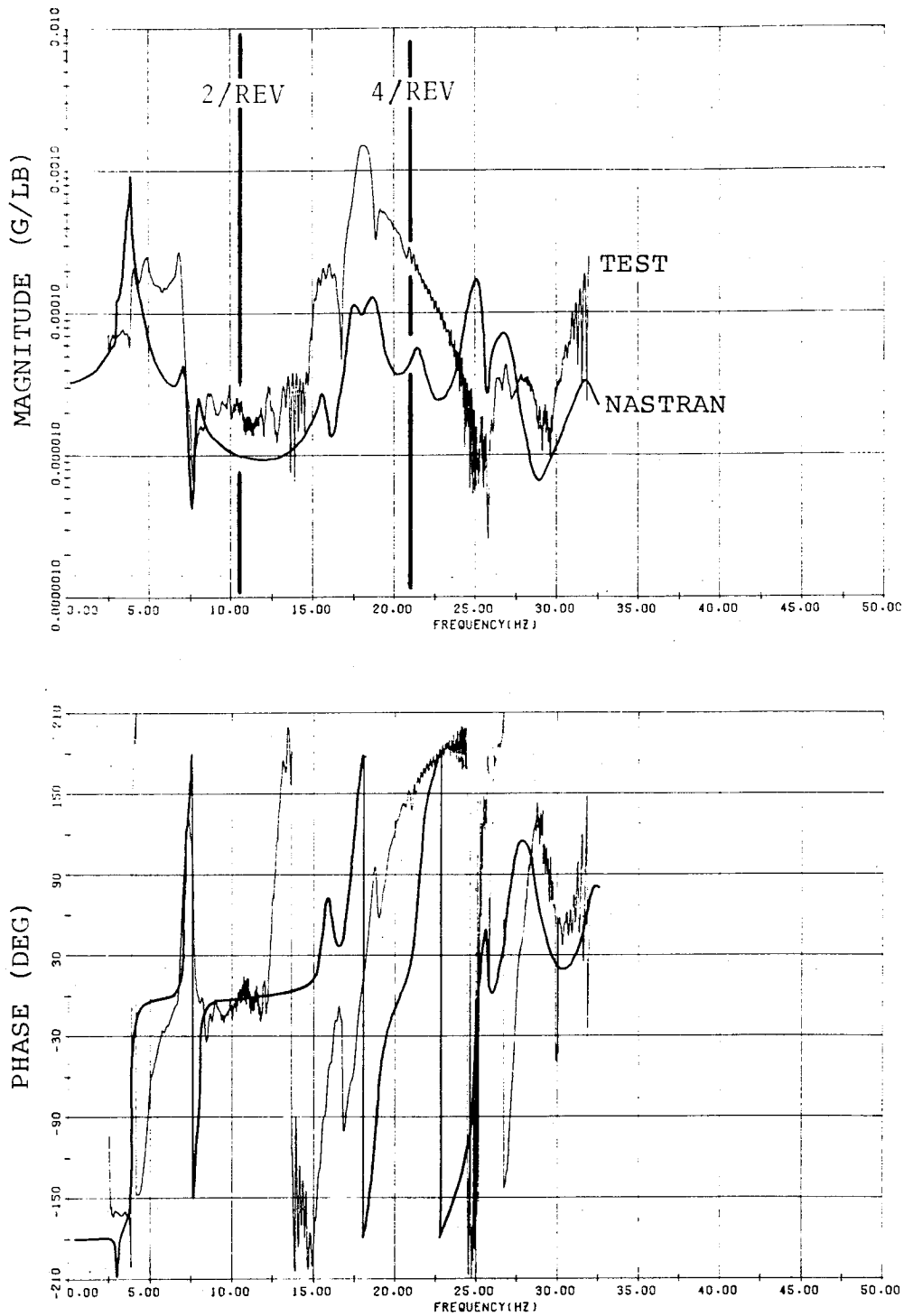

Figure B-45. Main Rotor Hub Lateral Shake (Clean Wing) Elevator Lateral Response.

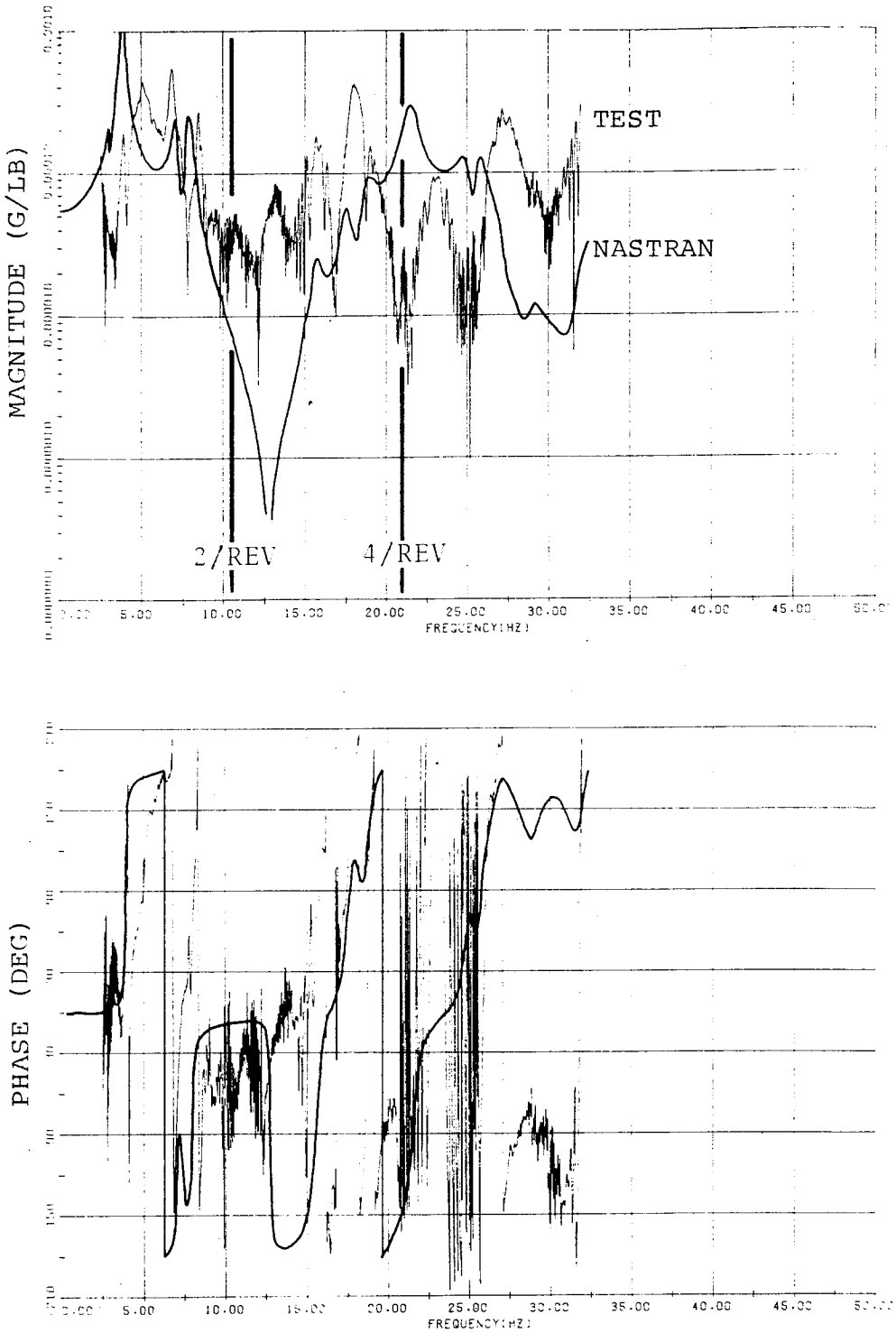

Figure B-46. Main Rotor Hub Lateral Shake (Clean Wing) 90° Gearbox Vertical Response.

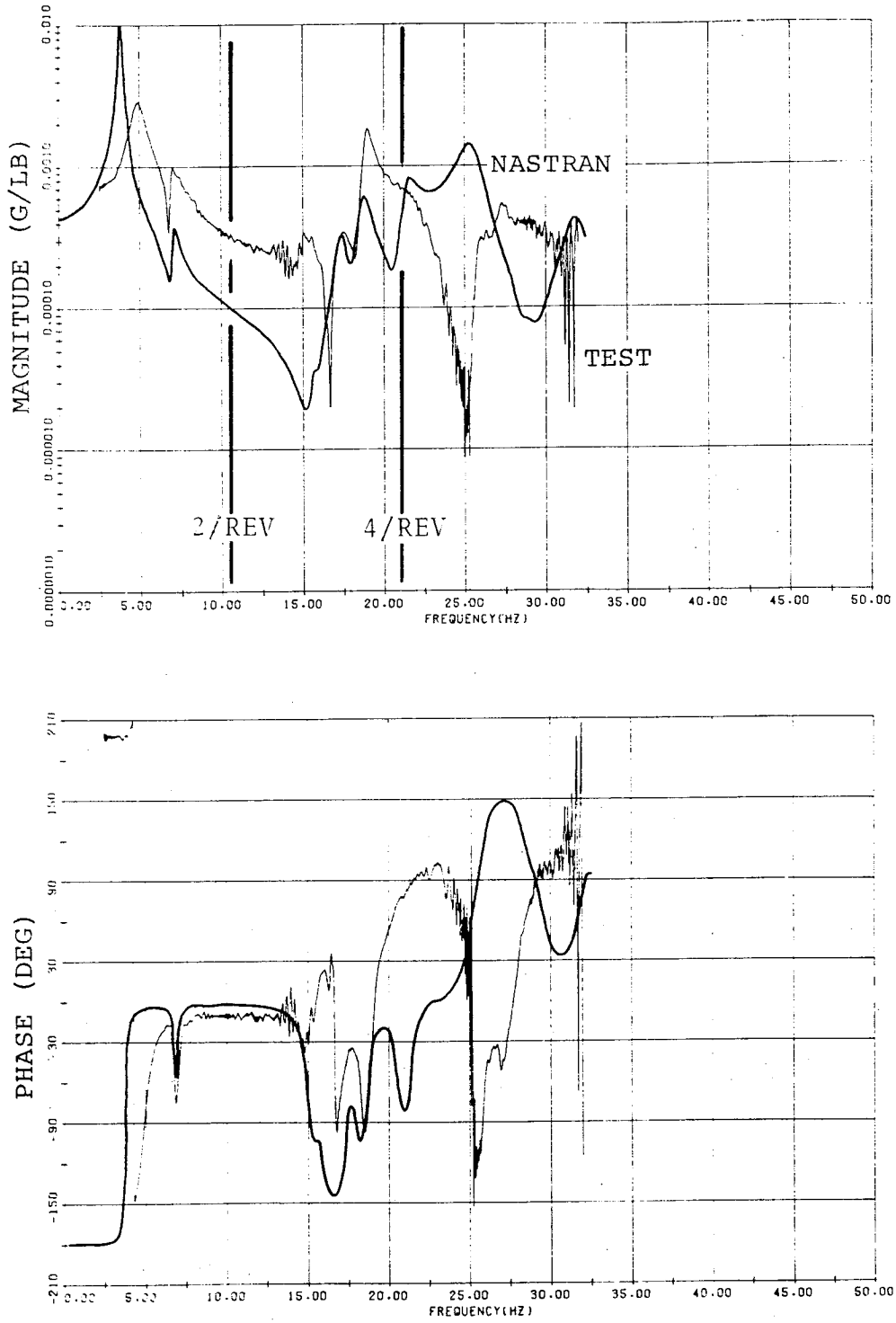

Figure B-47. Main Rotor Hub Lateral Shake (Clean Wing) Left Wing Tip Vertical Response.

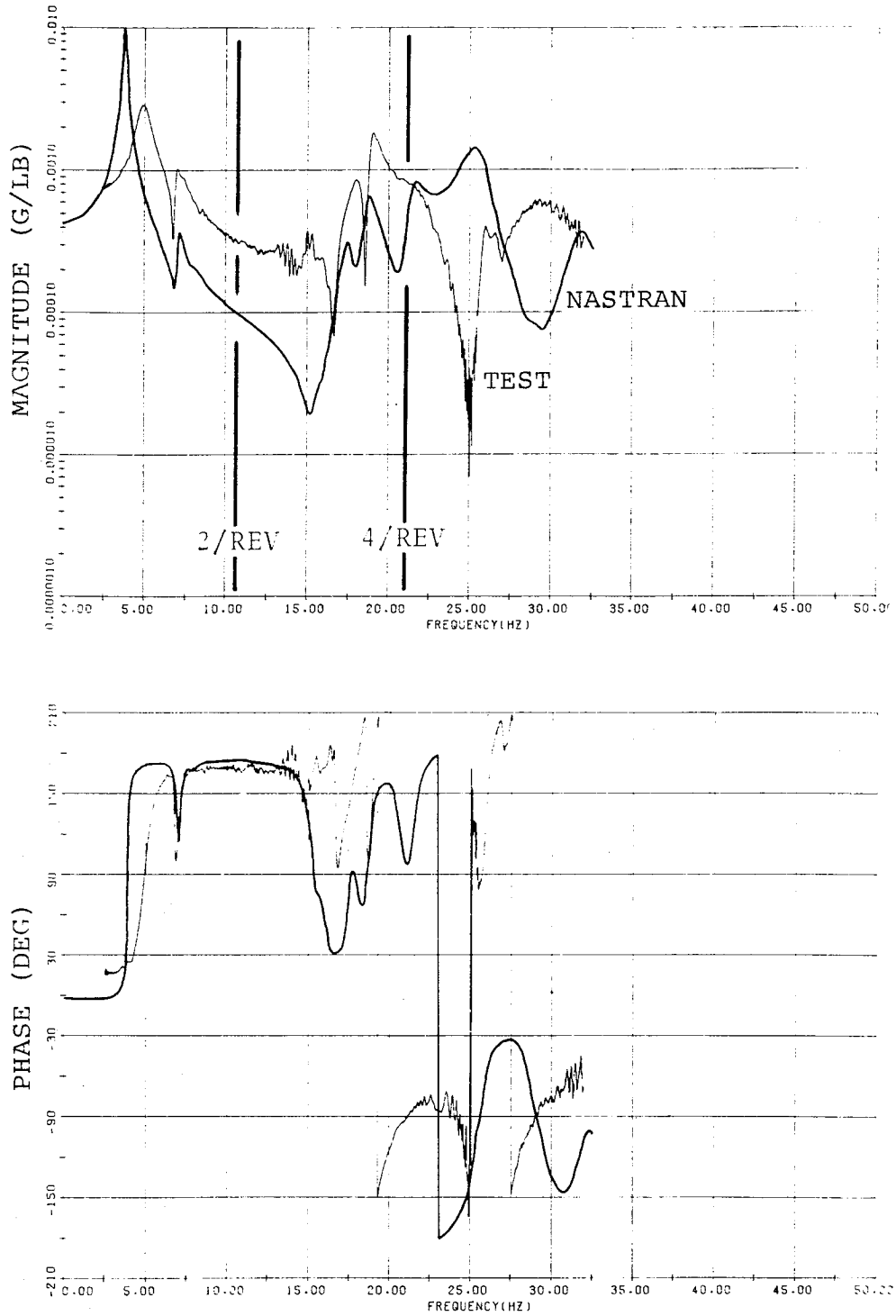

Figure B-48. Main Rotor Hub Lateral Shake (Clean Wing) Right Wing Tip Vertical Response.

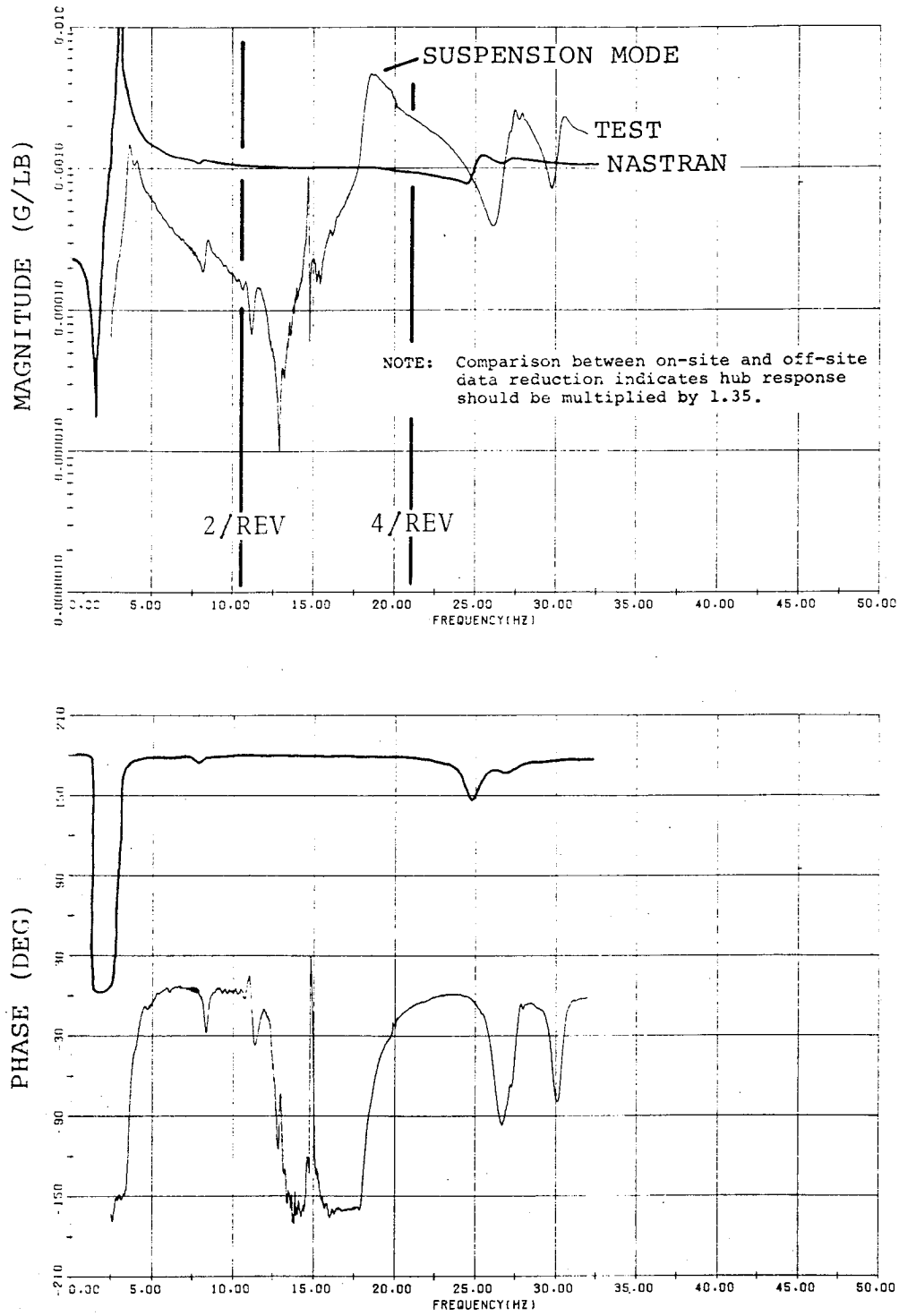

Figure B-49. Main Rotor Hub Fore-and-Aft Shake (Clean Wing) Hub Fore-and-Aft Response.

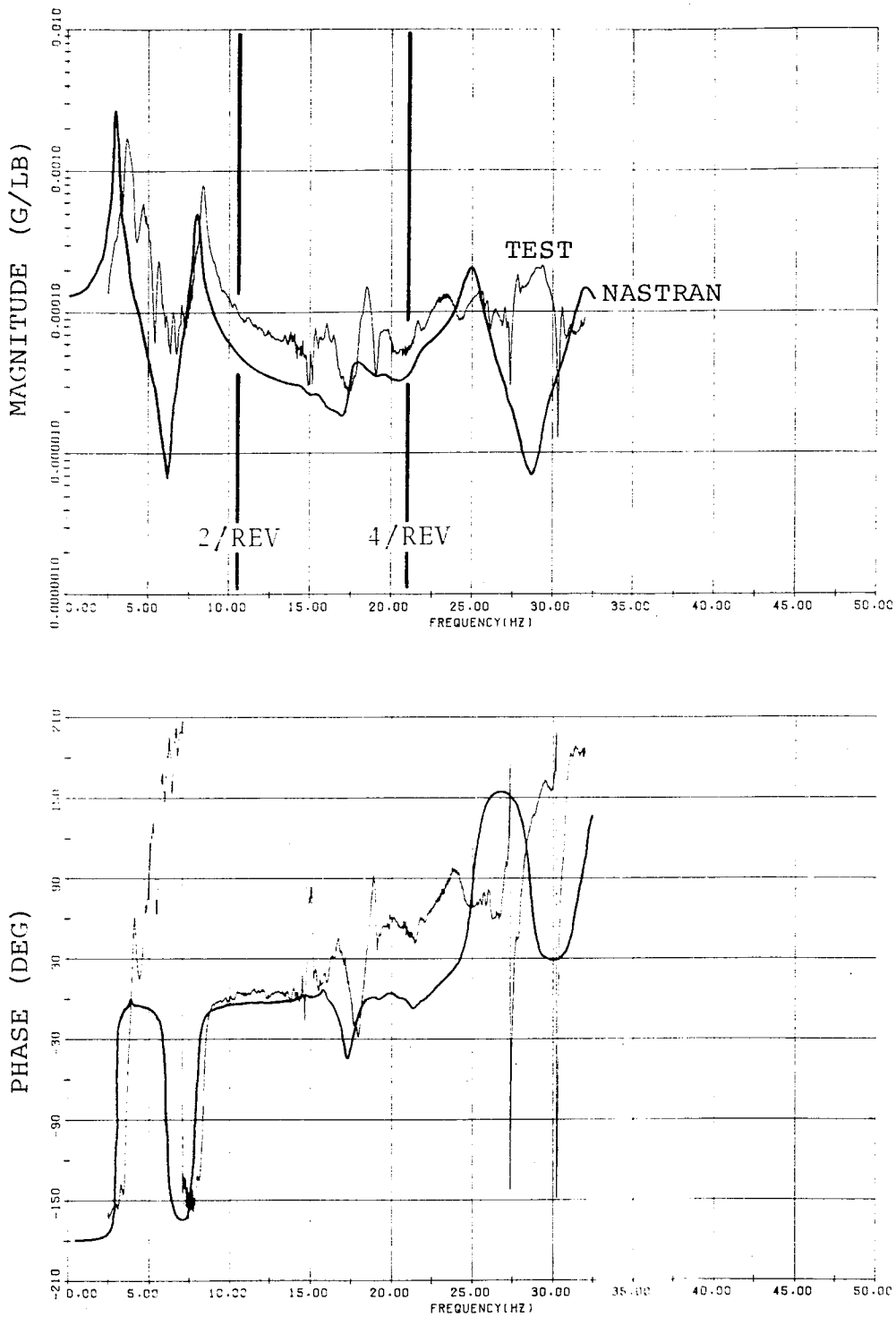

Figure B-50. Main Rotor Hub Fore-and-Aft Shake (Clean Wing) Gunner Seat Vertical Response.

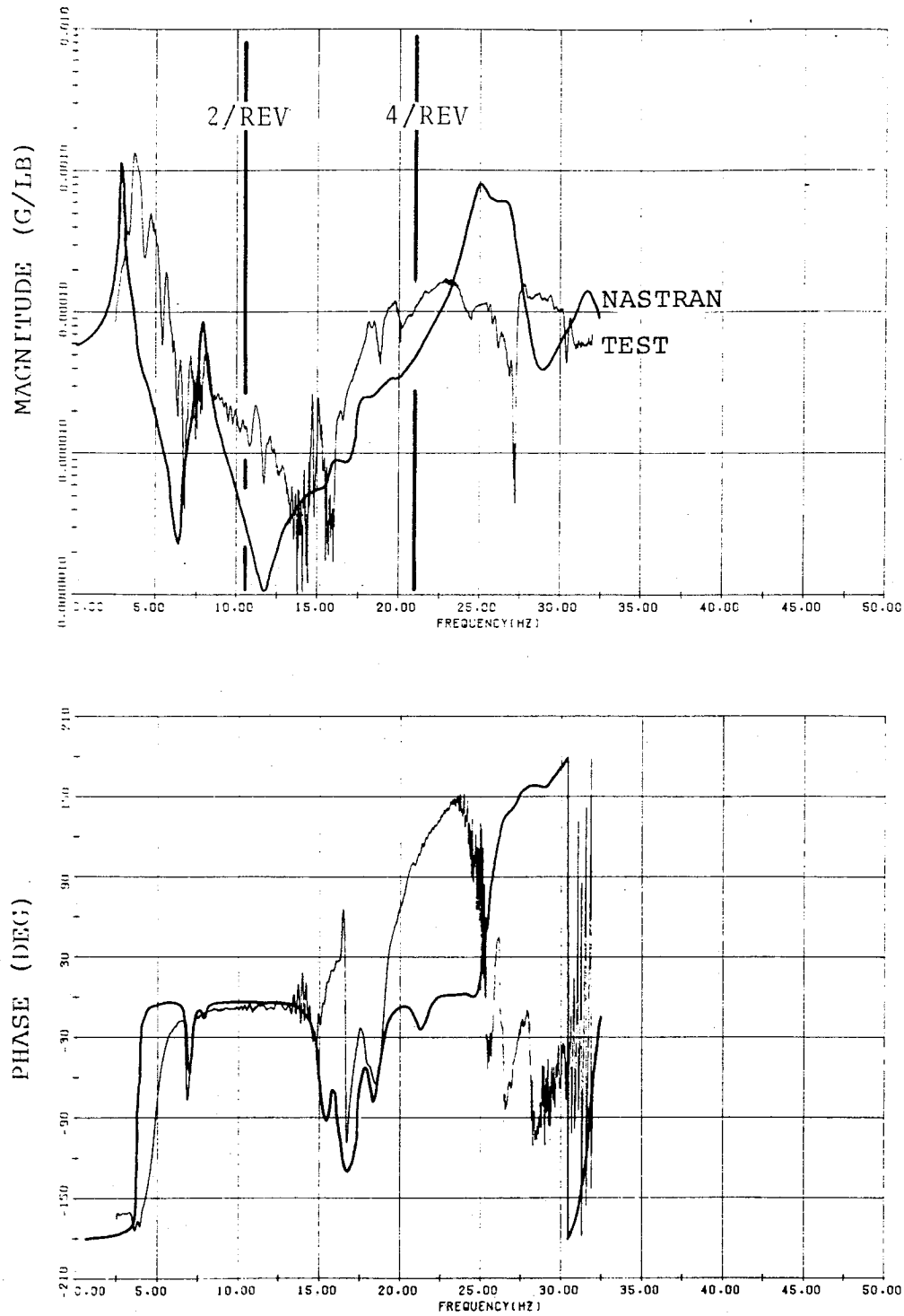

Figure B-51. Main Rotor Hub Fore-and-Aft Shake (Clean Wing) Pilot Seat Vertical Response.

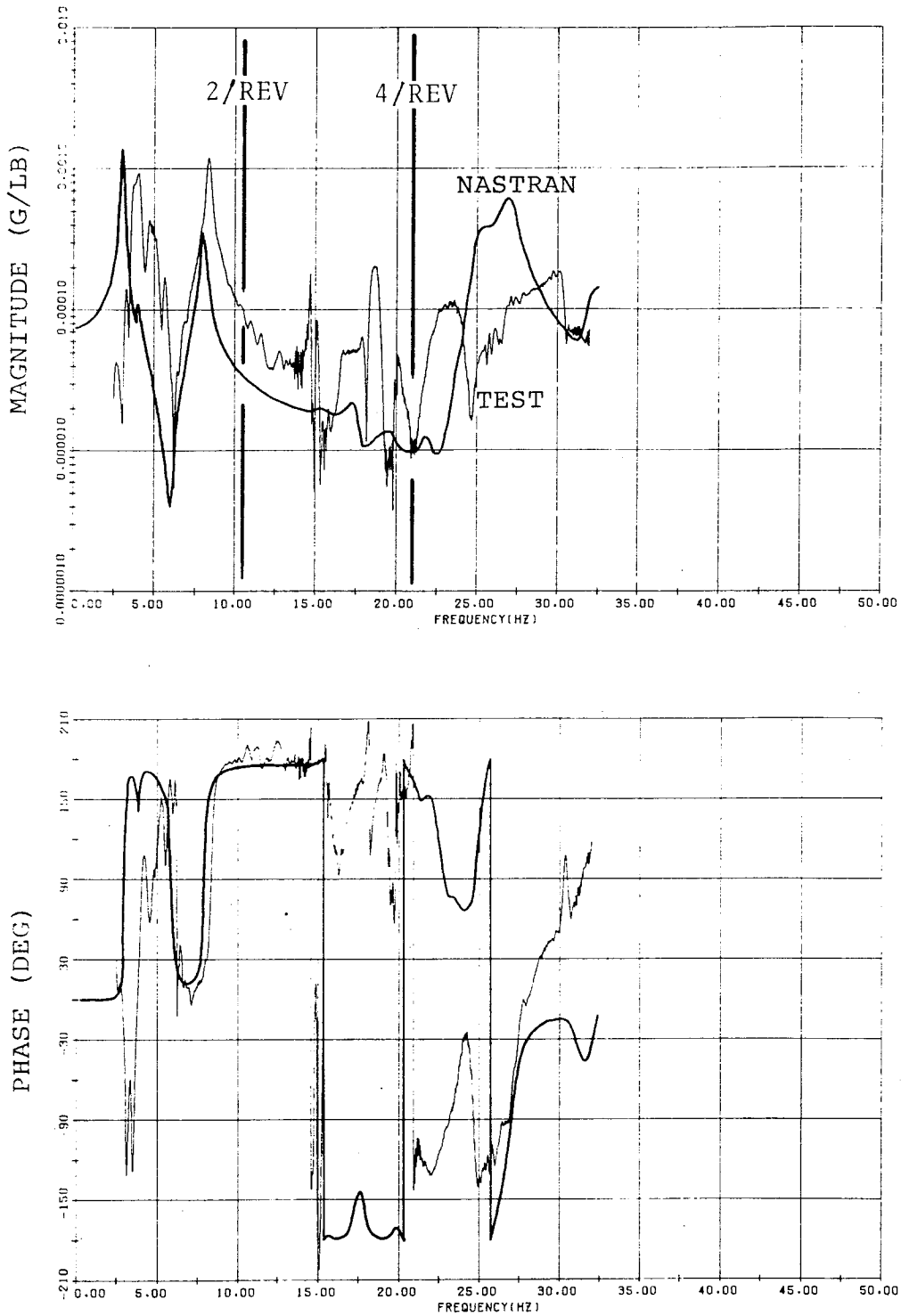

Figure B-52. Main Rotor Hub Fore-and-Aft Shake (Clean Wing) Engine Deck (FS 250) Vertical Response.

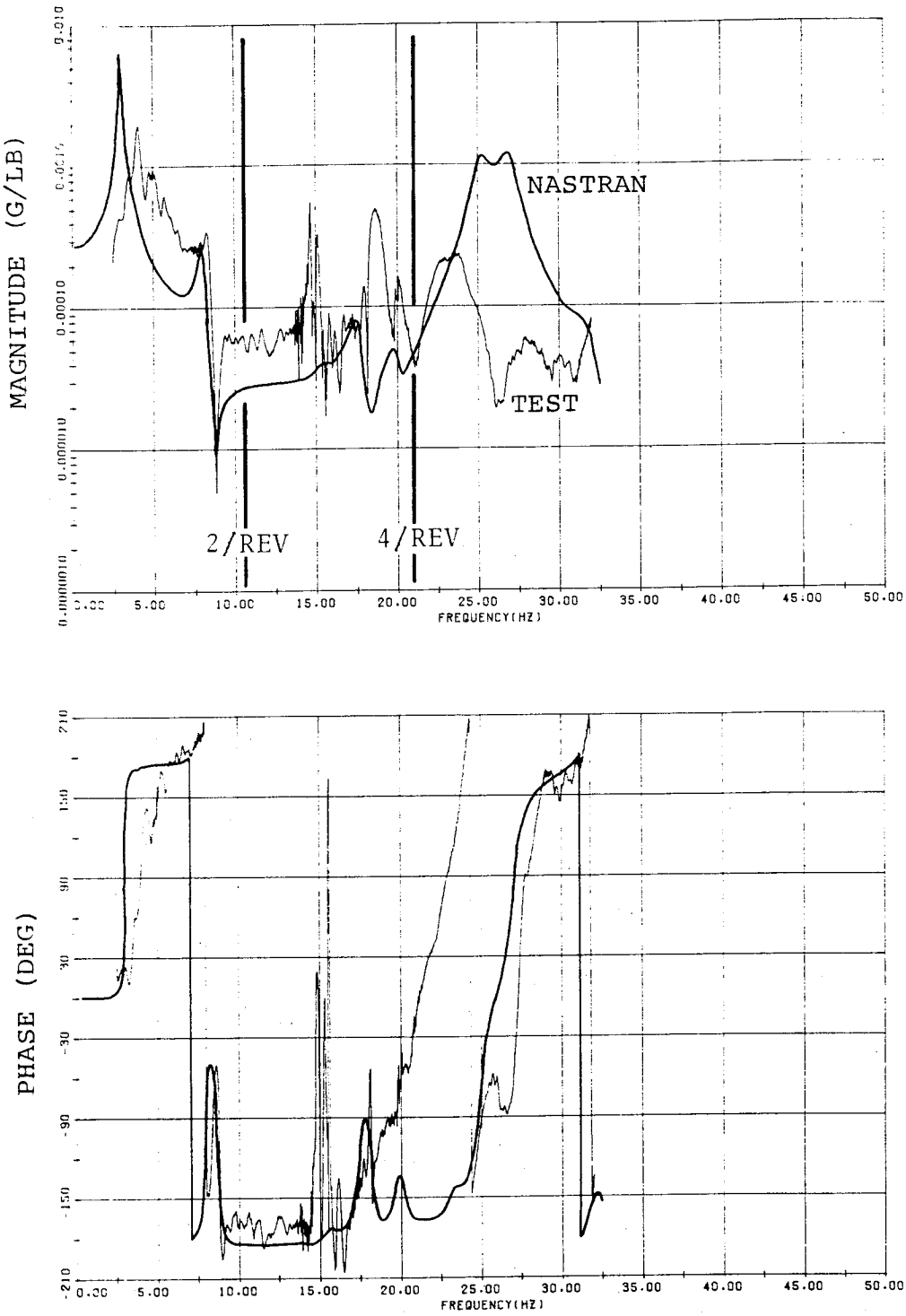

Figure B-53. Main Rotor Hub Fore-and-Aft Shake (Clean Wing) Elevator Vertical Response.

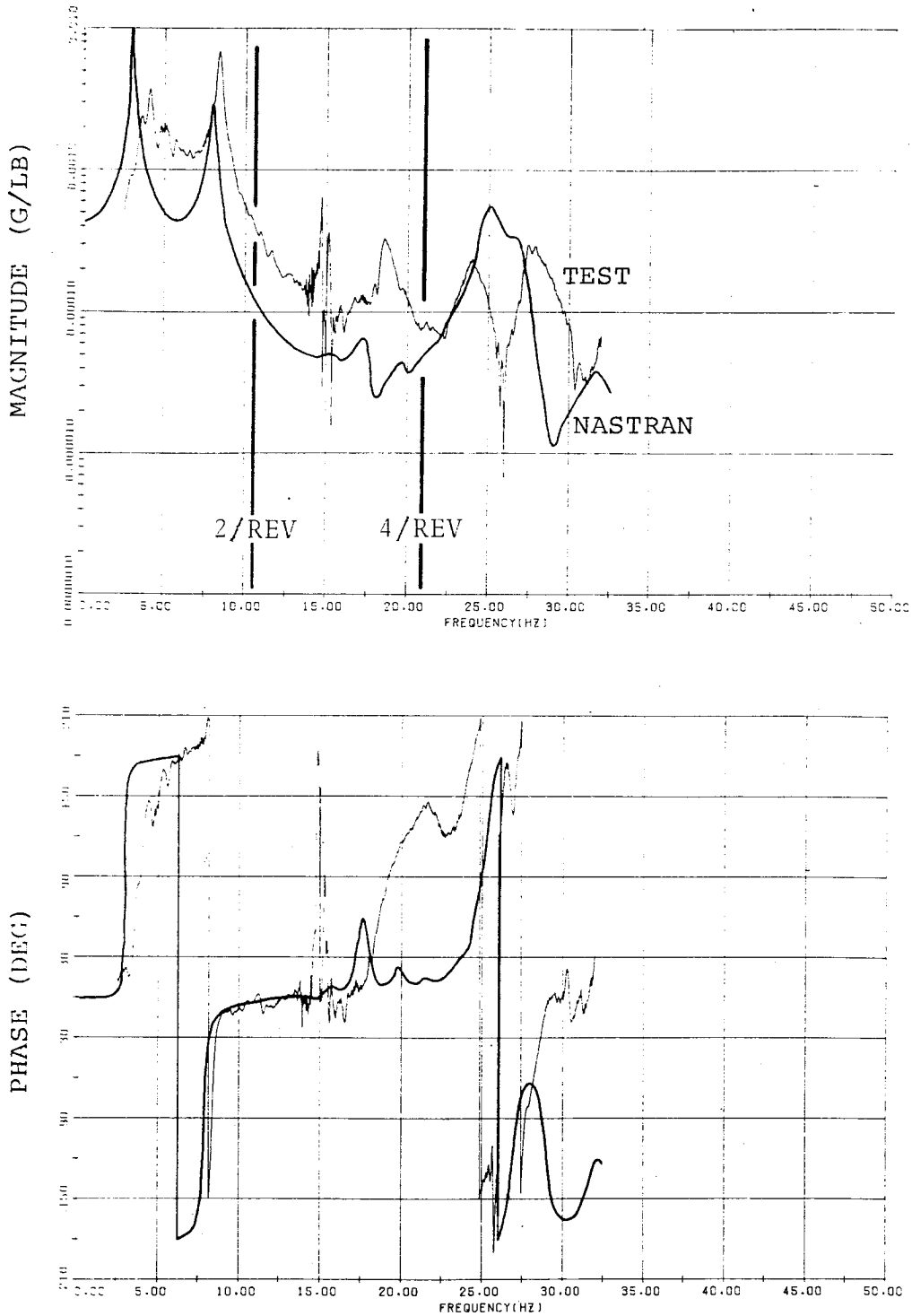

Figure B-54. Main Rotor Hub Fore-and-Aft Shake (Clean Wing) 90° Gearbox Vertical Response.

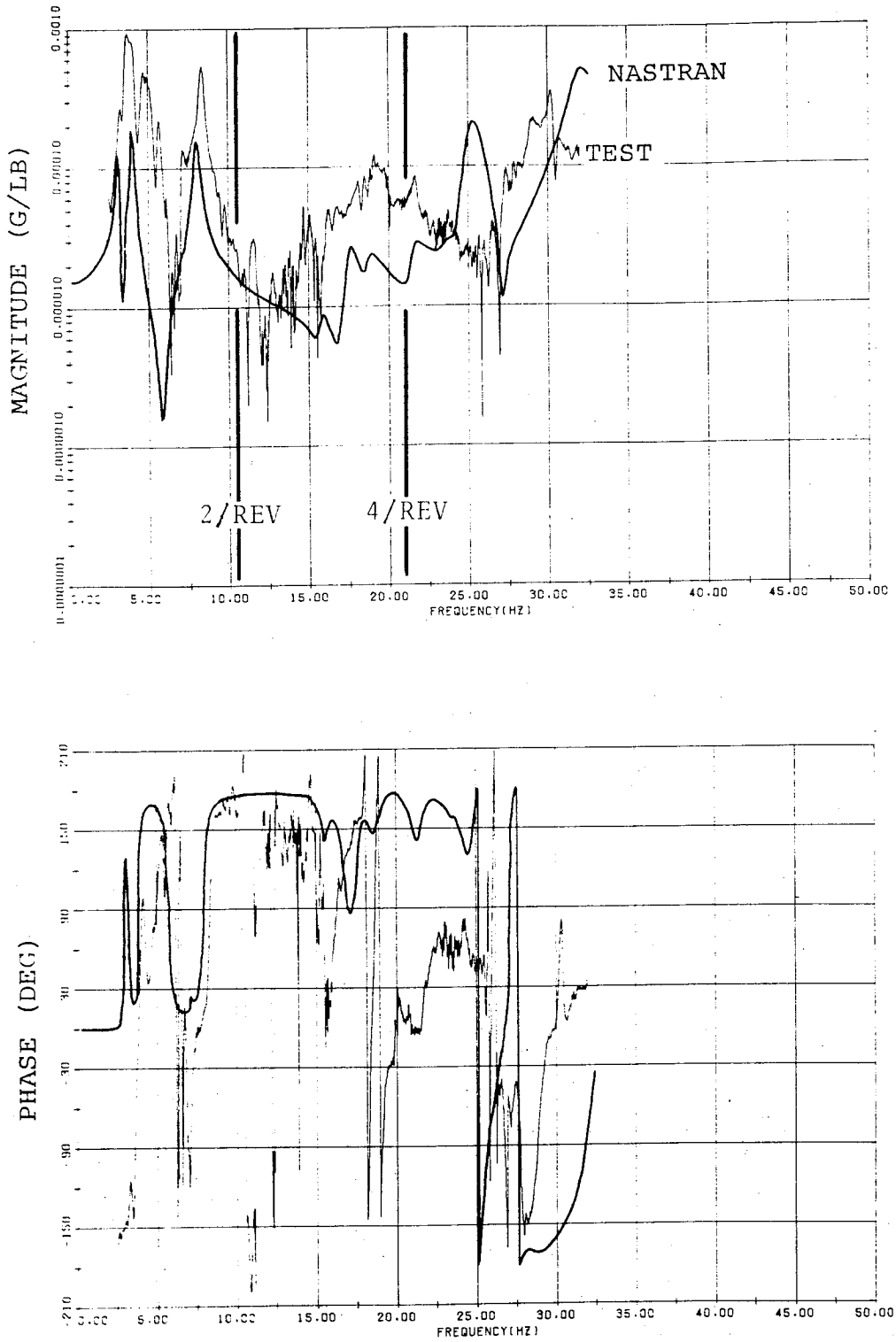

Figure B-55. Main Rotor Hub Fore-and-Aft Shake (Clean Wing) Left Wing Tip Vertical Response.

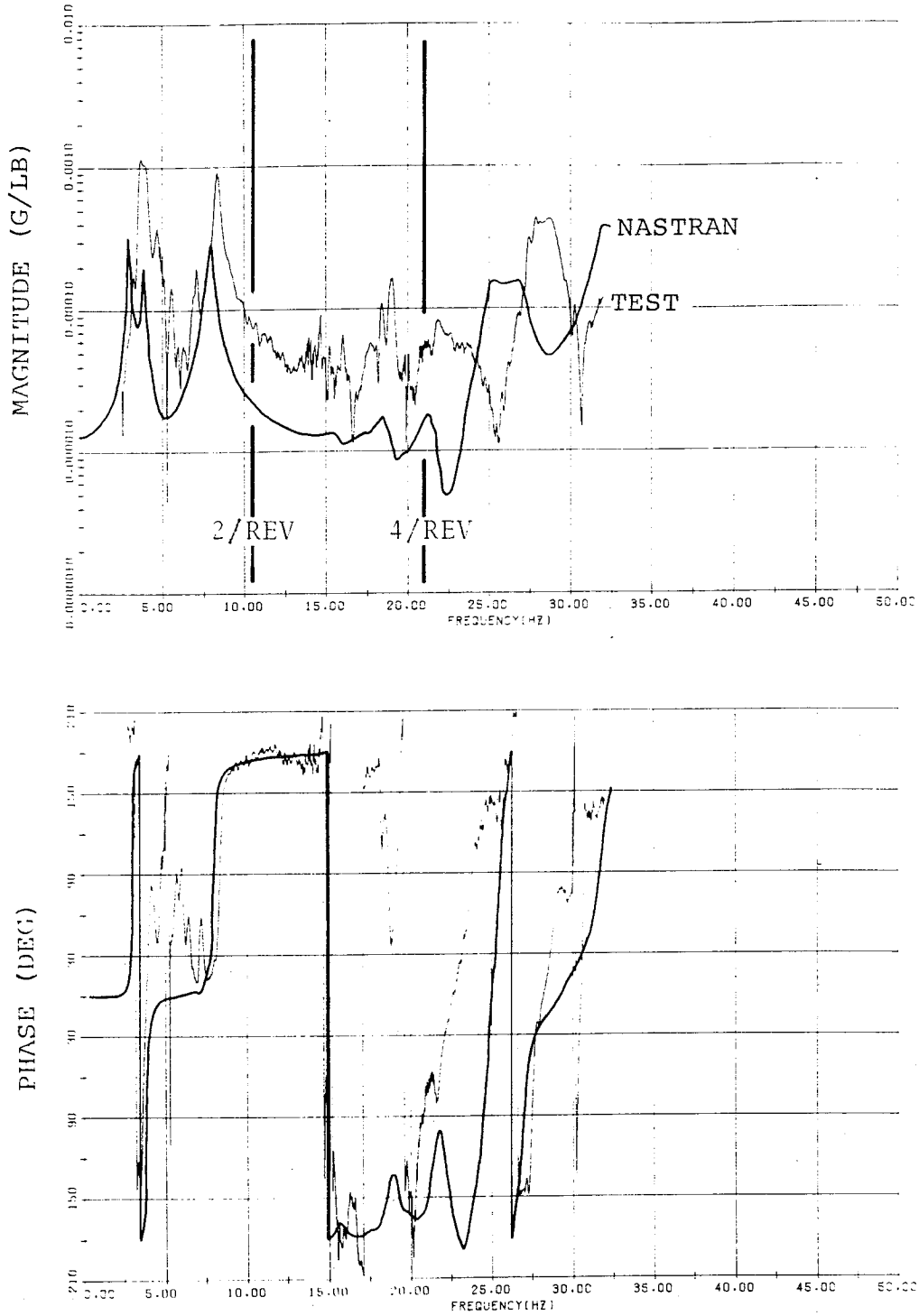

Figure B-56. Main Rotor Hub Fore-and-Aft Shake (Clean Wing) Right Wing Tip Vertical Response.

APPENDIX C

FORCED RESPONSE MODE SHAPE COMPARISONS

This appendix contains figures showing forced response mode shape comparisons between NASTRAN and test for the lateral and vertical tail shake tests. Comparisons shown are for the clean wing configuration at frequencies indicating resonances in the NASTRAN and test results. Figure number, forcing directions and frequencies for each mode comparison are given in Table C1.

TABLE C1. - FORCED RESPONSE MODE SHAPE COMPARISONS

Figure number	Applied force location/direction	Frequency - Hertz	
		Test	NASTRAN
C-1	Tail/vertical	3.9	3.0
C-2	Tail/vertical	8.0	8.0
C-3	Tail/vertical	15.5	15.7
C-4	Tail/vertical	18.0	17.5
C-5	Tail/lateral	7.1	7.15
C-6	Tail/lateral	15.5	15.7
C-7	Tail/lateral	18.9	17.5
C-8	Tail/lateral	24.4	25.8

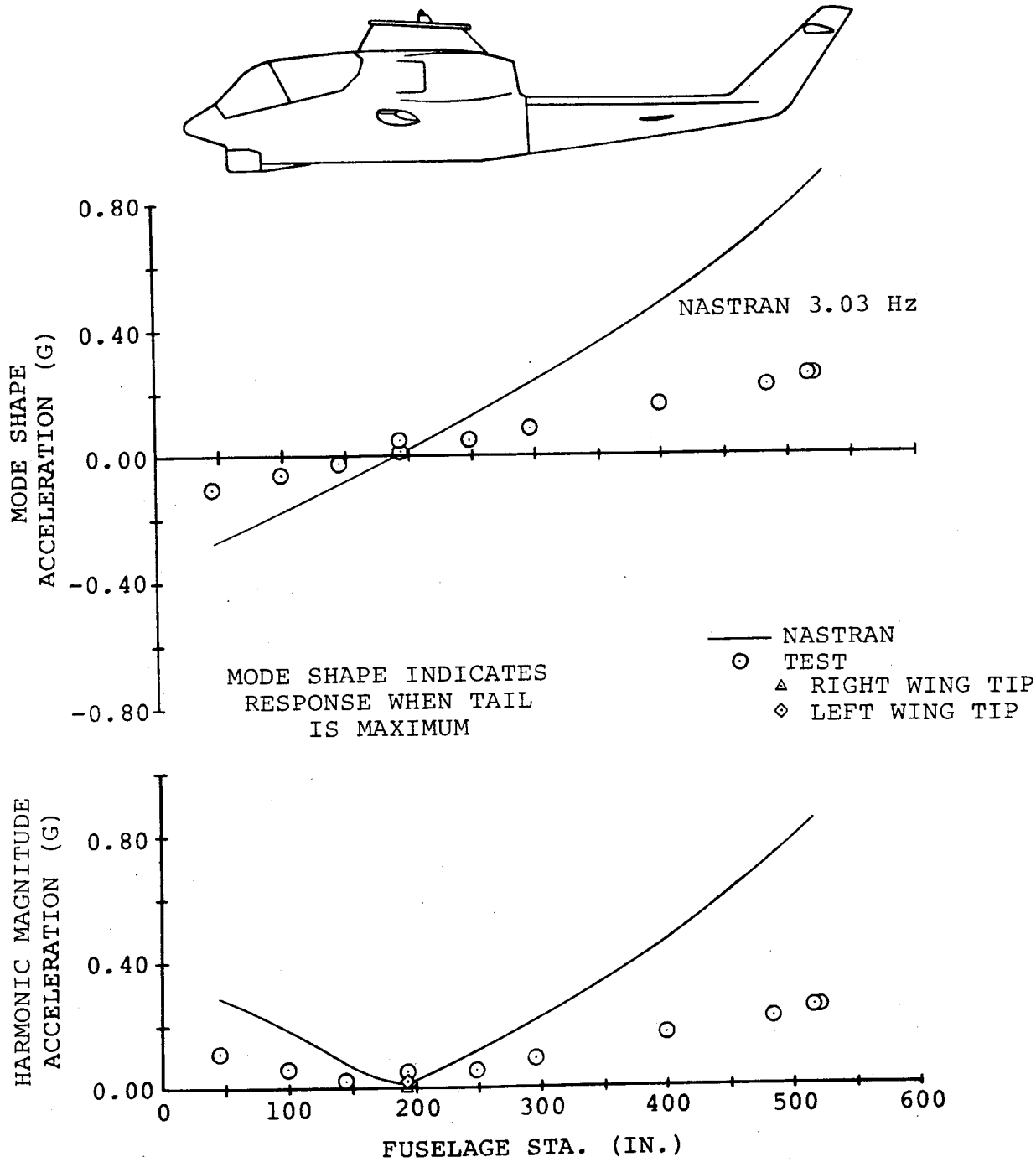

Figure C-1. Forced Response Mode Shape
Vertical Tail Shake at 3.92 Hz.

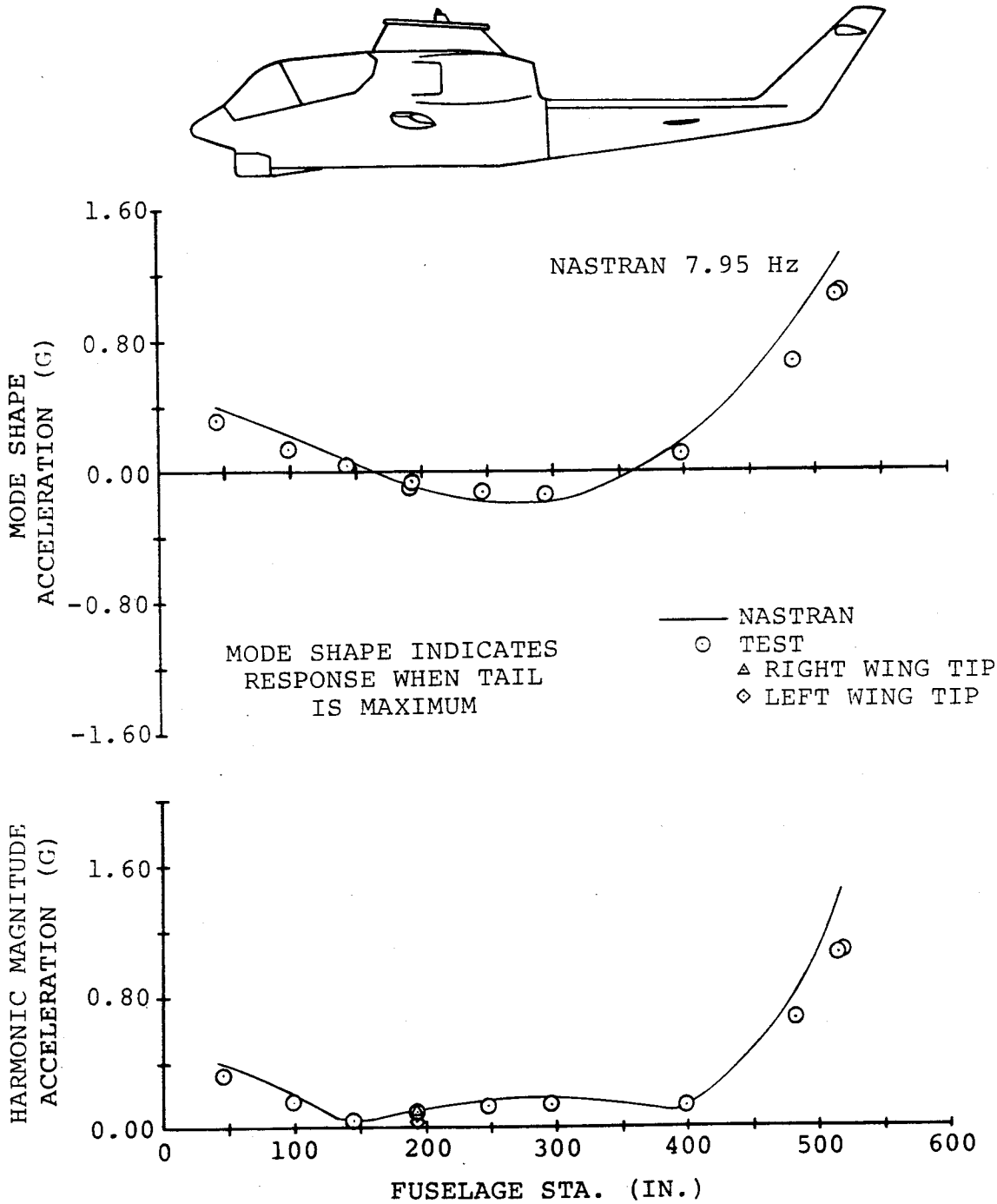

Figure C-2. Forced Response Mode Shape
Vertical Tail Shake at 8.06 Hz.

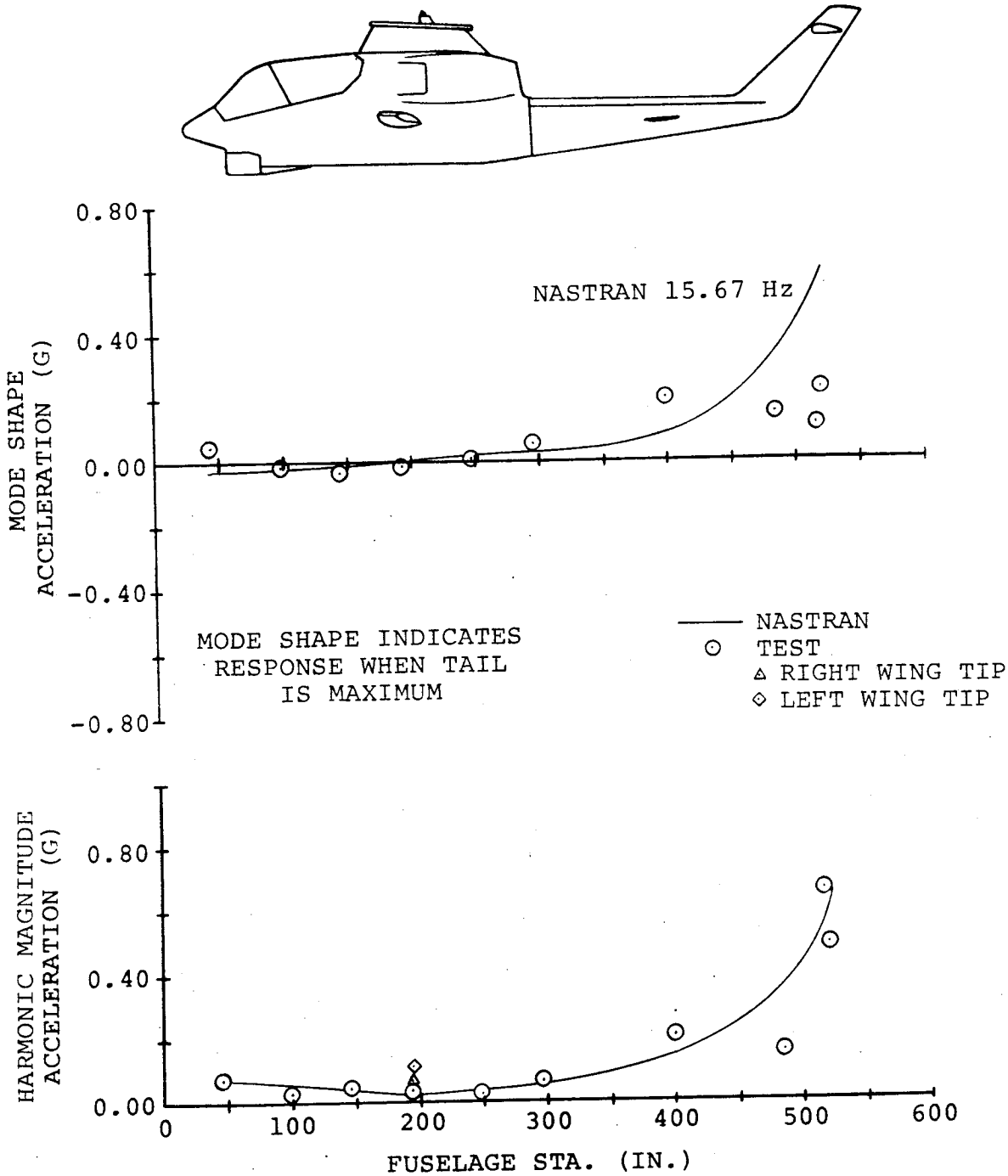

Figure C-3. Forced Response Mode Shape
Vertical Tail Shake at 15.52 Hz.

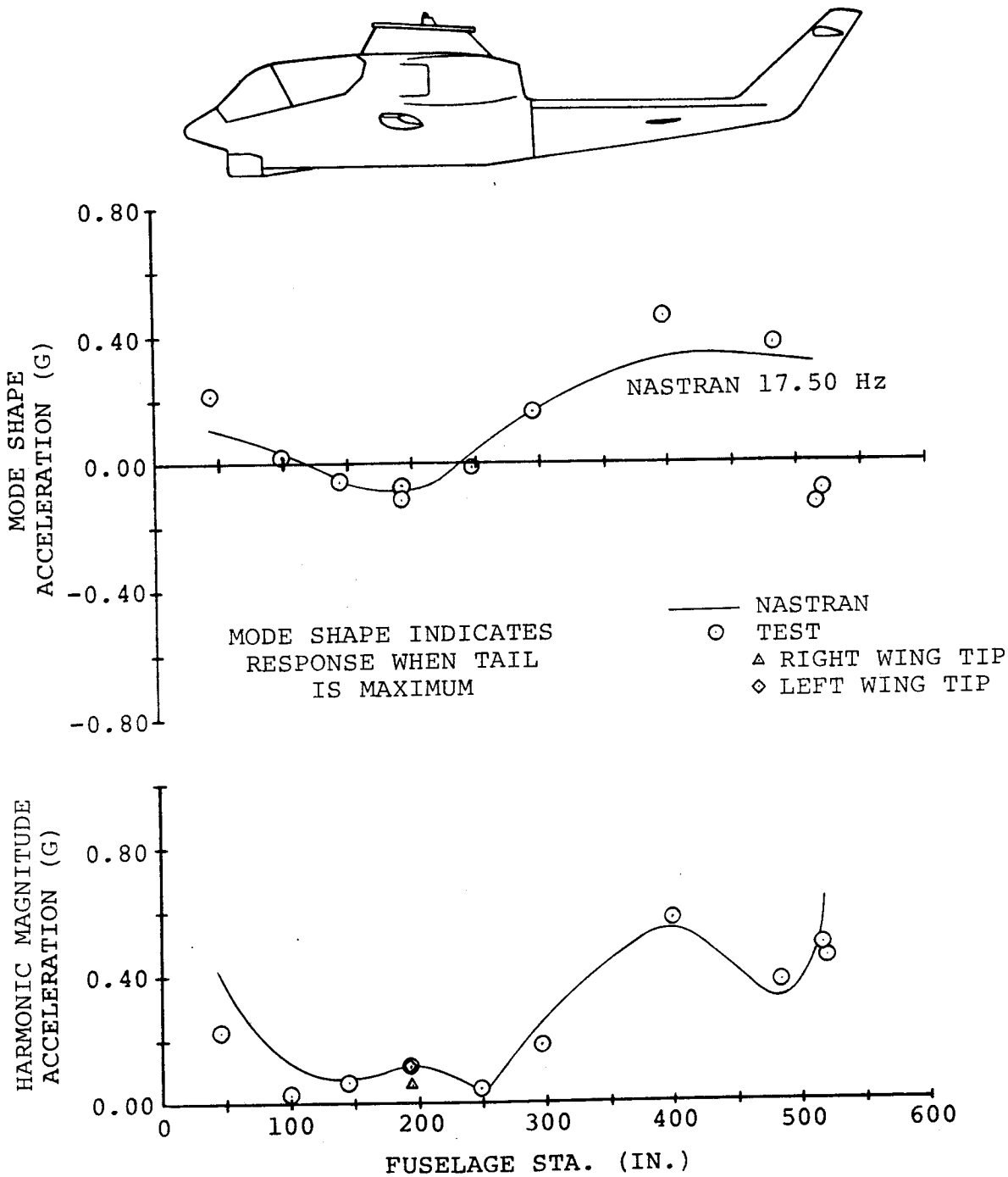

Figure C-4. Forced Response Mode Shape
Vertical Tail Shake at 17.97 Hz.

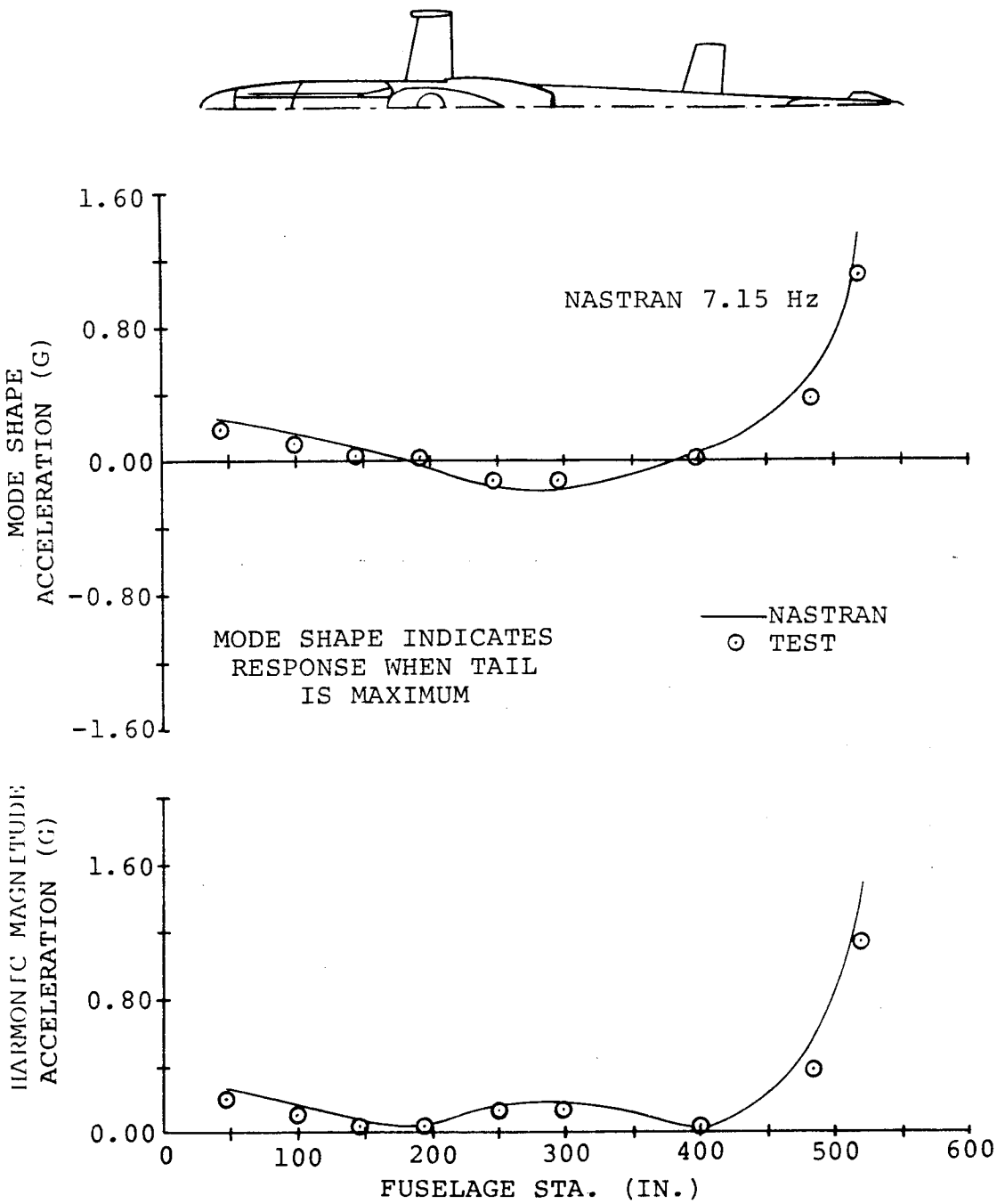

Figure C-5. Forced Response Mode Shape
Lateral Tail Shake at 7.06 Hz.

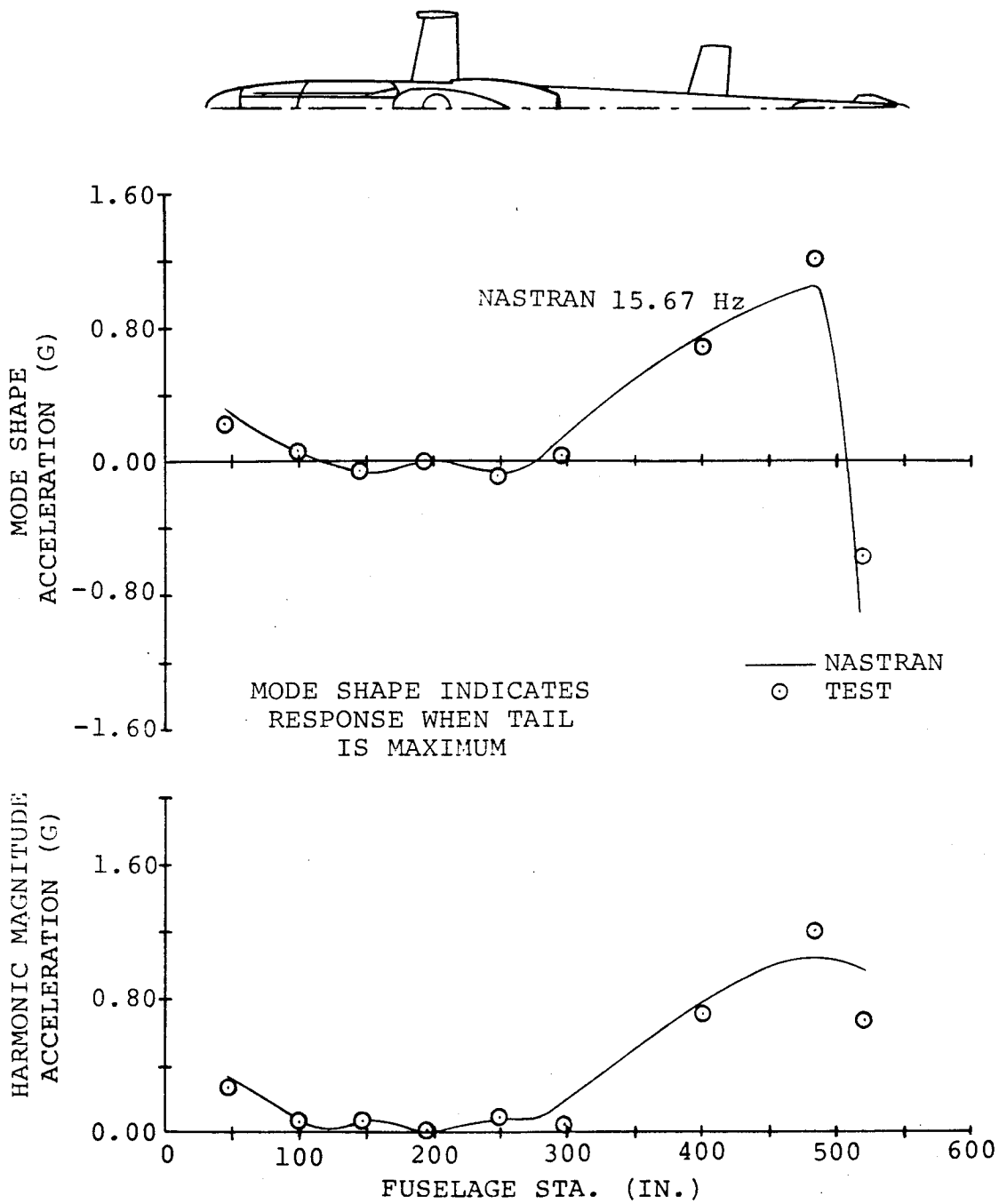

Figure C-6. Forced Response Mode Shape
Lateral Tail Shake at 15.52 Hz.

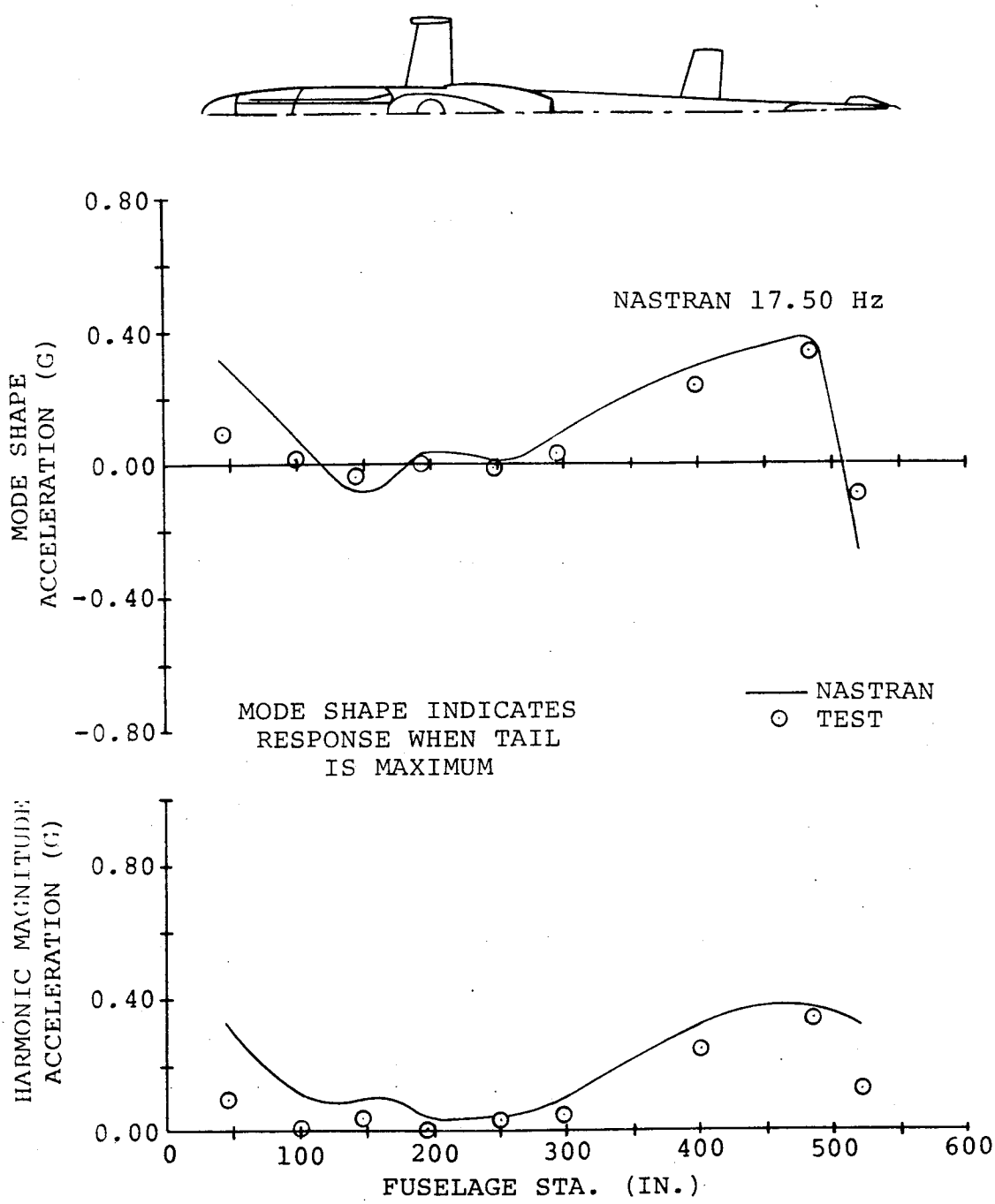

Figure C-7. Forced Response Mode Shape
Lateral Tail Shake at 18.96 Hz.

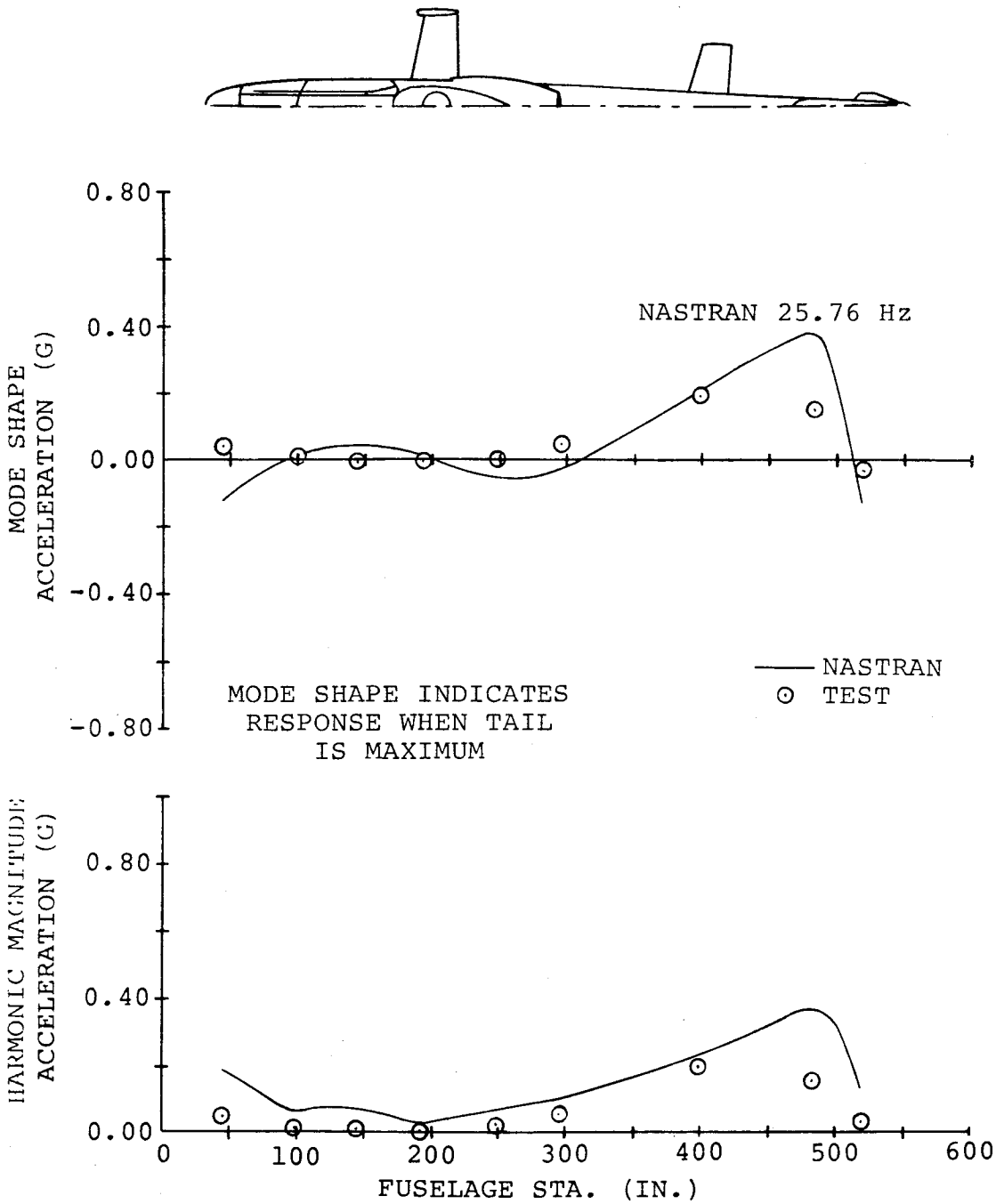

Figure C-8. Forced Response Mode Shape
Lateral Tail Shake at 24.38 Hz.

APPENDIX D

DESCRIPTION OF DIGITAL DATA REDUCTION TECHNIQUE

In the vibration testing, conducted at Bell Helicopter Textron, the sinusoidal forcing function is swept through all the frequencies of interest. Record lengths of 350 seconds with a sampling rate of 512 samples/second are not uncommon. This produces close to 180,000 data points to be analyzed, an amount which is unreasonably large for today's computers. It is necessary then to create an algorithm which will condense this data to a reasonable amount and retain the system responses for all the frequencies in the sweep. The system's transfer function (frequency response function) and phase plots can be calculated using this condensed data. The algorithm adapted for the IBM 370 computer used at Bell is described in this appendix.

SYMBOLS

$G_{\hat{x}\hat{x}}(f)$	power spectral density of the excitation (input)
$G_{\hat{x}\hat{y}}(f)$	cross power spectral density of the excitation (input) and response (output)
$H(f)$	transfer function or frequency response function
m	number of time segments representing complete time interval
N	number of samples
T	segment time length
Δt	sampling time
$x(t)$	excitation time history
$\hat{x}(t)$	excitation represented as a summation of time segments
$X(f)$	Fourier transform of $\hat{x}(t)$
$X^*(f)$	complex conjugate of $X(f)$
$y(t)$	response time history
$\hat{y}(t)$	response represented as a summation of time segments
$Y(f)$	Fourier transform of $\hat{y}(t)$

DIGITAL DATA REDUCTION TECHNIQUE

Using the assumption that the response of the system, y(t), is a linear function of the applied force, x, that is

$$y(t) = f(x_1 + x_2 + x_3 \ldots) = f(x_1) + f(x_2) + f(x_3) \ldots$$

a forcing function, $\hat{x}(t)$, can be formed as

$$x(t) = \sum_{k=0}^{m} x(t + kT)$$

where m is the number of sequential segments representing the original time history and T is the segment time length. It follows from the assumption of linearity that the system's response to this combined forcing function is the sum of the individual responses, i.e.

$$\hat{y}(t) = y[\hat{x}(t)] = y[\sum_{k=0}^{m} x(t + kT)] = \sum_{k=0}^{m} y[x(t + kT)]$$

Representative forcing function and response function time histories are shown in Figure D-1. Summing segments of the response to represent the total response is shown graphically in Figure D-2. This results in a response function which is only 1/m the length of these original time histories.

The transfer function or frequency response function, H(f), of the system, over all the measured frequencies, can be computed by using the Power Spectral density of the input, $G_{\hat{x}\hat{x}}(f)$, and the Cross Power Spectral density of the input and output, $G_{\hat{x}\hat{y}}(f)$.

$$H(f) = \frac{Y(f)}{X(f)}$$

then,

$$H(f) = \frac{G_{\hat{x}\hat{y}}(f)}{G_{\hat{x}\hat{x}}(f)}$$

where,

$$G_{\hat{x}\hat{y}}(f) = \frac{2\Delta t}{N} X^*(f)Y(f)$$

$$G_{\hat{x}\hat{x}}(f) = \frac{2\Delta t}{N} X^*(f)X(f)$$

$X(f)$ and $Y(f)$ are the Fourier transforms of $\hat{x}(t)$ and $\hat{y}(t)$ and are computed using the Cooley-Tukey Fast Fourier Transform algorithm. $X^*(f)$ is the complex conjugate of $X(f)$, Δt is the sampling interval and N is the number of samples. The amplitude of $H(f)$ can be found by the square root of sum of the squares of its components. The phase of $H(f)$ is the same as the phase of the cross power $G_{\hat{x}\hat{y}}$. For further information, see Reference 6.

Comparisons of data processed by the on-site data reduction system, which uses a tracking filter technique, and the digital data reduction technique explained above show good agreement between these two different methods.

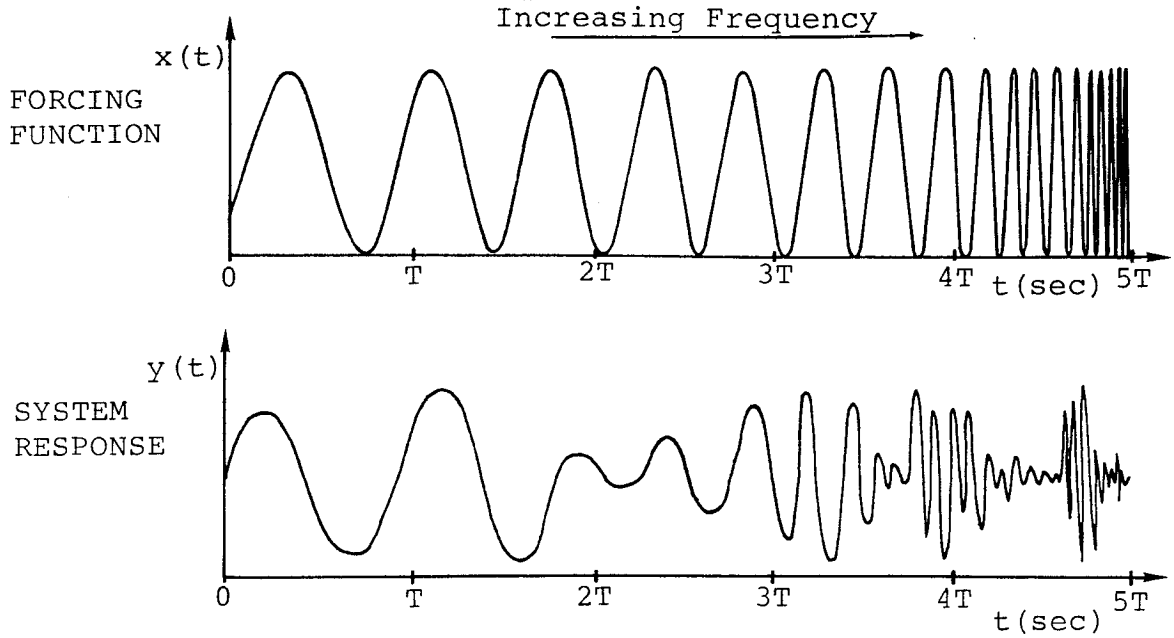

Figure D1. - Force and Response Time Histories.

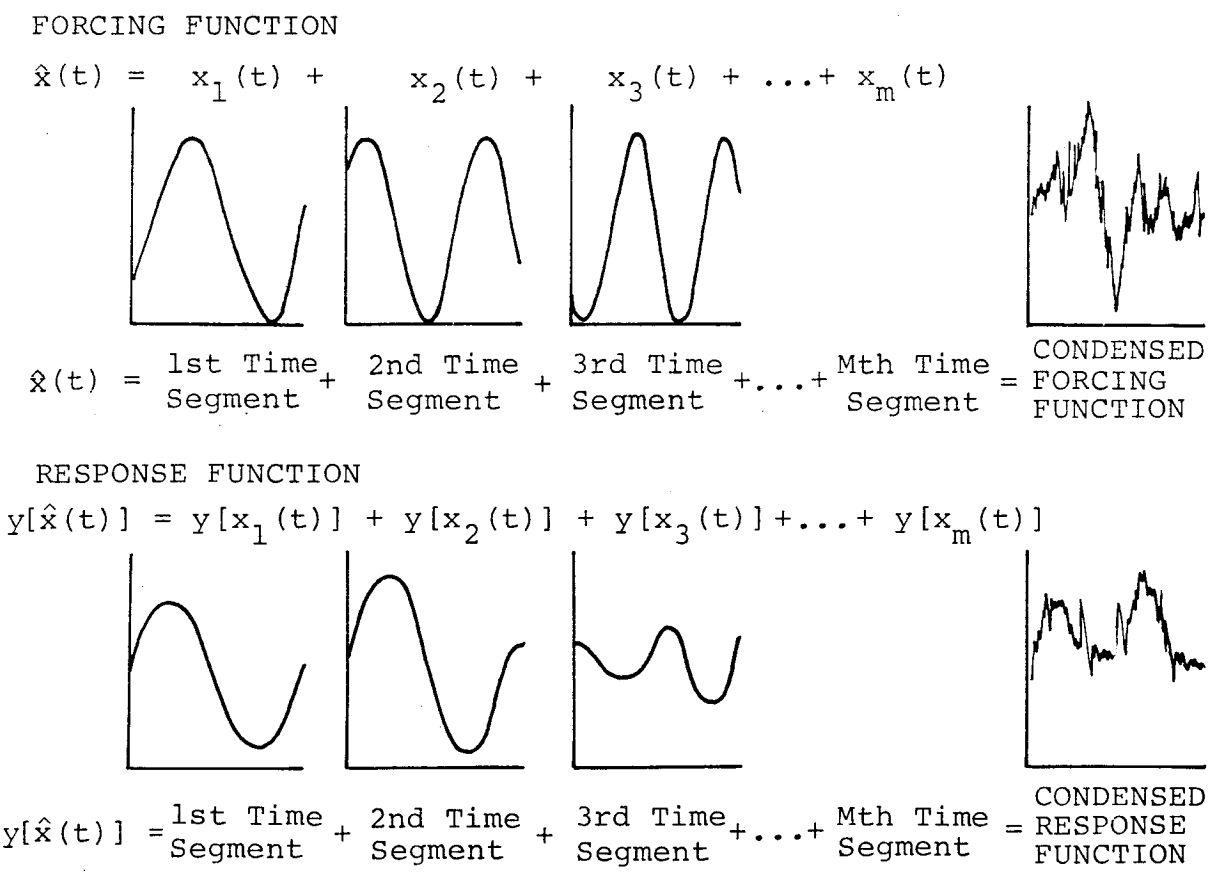

Figure D2. - Summation of Time History Segments to Represent Whole.

REFERENCES

1. McCormick, C. W. (editor): The NASTRAN User's Manual (Level 15), NASA Report No. SP-222(01), Scientific and Technical Information Office, National Aeronautics and Space Administration, Washington, D.C., June 1972.

2. Cronkhite, J. D., Berry, V. L., and Brunken, J. E.: A NASTRAN Vibration Model of the AH-1G Helicopter Airframe, U. S. Army Armament Command Report No. R-TR-74-045, Research Directorate, Gen. Thomas J. Rodman Laboratory, Rock Island Arsenal, Rock Island, Illinois, June 1974.

3. Frericks, D. E., et. al.: Measurement of the Static Influence Coefficients of the AH-1G Cobra Fuselage, U. S. Army Armament Command Report No. R-TR-76-005, February 1976.

4. Slack, J. R.: Static Load Deflection Test of Tailboom Installation for AH-1G Helicopter, Bell Helicopter Textron Report No. 299-095-003, Bell Helicopter Textron, Fort Worth, Texas, December 1975.

5. White, J. A.: Model AH-1G Airframe and Control System Ground Vibration Test Results, Bell Helicopter Textron Report No. 299-099-819, February 1976.

6. Enochson, L. D. and Otnes, R. K.: Programming and Analysis for Digital Time Series Data, the Shock and Vibration Information Center United States Department of Defense, 1968.